National Library
of Canada

Canadian Theses Service

Ottawa, Canada
K1A 0N4

Bibliothèque nationale
du Canada

Service des thèses canadiennes

NOTICE

The quality of this microform is heavily dependent upon the quality of the original thesis submitted for microfilming. Every effort has been made to ensure the highest quality of reproduction possible.

If pages are missing, contact the university which granted the degree.

Some pages may have indistinct print especially if the original pages were typed with a poor typewriter ribbon or if the university sent us an inferior photocopy.

Previously copyrighted materials (journal articles, published tests, etc.) are not filmed.

Reproduction in full or in part of this microform is governed by the Canadian Copyright Act, R.S.C. 1970, c. C-30.

AVIS

La qualité de cette microforme dépend grandement de la qualité de la thèse soumise au microfilmage. Nous avons tout fait pour assurer une qualité supérieure de reproduction.

S'il manque des pages, veuillez communiquer avec l'université qui a conféré le grade.

La qualité d'impression de certaines pages peut laisser à désirer, surtout si les pages originales ont été dactylographiées à l'aide d'un ruban usé ou si l'université nous a fait parvenir une photocopie de qualité inférieure.

Les documents qui font déjà l'objet d'un droit d'auteur (articles de revue, tests publiés, etc.) ne sont pas microfilmés.

La reproduction, même partielle, de cette microforme est soumise à la Loi canadienne sur le droit d'auteur, SRC 1970, c. C-30.

NL-339 (r. 88/04)

Canada

THE UNIVERSITY OF ALBERTA

SOLVENT STRUCTURE EFFECTS ON THE REACTIVITY OF SOLVATED ELECTRON IN ISOMERIC BUTANOL/WATER MIXTURES

by

©

PEMSARA CHANDANI SENANAYAKE

A THESIS SUBMITTED
TO THE FACULTY OF GRADUATE STUDIES AND RESEARCH
IN PARTIAL FULFILMENT OF THE REQUIREMENTS
FOR THE DEGREE OF DOCTOR OF PHILOSOPHY

DEPARTMENT OF CHEMISTRY

EDMONTON, ALBERTA
FALL, 1987

Permission has been granted to the National Library of Canada to microfilm this thesis and to lend or sell copies of the film.

The author (copyright owner) has reserved other publication rights, and neither the thesis nor extensive extracts from it may be printed or otherwise reproduced without his/her written permission.

L'autorisation a été accordée à la Bibliothèque nationale du Canada de microfilmer cette thèse et de prêter ou de vendre des exemplaires du film.

L'auteur (titulaire du droit d'auteur) se réserve les autres droits de publication; ni la thèse ni de longs extraits de celle-ci ne doivent être imprimés ou autrement reproduits sans son autorisation écrite.

ISBN 0-315-40856-1

THE UNIVERSITY OF ALBERTA

RELEASE FORM

NAME OF AUTHOR ..... Pemsara Chandani Senanayake

TITLE OF THESIS .... Solvent Structure Effects on the Reactivity of Solvated Electrons in Isomeric Butanol/Water Mixtures

DEGREE FOR WHICH THESIS WAS PRESENTED Doctor of Philosophy

YEAR THIS DEGREE GRANTED 1987

Permission is hereby granted to the UNIVERSITY OF ALBERTA LIBRARY to reproduce single copies of this thesis and to lend or sell such copies for private, scholarly or scientific research purposes only.

The author reserves other publication rights, and neither the thesis nor extensive extracts from it may be printed or otherwise reproduced without the author's written permission.

(Signed) P. C. Senanayake

Permanent Address:

28, Third Lane
Rathmalana
Sri Lanka

DATED Oct 14, 1987

THE UNIVERSITY OF ALBERTA

FACULTY OF GRADUATE STUDIES AND RESEARCH

The undersigned certify that they have read, and recommend to the Faculty of Graduate Studies and Research for acceptance, a thesis entitled

"SOLVENT STRUCTURE EFFECTS ON THE REACTIVITY OF SOLVATED ELECTRONS IN ISOMERIC BUTANOL/WATER MIXTURES"

submitted by P.C. Senanayake in partial fulfilment of the requirements for the degree of Doctor of Philosophy.

G R Freeman

Supervisor

John Stephens

James A. Plambeck

George Kotovych

Ashok Vij

External Examiner

15 June/87

Date

To My Parents

ABSTRACT

The reactivity of solvated electron with polar and charged scavengers was studied in water mixtures of *i*-BuOH , 2-BuOH and *t*-BuOH as a function of solvent composition and temperature. The kinematic viscosities and densities of these mixtures were also measured as functions of solvent composition and temperature.

The composition dependence of the nearly diffusion controlled rate constants is analysed according to the Stokes-Smoluchowski and Debye models and indicates four solvent composition zones that were also observed in the optical absorption spectrum of the solvated electron and the freezing point curves of the solvent. The rate constants depend more on the diffusion rates of the reactants than on the solvation energies of the participating ions. The difference in the composition dependence of the reactivity of polar and charged scavengers with electrons arise due to the difference in electron-dipole and electron-ion interactions. The latter has a greater dependence on the dielectric constant of the solvent.

The rate constants for the reactions with inefficient scavengers depend more on the solvation energies of the participating ions than on the solvent transport properties. The free energy of reaction for such a system is directly related to the electron affinity of the scavenger, the solvation energy of the electron and the polarizability of the solvent. The difference in reactivity between efficient and inefficient scavengers is due to entropies of activation rather than energies of activation.

TABLE OF CONTENTS

1 INTRODUCTION

1.1 The Solvated Electron 1
  1.1.1 Solvation Process 1
  1.1.2 Properties of the Solvated Electron 2
    1.1.2.1 Mobility 2
    1.1.2.2 Reactivity 2
  1.1.3 Optical Absorption 3
    1.1.3.1 Broadening of the Absorption Band 3
    1.1.3.2 Transitions 4
    1.1.3.3 Models 5
    1.1.3.4 Geometrical Structure 6
1.2 Optical and Kinetic Properties of the Solvated Electron in Alcohol/Water Mixtures 6
  1.2.1 Optical Properties 6
    1.2.1.1 Pure Solvents 6
    1.2.1.2 Mixed Solvents 8
  1.2.2 Kinetic Properties 10
    1.2.2.1 Composition Effects 10
      (a) Diffusion Controlled Reactions 11
      (b) Diffusion Coefficients 13
      (c) Slow Reactions 15
    1.2.2.2 Temperature Effects 15

1.3 Structure of Alcohol/Water Mixtures 16
1.3.1 Water 17
1.3.2 Alcohol 18
1.3.3 Alcohol/Water Mixtures 18
1.3.3.1 Static Properties 18
(a) Static Dielectric 18
(b) Thermodynamic 19
1.3.3.2 Dynamic Properties 21
(a) Viscosity 21
(b) Dielectric Relaxation 22
(c) Rotational Relaxation 23

Chapter 2 : EXPERIMENTAL

2.1 Materials 25
2.2 Apparatus 26
2.2.1 Sample Cells 26
2.2.2 Bubbling System 26
2.2.3 Irradiation, Detection and Control System 26
2.2.3.1 The Van de Graaff Accelerator 26
2.2.3.2 The Secondary Emission Monitor 28
2.2.3.3 Optical Detection System 30
(a) Light Source 30
(b) Monochromator, Grating and Filters 30
(c) Detectors and Amplifiers 32
(d) Digital Voltmeter, Oscilloscope and the Plotter 32

2.2.3.4 Temperature Control System 32
(a) Cooling and Heating System 32
(b) Cell Holder Box 33
2.2.4 Viscosity and Density Measuring Systems 34
2.2.4.1 Dilatometer 34
2.2.4.2 Viscometer 35
2.2.4.3 Temperature Regulating System 35

2.3 Techniques 37
2.3.1 Sample Preparation 37
2.3.2 Concentration Measurements 40
2.3.3 Measurement from Decay Curves 42
2.3.4 Effect of Impurities 46
2.3.4(a) Impurity in the Solvent 46
2.3.4(b) Impurity in the Solute 48
2.3.5 Viscosity Measurements 48
2.3.5(a) Calibration with Water 48
2.3.5(b) Calibration with Organic Liquids 49
2.3.6 Density Mesurements 49

Chapter 3 : RESULTS

3.1 Organic Scavengers 54
3.1.1 Tertiary Butanol/Water Mixtures 54
3.1.1(a) Reaction of e_s^- with Nitrobenzene 54
3.1.1(b) Reaction of e_s^- with Acetone 72
3.1.1(c) Reaction of e_s^- with Phenol 82

3.1.1(d) Reaction of e_s^- with Toluene 95

3.1.2 Secondary Butanol/Water and Iso-Butanol/Water Mixtures 106

3.2.1(a) Reaction of e_s^- with Nitrobenzene 106

3.2.1(b) Reaction of e_s^- with Acetone 126

3.2.1(c) Reaction of e_s^- with Phenol 139

3.2.1(d) Reaction of e_s^- with Toluene 154

3.2 Inorganic Scavengers 167

3.2.1 Reaction of e_s^- with Positive Ions 167

3.2.2 Reaction of e_s^- with Negative Ions 193

3.3 Viscosities and Densities of Butanol/Water Mixtures 217

3.3.1 Density 217

3.3.2 Viscosity 229

Chapter 4 : DISCUSSION

4.1 Solvent Structure Effects in t-butanol/Water Mixtures 243

4.1.1 Composition Effects 243

4.1.1.1 Diffusion Controlled Reactions 243

4.1.1.1(a) Solvent Viscosity Effects 243

4.1.1.1(b) Solvent Dielectric Effects 249

4.1.2 Slow Reactions 253

4.1.3 Changes for all Alcohols 259

4.1.4 Temperature Effects 261

4.1.4.1 Energies of Activation 261

4.1.4.2 Entropy Effects 261

4.1.4.3 Curved Arrhenius Behaviour 264

4.2 Solvent Isomer Effects in Butanol/Water Mixtures 267
4.2.1 Composition Effects 267
4.2.1.1 Efficient Scavengers 267
4.2.1.1(a) Stokes-Smoluchowski Model 265
4.2.1.1(b) Debye Model 269
4.2.1.1(c) Trap-depth Model 273
4.2.1.2 Inefficient Scavengers 273
4.2.1.2(a) Pure Alcohol 277
4.2.1.2(b) Alcohol/Water Mixtures 287
4.2.2 Energies and Entropies of Activation 290

4.3 Comparison of Electron Reactivities with Polar and Charged Scavengers in t-butanol/Water Mixtures 293
4.3.1 Positive Scavengers 293
4.3.2 Negative Scavengers 300
4.3.3 Temperature Dependence 304

4.4 Temperature and Composition Dependence of Densities and Viscosities of Butanol/Water Mixtures 306
4.4.1 Excess Volume 306
4.4.2 Viscosity 307
4.4.3 Energy of Activation for Viscous Flow 314

4.5 Conclusions 317

REFERENCES 318

LIST OF TABLES

Table Number

Table 2-1 : Comparison of viscosity values 53

Table 2-2 : Comparison of densities at 293.15K 53

Table 3-1 :The values of second order rate constants for nitrobenzene in *t*-butanol/water 67

Table 3-2 : Reaction rate parameters for nitrobenzene in *t*-butanol/water 70

Table 3-3 :The values of second order rate constants for acetone in *t*-butanol/water 78

Table 3-4 : Reaction rate parameters for acetone in *t*-butanol/water 80

Table 3-5 :The values of second order rate constants for phenol in *t*-butanol/water 90

Table 3-6 : Reaction rate parameters for phenol in *t*-butanol/water 93

Table 3-7 :The values of second order rate constants for toluene in *t*-butanol/water 101

Table 3-8 : Reaction rate parameters for toluene in *t*-butanol/water 104

Table 3-9 :The values of second order rate constants for nitrobenzene in *iso*-butanol/water 118

Table 3-10 :The values of second order rate constants for nitrobenzene in 2-butanol/water 119

Table 3-11 : Reaction rate parameters for nitrobenzene in *iso*-butanol/water and 2-butanol/water 122

Table 3-12 :The values of second order rate constants for acetone in *iso*-butanol/water 133

Table 3-13 : The second order rate constants for for acetone in 2-butanol/water 134

Table 3-14 : Reaction rate parameters for acetone in *iso*-butanol/water and 2-butanol/water 136
Table 3-15 :The values of second order rate constants for phenol in *iso*-butanol/water 147
Table 3-16 :The values of second order rate constants for phenol in 2-butanol/water 148
Table 3-17 : Reaction rate parameters for phenol in *iso*-butanol/water and 2-butanol/water 150
Table 3-18 :The values of second order rate constants for toluene in *iso*-butanol/water 160
Table 3-19 :The values of second order rate constants for toluene in 2-butanol/water 162
Table 3-20 : Reaction rate parameters for toluene in *iso*-butanol/water and 2-butanol/water 164
Table 3-21 : The values of k_2 in t-butanol/water mixtures for (+) scavengers .. 182
Table 3-22 : Reaction rate parameters for (+) scavengers in t-butanol/water .. 191
Table 3-23 : The values of k_2 in t-butanol/water mixtures for (-) scavengers ... 206
Table 3-24 : Reaction rate parameters for (-) scavengers in t-butanol/water ... 215
Table 3-25 : Density of butanol/water mixtures as a function of x_{H_2O} and T .. 219
Table 3-26 : Parameters for the temperature dependence of density 226
Table 3-27 : Parameters for the composition dependence of density in butanol/water mixtures 228
Table 3-28 : Experimental flow times (t) and kinematic viscosities (ν) of butanol/water mixtures as a function of composition and temperature 230
Table 3-29 : Temperature dependence of viscosity 238
Table 3-30 : The activation energies for viscous flow 240

Table 4-1 : The molar volumes and polarizabilities in pure alcohols and butanol/water mixtures 284

Table 4-2 : The excess volumes in butanol/water mixtures 309

LIST OF FIGURES

Figure # Page

2-1: The bubbling system 27

2-2: The secondary emission monitor 29

2-3: The path of the analyzing light 31

2-4: Viscometer 36

2-5: Temperature measurement system for the viscometer 38

2-6: Temperature regulator system 39

2-7: The sealing technique 41

2-8: Evaporation rate of toluene, and acetone in alcohol/water mixtures . 42

2-9: A Typical plot of solvated electron decay 44

2-10: The first order decay plot of solvated electron 45

2-11: Reproducibility of k_2 values 48

3-1 to 12: Values of k_{obs} for e_s^- + nitrobenzene reaction in *t*-butanol/water mixtures 56

3-13: Arrhenius plots for e_s^- + nitrobenzene reaction in *t*-butanol/water mixtures 69

3-14: The values of k_2 , E_2 and $\Delta S_2^{\neq}$ for e_s^- + nitrobenzene reaction in *t*-butanol/water mixtures 71

3-15 to 20: Values of k_{obs} for e_s^- + acetone reaction in *t*-butanol/water mixtures73

3-21: Arrhenius plots for e_s^- + acetone reaction in *t*-butanol/water mixtures 79

3-22: The values of k_2 , E_2 and $\Delta S_2^{\neq}$ for e_s^- + acetone reaction in *t*-butanol/water mixtures.... 81 item3-23 to 29:Values of k_{obs} for e_s^- + phenol reaction in *t*-butanol/water mixtures 83

3-30: Arrhenius plots for e_s^- + phenol reaction in *t*-butanol/water mixtures 92

3-31: The values of k_2 , E_2 and $\Delta S_2^{\neq}$ for e_s^- + phenol reaction in *t*-butanol/water mixtures 94

3-32 to 37: Values of k_{obs} for e_s^- + toluene reaction in *t*-butanol/water mixtures96

3-38: Arrhenius plots for e_s^- +toluene reaction in *t*-butanol/water mixtures 103

3-39: The values of k_2 , E_2 and $\Delta S_2^{\neq}$ for e_s^- + toluene reaction in *t*-butanol/water mixtures 105

3-40 to 47: Values of k_{obs} for e_s^- + nitrobenzene reaction in *iso*-butanol/water mixtures 108

3-48 to 56: Values of k_{obs} for e_s^- + nitrobenzene reaction in 2-butanol/water mixtures 109

3-57: Arrhenius plots for e_s^- +nitrobenzene reaction in *iso*-butanol/water , 2-butanol/water mixtures 121

3-58: The values of k_2 for e_s^- + nitrobenzene reaction in butanol/water mixtures 123

3-59: The values of E_2 for e_s^- + nitrobenzene reaction in butanol/water mixtures 124

3-60: The values of $\Delta S_2^{\neq}$ for e_s^- + nitrobenzene reaction in butanol/water mixtures 125

3-61 to 66: Values of k_{obs} for e_s^- + acetone reaction in *iso*-butanol/water mixtures 127

3-67 to 71: Values of k_{obs} for e_s^- + acetone reaction in 2-butanol/water mixtures 130

3-72: Arrhenius plots for e_s^- + acetone reaction in *iso*-butanol/water , 2-butanol/water mixtures 135

3-73: The values of E_2 for e_s^- + acetone reaction in butanol/water mixtures 137

3-74: The values of $\Delta S_2^{\neq}$ for e_s^- + acetone reaction in butanol/water mixtures 138

3-75 to 81: Values of k_{obs} for e_s^- + phenol reaction in *iso*-butanol/water mixtures 140

3-82 to 86: Values of k_{obs} for e_s^- + phenol reaction in 2-butanol/water mixtures144

3-87: Arrhenius plots for e_s^- +phenol reaction in *iso*-butanol/water , 2-butanol/water mixtures.......................................149

3-88: The values of k_2 for e_s^- + phenol reaction in butanol/water mixtures 151

3-89: The values of E_2 for e_s^- + phenol reaction in butanol/water mixtures 152

3-90: The values of $\Delta S_2^{\neq}$ for e_s^- + phenol reaction in butanol/water mixtures 153

3-91 to 96: Values of k_{obs} for e_s^- + toluene reaction in *iso*-butanol/water mixtures 155

3-97 to 100: Values of k_{obs} for e_s^- + toluene reaction in 2-butanol/water mixtures 158

3-101: Arrhenius plots for e_s^- +toluene reaction in *iso*-butanol/water , 2-butanol/water mixtures.......................................163

3-102: The values of E_2 for e_s^- + toluene reaction in butanol/water mixtures 165

3-103: The values of $\Delta S_2^{\neq}$ for e_s^- + toluene reaction in butanol/water mixtures 166

3-104 to 115: Values of k_{obs} for e_s^- + Ag^+ reaction in *t*-butanol/water mixtures (counter ion ClO_4^-).......................................169

3-116 to 120: Values of k_{obs} for e_s^- + Cu^{2+} reaction in *t*-butanol/water mixtures (counter ion SO_4^{2-}) 176

3-121 to 125: Values of k_{obs} for e_s^- + Cu^{2+} reaction in *t*-butanol/water mixtures (counter ion ClO_4^-) 179

3-126: Arrhenius plots for e_s^- +Ag^+ reaction in *t*-butanol/water mixtures 188

3-127a: Arrhenius plots for e_s^- +Cu^{2+} reaction in *t*-butanol/water mixtures189

3-127b: Arrhenius plots for e_s^- +Cu^{2+} reaction in *t*-butanol/water mixtures190

3-128: The values of k_2 , E_2 and $\Delta S_2^{\neq}$ for e_s^- reaction in t-butanol/water mixtures 192

3-129 to 135: Values of k_{obs} for e_s^- + NO_3^- reaction in *t*-butanol/water mixtures (counter ion K^+)........194

3-136 to 143: Values of k_{obs} for e_s^- + CrO_4^{2-} reaction in *t*-butanol/water mixtures (counter ion K^+)........198

3-143 to 150: Values of k_{obs} for e_s^- + NO_3^- reaction in *t*-butanol/water mixtures (counter ion Li^+) 202

3-151: Arrhenius plots for e_s^- +NO_3^- reaction in *t*-butanol/water mixtures (counter ion K^+)........212

3-152: Arrhenius plots for e_s^- +NO_3^- reaction in *t*-butanol/water mixtures (counter ion Li^+) 213

3-153: Arrhenius plots for e_s^- +CrO_4^{2-} reaction in *t*-butanol/water mixtures 214

3-154: The values of k_2 , E_2 and $\Delta S_2^{\neq}$ for e_s^- reaction in t-butanol/water mixtures 216

3-155: Composition and temperature dependence of viscosity of *t*-butanol/water mixtures 241

3-156: Composition and temperature dependence of viscosity in (a)*iso*-butanol/water and, (b)2-butanol/water mixtures 242

4-1: The composition dependence of rate constants k_2 in *t*-butanol/water mixtures 244
4-2: The values of k_2 against viscosity η in *t*-butanol/water mixtures . . . 246
4-3: Composition dependence of viscosity η and solvation energy of the electron E_r in *t*-butanol/water mixtures 248
4-4: Values of k_2 /f for nitrobenzene against viscosity η in *t*-butanol/water mixtures 251
4-5: Values of k_2 against η for inefficient scavengers in *t*-butanol/water mixtures 254
4-6: Encounter efficiency for inefficient scavengers against solvated electron trap depth in *t*-butanol/water mixtures 256
4-7: The composition dependence of ηk_2 in *t*-butanol/water mixtures for inefficient scavengers 258
4-8: The composition dependence of energies of activation in *t*-butanol/water mixtures 262
4-9: The composition dependence of activation entropies in *t*-butanol/water mixtures 263
4-10: Composition dependence of rate constants in butanol/water mixtures 268
4-11: Composition dependence of viscosity normalized rate constants in butanol/water mixtures 270
4-12: Values of (k_2 /f) normalized with that of water against viscosity in butanol/water mixtures 271
4-13: Composition dependence of $\epsilon\eta k_2$ in butanol/water mixtures 274
4-14: $\epsilon\eta k_2$ against the optical absorption energy of e_s^- 275
4-15: Dependence of e_s^- reactivities in alcohol/Water mixtures with electron affinity 276

4-16: Values of (k_2/k_N) against optical absorption energy 278

4-17: Change of the dependence of $\Delta G^{\neq}_{52}$ for the reaction of $e_s{}^-$ with inefficient scavengers, on the solvated electron optical absorption energy with dipole moment 280

4-18: Relationship between the electron affinity and the dipole moment .. 281

4-19: Change of $\log(k_2/k_N)$ at the same E_r value (1.34 eV), with the number of carbon atoms 282

4-20: Change of $\log(k_2/k_N)$ with $(1 + \frac{1}{\epsilon})$ in pure alcohols 286

4-21: Change of $\log(k_2/k_N)$ with E_r in butanol/water mixtures 288

4-22: Dependence of the dielectric constant in butanol/water mixtures on composition 289

4-23: Composition dependence of energies of activation E_2 291

4-24: Composition dependence of entropies of activation $\Delta S^{\neq}_2$ 292

4-25: Composition dependence of rate constants k_2 for $e_s{}^-$ reaction. in *t*-BuOH /water mixtures 294

4-26: Change of rate constant k_2 with viscosity η in *t*-butanol/water mixtures for Ag^+ and nitrobenzene 295

4-27: The viscosity η, dependence of normalized rate constants for Ag^+ and nitrobenzene (k_2 /f), in *t*-butanol/water mixtures 297

4-28: The composition η, dependence of normalized rate constants k_2 in *t*-butanol/water mixtures for Ag^+ and nitrobenzene 300

4-29: The viscosity η, dependence of rate constants k_2 in *t*-butanol/water mixtures for all charged scavengers 302

4-30: The composition dependence of normalized rate constants in *t*-butanol/water mixtures for all charged scavengers 303

4-31: The experimental and calculated densities of *t*-butanol/water (a), and 2-butanol/water (b) mixtures 308

4-32: Excess volumes V^E, in *t*-butanol/water (a) and 2-butanol/water (b and c) mixtures 311
4-33: Composition dependence of viscosity η 313
4-34: Composition dependence of activation energy for viscous flow, E_η . 315

1 INTRODUCTION

1.1 Solvated Electron

1.1.1 Solvation Process

Solvated electrons were first obtained by dissolving alkali metals in liquid ammonia(1), and later in other solvents such as amines(2) and alcohols(3). They can also be formed by other methods, radiolysis being one of them.

Radiolysis involves irradiating the liquid with ionizing radiation. Pulse radiolysis uses pulses of high energy electrons as the source of radiation. When ionizing particles such as electrons, penetrate the liquid medium, energy is lost by ionization and excitation of the liquid molecules. Along the path of these electrons (ionizing particles) local volumes of ionized, excited and dissociated molecules remain. These local volumes are called spurs. The spurs rapidly dissipate as the reactive intermediates diffuse into the bulk of the liquid(4).

Due to ionization more electrons are produced in the path of the high energy electron. These also dissipate their excess energy by ionization and excitation of molecules of the medium. Once the energy of the electron is sufficiently lowered it can form a localized state.

The localization process of an electron depends on whether the electron affinity of the medium (molecules) is positive or negative. If the molecules have positive electron affinity the electron gets localized in a solvent molecule and forms a negative ion. If it is negative, localization is affected by the polarity of the molecules: (i) the electron in a polar fluid gets trapped in a potential well created by several dipolar molecules; (ii) in a non-polar liquid, localization occurs due to the anisotropic polarizability of the molecules. If the molecules are isotropically polarizable, the electron is either delocalized or localized in a shallow potential well. Such electrons are called quasi-free electrons(5).

An electron electronically polarizes the medium in about 10^{-15}s. Thus the trapped electron immediately finds itself in an electronically polarized potential well (trap)(6). The electric field of the electron causes the medium molecules to reorient along the axes of permanent dipole or that of the maximum polarizability. The trap becomes deeper and the electron state more stable. The time for this process is related to the dielectric relaxation time of the medium (7). The completely relaxed state of the electron which is in equilibrium with the solvent is called the solvated electron. In polar liquids an electron becomes solvated in a time range of picoseconds (8).

1.1.2 Properties of the Solvated Electron

The physico-chemical properties of solvated electrons depend on the nature of the solvent. The shape and polarity of the solvent molecules affect the electron-solvent interaction, and therefore the energy of solvation.

1.1.2.1 Mobility

Solvated electrons are different from quasi-free electrons by being more localized and less mobile. Their mobility is several times higher than that of normal ions, but in water it is less than that of H^+(9).

1.1.2.2 Reactivity

The solvated electron has a negative free energy of formation. Therefore it is a thermodynamically stable reactant. It has a very high electron donor capacity (10). It reacts with chemical species that have positive electron affinity and becomes localized in a deeper trap in the reactant molecule. Its reactivity is a function of the electron affinity of the reactant.

1.1.3 Optical Absorption

Solvated electrons absorb light at wave lengths ranging from ultraviolet to infrared. The absorption band is broad and asymmetric with a long tail extending to higher energies. The energy at the absorption maximum, E_{Amax}, and the width of the band depend on the polarity of the solvent. In polar solvents, the maximum in the absorption spectrum occurs at higher energies because the energy of interaction of the electron with the permanent dipoles of the solvent is greater than that with the induced dipoles. The electron is solvated in a deeper trap in polar solvents.

In general, the E_{Amax} values of solvated electrons in organic solvents depend on:

(a) the types and number of functional groups, and
(b) the number of alkyl groups attached to the functional group.

Values of E_{Amax} are temperature (and density) dependent. The thermal agitation of the solvent makes the traps shallower.

1.1.3.1 Broadening of the Absorption Band

The shape of the solvated electron spectrum is similar in any solvent, it being broad and assymmetric, skewed to high energies. The shape of the band is attributed to:

(a) homogeneous broadening(11,12), and
(b) heterogeneous broadening (13,14).

Homogeneous broadening involves bandwidth that originates from the optical absorption of a single type of absorbing species. This requires to assume that all traps in the medium are of the same depth and that broadening is due to the specific nature of the excitation. But in a liquid where randomness persists the probability that all solvated electron traps are of the same depth is probably negligible.

Heterogeneous broadening is due to excitations from several traps, each giving rise to a spectrum slightly different from others. If broadening is due to a distribution of traps, the width should increase with increasing temperature. This is not always observed.

1.1.3.2 Transitions

The energy absorbed by the ground state solvated electron has been attributed to the following transitions (15-20):

(a) from the ground state discrete energy level to an excited state discrete energy level (15) (bound to bound transition) of the same trap,

(b) from the ground state discrete energy level to the higher energy continuum (16) (bound to continuum),

(c) from the ground bound level to an excited bound level or to the continuum (17-20) (bound to bound and bound to continuum),

(d) from the ground bound level in one trap to a similar ground bound energy level of a neighbouring trap (18,19) (trap to trap).

If the transitions are bound to bound type, the absorption spectrum is symmetrical. But the other three types of transitions could account for the asymmetry of the band. The skew to the high energy side is usually explained by bound to continuum transitions. The last two types of transitions are similar. The trap to trap model assumes two types of transitions: (a) short distance transfers in analogy to bound to bound transitions; (b) long distance transfers in analogy to bound to continuum transitions. Measurement of the photoconductivity spectra has given information about the type of transitions. A photoconductivity spectrum corresponds to bound ground level to continuum transitions. Comparison of the optical absorption spectrum with the photoconductivity spectrum allows the following to be estimated: (a) the threshold energy for photoconductivity, E_{th}, i.e. the lowest energy needed for the bound to continuum transition (20,21); (b) the relative amounts of absorption spectrum due to bound to bound and bound to continuum transitions (22,23). The value of E_{th} is a measure of the trap depth, i.e. the energy difference between the ground state energy level and the bottom of the conduction band. If E_{th} and the threshold for optical absorption E_{th}^{ab} were the same and the maxima of the two spectra overlapped, the optical transition would be entirely due to bound to continuum transitions.

Comparisons indicate that in all systems the optical absorption band consists of both bound to bound and bound to continuum transitions (14, 20-26). In most solvents E_{th} is less than E_{Amax}, indicating that a major portion of the transitions are bound to continuum type.

The depths of the shallowest and deepest traps have been estimated (14), indicating that there is a distribution of trap depths. Photoconductivity spectra of solvent mixtures of polar and non-polar solvents (23-26) indicate that as the non-polar component in the mixture decreases the traps become deeper and the extent of bound to bound transitions increase.

1.1.3.3 Models

The simplest model of the solvated electron consists of a spherical square-well potential (27). This is called the cavity model. The electron is localized in a physical cavity, with the positive ends of the dipoles aligned around it.

This model (28) considers the effect of medium polarization produced by the electron. The solvent is viewed as a dielectric continuum. This is called the continuum model.

Semi-continuum models (29,30) assume the electron to be at the center of a spherical cavity surrounded by a solvation shell of a fixed number of solvent molecules. The solvent beyond the solvation shell is regarded as a dielectric continuum.

The calculations done according to these models are successful in predicting the E_{Amax} value. But the line shape is more narrow and symmetrical than observed. A statistical mechanical model that considers the molecular properties of the solvent is being developed (31,32).

1.3.4 Geometrical Structure

The geometry of the solvated electron has been estimated for electrons in aqueous glasses(6). These indicate that the electron is solvated in the middle of an octahedran of 6 water molecules. The -OH bond points towards the electron. The theoretical models for the solvated electrons do not predict the -OH bond orientation geometry. Instead they predict orientation of the dipoles in the water molecules. In contrast to this, ESR spectrum in methanol indicates a tetrahedral structure, also with -OH bonds pointing towards the solvated electron (6). A planar geometry is suggested for the electron in methyltetrahydrofuran (6).

1.2 Optical and Kinetic Properties of Solvated Electrons in Alcohol/Water Mixtures

1.2.1 Physical Properties

1.2.1.1 Pure Solvents

The optical absorption energies of electrons in water and alcohol are greater than those in other polar solvents such as ammonia and amines (20,33). This indicates that in solvents with a hydroxyl group there are stronger electron-solvent interactions, leading to deeper electron traps. Thus the E_{Amax} value in a solvent depends on the functional group of the solvent molecule, because it reflects the polarity of the solvent. Even though the dielectric constant and the dipole moment are used as measures of the polarity of a liquid, values of E_{Amax} are better correlated with Kirkwood structure factors g_k (34). The g_k values reflect the amount of short-range order in the liquid. The correlation of E_{Amax} with g_k indicates that the details of the liquid structure dominate the determination of the energy levels of solvated electrons (33,35).

The E_{Amax} value of solvated electrons in alcohols are in the order: primary > secondary > tertiary (36,37). Electrons are solvated in shallower traps in tertiary alcohols. The degree of orderliness is least in the tertiary alcohols.

In the primary alcohols, the E_{Amax} values are almost independent of the chain length (for alcohols above ethanol) (38). It is probably independent of the type of the alkyl chain too(e.g. 1-butanol and *iso*-butanol) (36). The electron solvation depends only on the alkyl substitution of the α-carbon atom.

The similarity of E_{Amax} values of solvated electrons in primary alcohols indicates that the configuration of -OH groups in the solvation shells of the electrons are of the same type. The alkyl group has almost no effect on the interaction between the electron and the -OH groups (38,39). Most models of solvated electrons consider the interaction between the electron and the molecular dipoles (15-19). But the ESR spectra indicate that the geometry of the solvated electron in methanol is such that there are four methanol molecules in the corners of a tetrahedral structure, with the -OH dipoles pointing towards the central electron (6). This confirms that the energy levels of the potential well of the electron depends only on the -OH groups of the alcohol. Therefore respectively lower values of E_{Amax} in secondary and tertiary alcohols are probably due to the lower number of aligned dipoles in the solvation shell, that are limited because of : (a) steric hindrance by the alkyl group; (b) the need for greater disruption of the liquid structure.

Although the values of E_{Amax} are related to the short range order in the liquid structure, the widths of the absorption bands are not. In alcohols, the width of the absorption band at half height, $W_{\frac{1}{2}}$, are about twice as wide in water. The $W_{\frac{1}{2}}$ values in amines are also about twice as that in ammonia. Alkylation increases the bandwidth. This implies that the absorption band arises due to a distribution of trap depths (40). But as discussed in the previous section, the positive temperature coefficients of $W_{\frac{1}{2}}$ expected for such a system does not always occur. Actually in some alcohols such as 2-propanol and *t*-butanol it is negative (36). An alternative view is that the absorption band is due entirely to bound to continuum transitions (41,42). This argument is invalid since the photoconductivity threshold is greater than the optical absorption threshold in several solvents, which indicate the existence of bound to bound transitions (21).

In pure alcohols most of the absorption band of the solvated electron is due to the bound to continuum transition (22). Extent of the bound to bound transition may change with the type of the solvent.

The threshold energy for the bound to continuum transition, E_{th} , is a measure of the trap depth of the solvated electron (trap depth in this instance is the energy difference between the ground energy level and the bottom of the conduction band). In primary alcohols E_{th} is the same regardless of the alkyl chain length (26,43). This is in accordance with the view that only the -OH groups in the alcohols determine the extent of interaction between the solvated electron and the solvent alcohol molecules. Since the E_{Amax} and E_{th} values in primary alcohols are similar, the number of bound levels and the trap-depth in all primary alcohols are also probably similar.

1.2.1.2 Mixed Solvents

Spectral parameters of solvated electrons in alcohol-water mixtures display strong composition dependence. Based on the composition dependence trend, the alcohol-water mixtures are categorized into three groups of alcohols (36,37):

(1) methanol, (2) other primary alcohols, (3) secondary and tertiary alcohols. The E_{Amax} values of primary alcohols are quite close to that of water, while in secondary and tertiary alcohols they are lower.

The composition dependence of the E_{Amax} values falls into four composition zones:

(a) $0 \leq x_{H_2O} < 0.1$; E_{Amax} decreases sharply with increasing x_{H_2O} in group (2), decrease less sharply in (1), and increases sharply in group (c),

(b) $0.1 < x_{H_2O} \leq 0.5$; gradual increase of E_{Amax} ,

(c) $0.5 < x_{H_2O} < 0.98$; almost no change in E_{Amax} values,

(d) $0.98 < x_{H_2O} \leq 1.00$; slight decrease in E_{Amax} with composition,

where x_{H_2O} is the mol fraction of water in alcohol. The same four zones are also observed in the phase diagram of tertiary butanol-water mixtures (44,45).

The minimum of E_{Amax} values in primary alcohol/water mixtures is attributed to a water nucleated solvent structure at that composition. The similarities of trends in zones (b), (c) and (d) among alcohol/water mixtures indicate that the liquid structure in these change in the same way. The near constant values in zone(c) are probably due to selective solvation of the electron in the same environment. This indicate the existence of clusters of pure water, alcohol or alcohol-water complexes.

The E_{Amax} values of the electron solvated in mixtures of amides/water (46) also display composition dependence. The E_{Amax} values in pure amides are lower than that of water. The composition dependence of E_{Amax} is similar to that in aqueous mixtures of secondary or tertiary alcohols, except in zone(d). The zone(c) in these mixtures also display selective solvation of the electron by water. The composition range of zone(c) in amide/water mixtures is shorter than that in alcohol/water mixtures. The reason may be the large size of the amide molecule.

Similar behaviour is observed in several other systems (47-50). In the spectra of electrons in alcohol/ammonia mixtures selective solvation in the middle composition regions indicate the existence of clusters of molecular complexes (49,50). If there are clusters of a certain type of molecules in a mixture, it indicates micro-heterogeneity. Micro-phase separations have occurd. This kind of microscopic structure changes are not evident in physical properties of these polar solvent systems (see 1.3). Hence optical absorption is valuable to understand the microscopic structure changes.

1.2.2 Kinetic Properties

In addition to the optical properties another way to gain an understanding of the solvated electron is through its reactivities with different types of solutes. These reactivities depend on the solute, the solvent and the thermodynamic conditions. The solvent composition effects of alcohol/water mixtures and temperature effects on the reactivity of the solvated electron with different solutes are discussed below.

1.2.2.1 Composition Effects

The microscopic structure of the solvent that surround the electron and the scavenger (solute) affects the solvation energies of the reactants (in the present case solvated electron and the scavenger), the transition state and the products. It also affects the transport of the reactants. Therefore the kinetics of the solvated electron reactions reflect the structural changes in the solvent system.

The rate of reaction of the solvated electron in a specific solvent at constant temperature and pressure depends on the type of the scavenger. For electron scavenging reactions to occur the scavenger should have positive electron affinity. The reactivity is a function of the electron affinity of the scavenger (51).

Reactions with high electron affinity scavengers such as nitrobenzene are nearly diffusion controlled in water (52,53).

1.2.2.1(a) Diffusion Controlled Reactions

When the rate of the reaction is controlled by the diffusion rate of the reactants, it is called a diffusion controlled reaction. A theoretical model for such reactions is provided by the Smoluchowski equation (54),

$$k = 4\pi N(D_A + D_B)R_{eff} \tag{1}$$

where D is the diffusion coefficient of the reactant, R_{eff} is the reaction distance (reaction radius for the encounter pair) and N is the Avogadro's number. The diffusion coefficients reflect changes in the solvent viscosity and the dielectric relaxation time. The reaction radius reflects changes in the dielectric constant. The value of R_{eff} for neutral reactants is given by the sum of the effective molecular radii. For the electron reactions, one of the reactants is charged, and the reaction radius depends on the type of the solute:

(a) if the scavenger is polar, the interaction is ion-dipole;

(b) if it is nonpolar and polarizable, then the interaction is ion-induced dipole.

In both cases the interaction between the solvated electron and the scavenger depends on the microscopic dielectric constant of the solvent. This is different from the bulk dielectric constant of the polar solvents, because the charge of the electron tends to align the solvent dipoles that lie between the electron and the scavenger.

When a potential energy difference exists between the reactants the above equation extends to the Debye-Smoluchowski equation(55):

$$k = 4\pi N(D_A + D_B)R_{eff}\frac{Q}{e^Q - 1} \tag{2}$$

where Q is a function that is related to the probability of interaction depending on the type of the potential energy difference between the reactants. For coulombic type electron-ion interactions,

$$Q = \frac{Ze^2}{4\pi\epsilon_0\epsilon R_{eff}k_BT} \tag{3}$$

where Z is the charge in the scavenger, ϵ_0 the permittivity in the vacuum, ϵ the relative permittivity of the solvent, T the temperature and k_B the Boltzmann constant.

There are numerous extensions to the Smoluchowski equation (56), but in addition to the generalization by Debye to include interaction potentials, the only other form of interest here is the concentration dependence (57) of the rate constant.

The original Smoluchowski relation is derived for dilute concentrations of the reactants. When one of the species (such as the scavenger) is of much higher concentration, the rate constant reduces to,

$$k = 4\pi DR_{eff}[1 + (4\pi R_{eff}^3C)^{\frac{1}{2}}] \tag{4}$$

where C is the concentration of the reactant that is in excess.

Application of the Smoluchowski equation to electron scavenging reactions to calculate the theoretical rate constant is possible only if the diffusion coefficients and the reaction radius are known. It is usually applied to estimate the diffusion coefficients of the solvated electron, using an approximate value for R_{eff} (58-61). If the diffusion coefficients are known this relation is applied to obtain values of R_{eff} (62,63). Based on such comparisons a tunneling machanism for electron scavenging was proposed (62).

1.2.2.1(b) Diffusion Coefficient

The greatest problem in the application of the Smoluchowski relation to diffusion controlled reactions of solvated electrons arises in choosing a value or an expression for the diffusion coefficient of solvated electrons.

Substitution of the Stokes relation,

$$\zeta = 6\pi\eta r \tag{5}$$

where ζ is the friction coefficient, η the solvent viscosity and r the diffusion radius, to the Einstein relation,

$$D = \frac{kT}{\zeta} \tag{6}$$

gives a diffusion coefficient that depends on the solvent vicosity η (64).

The nearly diffusion controlled rate constants of solvated electron in pure alcohols or mixtures of alcohol and water relate to the solvent viscosity by the empirical relationship (52,53,65,66),

$$k \propto \eta^{-x} \qquad where\ x < 1 \tag{7}$$

The value of x varies from 0.45 for the reaction of solvated electron with phenanthrene (65,66) to 0.6 for that with nitrobenzene (53). This empirical relation indicates that the diffusion coefficient of the solvated electron in alcohols or alcohol/water mixtures does not vary inversely with only bulk viscosity. It is also not applicable to every solute (66) in pure solvents.

Application of Stokes-Smoluchowski relation to water/alcohol mixtures (67,68) have enabled recognition of four solvent composition zones, that are similar to the ones seen in optical absorption energies of the solvated electron and in the freezing point curves. Only one zone (zone(c)) obeys the relation. In this zone the rate constant is inversely proportional to the solvent viscosity. Selective solvation of the solvated electron also occurs in the same zone (optical absorption energy is approximately constant). This probably means that the diffusion radius of the solvated electron is constant throughout zone(c).

The Stokes-Einstein relation was first derived for the movement of a hard-sphere through a continuum medium. It works quite well for small molecules moving in solvents with slightly smaller molecules (69). Even though the application of this relation to solvated electron is uncertain it helps us to formulate a picture of electron diffusion.

This relation was derived also for neutral species. When the species is charged the effect of the solvent is twofold: the viscous friction and the dielectric friction. Thus when the Stokes-Einstein relation is applied to a charged species, the effect due to the charge is reflected in the diffusion radius.

Modification of the above relation so that it could be applied to a charged species diffusing in a polar medium has been done by several researchers (70). The best results for polar solvents are obtained by the Hubbard-Onsager theory (71-73). In this theory, in addition to the viscous friction, the friction due to relaxation of the solvent dipoles around the moving ion is also considered. These two types of friction, electrodynamic and hydrodynamic, are coupled together to calculate the solvent effect. The Hubbard-Onsager theory gives an effective diffusion radius that depends on viscosity, dielectric constant and dielectric relaxation time of the solvent. It is possible to use this radius to evaluate the friction coefficient. Substitution of it in the Einstein relation (equation(7)) gives a diffusion coefficient that depends more on solvent properties than that obtained using the Stokes radius.

1.2.2.1(c) Slow Reactions

Scavengers with low electron affinities react with the solvated electron at rates reduced from the diffusion controlled rate. Rates of solvated electron with these inefficient scavengers depend on the solvation energies of the electron rather than on the solvent viscosity (53, 68, 74-76).

A measure of the solvation energy is provided by the optical absorption energy, which is an indication of the trap-depth of the solvated electron. When the electron affinity of the scavenger is small, it is more difficult for an electron to jump from a deeper trap than from a shallower trap. Electrons in shallower traps have a greater probability of reactivity.

The threshold energy, E_{th} indicates the depth of the shallowest traps. In the absence of E_{th} values, the energy at half-height on the red (low energy) side of the absorption band, E_r , is chosen as a measure of the shallower trap depths.

$$E_r = E_{Amax} - W_r \tag{8}$$

where W_r is the portion of width at half-height that is on the red side of E_{Amax} .

The slow reactions also involves the solvation energies of the participating ions in the following two reactions by which the electron reacts:

$$e_s^- + S \longrightarrow S^- \tag{10}$$

$$S^- + ROH \longrightarrow RO_s^- + SH \tag{11}$$

When the efficiency of the scavenger is low the rate costant of electron capture depends on the relative solvation energies.

1.2.2.2 Temperature Effects

Many chemical reactions follow the Arrhenius relation:

$$k = Ae^{-E_a/RT} \tag{12}$$

where A is the frequency factor and E_a the energy of activation for the reaction of the solvated electron with the scavenger. Information about the energies of activation are helpful to achieve a better understanding of the reaction mechanism.

The energies of activation are not necessarily the energies required for diffusion (74, 75). But in alcohol/water mixtures they follow the trend of the activation energies for the viscous flow.

Since the reaction of solvated electrons with inefficient scavengers involves the solvation energies of the participants in reactions (10) and (11), the energies of activation for these should depend on the energies of activation for dielectric relaxation more than on that of diffusion.

1.3 Structure of Alcohol/Water Mixtures

An alcohol contains a hydrophilic -OH group and a hydrophobic alkyl group. This bifunctional nature of the alcohol molecule gives rise to strong composition-dependent physical properties in alcohol-water mixtures. The amount of hydrogen bonding between the alcohol -OH group and water depends on the size of the hydrophobic group and the number of hydrophilic groups in the alcohol. Monoalcohols with small hydrophobic (alkyl) groups are completely soluble in water. As the hydrophobic group becomes larger the solubility decreases (77). Among n-alkanols, alcohols up to 1-propanol are completely miscible with water. Of the alcohols with the same number of carbon atoms, the one with the most compact alkyl group has increased miscibility. An example can be given in the butanol series. Miscibility increases in butanols as the alkyl group becomes more compact, tertiary butanol being completely miscible. If the alcohol has another hydrophilic -OH group, such as glycol, miscibility with water is even more increased (78). Only the structure of mono alcohol/water mixtures is discussed in the present study.

1.3.1 Water

The earliest model of the structure of water was based on the radial distribution functions (79) which had a pattern similar to that of a "broken down" ice structure (80). In ice, each water molecule is hydrogen-bonded tetrahedrally to four other molecules. The distribution functions of water (81) indicate slightly more than four nearest neighbours. At higher temperatures it becomes closer to five indicating a more random order. This is not consistent with the idea that all molecules in water are centrally hydrogen bonded to other molecules.

Since this early model, numerous models have been proposed for the structure of water. These models fall into two broad categories: (a) uniformist models; (b) mixture models.

(a) Uniformist Models (82-85): These models assume water to consist of a single type three-dimensional random hydrogen bond network. There are no significant amounts of monomer water (molecules without hydrogen bonds). Water is treated as a simple chemical equilibrium between free and bonded -OH groups. The structure is visualized as a network of cavities (voluminous) and the structural order as only short range with the local structure being approximately tetrahedral.

(b) Mixture Models (86-89): These assume water to consist of a mixture of two or more species. There are water molecules with no hydrogen bonds (monomers), or with up to four hydrogen bonds. The hydrogen bonded water molecules form an open network full of cavities or clusters of water molecules. These exist in equilibrium with monomer water which forms a dense medium. Cluster concentration or size changes with temperature.

None of these models are able to explain all properties of water. Because of the uncertainty of the structure of water, experimental results are usually explained in terms of one model or the other. Computer simulations of water are being done in order to develop a better model for water (90, 91).

1.3.2 Alcohols

In contrast to water, the structures of alcohols are simpler because there is only one hydroxyl group per molecule. Alcohols have the ability to form up to three hydrogen-bonds while water can form four hydrogen-bonds. But various spectroscopic studies have shown the presence of monomers, dimers and molecular aggregates of polymers (92-94). At room temperature these are linear or ring polymers, indicating that mostly two hydrogen bonds per alcohol molecules are formed. A higher monomer concentration exists in alcohols with larger alkyl chains (98).

Comparison of primary, secondary or tertiary lower alcohols (99, 100) (all completely miscible with water) show that: (a) these have similar monomer concentrations, except in tertiary butanol where it is slightly greater; (b) molecules are associated in linear chains; (c) about 5-10% of small alcohol molecules form a third hydrogen bond. Formation of a third hydrogen bond might lead to cross-linking of polymer chains.

The monomer concentration in tertiary butanol is slightly larger because the number of hydrogen-bonds are limited due to steric hindrance. Considering this steric hindrance the possibility of long chain formation in this alcohol is questionable. If polymer chains exist they probably are ring-like.

1.3.3 Alcohol/Water Mixtures

1.3.3.1 Static Properties

1.3.3.1(a) Static Dielectric Properties

Dielectric properties give information about the short-range order in a liquid. The Kirkwood structure factor, g_k, which is calculated from the dielectric constant and dipole moment is a measure of the short-range order (34). If $g_k > 1$, the molecular dipoles are oriented in series: the dipole moment in the liquid phase is greater than that measured in the gas phase. If $g_k < 1$, they are in anti-parallel orientation, and the liquid phase dipole moment is less than that in the gas-phase. Random orientation gives $g_k = 1$.

The g_k values in water and primary alcohols are greater than one (101, 102), indicating short-range order. In primary alcohols, the value of g_k increases with increasing chain length; the alcohols with longer chains are more aligned. Since the small alcohols have the ability to form a third hydrogen bond (99, 100), cross-linking of the polymer chains probably makes it difficult to align. This leads to lower g_k values.

Among alcohols with the same number of carbon atoms (102-104), tertiary alcohols have the lowest g_k values. This perhaps implies that chain formation ability is lower in tertiary alcohols. The g_k values in larger tertiary alcohols are slightly lower than one. These values are justified only if ring like polymers are assumed (103, 104).

When water is added to methanol or tertiary alcohols (102, 103), the structure factors increase slightly. Water hydrogen bonds with these alcohol molecules to order these into a better linear arrangement of dipoles. Water has a structure making effect.

The g_k values decrease when water is added to other alcohols, and go through a minimum in the mid-composition range (102). Water has a structure breaking effect on these alcohols.

1.3.3.1(b) Thermodynamic Properties

The thermodynamic functions of mixing alcohol and water were among the first properties employed to suggest a structure for alcohol/water mixtures. In the composition dependence of these properties of water and any alcohol, the extent of change depends on the size of the alkyl group (105-107).

In associated systems, negative heat of mixing implies hydrogen bond formation and a positive value implies hydrogen bond rupture. Dissolution of a small amount of alcohol in water is accompanied by loss of enthalpy (exothermicity) and loss of entropy. This occurs for the addition of a small amount of any non-electrolyte to water. This observation is interpreted according to one of the following: (a) the non-electrolyte molecule promotes water-water hydrogen bonding, in clusters that form small domains (108 -110); (b) water molecules order around the non-electrolyte and form oligomers similar to clathrates (111-113). In both cases the non-electrolyte molecules cluster together. This effect is called hydrophobic interaction and structure building of water is called ice-berg formation. Hydrophobic interaction is also evident in apparent molar volumes and heat capacities of alcohol-water mixtures.

The alcohol molecules thus promote the water structure. The composition at which the maximum strengthening occurs, depends on the size of the alkyl group of the alcohol. This composition is lower when the alkyl group of the alcohol is larger (107-111). Among alcohols with the same number of carbon atoms, the one with the most compact alkyl group stabilizes the water structure at the highest composition of alcohol (e.g. tertiary butanol among butanols).

Further addition of the alcohol into water does not break the clathrates or the stabilized water structure. Instead micro-phase separation of clathrates and alcohol clusters is assumed to occur. Clustering of alcohols in alcohol-water mixtures is also suggested in studies other than thermodynamic (114-116).

When water is added to small alcohols, some of these alcohol molecules make hydrogen bonds with water;heat of mixing is negative (exothermic) (105,106) and water acts as a structure maker. Heat of mixing of higher alcohols with water is positive (endothermic); water acts as a structure breaker.

1.3.3.2 Dynamic Properties

1.3.3.2(a) Viscosity

The dynamic structure of a system is much different from the steric structure and contains information about the motion of the molecules. Dynamics is important for the study of kinetics in liquids, because it involves movement of reaction species. Diffusion of a species in a liquid depends on its viscosity.

Viscosities of pure alcohols are either close to or higher than that of water at the same temperature. The viscosity is higher in alcohols with longer and more branched alkyl groups. Such alcohols flow less easily because of the bulkiness of the molecule.

Viscosities are strongly composition dependent in mixtures of alcohol and water. Composition dependency is characterized by (89, 117):

(a) a maximum in viscosity at compositions ranging from 0.65 to 0.75 mole fraction of water;

(b) a sharp increase in viscosity when a few mole percentage of alcohol is added to water;

(c) small changes in viscosity when a few mole percentage of water is added to alcohol.

The maximum in viscosity does not correspond to the stabilization of water structure that is associated with the hydrophobic effect. Instead, the maximum in the first derivative of the viscosity curve, $\frac{\Delta\eta}{\Delta x}$, occurs at this composition (118).

Addition of alcohol to water increases the viscous resistance to flow. This perhaps is due to the clathrate formation.

Water acts as a structure maker in small alcohols, increasing the viscosity. In larger alcohols, the addition of water is accompanied by a decrease in viscosity. One of the following is suggested to occur: (a) formation of water nucleated alcohol complexes (103, 106); (b) breakdown of alcohol structure by water (119).

1.3.3.2(b) Dielectric Relaxation

The dielectric properties of a liquid is used to obtain information about the reorientation of a solute (120). If the solute is neutral its reorientation depends on the viscosity, and if it is charged it also depends on the dielectric nature of the liquid.

The dielectric structure of a liquid is two fold. The dynamic differences, as expressed by dielectric relaxation times, are much greater than the static differences given by the Kirkwood structure factor (121) (discussed earlier).

Water has a single dielectric relaxation process, with a response time τ_d equal to 10^{-11} s at normal temperatures and pressures. In contrast several relaxation processes are observed in alcohols. These are interpreted as follows (122):

(a) τ_1 : the time required for the breaking of intermolecular hydrogen bonds and reorientation of the molecule;

(b) τ_2 :reorientation time of a free monomer;

(c) τ_3 :reorientation time of free -OH dipoles.

The process that relates to the liquid structure is given by τ_1. This is called the primary relaxation process. The reorientation of large alcohol molecules depends on the steric hindrance of the alkyl group and the hydrogen-bonds (123). Reorientation of these molecules needs the cooperation of the other molecules. Small alcohol molecules display relatively small steric effects, hence reorientation depends mostly on hydrogen bond breaking; relaxation times in these alcohols are lower.

When a small amount of water is added to an alcohol at room temperature, the dielectric relaxation time varies as follows: (a) in a small alcohol such as methanol, it increases slightly (120); (b) in other lower alcohols it decrease (124, 125).

Water has a structure breaking effect on alcohols. Thermal agitation of the molecules increase with increasing temperature. Dielectric relaxation times decrease and viscous flow become easier.

1.3.3.2(c) Rotational Relaxation

Rotational relaxation time, τ_{rot} of a large solute (dye molecules) in a liquid depends on the solvent properties of the medium molecules. In a polar medium τ_{rot} is a function of the solvent viscosity and the dielectric relaxation time.

Values of τ_{rot} for dye molecules in pure alcohols are directly proportional to the solvent viscosity (126 -129) and dielectric relaxation time, τ_d . But solvents with the same viscosity or τ_d values do not lead to the same rotational relaxation times (128) of the solute molecule. The direct correlation exists because all these properties are interrelated by another variable, liquid structure.

In alcohol/water mixtures (130), τ_{rot} of the dye molecule is not linearly correlated to either viscosity or dielectric relaxation time of the solvent. This is probably due to vast differences among alcohol/water structures at various compositions, whereas among pure alcohols the structures are similar. Based on the rotational relaxation times in alcohol/water mixtures, selective solvation of ions by water or alcohols is suggested (131).

Summary

The structure of water is a three dimensional hydrogen bonded network, while that of alcohols tends to be linear or ring like polymers.

Addition of a small amount of alcohol to water corresponds to a strengthening of the water structure and probably involves clathrate formation; an increase in viscosity, loss of enthalpy (change on mixing) and loss of entropy confirm this view. Further addition causes micro-phase separation into clathrates and a random mixture of alcohol and water molecules.

When a small amount of water is added to a small alcohol like methanol, it probably hydrogen-bonds with the alcohol chains and acts as a structure promoter. This is consistent with an increase of the Kirkwood structure factor, loss of enthalpy (change) of mixing and a slight increase in the dielectric relaxation time. In larger alcohols, water tends to break hydrogen-bonds between alcohol molecules or promote formation of water centered alcohol aggregates; the Kirkwood structure factor decreases, the enthalpy change of mixing increases and the dielectric relaxation time decreases.

2 EXPERIMENTAL

2.1 Materials

iso-butanol and *t*-butanol were obtained from British Drug House (BDH) and 2-butanol from Aldrich Chemical Company. These alcohols were dried for three weeks with Davison 3A Molecular Sieves and then treated for 1 day under argon (99.999%, Ultra High Purity Grade, Liquid Carbonic Ltd.) with sodium borohydride (1 g/l) at 323K. The alcohol was then fractionally distilled under argon, through a 80 x 2.3 cm column packed with 0.3 cm glass helices, discarding the first 15% and last 35%. The middle 50% was collected and kept in an argon-pressurized syphon system. The water content measured by Karl-Fischer titration was 0.04 ± 0.01 mol%. The solvated electron half-life after a 100ns pulse of 1.9 MeV electrons (2×10^{16} eV/g) at 298K was 20 μs for *iso*-butanol , 25 μs for 2-butanol and 15 μs for *t*-butanol .

Nitrobenzene (Fisher Scientific) and acetone (Terochem) were purified by simple distillation. Toluene (BDH) was distilled over potassium metal. In each case the middle fraction was collected and stored under argon in a syphon system. Phenol (Aldrich),silver perchlorate (General Intermediates),copper sulphate (Fisher Scientific), copper perchlorate (Aldrich), lithium nitrate, potassium nitrate (BDH), and potassium chromate (Aldrich) were used as received.

Water from two sources was used. Laboratory distilled water supply was used as the starter in both cases. In one method this water was distilled from, (a) acidic dichromate, (b) alkaline permanganate, and (c) without additive. The final collection flask was protected from laboratory atmosphere by a U-tube and a bubbler containing distilled water. In the other method distilled water was passed through a Barnstead Nanopure 2 Ion Exchange system.The solvated electron half-life after a 100 ns pulse of radiation was 20μs.

The alkanes, n-heptane (Aldrich HPLC 99.9%) and n-pentane, (99.93 mol%), n-hexane (99.99 mol%), methylcyclohexane (99.86 mol%), and n-octane (99.88 mol%, Phillips Petroleum Research Grade) were purified as follows: (a) stirred with conc. sulphuric acid for one day to remove alkenes; (b) decanted and swirled for 10 min with Davison 5A Molecular Sieves; and (c) bubbled with argon.

2.2 Apparatus

2.2.1 Sample Cells

Cells of Suprasil Quartz from Terochem Laboratories were used at atmospheric pressure for temperatures varying from -50C to 115C. The inside dimensions of the cell was 1 x 1 x 4.5 cm, and the optical path length 1 cm. The cell was topped by a graded seal so that it could be attached to a pyrex glass tube.

2.2.2 Bubbling System

Samples in quartz cells were bubbled with UHP argon and sealed before the experiment. The bubbling system (Fig. 2-1)

was made by connecting 1 ml syringes to a long pyrex tube. Pyrex/Teflon stopcocks (no. 72 Canadian Laboratory Supplies Ltd.) at the top of the syringes controlled the gas flow. Bubbling was done by long stainless needles (30cm long, and 0.625mm i.d.) fixed to the syringes. The rate of bubbling was $17cm^3/min$.

2.2.3 Irradiation Detection and Control System

2.2.3.1 The Van de Graaff Accelerator (VDGA)

The source of high energy electrons was a VDGA (type AK-60, 2 MeV) manufactured by High Voltage Engineering Coorporation. The maximum peak current delivered during a pulsed operation was 150 mA. Pulse widths of 3, 10, 30, 100 ns and 1.0 μs were available. Of these only 100 ns pulse width was used.

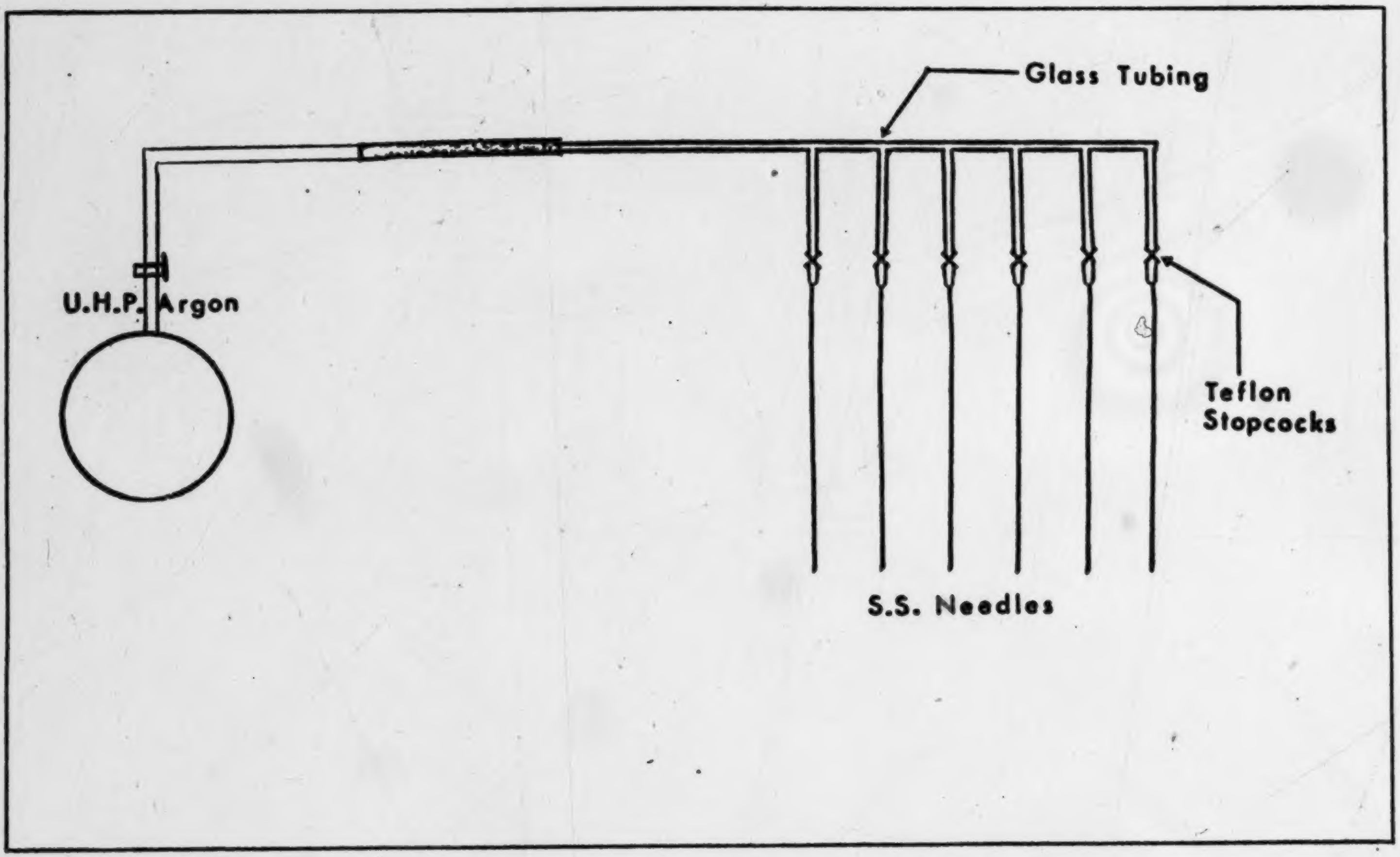
Glass Tubing
U.H.P. Argon
Teflon
Stopcocks
S.S. Needles

Fig. 2-1: The Bubbling System

The entrance from the control room to the accelerator and target room was shielded by a concrete maze. Closing and locking the iron-gate at the control room end of the maze sounded a warning buzzer for 15 s. Accelerator operation was possible only after cessation of the buzzer. Opening of the iron-gate resulted in immediate shutdown of the VDGA.

The method commonly used to monitor the steering and focussing of the electron beam was to fix a piece of phosphorescent paper to the end of the accelerator beam pipe. The paper could be viewed by a closed circuit television. Each pulse of electrons caused a visible glow where it struck the phosphor, enabling accurate steering and focussing by adjustment of the current in the electro-magnets. When equipment blocked visual observation, the beam could be steered by maximizing either the secondary emission monitor (SEM) dose or the absorption from a dummy sample.

2.2.3.2 The Secondary Emission Monitor

The relative dose for each electron pulse was indicated by the SEM. It consisted of three thin metal foils placed inside the accelerator beam pipe perpendicular to the path of the high energy electrons (Fig. 2-2).

It was positioned as near as possible to the beam pipe electron window, because of beam scattering at the foils.

Havar, a cobalt based high strength alloy was used for the foils. It was obtained in thin sheets (0.0025 mm) from the Hamilton Watch Company, Precision Metal Division. The low average atomic number (~27), of this material made it superior to gold (atomic number 79) because of less beam attenuation by electron scattering.

The 5 cm diameter foils were separated by 0.5 cm. The outer two were maintained at a potential difference of 50 V. Passage of an electron pulse generated

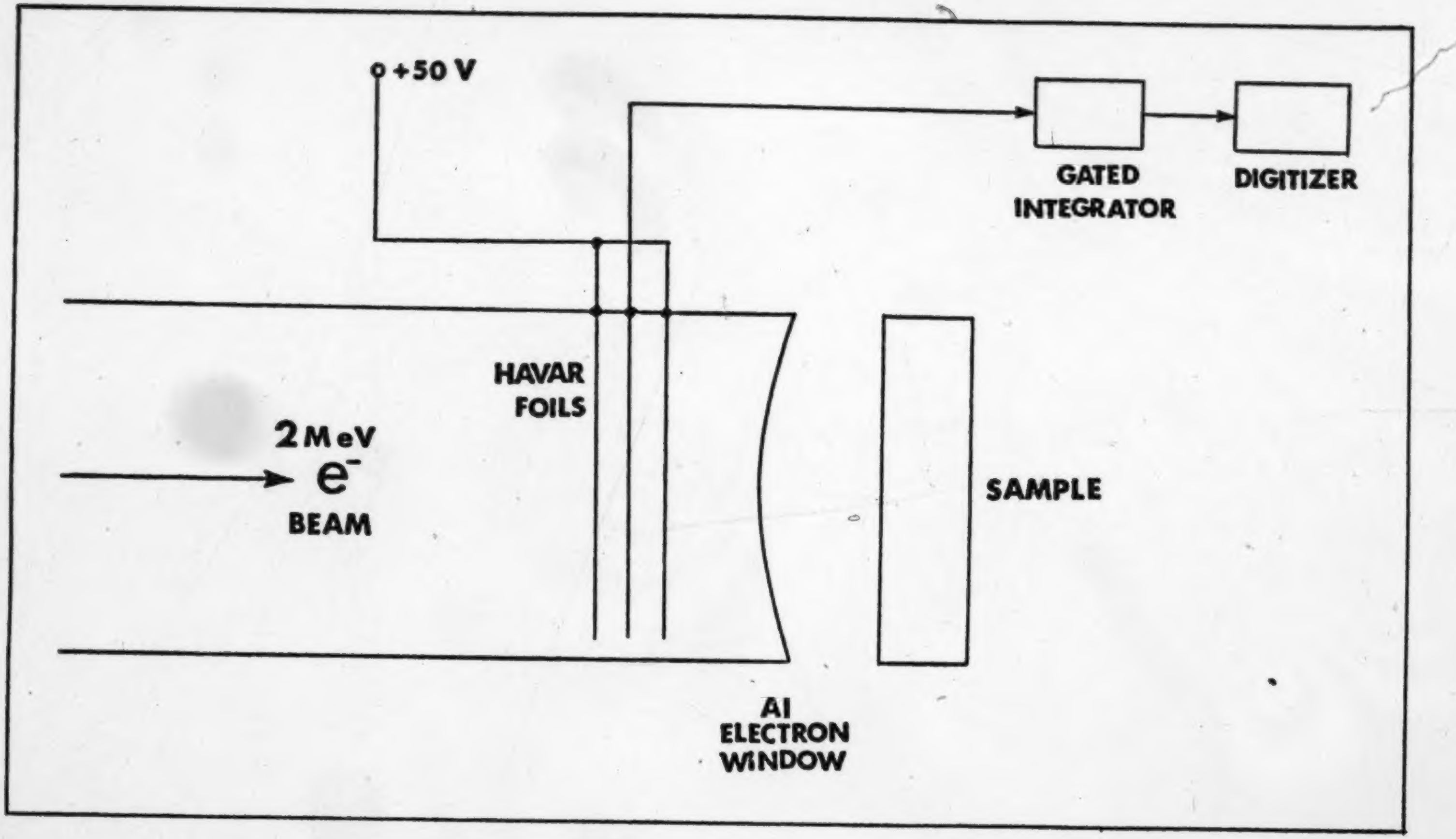
+50 V
GATED INTEGRATOR
DIGITIZER
HAVAR FOILS
2 MeV
e^-
BEAM
SAMPLE
Al ELECTRON WINDOW

Fig. 2-2: The Secondary Emission Monitor

secondary electrons at the foils. The electrons ejected from the center foil were collected by the outer foils, the net result being a current flow from the center foil. Current flow occured only during a high energy electron pulse and was measured and held by a gated integrator, digitized and displayed by a digital readout.

2.2.3.3 Optical Detection System

2.2.3.3(a) The Light Source

A schematic diagram of the path of the analyzing light is given in Fig. (2-3).

The source was a high pressure Xenon arc lamp (Optical Radiation Coorporation, model XLN 1000W) contained in a lamp housing (Photochemical Research Associates, model PRA ALH 220). A rhodium coated off axis parabaloid mirror (Melles Griot-02 POA 015) placed in the beam path absorbed the UV light with wavelength λ¡320 nm. This prevented ozone formation in the room. The lamp was run at 1000 W and pulsed to 9.75 kW for 500 μs when a decay signal was desired.

A light shutter protected the sample from unnecessary exposure by opening for only 55 ms. The above mentioned mirror was used to focus the light beam at the center of the irradiation cell. Front surface aluminumized mirrors coated with silicone monoxide were used to direct the light beam and to make it parallel. In this way, the light was transported from the irradiation room through a hole in the 1.2 m thick concrete wall. Total path length of the optical system was 12 m. Finally a concave mirror was used to focus the light into the monochromator housing.

2.2.3.3(b) Monochromator Grating and Filters

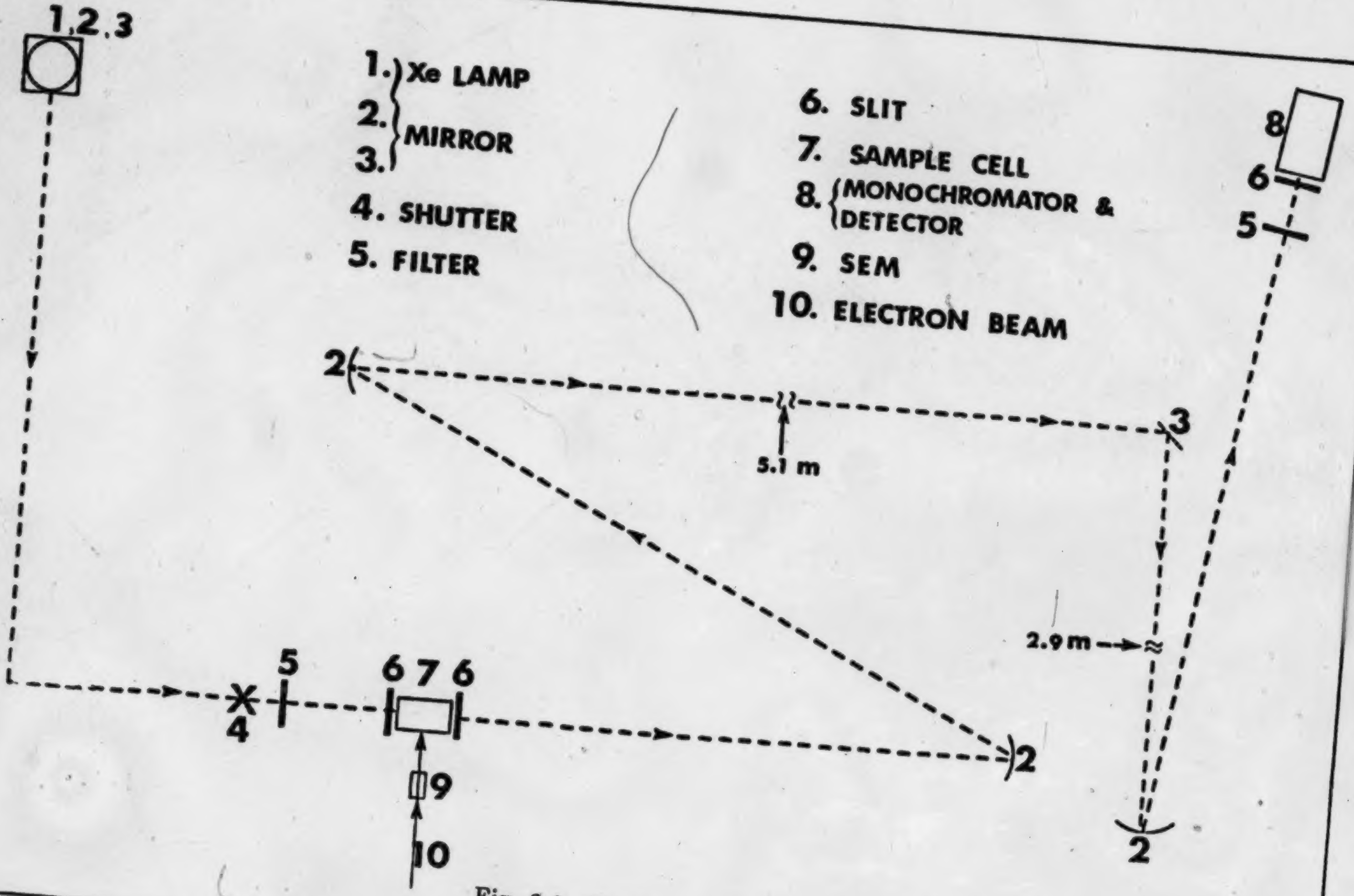
1,2,3
1. Xe LAMP
2. MIRROR
3. MIRROR
4. SHUTTER
5. FILTER
6. SLIT
7. SAMPLE CELL
8. MONOCHROMATOR & DETECTOR
9. SEM
10. ELECTRON BEAM
2
3
5.1 m
2.9 m
2
2
4
5
6 7 6
9
10
8
6
5

Fig. 2-3: The Path of the Analyzing Light

The monochromator was Bauch and Lomb type 33-86-25. The two gratings used were type 33-86-02 for light from 350nm to 800nm and 33-86-03 for light from 700nm to 1000nm. For all wave lengths used in these experiments filter CS-2-64 was used to minimize the second order effects of the light. The front and back slit widths of the monochromator were 2.5mm and 1.4mm.

2.2.3.3(c) Detectors and Amplifiers

The light that exited from the back monochromator slit fell on a silicon photodiode detector (EG and G Incorporated, model SGD-444-2) with a spectral range of 350-1050nm. The detector was connected to an amplifier (AD 50-J) with transresistance gain of 25kΩ for the continuous light and 2.5kΩ for the pulsed light. The overall rise and fall times for 3-97% response of the detector and amplifier was $1\mu s$ for the continuous and 100ns for the pulsed light, with 5MHz bandwidth in the 7A13 plugin of the Tektronix R7912 transient digitizer.

2.2.3.3(d) Digital Voltmeter (DVM) Oscilloscope and Plotter

Incident light was recorded as a voltage on a digital multimeter (Fluke 8810A), displayed on an oscilloscope (Tektronix R7623) and plotted on a digital plotter (Zeta 1200). The signals were displayed as plots of voltage against time. All the information related to the particular reading such as total light, dose, temperature, sensitivity, time scale and cell holder number were also printed.

2.2.3.4 The Temperature Control System

2.2.3.4(a) Cooling and Heating Systems

Temperatures from 223K to 298K were achieved by boiling liquid nitrogen and regulating the temperature of the nitrogen gas by using another heater. Liquid nitrogen was boiled at a controlled rate from a 50 L, narrow necked aluminum Dewar vessel (Lakeshore Cryotonics Inc.). A stainless steel pipe (5cm diameter) extended to the bottom of the Dewar. It was fixed to a lid which fit snuggly into the neck of the Dewar. A 600W nichrome heating coil was attached to inside of the steel pipe about 7cm from the bottom. When being used, only 190W was applied to this heating coil.

Cold nitrogen gas was transported to the sample box through one meter of Rubatex foam-rubber pipe. Both ends had glass inserts to which a leather seal was connected. Cold air that came from this pipe flowed through another stainless steel pipe (2.5cm diam.) that had a Nichrome heating wire (0.024cm diam. x 4m long) inserted inside it, before going to the cell box. This heating coil regulated the nitrogen gas that goes through it to the required temperature.

Temperatures from 296K to 390K were obtained using air from a laboratory heat gun fan (Master Appliance Coorporation, model AH 0751). The fan speed was powered from a normal 60 cycle outlet. Room temperature air travelled through a 0.5 m foam-rubber pipe to the same stainless steel pipe with the nichrome wire in it before going into the cell holder box. The nichrome wire heated the air to the required temperature.

2.2.3.4(b) Cell Holder Box

Eight cell holders were mounted on a circular (7cm diam.) aluminum base which had holes in it for the air to flow through. The base was fixed to a steel tube (1.9cm diam.) which was connected to a motor that allows it to make rotations clockwise or counterclockwise.

The whole system was fixed inside a box of height 40cm and 8cm i.d.. The box was insulated by foam glass (Pittsburg Corning Coorporation) 15mm thick. The cell holder made continuous rotations when the cells were not being pulsed. Just before a pulse was given a pre-selected cell stopped in front of the electron window. The electron window was doubly insulated by a 3mm thick styroform plug and a 0.02mm thick aluminized polyamide film.

The optical windows were evacuated quartz cylinders with Suprasil ends. The gas entered from one side of the box below the aluminum base and was allowed to circulate by the rotating cell holder before leaving through a 2.5mm diameter hole in the lid. A copper-constantan thermocouple was mounted in a cell filled with the measuring solvent. A temperature sensor (thin film platinum resistance element, 3mm x 10mm x 0.7mm) was fixed to one of the cell holders other than the one with the thermocouple cell and was used by the temperature controller (Taylor Microscan 1300). Another thermocouple was situated inside the electron window to monitor the temperature of the air beyond the styroform plug. The temperature of the system was monitored using the thermocouple in the cell.

The temperature was measured by a Fluke Digital Thermometer (model 2100A). Temperature equilibrium in the system was assumed to exist when the thermocouple inside the cell indicated the same temperature for a period of 15min. Once equilibrium is achieved, the temperature of the thermocouple cell varied only 0.10K.

2.2.4 Density and Viscosity Measurement

2.2.4.1 Dilatometer

A dilatometer consisting of two Pyrex pipettes sealed to a bulb of 10, 20 or 25 ml was used. The dilatometer was fitted with ground glass tops that could be sealed using steel springs. The volume scale was readable to 1 mm^3.

Before each experiment the dilatometer was cleaned using (a)soapy water, (b)hexane, (c)ethanol and (d)triply distilled water, in that order. The two arms were useful in the cleaning and the filling process. The masses of samples were obtained from the differences in mass between the filled and the empty dilatometer. These were weighed on a Stanton Unimatic analytical balance readable to 0.1 mg.

2.2.4.2 Viscometer

The viscometer used (Schott Gerate, type 24 501) was fitted with light pipes to ensure high precision readings (Fig. 2-4).

The optical path for each timing mark consisted of fibre optic light pipes (Dolan Jenner, type BA 636) fitted with a high intensity light emitting diode (International Devices, type ID 2000-UR) at one end and a detector (Motorola MRD 360) at the other end. The light pipe was cut in the middle and fitted with clamps to give a rectangular cross section light beam 3.9 mm wide and 0.5 mm high. The high temperature limit of 423K is due to the epoxy cladding on each individual glass fibre. The detectors were connected to a timing device that responds to any change in the light level that results from a combination of reflection, refraction and transmission as the falling meniscus passes a detector. The timing device could be read to 0.01 seconds.

2.2.4.3 Temperature Regulating System

Viscosity measurements at high temperatures were done in a 4 L glass Dewar vessel filled with light parafin oil (Fisher Scientific). The Dewar was equipped with a knife heater (53Ω, 350W) and a motor controlled stirrer (laboratory type). Bath temperature was manually regulated by 2 variacs (Standard Electrical Products) in series connected to a knife-heater (Cenco). The temperature was measured with a platinum resistance digital thermometer (Fluke, model 2189A) with resolution 0.01 K. Temperature variations in the bath were recorded in a Sargent model SR chart recorder, using a platinum resistance detector (Omega Engineering Inc., model TFD).

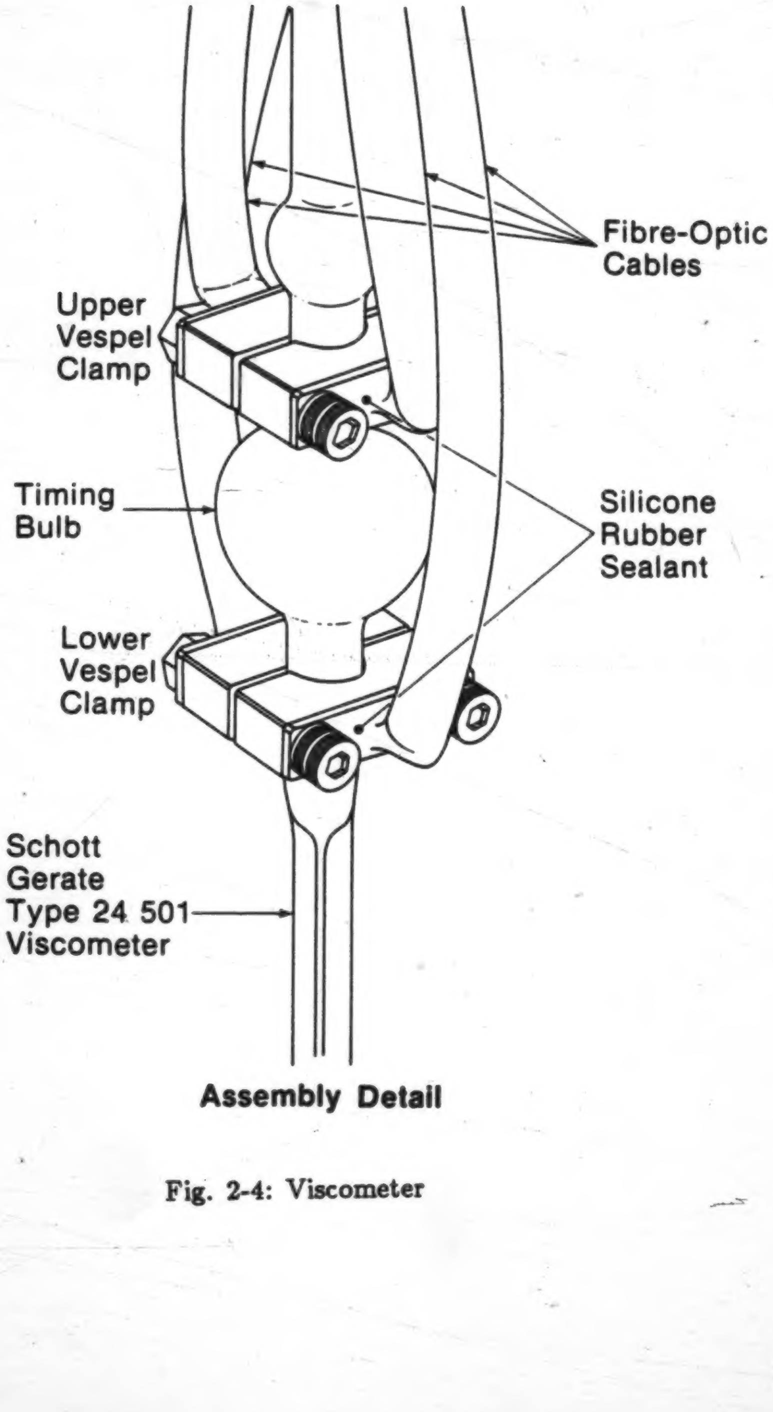
Fibre-Optic Cables
Upper Vespel Clamp
Timing Bulb
Silicone Rubber Sealant
Lower Vespel Clamp
Schott Gerate Type 24 501 Viscometer
Assembly Detail

Fig. 2-4: Viscometer

Viscosities at low temperature and densities were measured in a water bath. A 6L Dewar flask covered with; (a) aluminized polyamide film (Deposition Technology Inc., 10^{-3} inches thick); (b) foam sheet (Styrofoam) was used. A 6 inch wide opening along the length of the Dewar was used to observe the viscometer and the dilatometer. A knife-heater, a stirrer and a temperature sensor as described above were immersed in the water. In addition to these, a heat/cool module connected to a temperature regulating system and a refrigeration unit were immersed in the water (Fig. 2-5). Liquid Freon-12 flowing through a refrigerator unit (Tecumseh, model AE 1343 AA, 45W) was used as the coolant, while a temperature sensor (thin film platinum, Omega Inc.,) and a heater (thick film ceramic, Hittman Inc.,) regulated the temperature (Fig. 2-6).

The stability of the bath temperature measured using the Omega FTD detector was ±0.002K for >2h. The bath temperature during measurements was recorded to 0.01K with the Fluke digital thermometer. Before use the system was adjusted at ice-point to 273.15K. After the measurements were finished the ice-point check was repeated. The drift over measurement period was less than 0.01K.

2.3 Techniques

2.3.1 Sample Preparation

Quartz cells and other glassware were cleaned by performing the following sequence of operations. First the vessel was rinsed twice with ethanol. While the surface was still alcohol wetted, concentrated nitric acid was added. The resulting exothermic reaction caused the acid to boil vigorously. The acid was then removed by rinsing twice with dilute potassium hydroxide and distilled water. Finally the vessel was washed several times with triply distilled water. The glassware

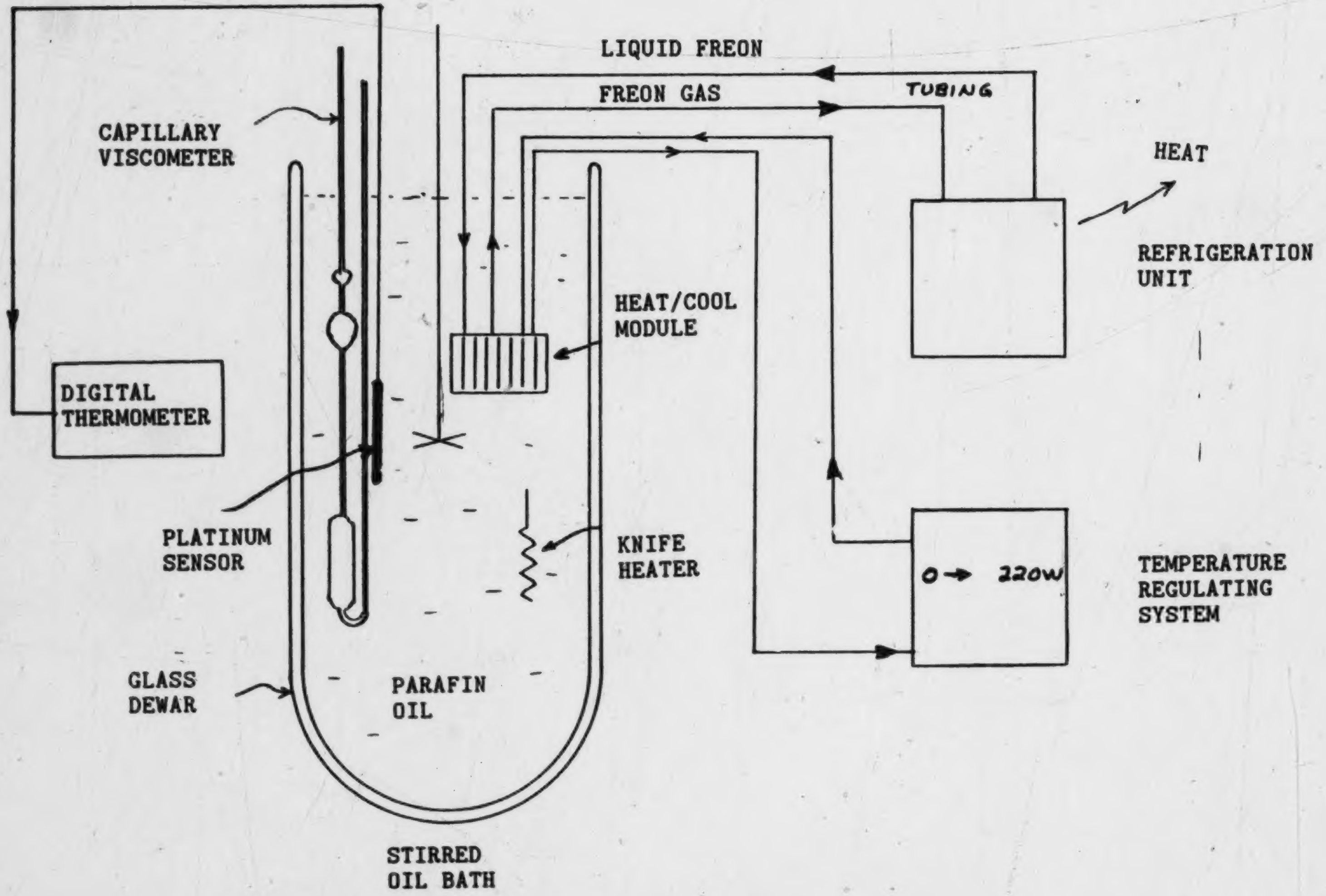
CAPILLARY VISCOMETER
LIQUID FREON
FREON GAS
TUBING
HEAT
REFRIGERATION UNIT
HEAT/COOL MODULE
DIGITAL THERMOMETER
PLATINUM SENSOR
KNIFE HEATER
0 → 220W
TEMPERATURE REGULATING SYSTEM
GLASS DEWAR
PARAFIN OIL
STIRRED OIL BATH

Fig 2-5: Temperature Measurement System for the Viscometer

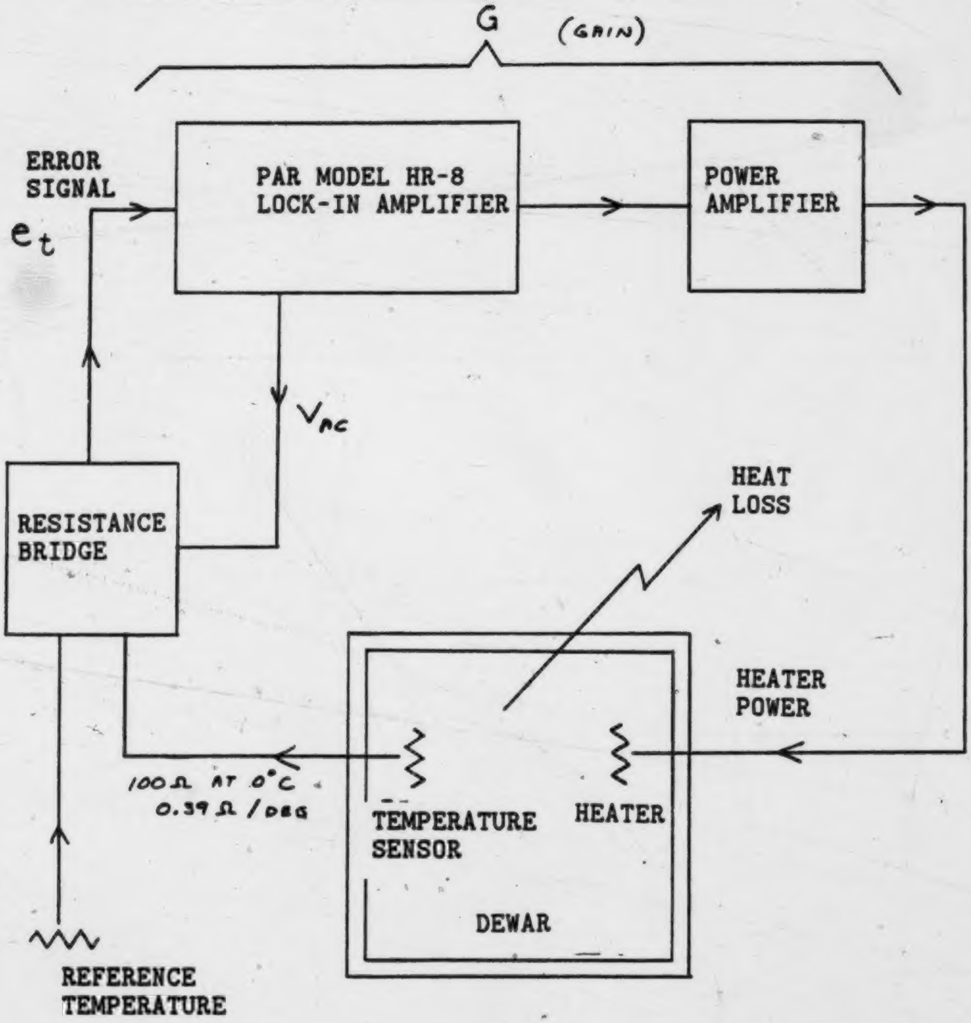
G (GAIN)
ERROR SIGNAL
e_t
PAR MODEL HR-8 LOCK-IN AMPLIFIER
POWER AMPLIFIER
V_{AC}
HEAT LOSS
RESISTANCE BRIDGE
HEATER POWER
100 Ω AT 0°C
0.39 Ω / DEG
TEMPERATURE SENSOR
HEATER
DEWAR
REFERENCE TEMPERATURE

1 mΩ : 2½ m°C

Fig 2-6: Temperature Regulating System

TEMPERATURE
REGULATOR
SYSTEM

and quartz cells were dried at 393K in an oven reserved for that purpose. Syringe needles were washed first with hexane, then with soap and hot water. They were finally rinsed many times with triply distilled water and oven dried. Before use they were rinsed several times with the solvent or the solution being used.

Alcohol/water mixtures were prepared in Pyrex volumetric flasks by volume measurement. Stock solutions of scavengers were prepared in 10ml volumetric flasks. Nitrobenzene, toluene and acetone were measured with microlitre syringes; phenol and all the inorganic scavengers were measured by weight using a Stanton Automatic Analytical Balance. The balance is readable to 0.1 mg with a precision of 0.1 mg determined by repeated weighings of a constant weight. Aliquots of the stock solutions were injected into the sample cells by microsyringes. The samples were bubbled with UHP argon at room temperature at a rate of $17cm^3/min$ for 30 minutes to de-aerate and sealed as illustrated in Fig.(2-7).

Step 1 took place at room temperature. The syringe needle was then withdrawn to just above the liquid as shown in step 2 and the argon flow rate was increased. The area around the sealing position was heated by a low flame to flush the volatile substances from the glass wall. The syringe needle was then further withdrawn as illutrated in step 3 and the seal made as rapidly as possible.

Bubbling the solution for 30 minutes as explained minimizes the dissolved gaseous impurities such as oxygen and carbon dioxide. When the solute evaporates easily (acetone and toluene, Fig. 2-8)

and when its solubility is quite low this proves to be a problem. Under these circumstances the solute was bubbled with argon and then injected into the solvent that had been bubbled for 30 minutes and the solution was again bubbled for 2 minutes and sealed. The effect of such impurities in the system on the efficient scavenger reactivities is quite small.

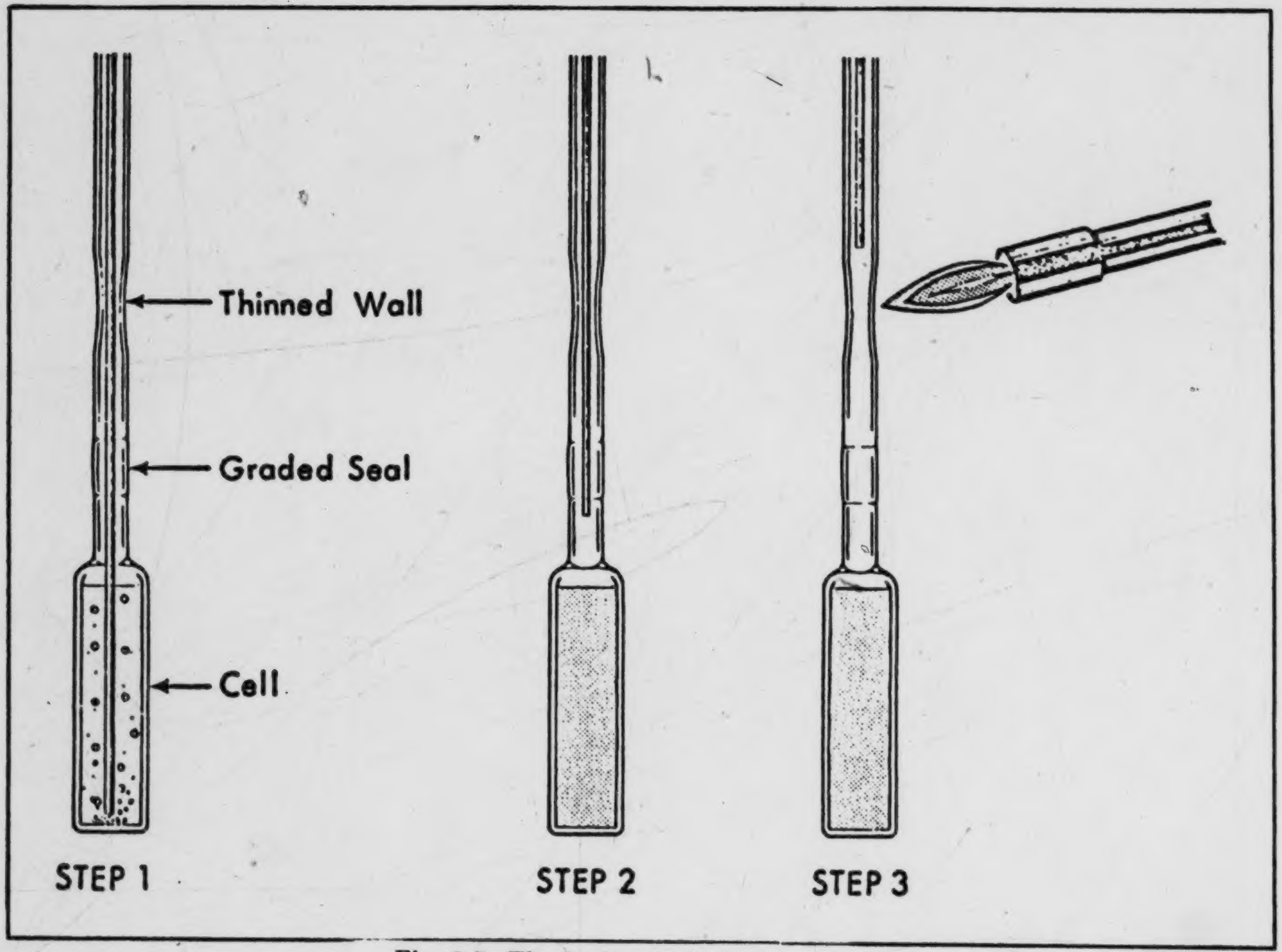
Thinned Wall
Graded Seal
Cell
STEP 1
STEP 2
STEP 3

Fig. 2-7: The Sealing Technique

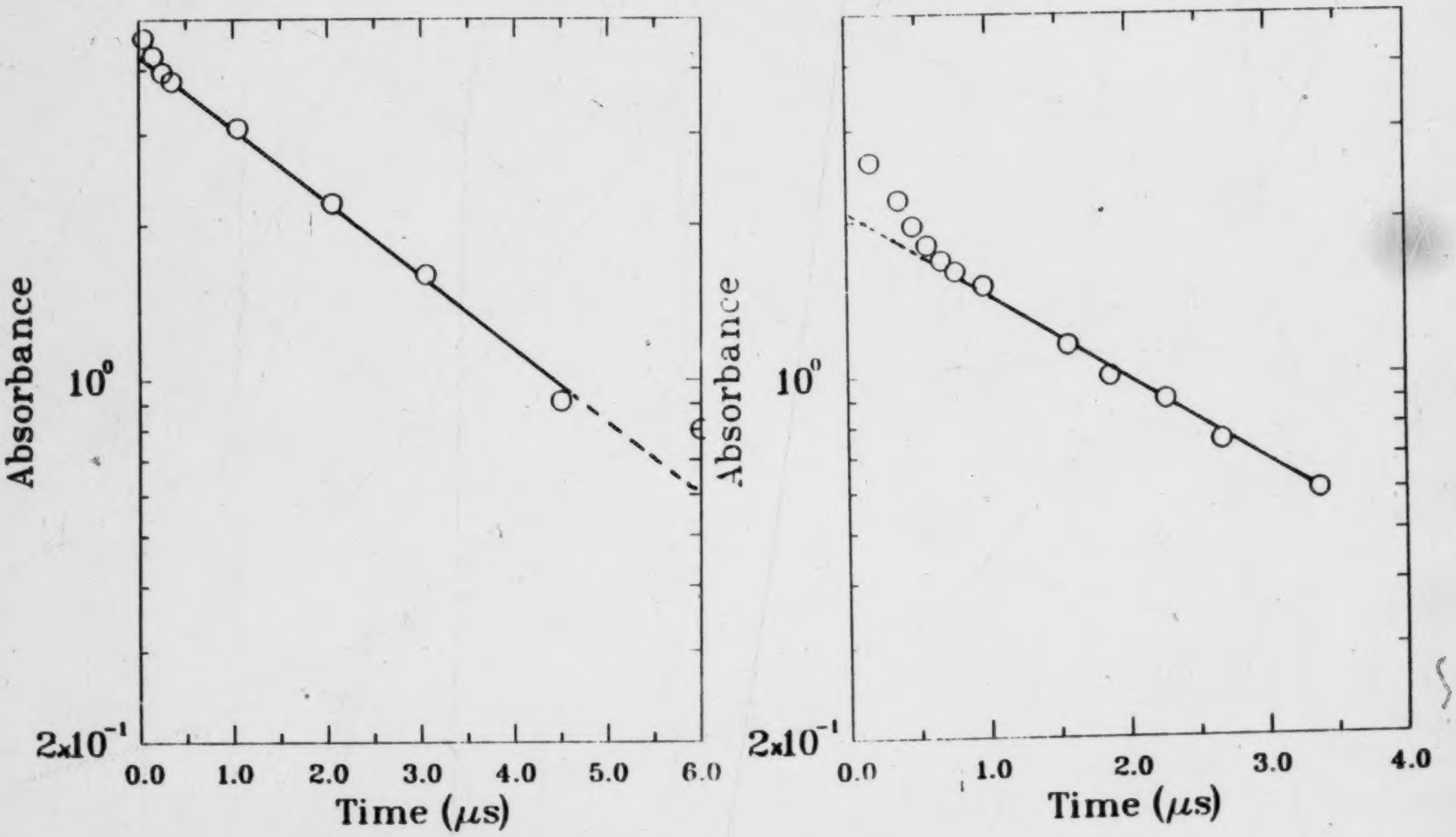

Fig. 2-10: The First Order Decay Plot of Solvated Electron

2.3.2 Concentration Measurement

The concentration of scavengers in the cells was measured by a UV spectrophotometer. Calibrations were done for each solvent. The wavelength of the absorption maximum and the molar absorbancy varied slightly with solvent composition.

The absorbance of the sample was measured, before bubbling, for solutions of nitrobenzene at 258nm and for solutions of toluene at 262nm. It was again measured after it was bubbled and sealed with the injected scavenger. Measurement of the low absorbancy acetone was done as follows: the purified solvent was bubbled for 30 min in the cell, and the absorption spectrum was measured from 276nm to 258nm. The required amount of acetone was injected into the solvent the solution was bubbled for 5 min and the cell was sealed as above. The absorption spectrum was measured and the difference taken at the wave length corresponding to the maximum wave length, λ_{max} (268nm).

Phenol samples had to be diluted before spectrophotometry. Therefore the concentrations were determined after irradiation. The samples were diluted 10 or 20 times with the solvent. The absorbance was measured using the same cell at 273nm.

2.3.3 Measurement from Decay Curves

The decay curve of the solvated electrons, e_s^- , displays an initial faster decay portion and a first order tail (Fig. 2-9, 2-10).

The fast decay is due to the reaction of e_s^- inside spurs (geminate reaction), whereas the first order decay is due to the reaction in the bulk solvent.

The electron in the bulk alcohol/water mixed solvents reacts with the alcohol according to equation 13,

$$e_s^- + ROH \longrightarrow RO_s^- + H \tag{13}$$

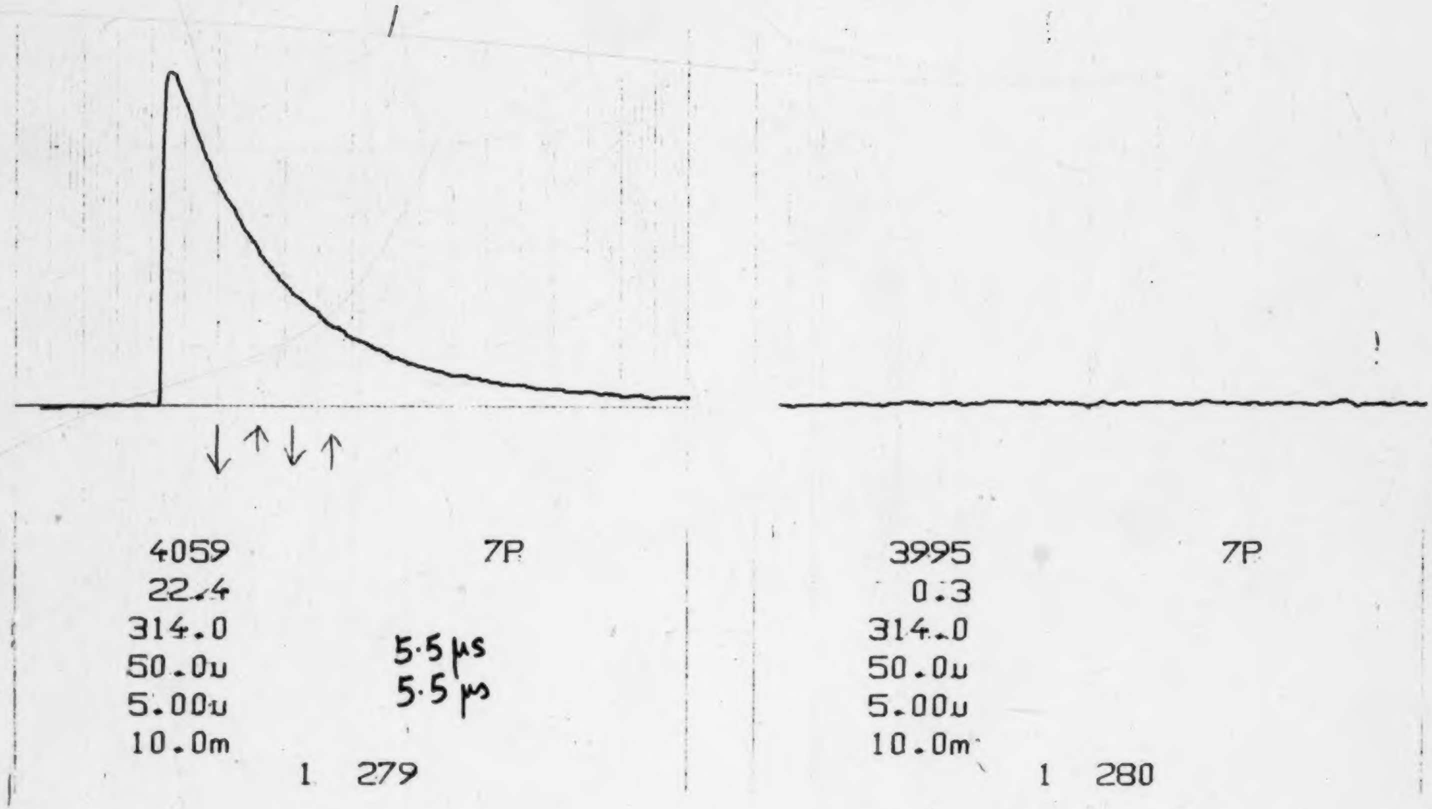

Fig. 2-9: A Typical Plot of Solvated Electron Decay

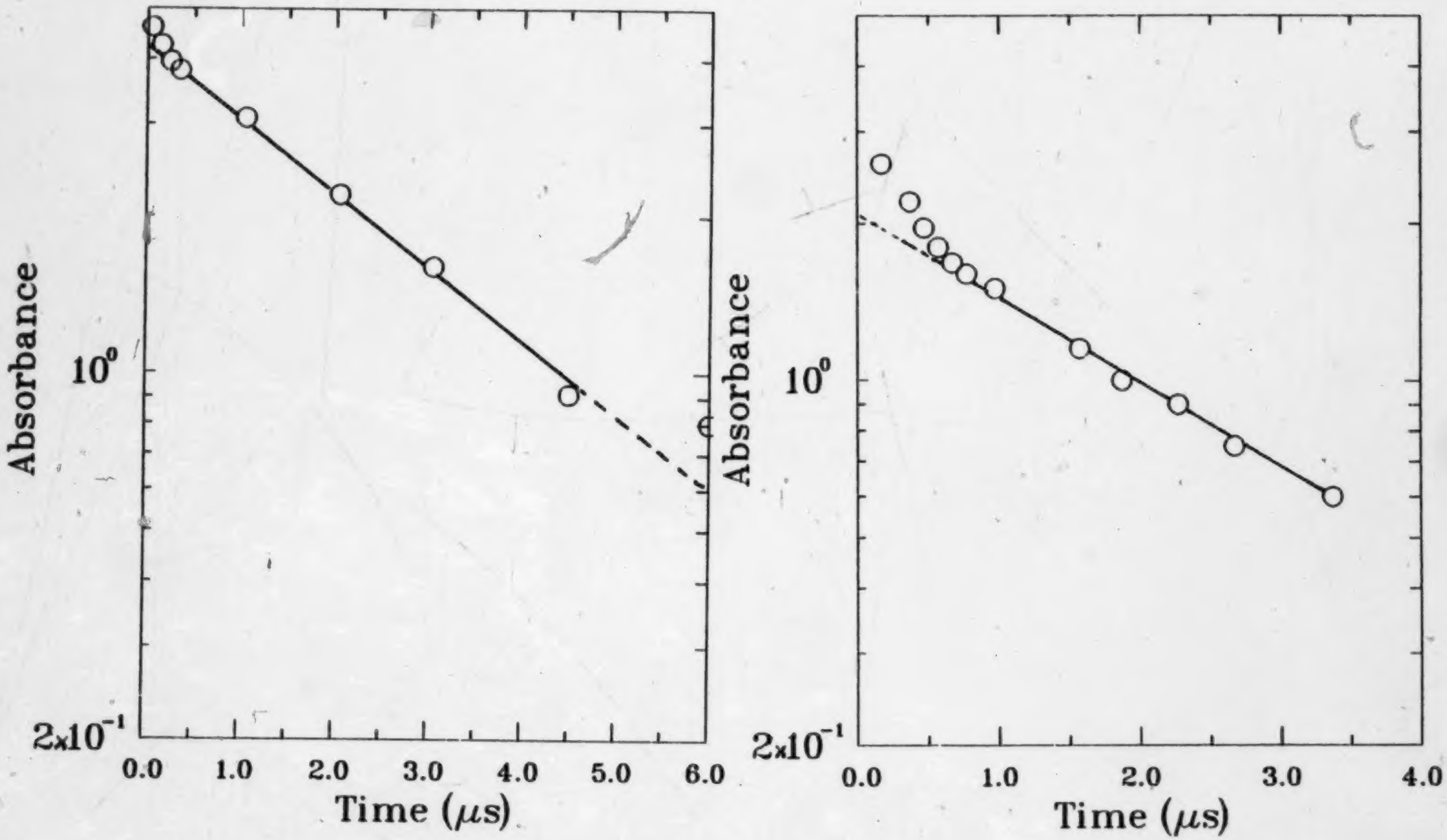

Fig. 2-10: The First Order Decay Plot of Solvated Electron

and in the presence of a scavenger it reacts according to equation 14,

$$e_s^- + S \longrightarrow products \tag{14}$$

Both reactions are first-order since the concentration of the solvent and the scavenger are much higher than that of e_s^- . The observed first-order decay rate constant is,

$$k_{obs} = k_1 + k_2[S] \tag{15}$$

where k_1 is the first order rate constant of reaction 13 and k_2 is the second order rate constant of reaction 14. The value of k_{obs} is obtained by,

$$k_{obs} = \frac{ln2}{t_{\frac{1}{2}}} \tag{16}$$

where $t_{\frac{1}{2}}$ is the half-life of the first order decay. The k_{obs} value in each system was calculated using an average of four half-lives secured from two consecutive decay curves. There was a two minute interval between succesive electron pulses given to one system.

The decay at a much slower time scale was observed for each system to check whether the first-order tail decays down to the base-line. If it does not decay down to the base-line it may be due to several reasons. Two most common are: (a) absorption of light by colour centers in the glass, which occurs when the cell does not fit properly in the cell holder, (b) drift of the base-line.

The decay curves in each solvent were measured at the wave-length that corresponds to the maximum absorption of e_s^- (λ_{max}). Measurements of pure *t*-butanol were different from the other results in two ways: (a) these were done at 250 nm below that of λ_{max} since the detector allowed measurements only up to about 1000 nm; (b) the rate constants at 298K were obtained by extrapolation.

The values of k_2 were obtained from the slope of a plot of k_{obs} against scavenger concentration. The scavenger concentration was measured before and after irradiation whenever possible, to ensure that there are no significant changes of concentration due to radiation.

Half-life values were obtained over a temperature range of 100 degrees. To minimize systematic errors the temperature was measured randomly. The temperature measurements were limited by: (a) freezing point of the solvent; (b) boiling point of the solvent; (c) phase separation of the solvent; and (d) sensitivity of the detector.

The repeatability of the measurements was examined using independent solvent and scavenger samples. The k_2 values thus obtained for two extreme solvent systems indicate fairly good reproducibility (Fig. 2-11(a) and (b)).

2.3.4 Effect of Impurities

In the presence of an impurity I, the solvated electron reacts as follows:

$$e_s^- + ROH \longrightarrow RO_s^- + H \qquad (17)$$

$$e_s^- + S \longrightarrow products \qquad (18)$$

$$e_s^- + I \longrightarrow products \qquad (19)$$

where k_1, k_2 and k_i are the rate constants of eqns. (17), (18) and (19) respectively. The effect of the impurity on the rate constant depends on whether it originates in : (a) the solvent or (b) the scavenger

2.3.4(a) Impurity in the Solvent

When the impurity originates in the solvent, the amount of the impurity at each scavenger concentration is the same. Therefore (k_1 + k_i [I]) in equation

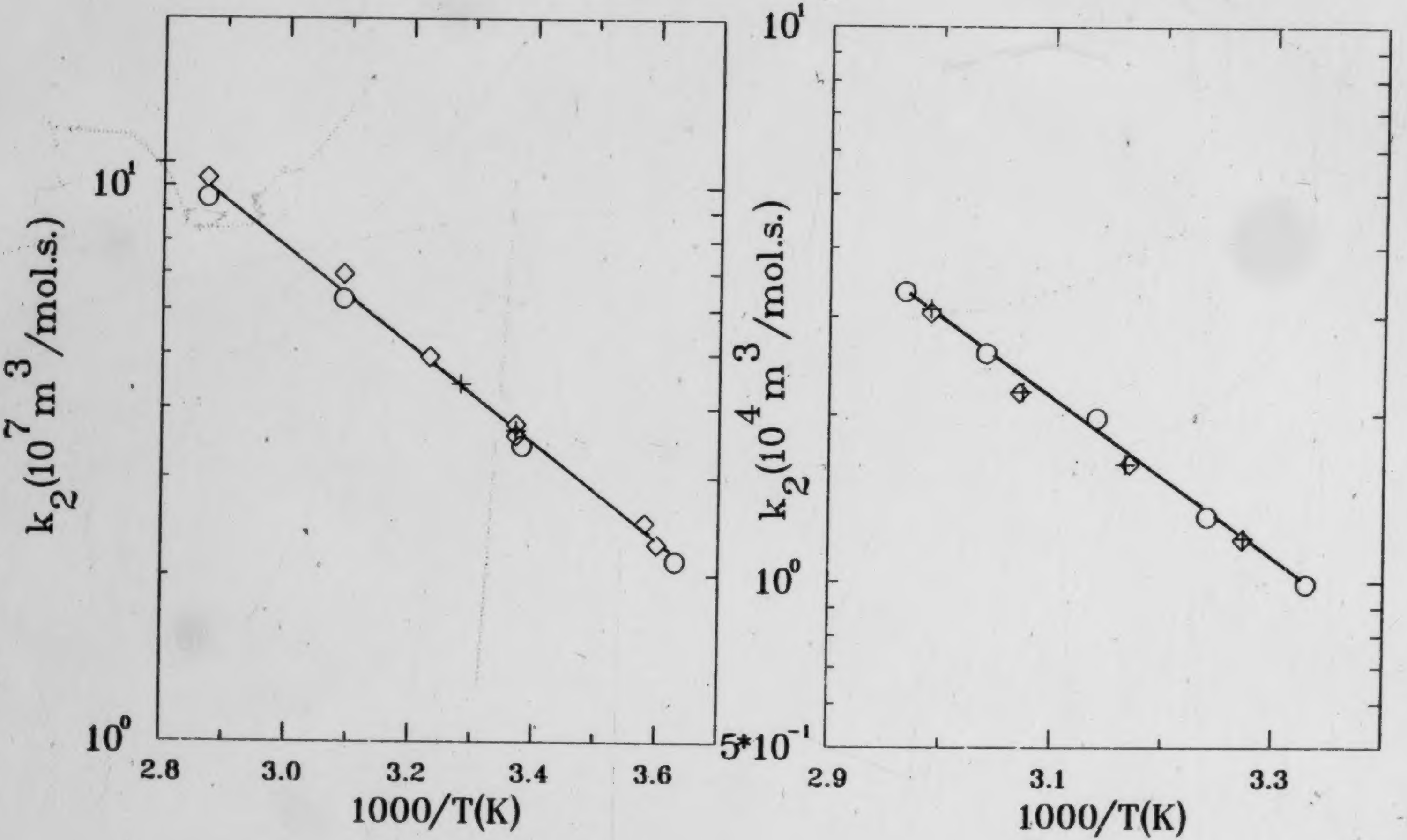

Fig. 2-11: Reproducibility of k_2 Values

(20) is constant.

$$k_{obs} = k_1 + k_i[I] + k_s[S] \tag{20}$$

The effect of the impurity appears in the intercept of the k_{obs} versus [S] plot and has no bearing on k_2 which is the slope.

If k_i [I] ¿¿ k_s [S] then all half lives are the same regardless of different solute concentrations. This occurs when the solute is an inefficient electron scavenger such as toluene ($k_2 \sim 10^3 - 10^4 m^3/mol.s.$) and the impurity an efficient electron scavenger. In alcohols the occurance of ketones ($k_2 \sim 10^7 m^3/mol.s.$) as impurities are common. During distillation the amount of ketones and other impurities in alcohols was checked by observing the UV spectrum of the alcohol (ketone peak ~ 275 nm) and the sample was collected when no ketone peak was visible. Absence of efficient impurities was confirmed by measuring the half-life of the purified alcohol.

2.3.4(b) Impurity in the Solute

When the impurity originates in the solute, the amount of impurity is a fraction p of the solute concentration [S].

$$k_{obs} = k_1 + (pk_i + k_s)[S] \tag{21}$$

Since p is small (probably $p < 0.01$) for an efficient solute,

$$k_2 = pk_i + k_s \approx k_s \tag{22}$$

If the impurity is an efficient scavenger and the solute an inefficient scavenger, the value of pk_i is comparable to that of k_s hence the second order rate constant $k_2 =$ pk_i + k_s .

2.3.5 Viscosity Measurements

2.3.5(a) Calibration with Water

The kinematic viscosity ν (m^2/s) was calculated from the efflux time t measured in Ubbelohde suspended level viscometers 0_c (Schott Gerate #24501-03) and I (Schott Gerate #24501-01). An optical meniscus detection system determined t in units of 0.01 s with a precision of ±0.009% (132).

The viscometer 0_c was calibrated by measuring t for water at $283 \leq T/K \leq 342$ and compared with literature ν values using

$$\nu = At - \frac{B}{t} \tag{23}$$

where A and B are the viscometer constants. Each t was the average of 6 determinations. Values of ν were obtained from

$$\nu = \frac{\eta}{\rho} \tag{24}$$

where the dynamic viscosities η were taken from a critical review (133) and densities ρ were taken from ref. 134(a). Values of ν (m^2/s) calculated using A = 2.8550 x 10^{-9} m^2/s^2 and B = 2.2823 x 10^{-6} m^2 agreed with those in ref.133 within an average deviation of 0.08%. Eq. (23) is the usual calibration relation in the literature. However the manufacturer's table of Hagenbach corrections to t (135) showed that it used

$$\nu = Kt - \frac{K_E}{t^2} \tag{25}$$

where K and K_E are the constants instead of A and B. Eq. (25) was also used in another work (136). Fitting the present t values for water to literature values of ν (m^2/s) yielded K = 2.8458 x $10^{-9} m^2/s^2$ and K_E = 3.4223 x $10^{-4} m^2.s$; however the average deviation between ν calculated from eq. (25) and the literature values increased to 0.10%. Hence ν was calculated from measured t using eq. (23).

2.3.5(b) Calibration with Organic Liquids

To calibrate the viscometer I, water could not be used, because its ν values have too small a range. Therefore organic liquids were used. Although suspended level viscometers were designed to minimize the surface tension effect (137), ref. 138 suggested calibrating with water, which at 293K has a surface tension $\sigma = 73 \times 10^{-3}$ N/m (134b). Such an effect was absent in ref.136 where the constants obtained by water calibration gave viscosities of toluene [$\sigma = 29 \times 10^{-3}$ N/m at 293K (134b)] at $298 \leq T/K \leq 368$ agreeing within an average deviation of 0.15% from other values in the literature.

A surface tension effect would affect studies in alcohol/water mixtures as σ changes with composition (134b). The possibility of a surface tension effect in the viscometers was investigated by determining flow times t (each being the average of at least three measurements) of n-heptane, n-octane and n-butanol in the water calibrated viscometer 0_c. The densities ρ used to calculate the present η are the average of values cited in the viscosity literature sources (139-141). The η values (table 1) are in general agreement with the rather scattered earlier works and do not support consideration of a surface tension effect in the present work.

At the same time the organic solvent measurements were done in viscometer 0_c, viscometer I was filled with that solvent and stabilized in the same bath. To calibrate the viscometer I values were correlated by eq. (23); the resulting $A = 1.0303 \times 10^{-8} m^2/s^2$ and $B = 2.3128 \times 10^{-6}$ gave calculated ν values that agree with measured values, with an average deviation of 0.06%.

2.3.6 Density Measurements

The liquid densities were determined from volume changes of a known mass of sample (142). Six pyrex dilatometers, each consisting of two 1.000 ml pipettes sealed to a 10, 20 or 25 cm^3 bulb were used. The two pipettes connected in parallel made the dilatometer easier to clean and fill. The samples were sealed in the dilatometer using ground-glass-jointed caps and springs. The mass of the sample was the difference between the filled and the unfilled dilatometer, weighed at 294±1K on a Stanton Instruments Ltd. (model C.L.I.) analytical balance. Sample masses of about 9 to 20g were measured to 0.1 mg with a precision of ±0.1 mg as determined by repeated weighings of a given mass. The pipette scales were readable to 0.001 ml with a precision of ±0.001 ml. Each dilatometer was calibrated with water with the meniscus at positions covering the entire length of the pipette portion, and at $274.16 \leq T/K \leq 347.93$.

To estimate the reliability of the measurements, densities were measured in four liquids at 293.15K and compared with values in the literature (Table 2). The percent deviation Δ

$$\Delta_{av} = 100(1 - \frac{lit}{present}) \qquad (26)$$

where *lit* are the literature values and *present* are the present values, varied from 0.09% to -0.11%. The reliability of the present densities is indicated by the average percent deviation,

$$\Delta_{av} = \frac{100}{n}\Sigma\Delta_i \qquad (27)$$

(n is the number of samples and the subscript i denotes the i'th sample) which for the liquids in Table 3 was 0.06%.

Table 2-1 : Comparison of Viscosity Values

liquid	T	ν^a	ρ	η^b			
	K	$10^{-6} m^2/s$	kg/m^3	present	ref 134(c)	ref 139	other
nC_5H_{12}	626.8	626.2	626.3^b	0.09			
nC_7H_{16}	298.17	0.569	683.8^c	0.389	0.386	0.392	0.396^d
nC_8H_{18}	298.24	0.726	698.4^c	0.507	0.511	0.514	0.514^d
nBuOH	307.84	2.538	798.5^e	2.027	2.034	2.026	1.993^f
nBuOH	318.23	2.005	790.7^e	1.585	1.579	1.580	1.549^f

a. Average of percent differences from eq. [4].

b. Ref. 140.

c. Ref. 134.

d. Ref. 141.

Table 2-2 : Comparison of Densities at 293.15K

liquid	$\rho(kg/m^3)$			
	present	ref 139	other	$\Delta(\%)$
nC_5H_{12}	626.8	626.2	626.3^b	0.09
nC_6H_{14}	658.7	659.4	-	-0.11
$nC_6H_{11}CH_3$	769.2	-	769.4^c	-0.03
$nBuOH$	809.5	809.6	809.4^d	0.00

a. Measured in Viscometer 0_c calibrated with water at $283.15 \leq T/K \leq 342.42$, $10^{-4} m^2/s$ = Stokes.

b. Dynamic viscosity in $10^{-3} Pa.s = 10^{-2} p$, see eq.(24).

c. Average of references 139 and 140.

d. Ref 140.

e. Average of refs. 139 and 141.

f. Ref 141.

3 RESULTS

3.1 Organic Scavengers

3.1.1 Tertiary Butanol/Water Mixtures

Tertiary butanol (t-BuOH), is completely miscible with water, whereas secondary butanol (2-BuOH) and *iso*-butanol (*i*-BuOH) are partially miscible. Solvent compositions were chosen so that they define the composition zones observed in the optical absorption spectrum of the solvated electrons and the viscosity of *t*-butanol/water mixtures: $x_{H_2O} = 0$ (pure alcohol), 0.10 (composition at viscosity minimum and at which there has been a large increase in optical absorption energy), 0.64 (composition at maximum viscosity), 0.97 (composition at maximally stabilized water structure) and 1.00 (pure water). Additional compositions were added as necessary to observe the intermediate changes. Scavengers were chosen so that their electron capture efficiencies and polarities span a wide range (the k_2 values vary from $\sim 10^7$ for nitrobenzene to $\sim 10^3$ for toluene).

3.1.1(a) Reaction of e_s^- with Nitrobenzene

The reaction with nitrobenzene ($C_6H_5NO_2$), was studied at the following compositions: x_{H_2O} = 0, 0.10, 0.30, 0.40, 0.56, 0.64, 0.90, 0.92, 0.94, 0.97, 0.98 and 1.00.

The first-order rate constants at each nitrobenzene concentration and temperature for all *t*-butanol/water mixtures are in Figs.(3-1) to (3-12). The concentration range of nitrobenzene was 5-300 x 10^{-3} mol/m^3. The second-order rate constants at each temperature are in Table(3-1). These rate constants fit the Arrhenius model at the given temperature range. The Arrhenius plots are in Fig.(3-13). The rate constant k_2 at 298K was obtained from a best fit line drawn through the points in the Arrhenius plot. Since pure *t*-BuOH is a solid at room temperature its k_2 value was obtained by extrapolation. The reaction rate parameters for the e_s^- + nitrobenzene reaction are given in Table(3-2).

Nitrobenzene is an efficient scavenger of electrons. At T = 298K the rate of reaction in water, 3.8 x $10^7 m^3/mol.s.$ is nearly diffusion controlled. This agrees with other recent experimental results (53,67) to within ±2%. However, the earlier results vary from 3.5 x $10^7 m^3/mol.s.$ (62) to 4.2 X $10^7 m^3/mol.s.$ (61). Those experiments were conducted only at one temperature , in contrast to the range of temperatures used in the later studies. When rate constants at several different temperatures were available the k_2 value at a specific temperature was always obtained from a best fit line drawn through the points. The rate of e_s^- reaction in pure t-BuOH , 1.1 x $10^7 m^3/mol.s.$ is the same as that in literature (53).

The rate constants decrease when water is added to alcohol up to $x_{H_2O} \approx 0.1$ (Fig. 3-14). They are relatively constant in the range $0.1 < x_{H_2O} < 0.7$, but then gradually increase until $x_{H_2O} = 1.0$. The extent of change in k_2 when one pure solvent is mixed with a small amount of the other is greater in water-rich solvents. Therefore more solvent compositions were studied in this region.

The temperature variation of k_2 fits the Arrhenius model (Fig. 3-13) and the energy of activation of this model E_2 decreases up to $x_{H_2O} \approx 0.1$, then does not change until $x_{H_2O} \approx 0.7$, then gradually decreases as the water content increases further. The energy of activation for e_s^- + nitrobenzene reaction in t-BuOH is about twice that in water. As the reaction is nearly diffusion controlled the activation energies probably reflect those of diffusion. The energy of activation for viscous flow, E_η, in pure water is 18 kJ/mol, while that in t-BuOH is 39 kJ/mol (74).

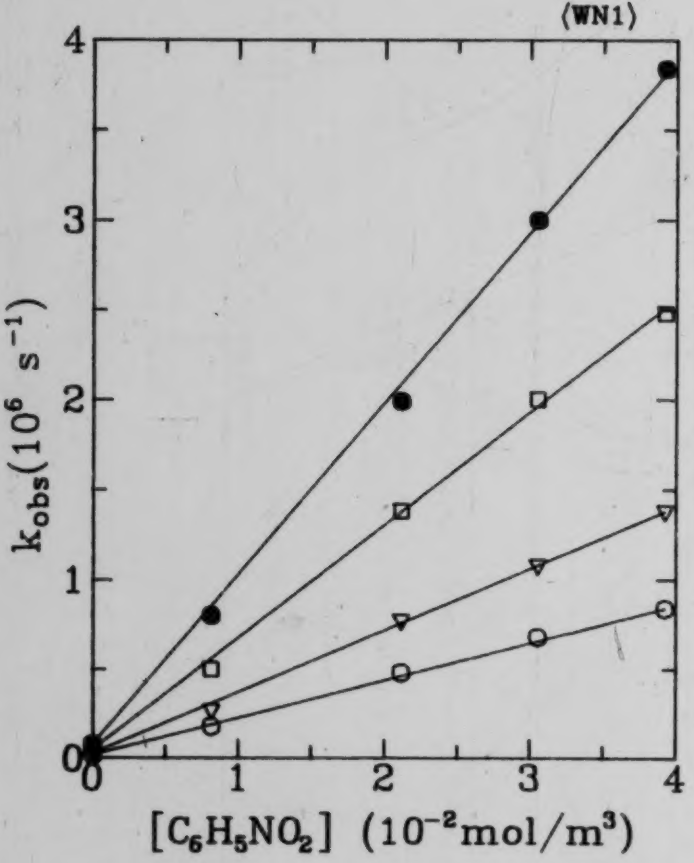

Fig. 3-1a: H_2O

○ 275.8K ▽ 296.1K □ 323.3K
● 348.2K

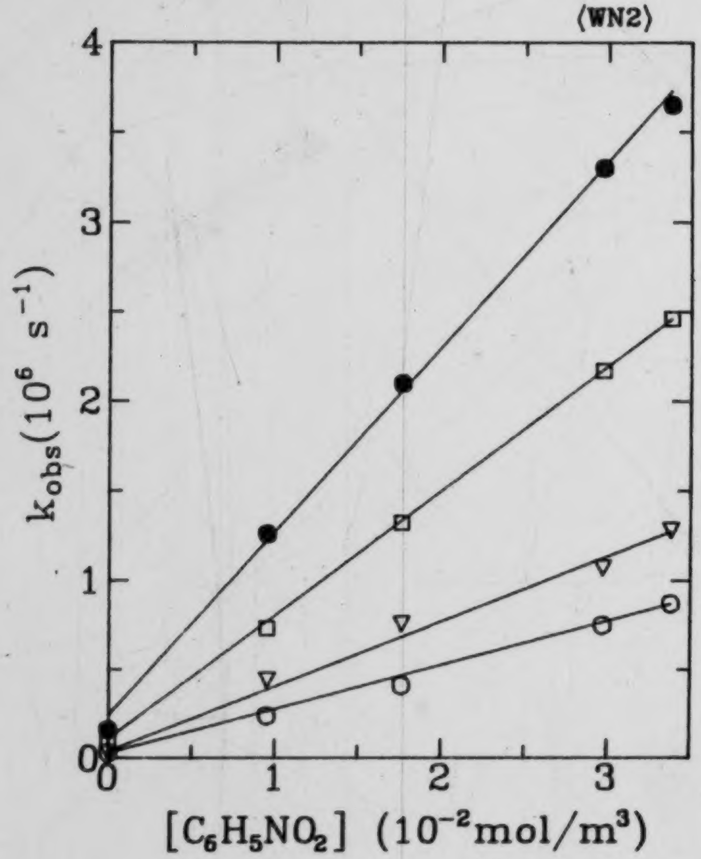

Fig. 3-1b: H_2O

○ 279.2K ▽ 296.6K □ 323.2K
● 348.3K

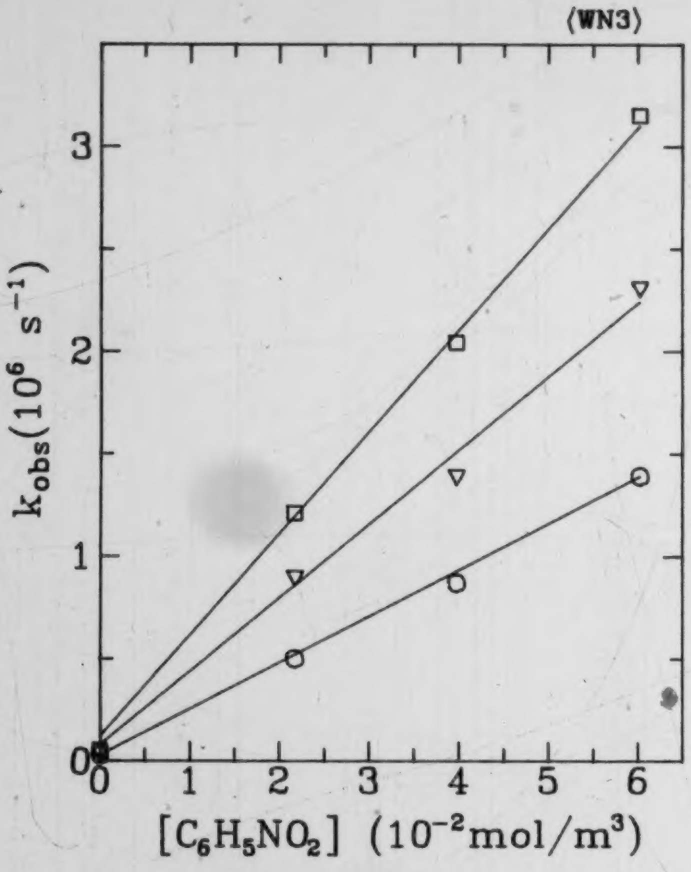

Fig. 3−1c: H_2O

○ 278.0K ▽ 296.7K □ 309.2K

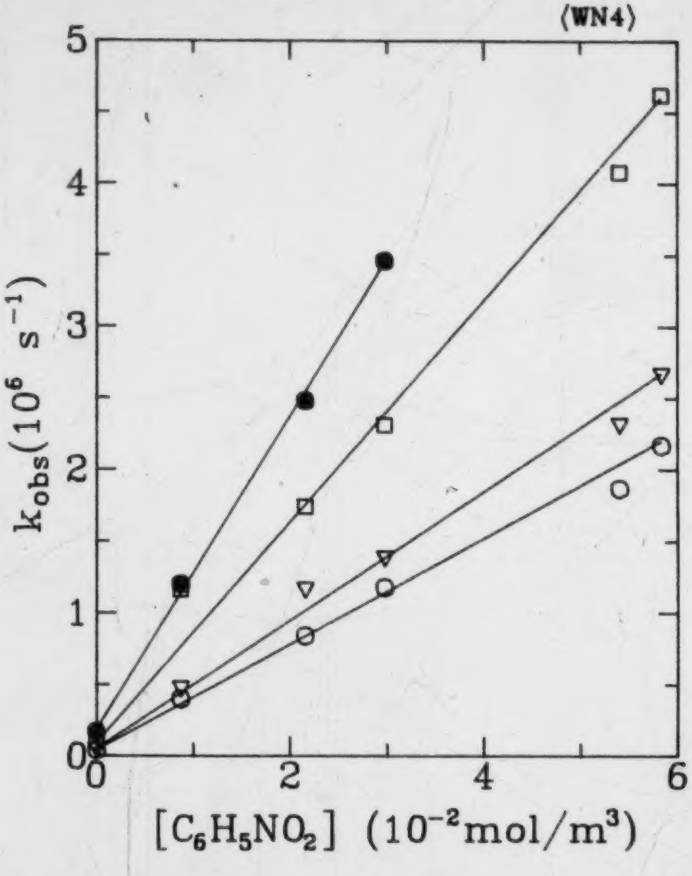

Fig. 3−1d: H_2O

○ 296.7K ▽ 305.3K □ 348.0K
● 357.5K

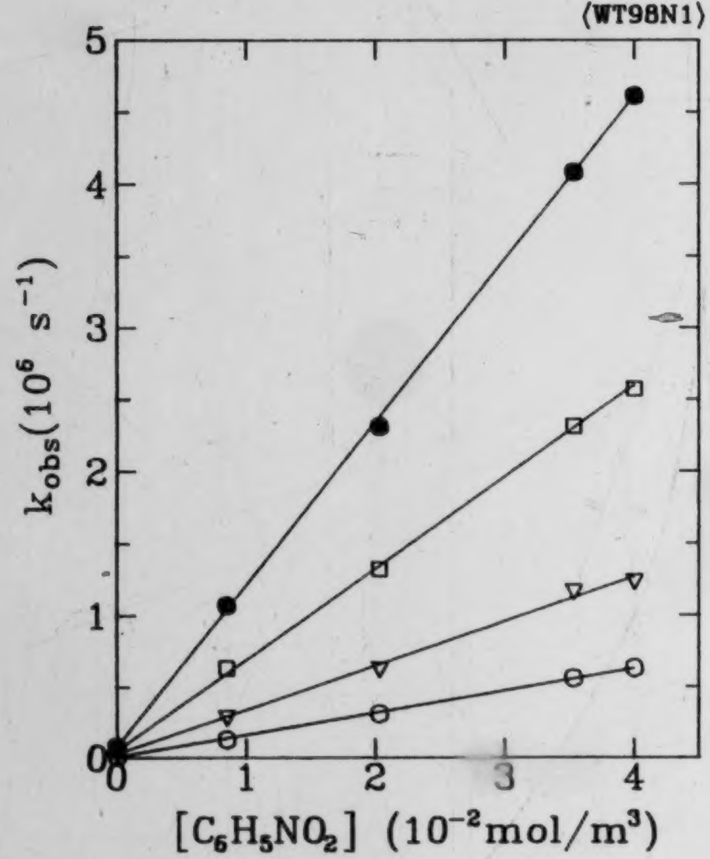

Fig. 3-2 : t-BuOH/H_2O:2/98
○ 273.8K ▽ 296.3K □ 330.2K
● 363.2K

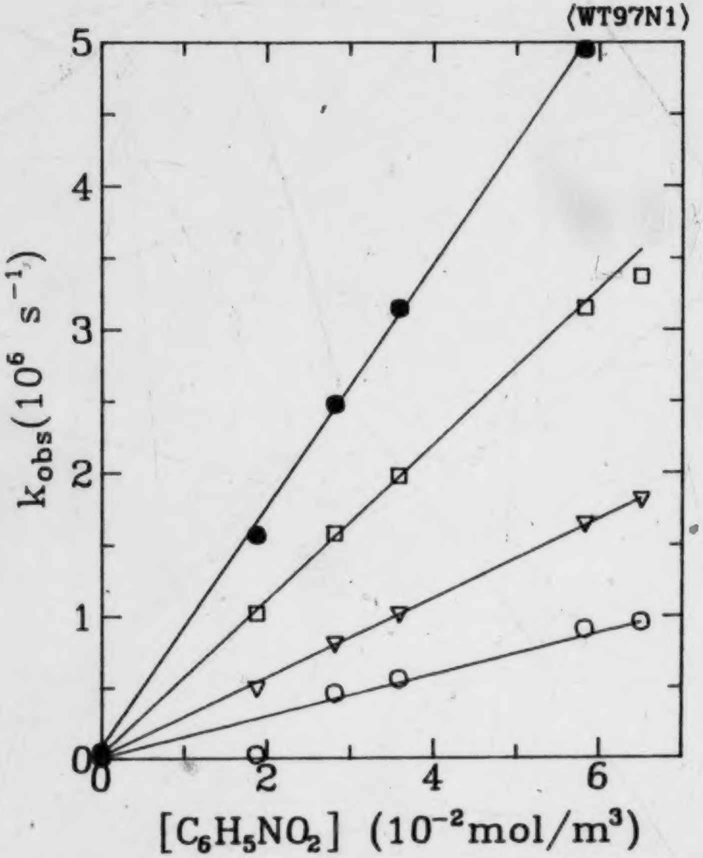

Fig. 3-3a : t-BuOH/H_2O:3/97
○ 274.7K ▽ 296.1K □ 323.2K
● 347.8K

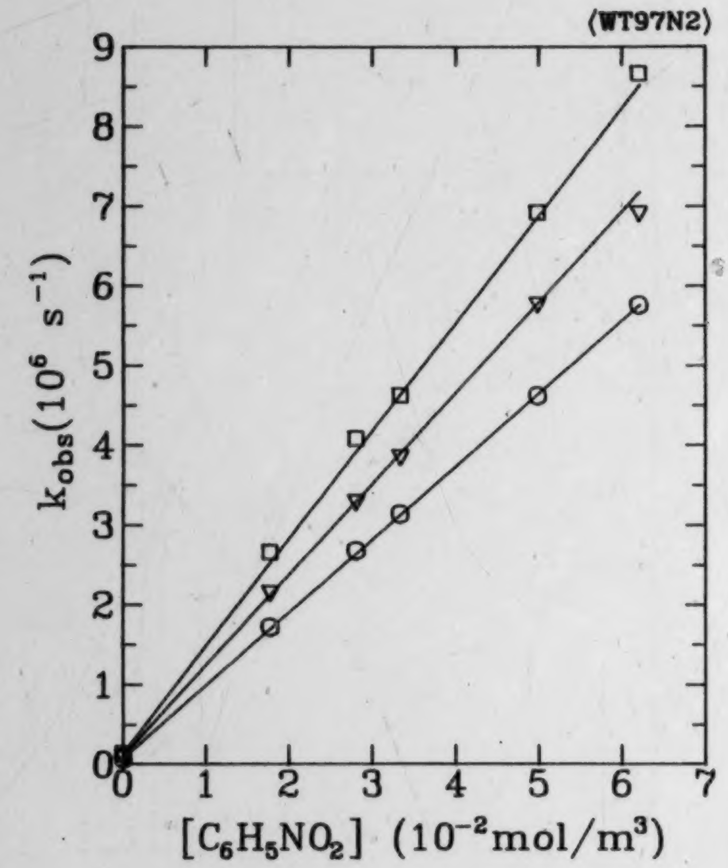

Fig. 3-3b: t-BuOH/H_2O:3/97

○ 354.6K ▽ 367.9K □ 383.4K

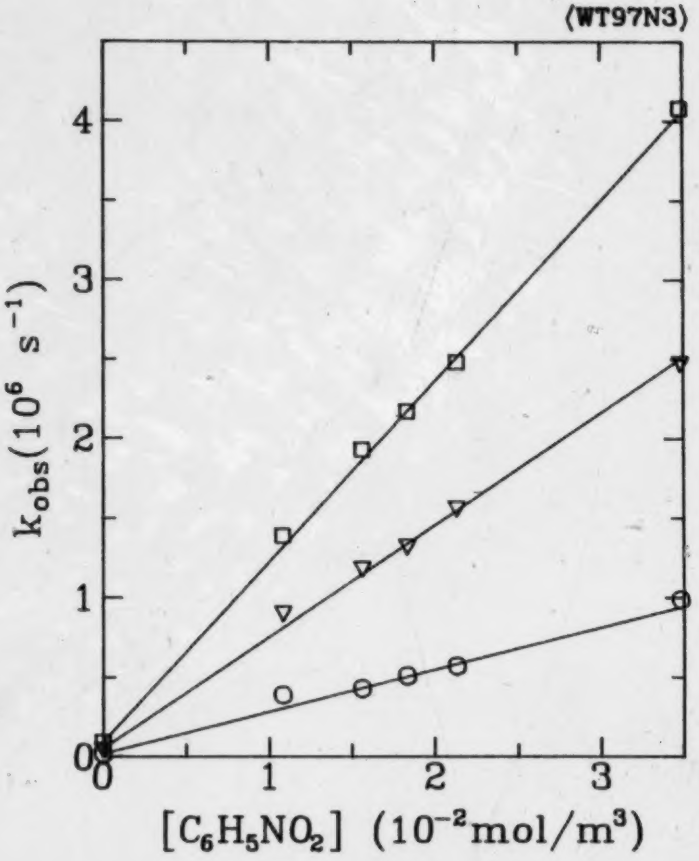

Fig. 3-3c: t-BuOH/H_2O:3/97

○ 296.3K ▽ 340.1K □ 371.7K

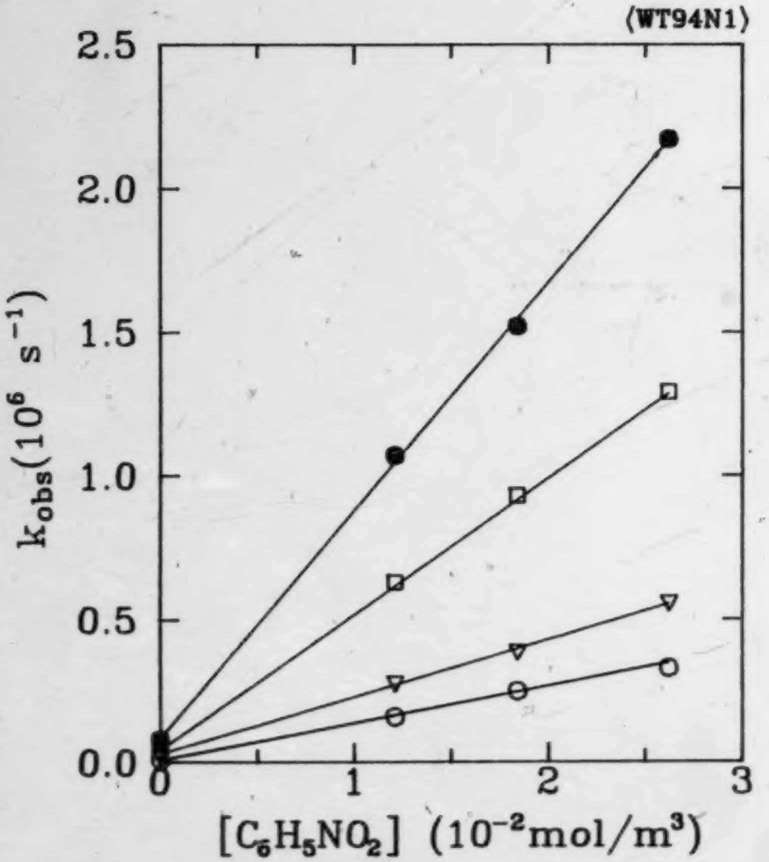

Fig. 3–4: t–BuOH/H_2O:6/94

○ 282.2K ▽ 297.3K □ 329.0K
● 357.3K

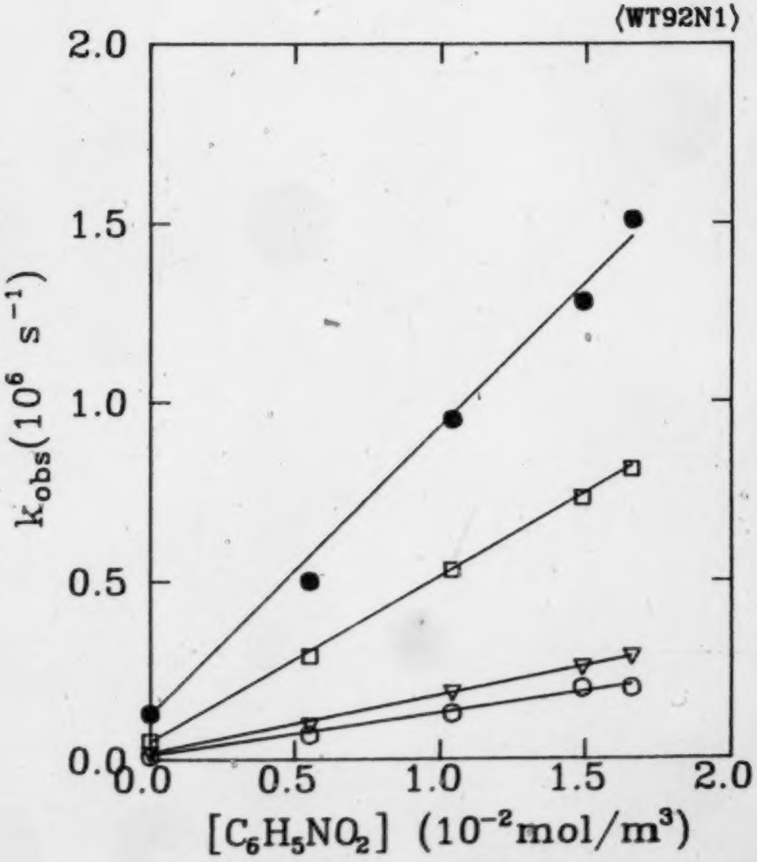

Fig. 3–5: t–BuOH/H_2O:8/92

○ 284.8K ▽ 296.4K □ 333.8K
● 369.0K

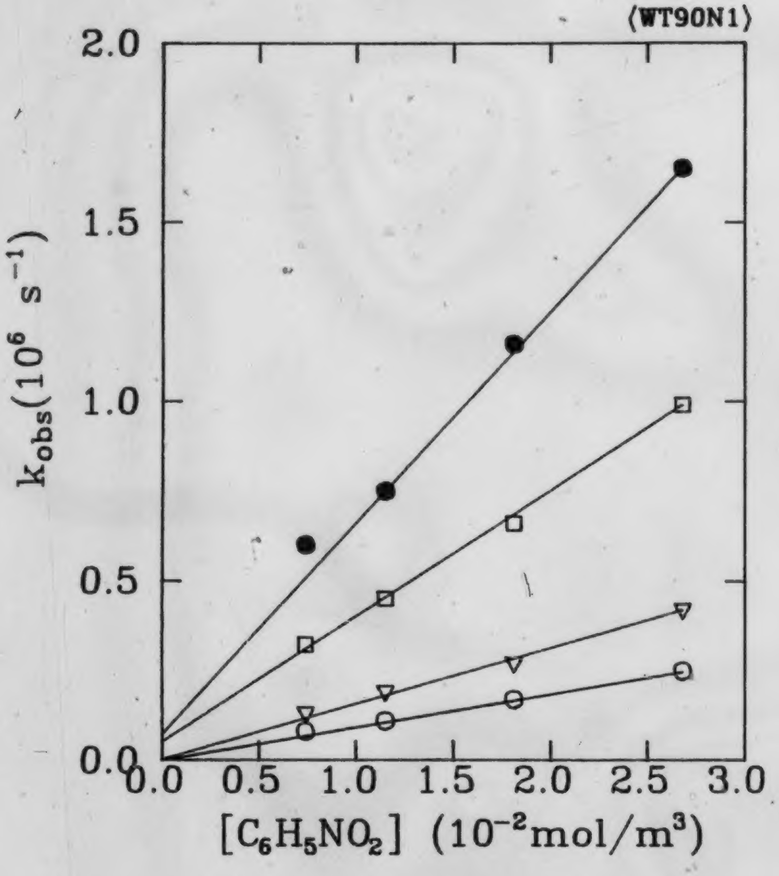

Fig. 3-6: t-BuOH/H_2O:10/90

○ 282.2K ▽ 296.7K □ 329.0K

● 357.4K

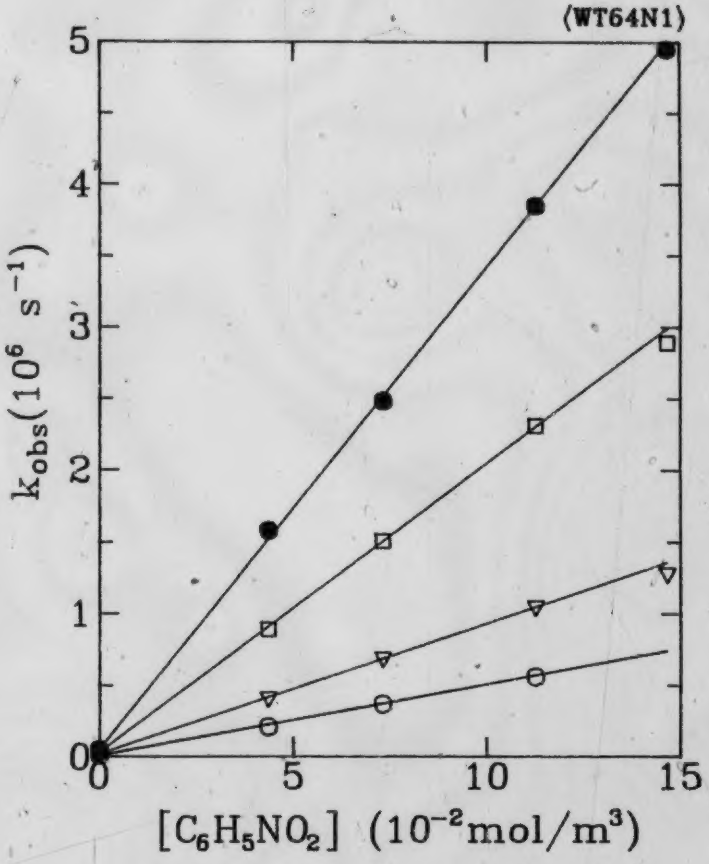

Fig. 3-7a: t-BuOH/H_2O:36/64

○ 282.2K ▽ 295.8K □ 323.6K

● 348.8K

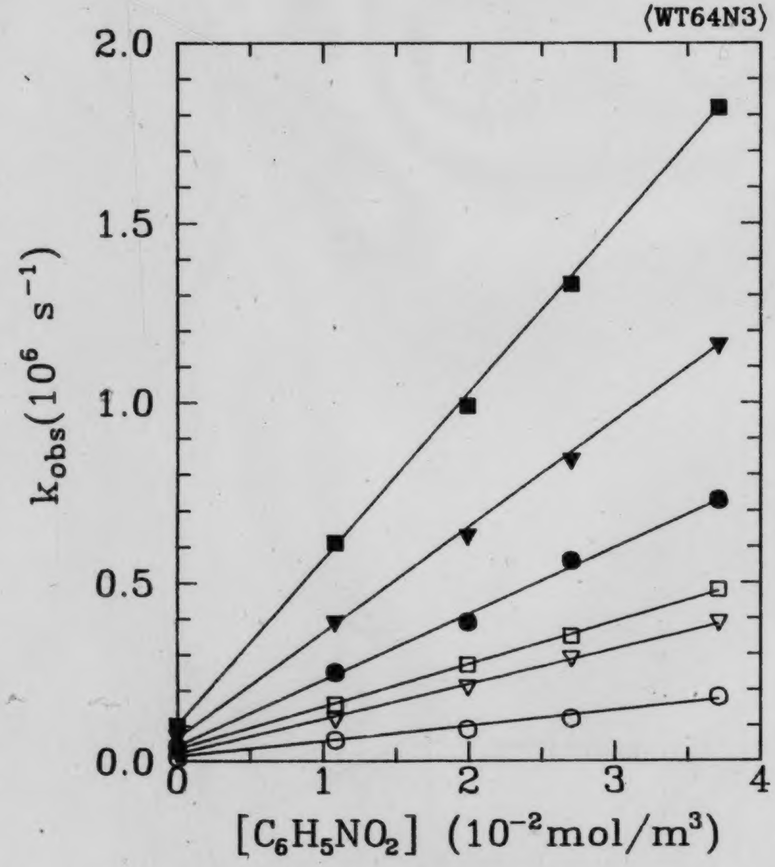

Fig. 3– 7b: t–BuOH/H_2O:36/64

○ 280.2K ▽ 297.6K □ 306.0K
● 319.5K ▼ 338.6K ■ 361.0K

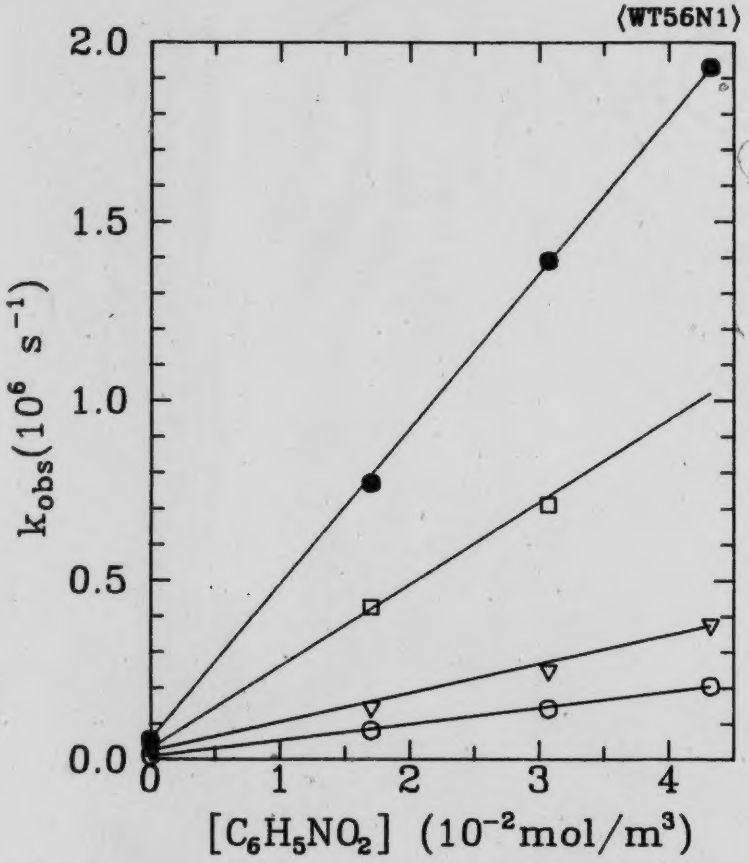

Fig. 3-8 : t-BuOH/H_2O:44/56
○ 283.5K ▽ 296.3K □ 330.2K
● 363.3K

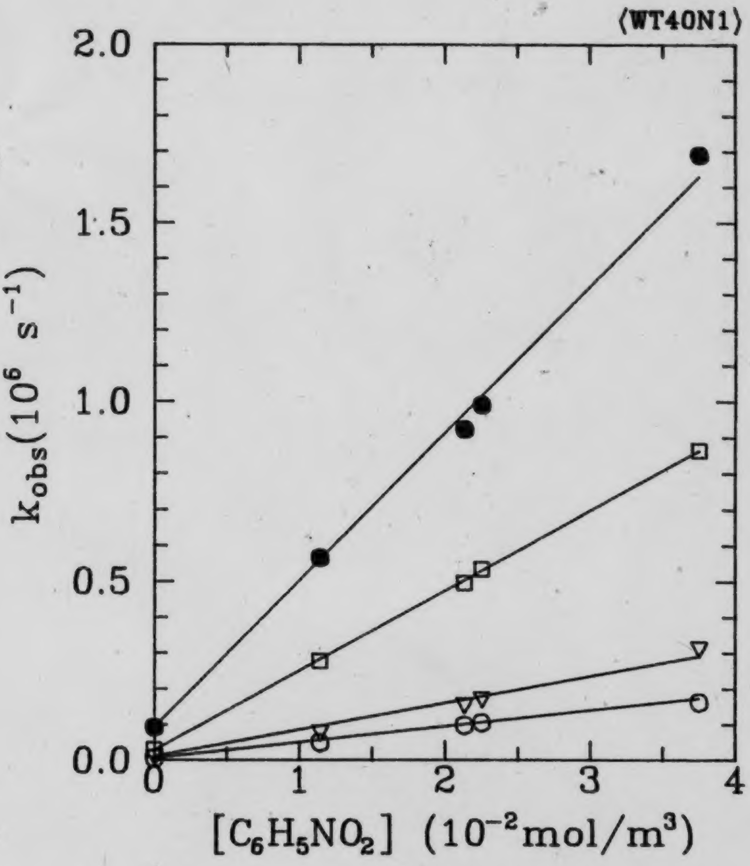

Fig. 3- 9: t-BuOH/H_2O:60/40
○ 283.5K ▽ 296.5K □ 332.1K
● 364.1K

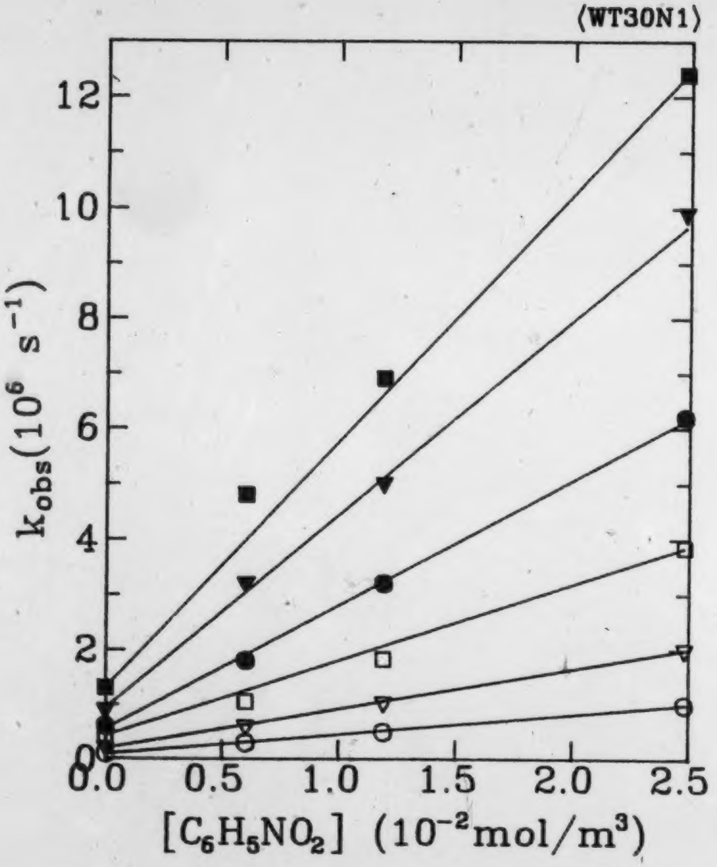

Fig. 3−10: t−BuOH/H_2O:70/30

○ 279.6K ▽ 295.5K □ 313.5K
● 333.0K ▼ 352.8K ■ 367.8K

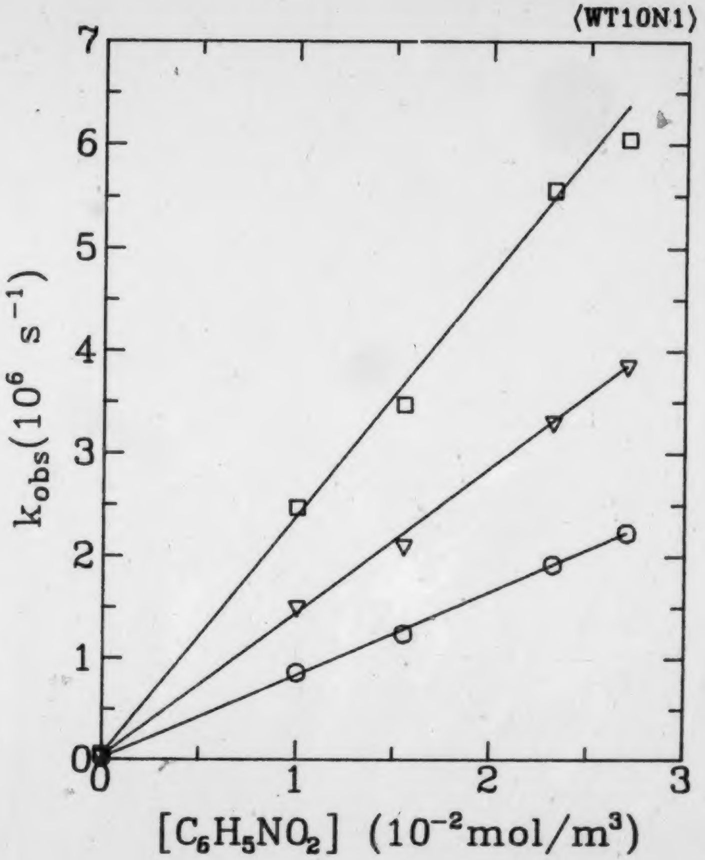

Fig. 3-11a: t−BuOH/H_2O:90/10

○ 296.1K ▽ 313.1K □ 332.8K

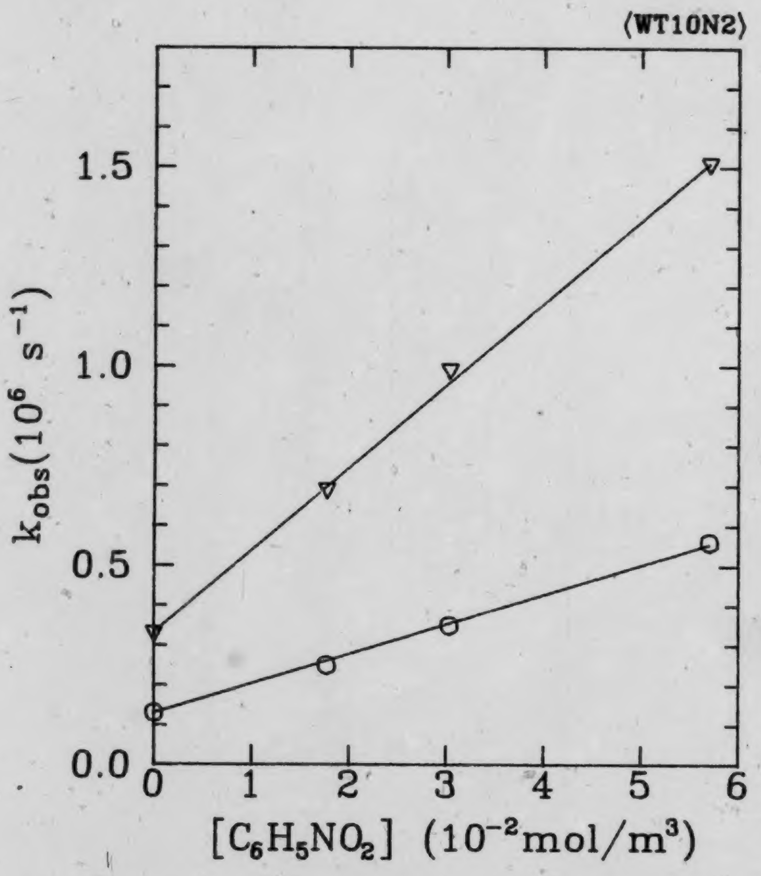

Fig. 3−11b: t−BuOH/H_2O:90/10
○ 295.6K ▽ 324.3K

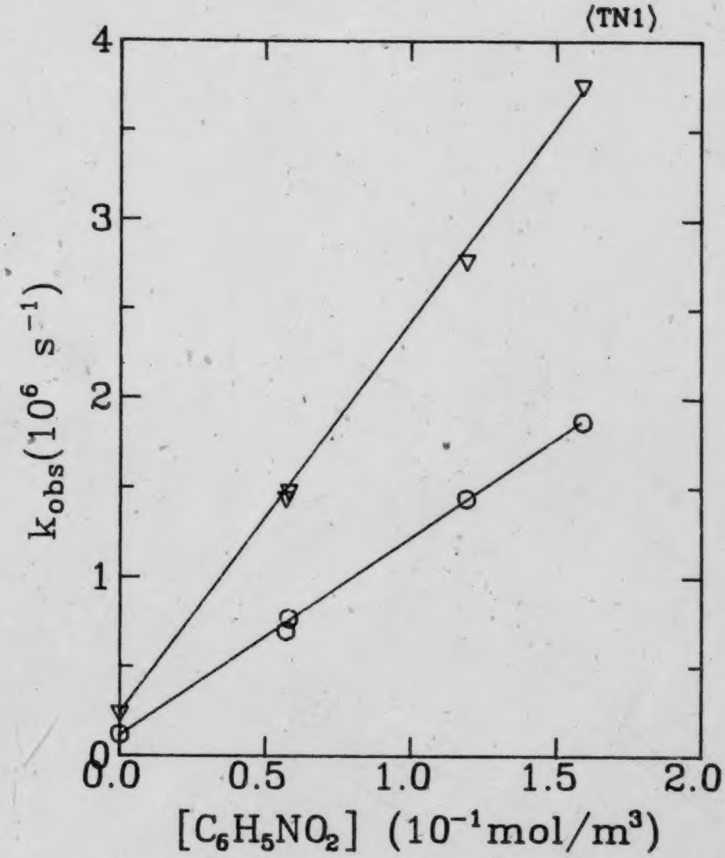

Fig. 3−12a: t−BuOH $_2$
○ 300.1K ▽ 314.1K

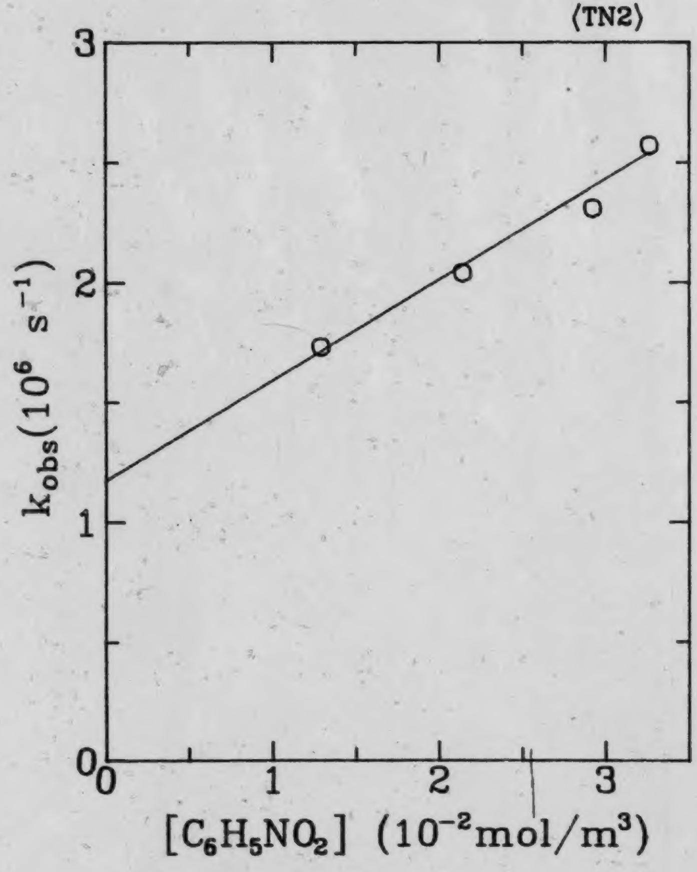

Fig. 3–12b: t–BuOH
○ 332.6K

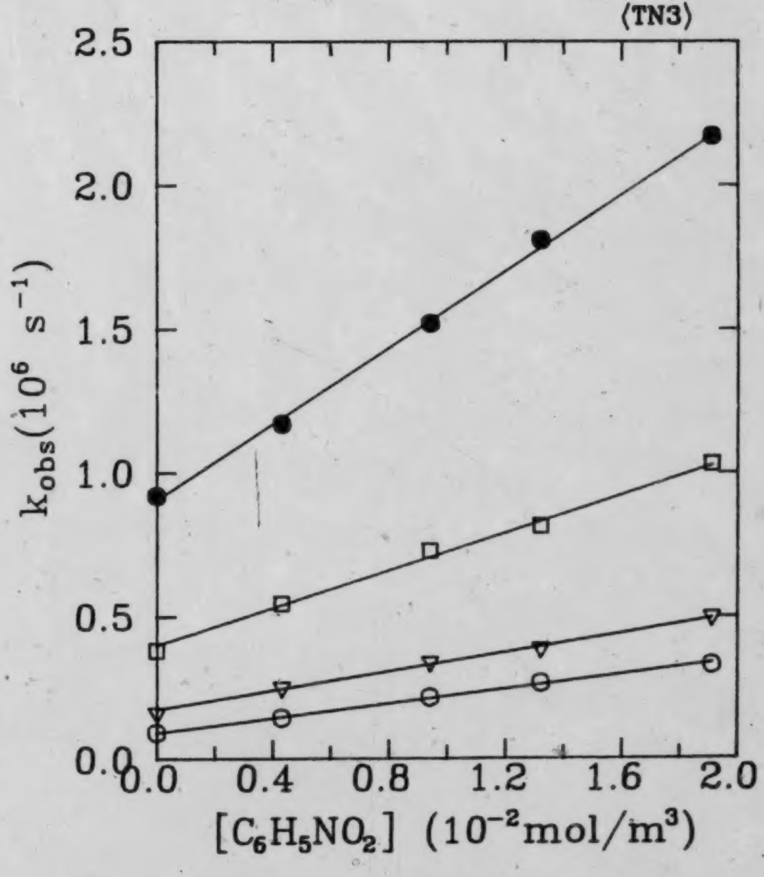

Fig. 3–12c: t–BuOH
○ 300.9K ▽ 307.6K □ 323.1K
● 337.4K

Table 3-1:The values of second order rate constants for nitrobenzene in *t*-butanol/water

x_{H_2O}	T (K)	k_2 $10^7 m^3/mol.s$	x_{H_2O}	T (K)	k_2 $10^7 m^3/mol.s$
0	300.1	1.1	0.40	283.5	0.44
	314.1	2.2		296.5	0.75
	332.6	4.2		332.1	2.2
0	300.9	1.3		364.1	4.2
	307.6	1.7	0.56	283.5	0.47
	323.1	3.3		296.3	0.82
	337.4	6.7		330.2	2.3
0.10	296.1	0.83		363.3	4.3
	313.1	1.4	0.64	282.2	0.51
	332.8	2.4		295.8	0.92
0.10	295.6	0.79		323.6	2.0
	324.3	2.1		348.8	3.4
0.30	279.6	0.40	0.64	280.2	0.47
	295.5	0.73		297.6	0.97
	313.5	1.4		306.0	1.2
	333.0	2.3		319.5	1.8
	352.8	3.5		338.6	2.9
	367.8	4.6		361.0	4.7
0.90	282.2	0.93	0.97	296.3	2.58
	296.7	1.5		340.1	7.0
	329.0	3.5		371.7	11.30
	357.4	5.9	1.00	275.8	2.12

0.92	284.8	1.2		296.1	3.42
	296.4	1.6		323.3	6.27
	333.8	4.5		348.2	9.53
	369.0	8.0	1.00	279.2	2.48
0.94	282.2	1.27		296.6	3.74
	297.3	1.98		323.2	6.95
	329.0	4.68		348.3	10.30
	357.3	7.97	1.00	278.0	2.27
0.97	274.7	1.59		296.7	3.57
	296.1	2.78		309.2	4.94
	323.2	5.43	1.00	296.7	3.65
	347.8	8.55		305.3	4.43
0.97	354.6	9.07		357.5	11.00
	367.9	11.30			
	383.4	13.70			

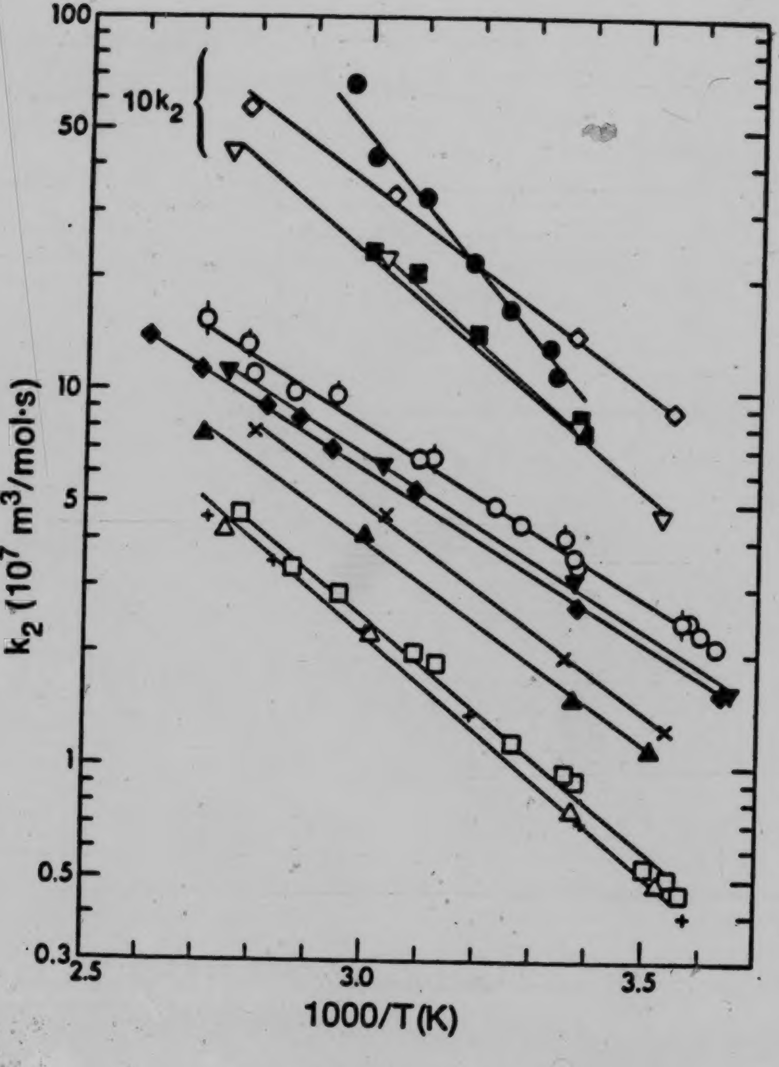

Fig. 3–13: e_s^- + $C_6H_5NO_2$ reaction in t–BuOH water mixtures.

x_{H_2O}: ● 0.00; ■ 0.10; + 0.30; △ 0.35; ▽ 0.56; □ 0.64; ◇ 0.90; ▲ 0.92; × 0.94; ◆ 0.97; ▼ 0.98; ○ 1.00

Table 3-2: Reaction rate parameters for the reaction of e_s^- with nitrobenzene in *t*-butanol/water .

x_{H_2O}	k_2 $10^7 m^3/mol.s$	E_2 J/mol	log A	$\Delta S_2^{\neq}$ J/mol.K
0	11.0	35	13.18	65
0.10	8.4	25	11.37	30
0.30	7.9	24	11.14	26
0.40	7.9	24	11.14	26
0.56	8.2	24	11.14	25
0.64	9.0	24	11.10	25
0.90	15	21	10.86	20
0.92	16	21	10.82	19
0.94	20	21	10.98	22
0.97	29	18	10.56	14
0.98	31	18	10.63	16
1.00	38	17	10.61	16

Fig.3–14: k_2, E_2 and ΔS_2 for Nitrobenzene in t–BuOH/Water Mixtures.

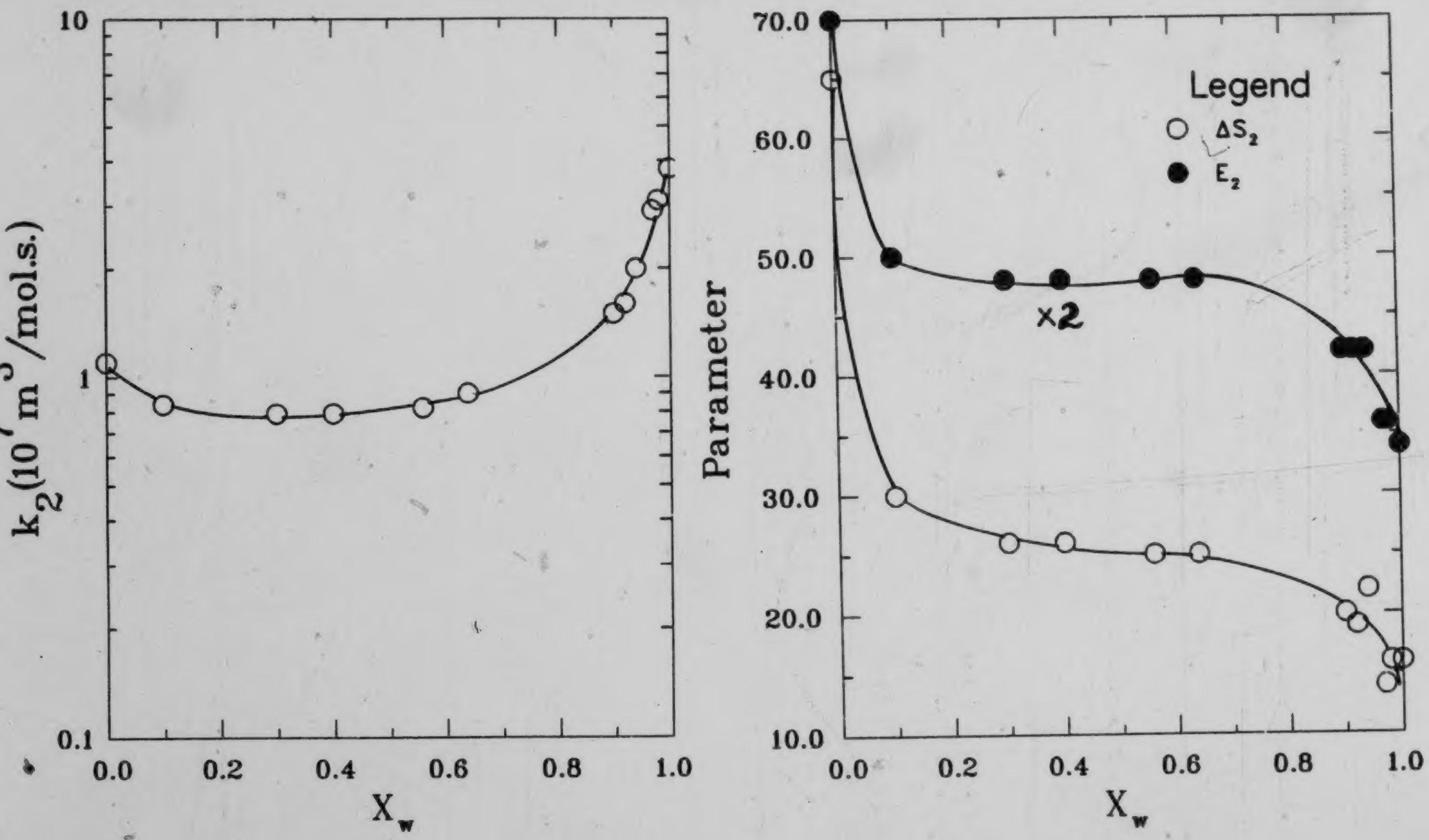

3.1.1(b) Reaction of e_s^- with Acetone

The different behavioral zones were firmly established by studying the reaction with nitrobenzene. Once this was done the reaction of e_s^- with the other scavengers were studied at the following compositions: x_{H_2O} = 0, 0.10, 0.64, 0.92, 0.97, 1.00. The observed rate constants (first-order) at each composition and temperature are in Figs.(3-15) to (3-20). The concentration range of acetone was 30-300 x $10^{-3} mol/m^3$.

The k_2 values at each temperature are listed in Table(3-3) and plotted according to the Arrhenius model in Fig.(3-21). The parameters for the reaction of e_s^- with acetone are in Table(3-4). The rate constant in water at 298K is 7.7 x $10^6 m^3/mol.s$. The literature results are 7.2 x $10^6 m^3/mol.s$. (53) and 8.0 x $10^6 m^3/mol.s$. (67). In pure alcohol the value of k_2 is 6.3 x $10^6 m^3/mol.s$. This value is within ±2% of that listed in the literature (53).

The composition dependence of k_2 for acetone is similar to that for nitrobenzene (Fig. 3-22). The temperature dependence fits the Arrhenius model. The composition dependence of activation parameters is also similar to that of nitrobenzene.

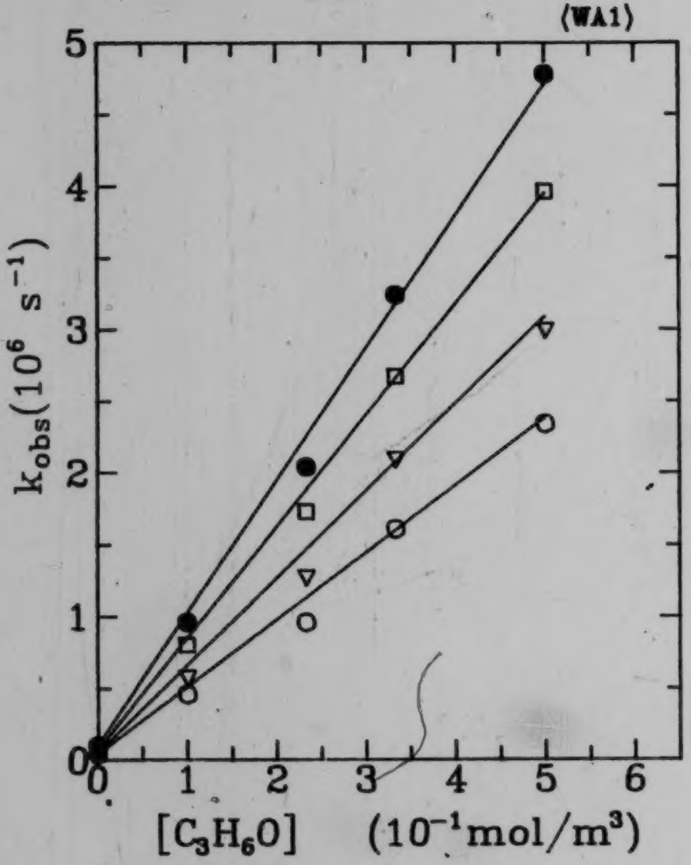

Fig. 3−15: H_2O

○ 275.3K ▽ 284.8K □ 298.1K
● 310.4K

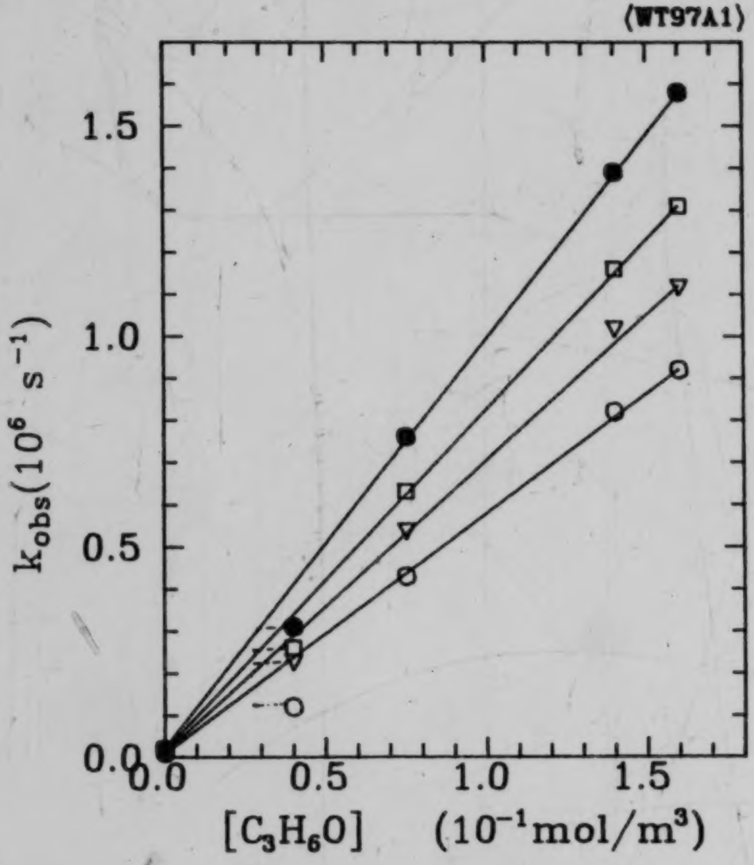

Fig. 3- 16a: t−BuOH/H_2O:3/97

○ 280.1K ▽ 288.1K □ 295.8K
● 305.7K

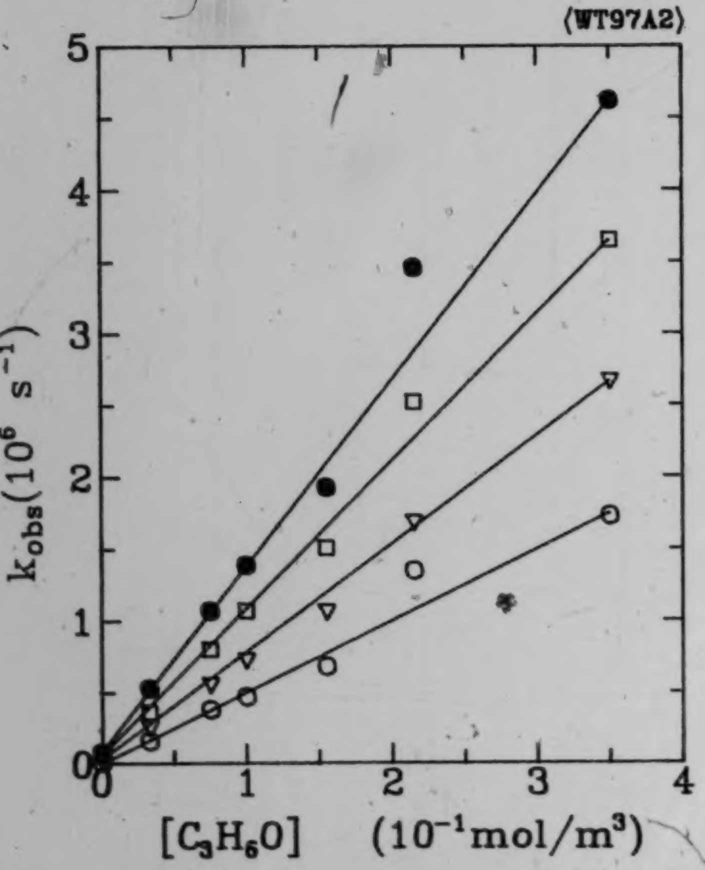

Fig. 3–16b: t–BuOH/H_2O:3/97

○ 276.6K ▽ 296.2K □ 314.2K

● 333.2K

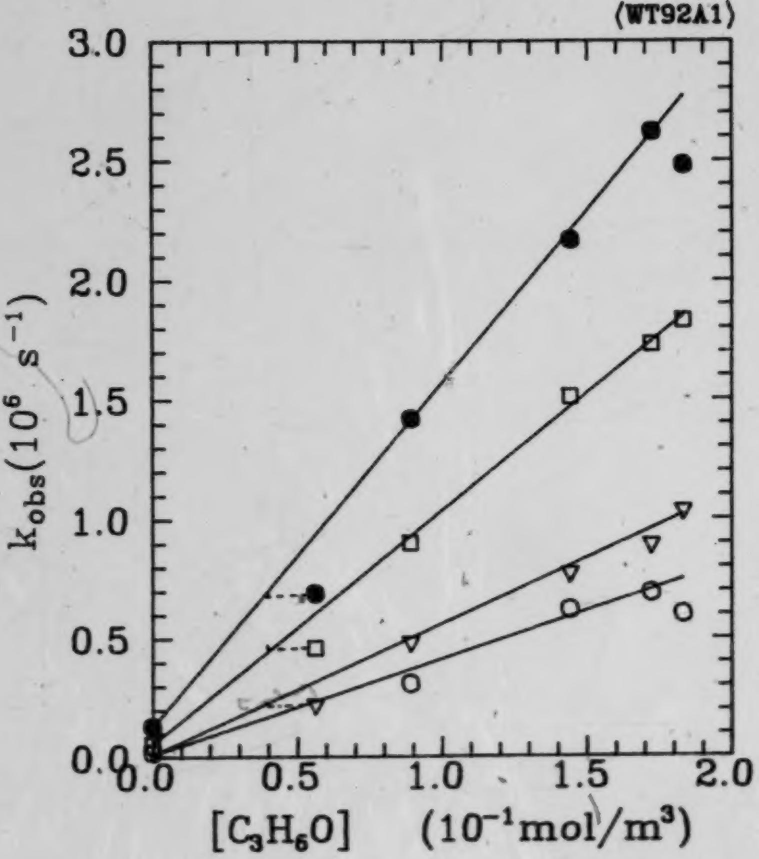

Fig. 3–17: t–BuOH/H_2O:8/92

○ 284.9K ▽ 296.6K □ 333.9K

● 368.9K

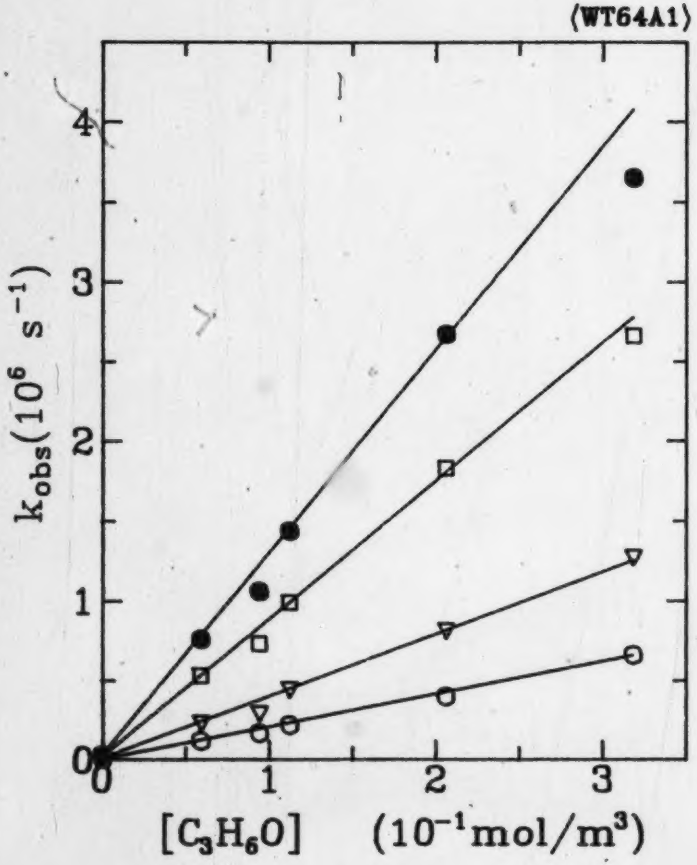

Fig. 3–18 a: t–BuOH/H_2O:36/64
○ 278.6K ▽ 295.8K □ 323.2K
● 348.5K

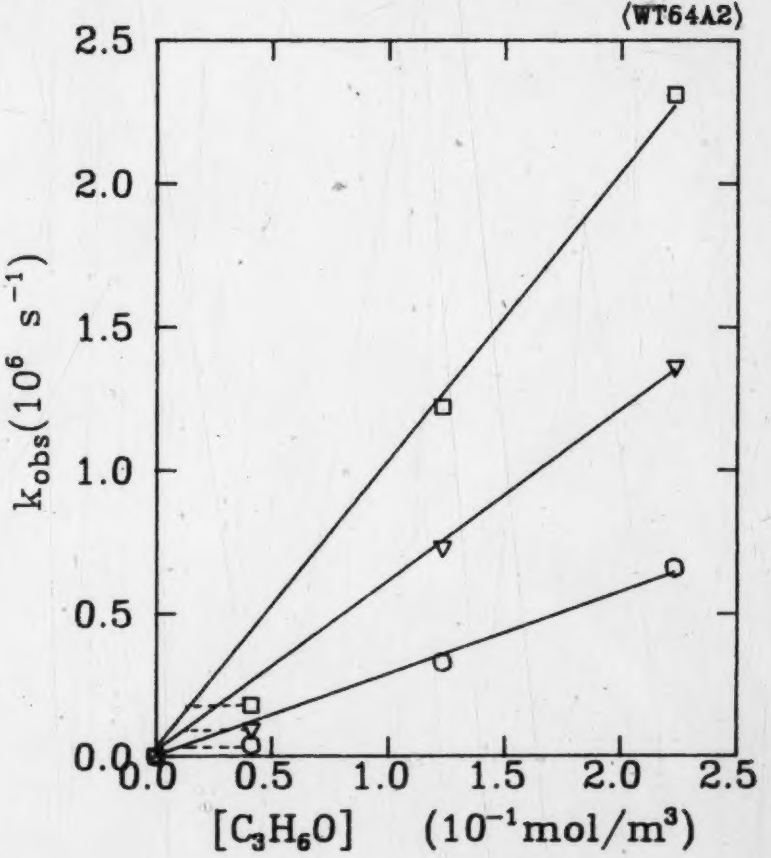

Fig. 3–18b: t–BuOH/H_2O:36/64
○ 285.2K ▽ 309.3K □ 337.0K

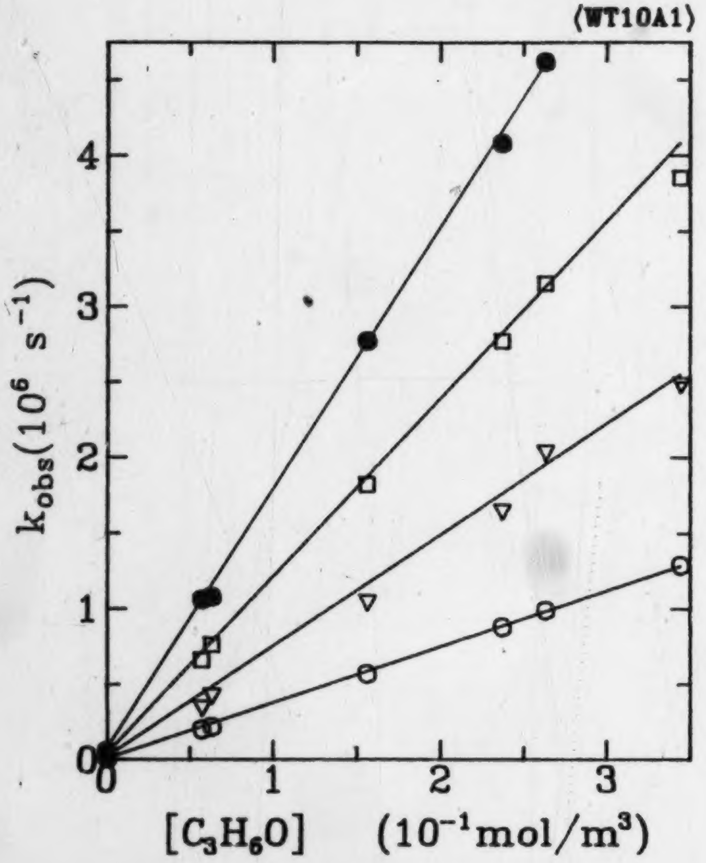

Fig. 3-19: t-BuOH/H_2O:90/10

○ 295.8K ▽ 314.1K □ 332.9K

● 352.5K

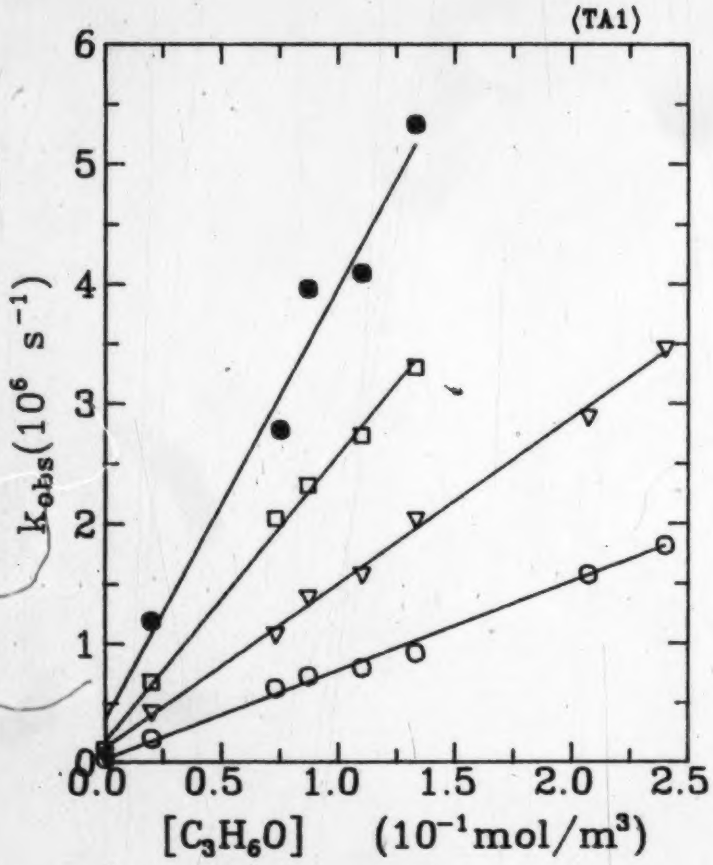

Fig. 3-20a: t-BuOH

○ 300.1K ▽ 313.2K □ 322.7K
● 332.6K

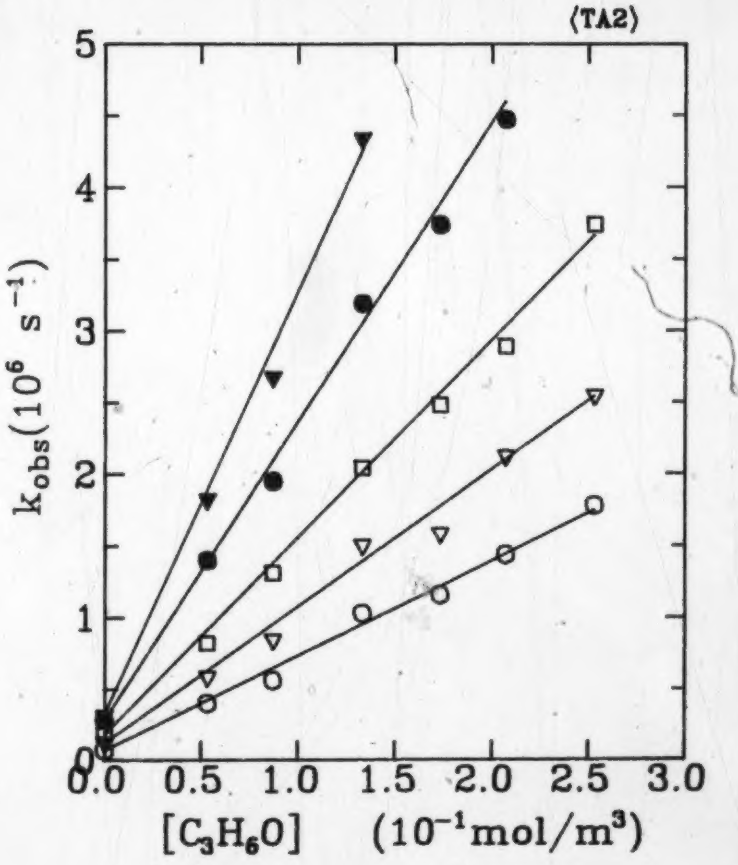

Fig. 3-20b: t-BuOH

○ 301.0K ▽ 308.2K □ 315.7K
● 323.5K ▼ 330.7K

Table 3-3:The values of second order rate constants for acetone in *t*-butanol/water

x_{H_2O}	T (K)	k_2 $10^7 m^3/mol.s$	x_{H_2O}	T (K)	k_2 $10^7 m^3/mol.s$
0.0	300.1	0.74	0.64	285.2	0.29
	313.2	1.38		309.3	0.60
	322.7	2.39		337.0	1.00
	332.6	3.56	0.92	284.9	0.42
0.0	301.0	0.67		296.6	0.55
	308.2	0.99		333.9	0.98
	315.7	1.41		368.9	1.44
	323.5	2.09	0.97	280.1	0.57
	330.7	2.96		288.1	0.69
0.10	295.8	0.37		295.8	0.81
	314.1	0.73		305.7	0.97
	332.9	1.18	0.97	276.6	0.50
	352.5	1.72		296.2	0.76
0.64	278.6	0.19		341.2	1.04
	295.8	0.39		333.2	1.31
	323.2	0.87	1.00	275.3	0.48
	348.5	1.28		284.8	0.61
				298.1	0.77
				310.4	0.92

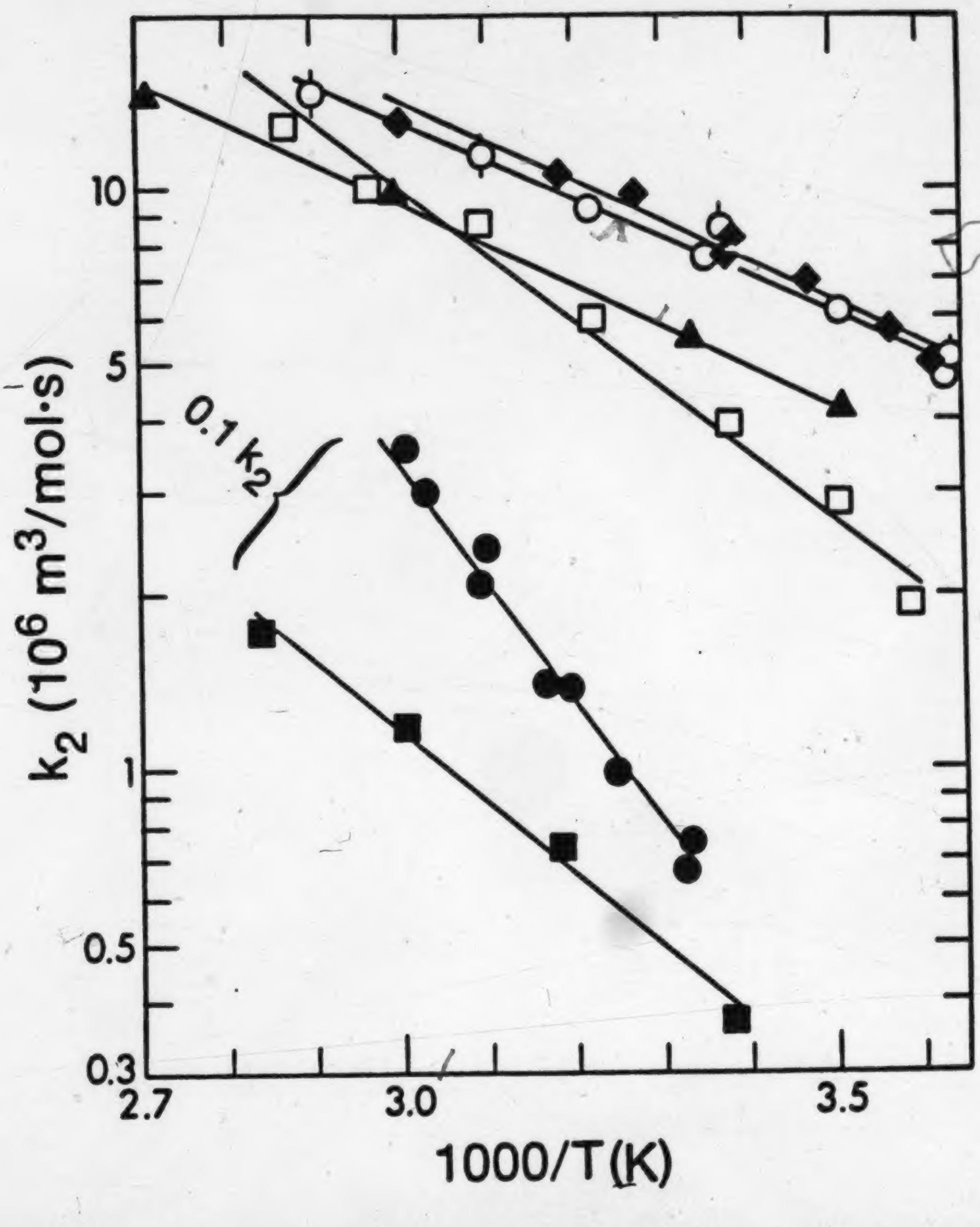

Fig. 3- 21 : e_s^- + acetone reaction in t-BuOH water mixtures.

x_{H_2O} : ● 0.00; ■ 0.10; □ 0.64; ▲ 0.92; ◆ 0.97; ○ 1.00.

Table 3-4: Reaction rate parameters for acetone in *t*-butanol/water

x_{H_2O}	k_2 $10^6(m^3/mol.s)$	E_2 (J/mol)	log A	$\Delta S_2^{\neq}$ (J/mol.K)
0.0	6.3	39	13.63	73
0.10	4.3	23	10.72	17
0.64	3.9	22	10.44	12
0.92	5.3	14	9.11	-13
0.97	8.0	13	9.23	-11
1.00	7.7	13	9.07	-14

Fig.3–22: k_2, E_2 and ΔS_2 for Acetone in t–BuOH/Water Mixtures.

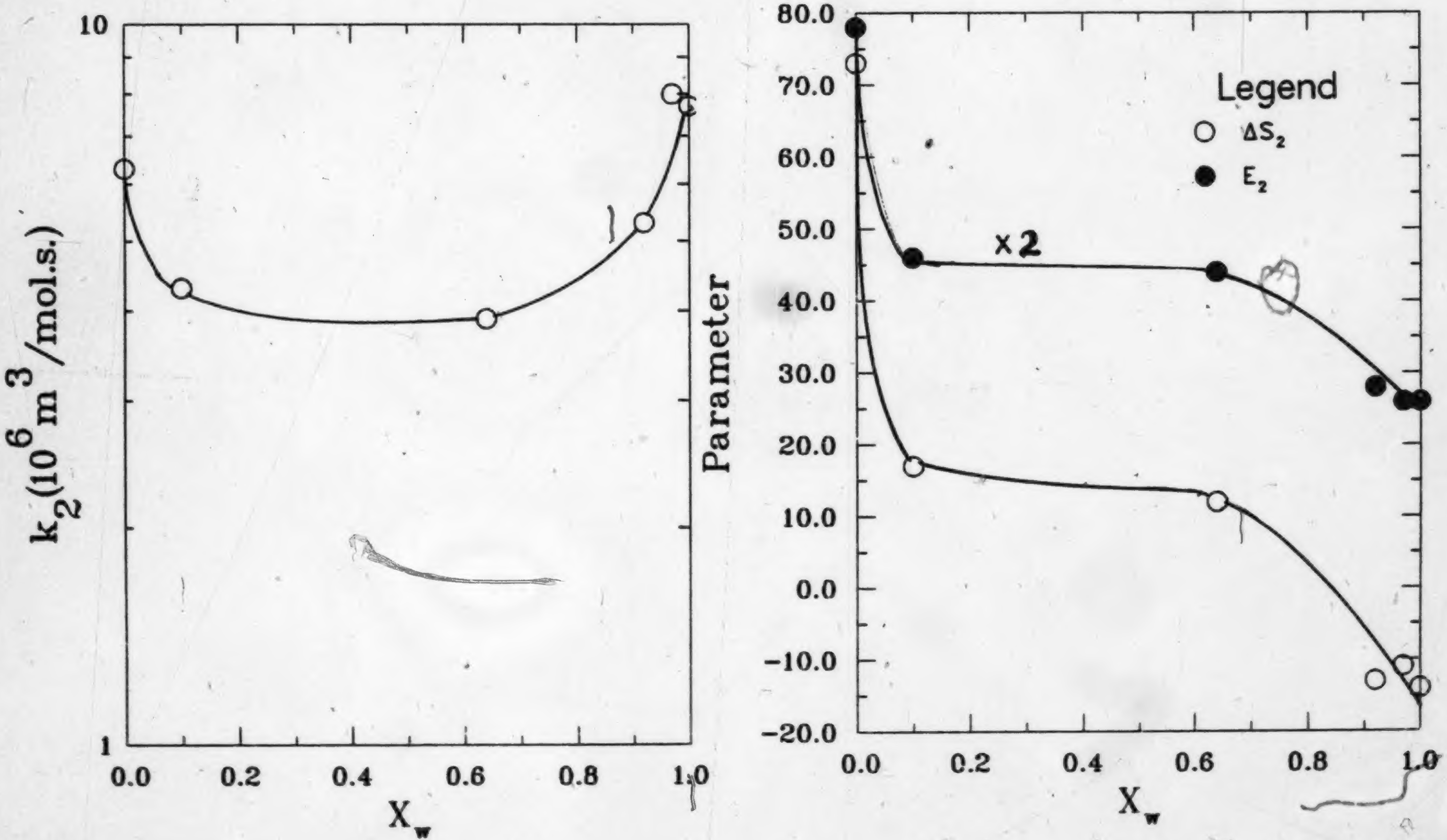

3.1.1(c) Reaction of e_s^- with Phenol

The observed rate constants are in Figs.(3-23) to (3-29). The concentration range of phenol is 1-20 mol/m^3. The second order rate constants at each temperature is listed in Table(3-5) and the Arrhenius plot are in Fig.(3-30). The rate parameters are in Table(3-6).

Phenol is a poor scavenger of electrons. The value of k_2 in water at room temperature is about three orders of magnitude less than that for the nearly diffusion controlled e_s^- + nitrobenzene reaction. But in pure alcohol k_2 for phenol is lower than that for nitrobenzene by only one order of magnitude. When water is added to *t*-BuOH , k_2 decreases through x_{H_2O} =0.1, in contrast to k_2 for the reaction with efficient scavengers nitrobenzene and acetone (Fig. 3-31). Thus solvent effects play a larger role in the reactions of inefficient scavengers.

The energies of activation for the e_s^- + phenol reaction in *t*-butanol/water mixtures are similar to that for the nitrobenzene reaction (Fig. 3-31). Therefore the differences in rate constants are due to changes of entropies of activation rather than that of energies.

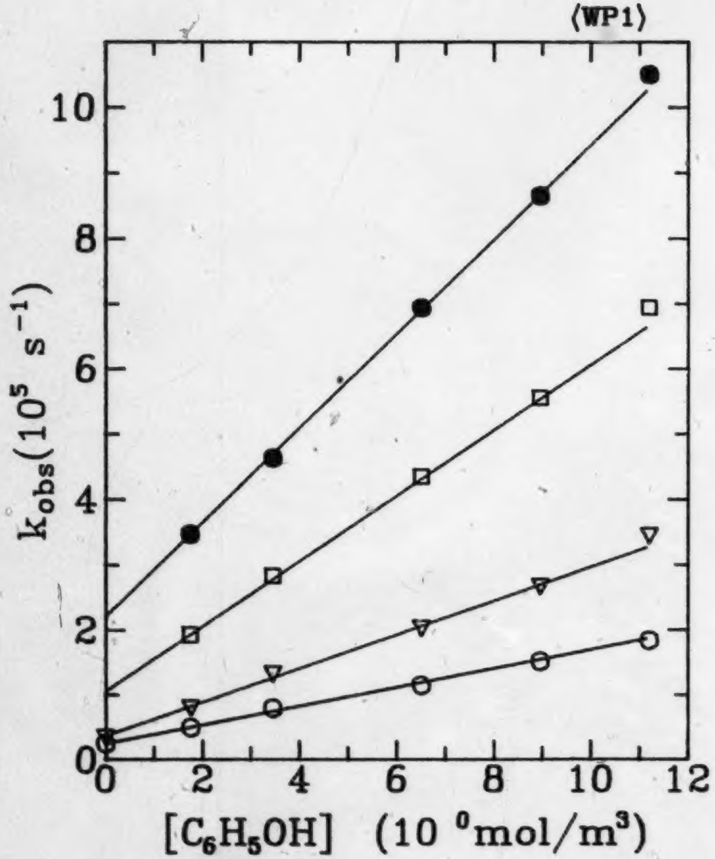

Fig. 3−23a: H_2O

○ 278.9K ▽ 296.1K □ 323.4K
● 350.6K

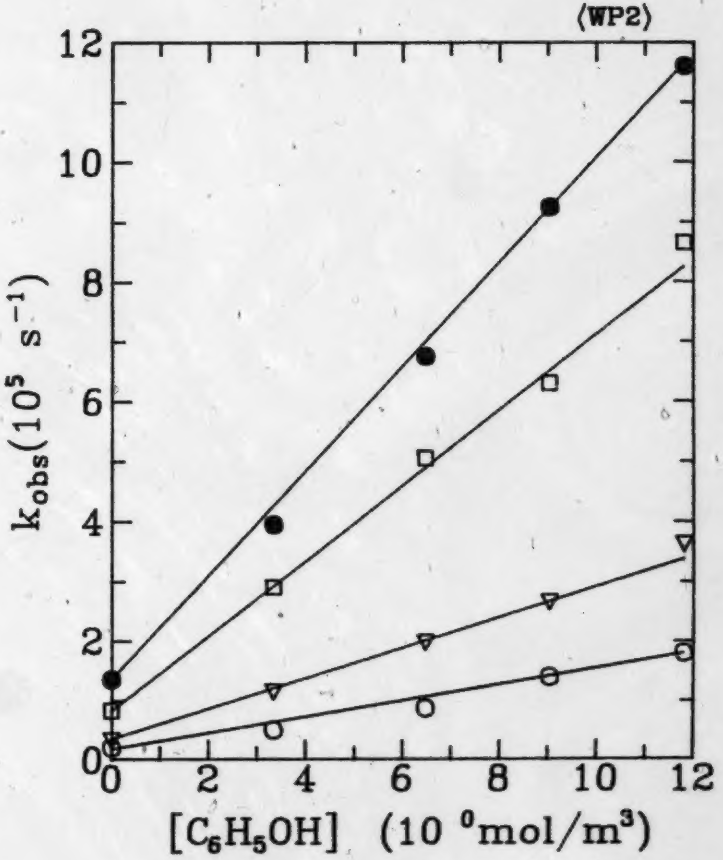

Fig. 3−23b: H_2O

○ 274.7K ▽ 296.0K □ 334.3K
● 362.6K

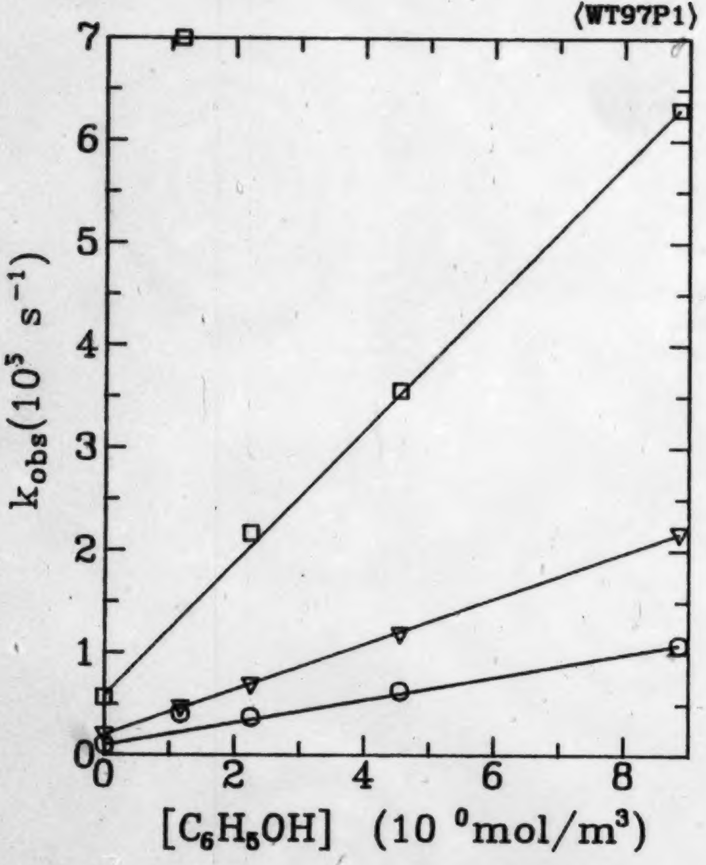

Fig. 3–24a: t–BuOH/H_2O:3/97

○ 274.9K ▽ 296.0K □ 347.9K

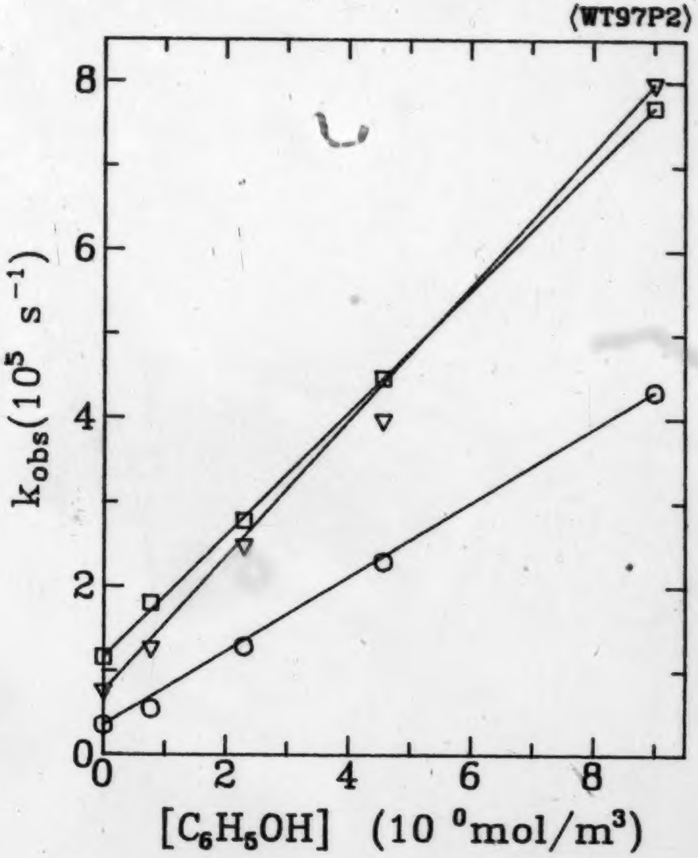

Fig. 3–24b: t–BuOH/H_2O:3/97

○ 323.2K ▽ 388.8K □ 368.0K

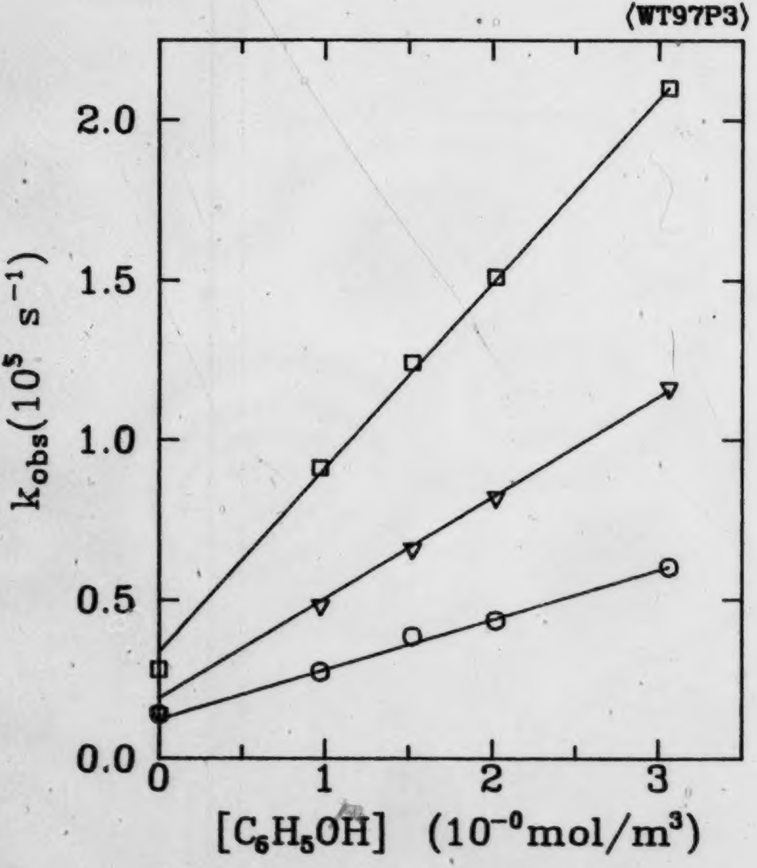

Fig. 3–24C: t–BuOH/H_2O:3/97

○ 284.7K ▽ 305.3K □ 334.9K

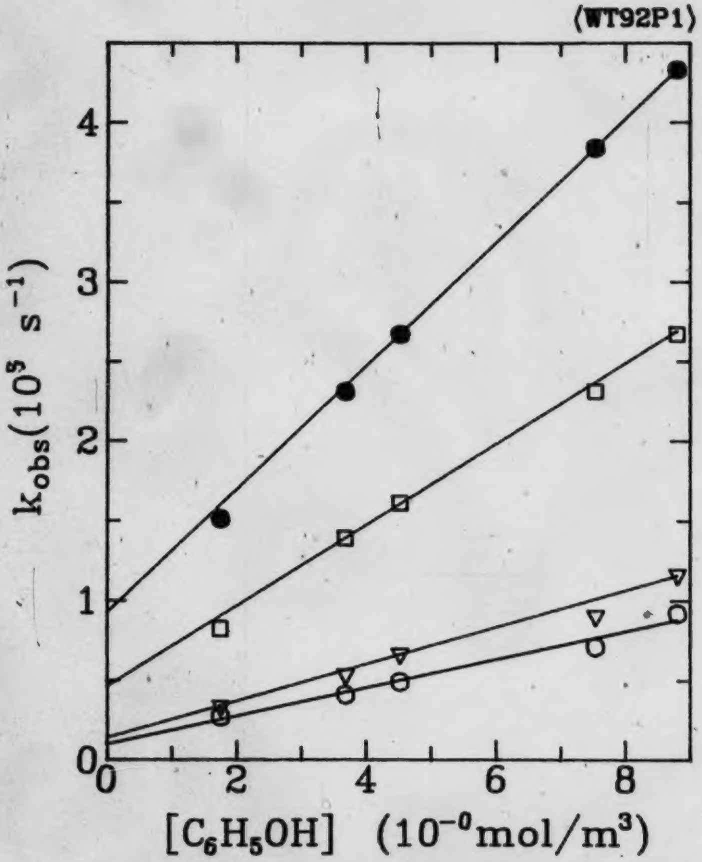

Fig. 3–25a: t–BuOH/H_2O:8/92
○ 284.1K ▽ 296.4K □ 333.8K
● 368.9K

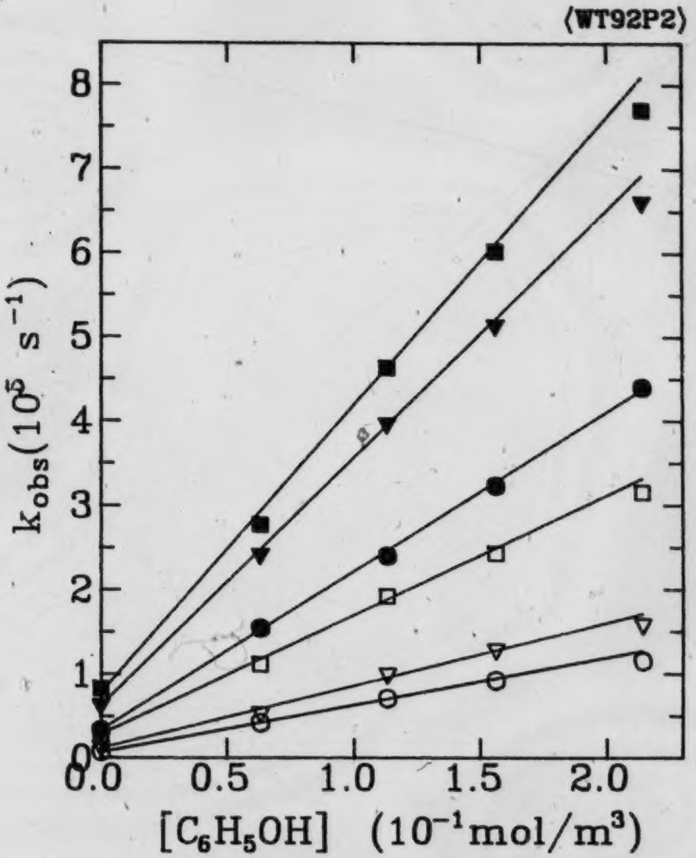

Fig. 3–25b: t–BuOH/H_2O:8/92
○ 275.9K ▽ 286.3K □ 309.2K
● 323.6K ▼ 345.7K ■ 358.1K

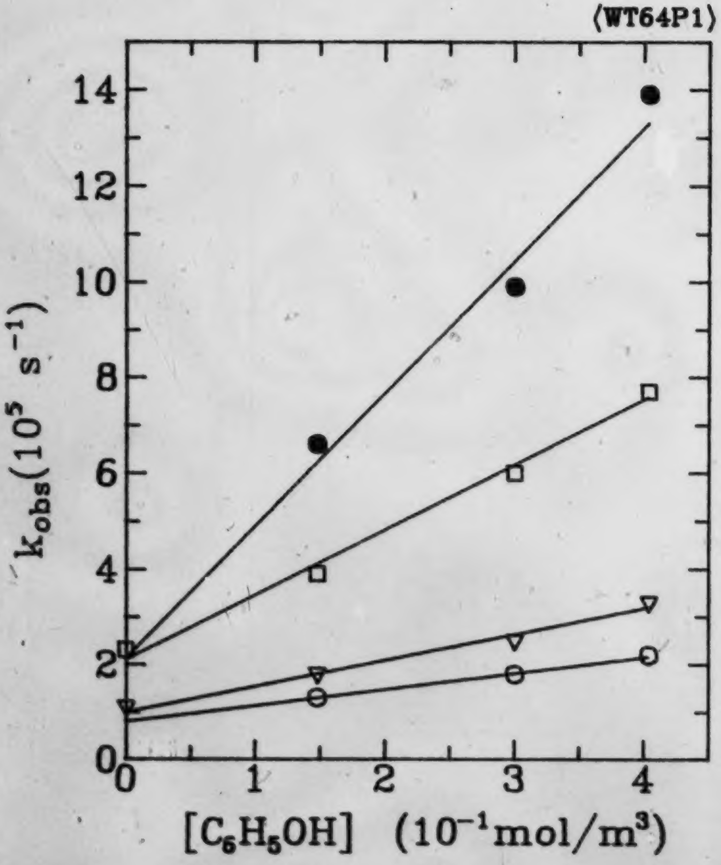

Fig. 3−26a: t−BuOH/H_2O:36/64
○ 282.4K ▽ 296.1K □ 323.6K
● 348.8K

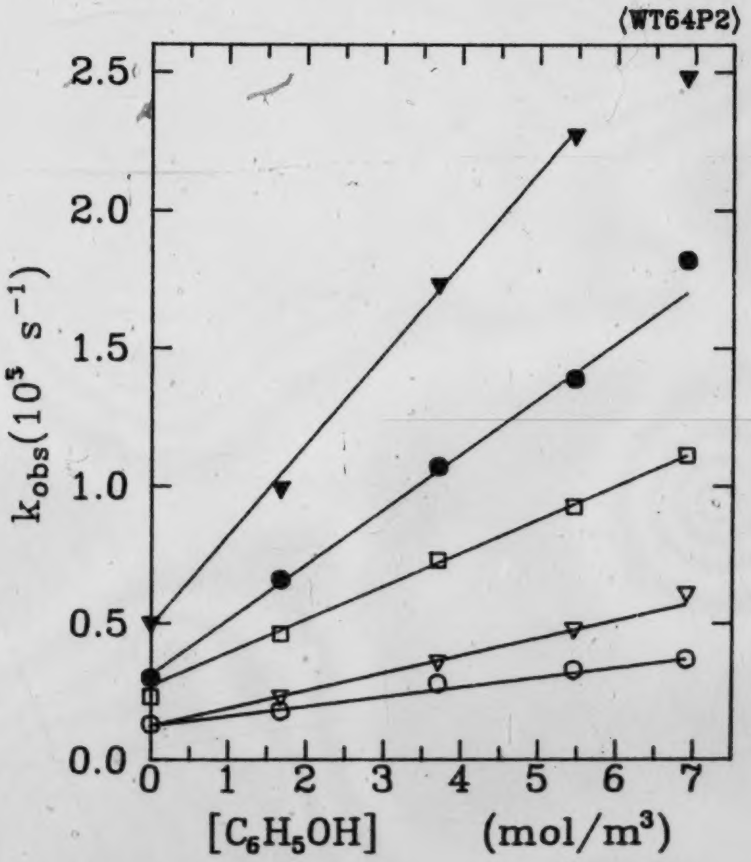

Fig. 3−26b: t−BuOH/H_2O:36/64
○ 283.1K ▽ 296.3K □ 318.6K
● 338.6K ▼ 358.0K

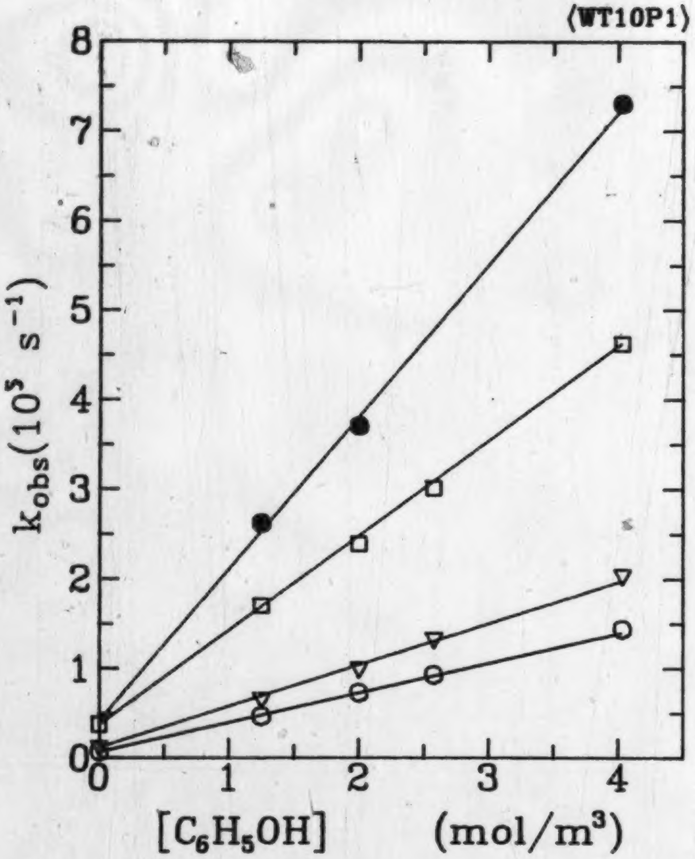

Fig. 3-28: t-BuOH/H_2O:90/10

○ 283.4K ▽ 295.4K □ 324.2K
● 348.9K

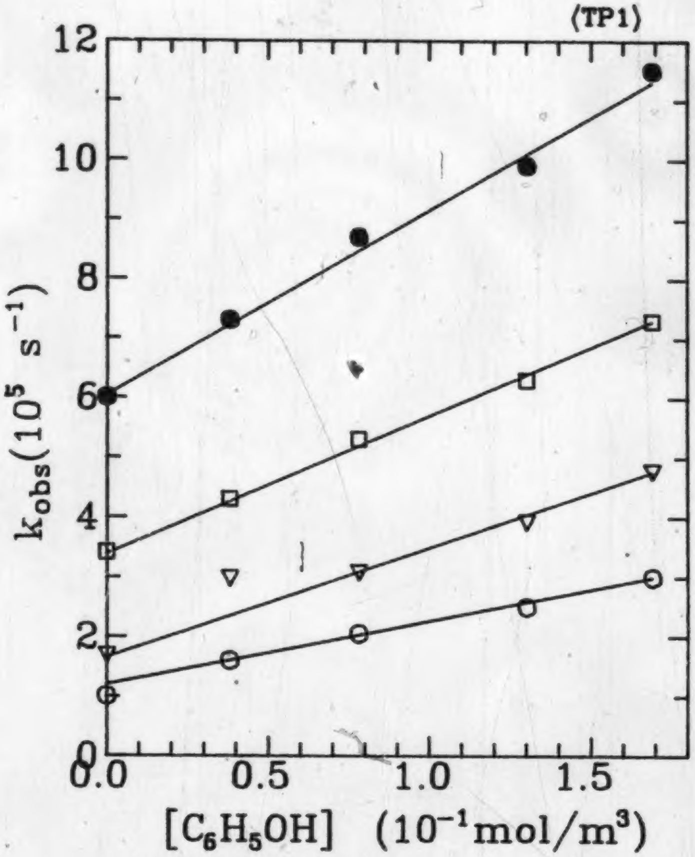

Fig. 3-29a: t-BuOH

○ 300.8K ▽ 314.1K □ 323.6K
● 333.0K

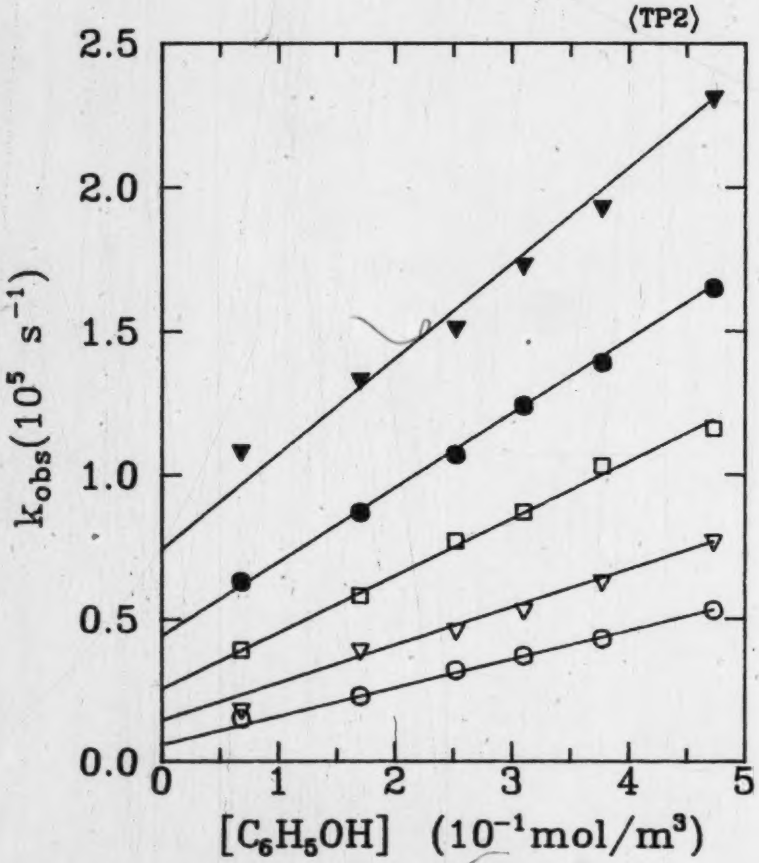

Fig. 3-29b: t-BuOH

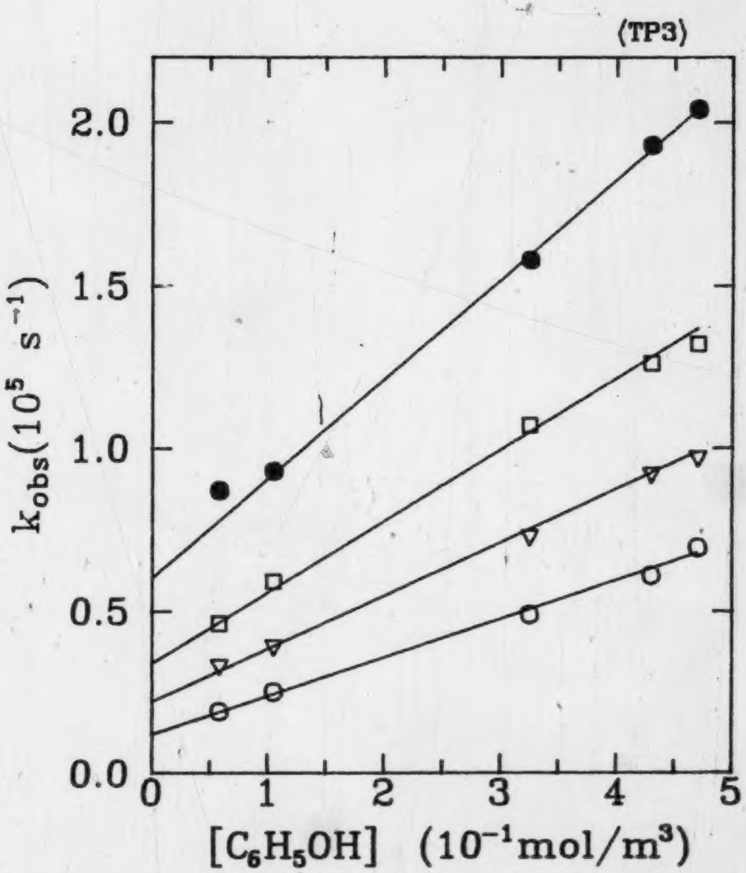

Fig. 3-29c: t-BuOH

Table 3-5:The values of second order rate constants for phenol in *t*-butanol/water

x_{H_2O}	T (K)	k_2 $10^4(m^3/mol.s)$
0.0	300.8	10.60
	314.1	17.60
	323.6	22.8
	333.0	30.80
0.0	300.8	9.90
	308.4	13.10
	318.6	19.7
	328.9	25.80
	337.0	33.30
0.0	305.6	11.90
	315.8	16.30
	325.4	21.90
	334.5	30.50
0.10	283.4	3.30
	295.4	4.70
	324.2	10.60
	348.9	16.90
0.64	282.4	0.34
	296.1	0.54
	323.6	1.36
	348.8	2.76
0.64	283.1	0.39

	296.3	0.63
	318.6	1.21
	338.6	2.00
	358.0	3.31
0.92	284.1	0.89
	296.4	1.10
	333.8	2.54
	368.9	4.10
0.92	275.9	0.56
	286.3	0.74
	309.2	1.43
	323.6	1.88
	345.7	2.96
	358.1	3.44
0.97	274.9	1.16
	296.0	2.18
	347.9	6.47
0.97	323.2	4.56
	368.0	8.10
	388.8	7.20
0.97	284.7	1.55
	315.3	3.15
	334.9	5.82
1.00	278.9	1.45
	296.1	2.60
	323.4	4.90

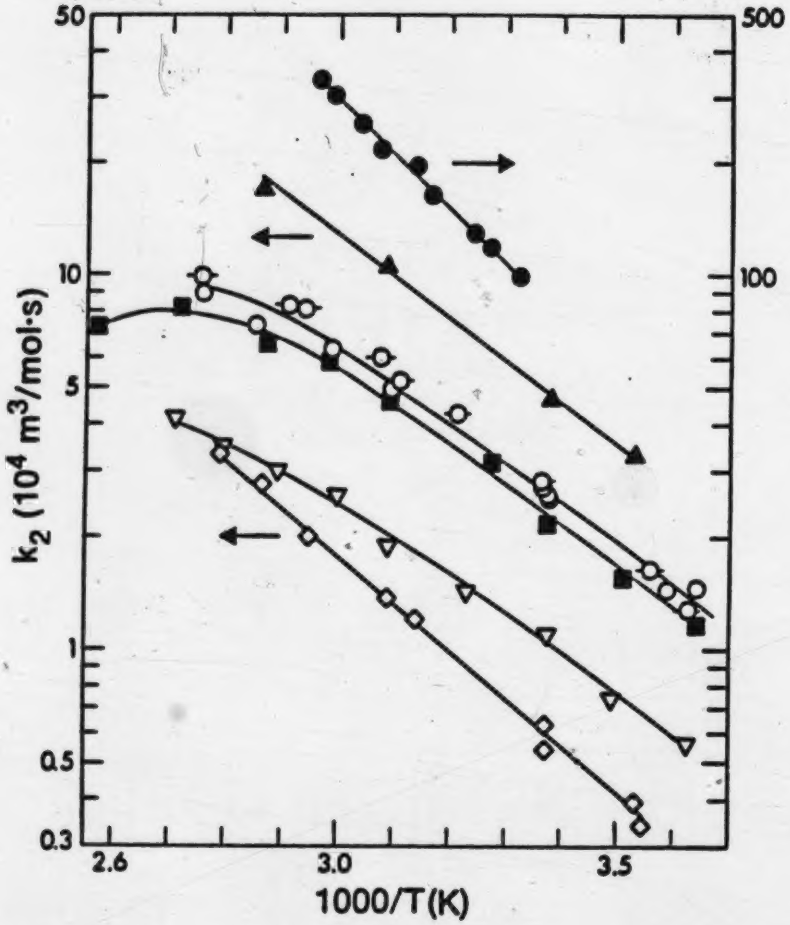

Fig. 3–30: e_s^- + C_6H_5OH reaction in t–BuOH water mixtures.

x_{H_2O}: ● 0.00; ■ 0.10; □ 0.64; ▲ 0.92; ◆ 0.97; ○ 1.00.

Table 3-6: Reaction rate parameters for phenol in *t*-butanol/water

x_{H_2O}	k_2 $10^4(m^3/mol.s)$	E_2 (J/mol)	log A	$\Delta S_2^{\neq}$ (J/mol.K)
0	89	28	10.84	20
0.10	5.1	22	8.56	-23
0.64	0.63	24	7.99	-34
0.92	1.1	19	7.40	-46
0.97	2.4	18	7.53	-44
1.00	2.7	18	7.60	-42

Fig.3–31: k_2, E_2 and ΔS_2 for Phenol in t–BuOH/Water Mixtures.

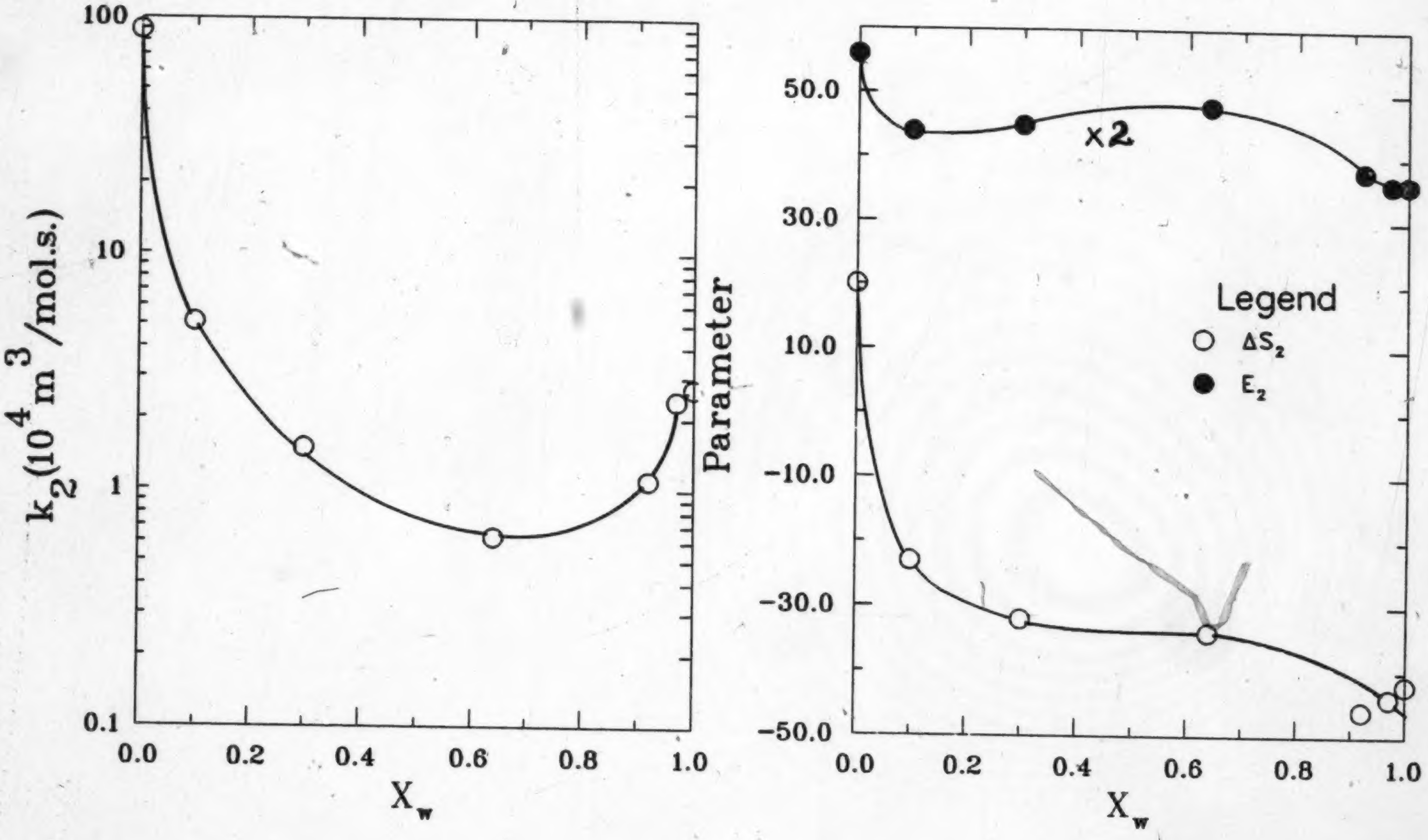

3.1.1(d) Reaction of e_s^- with Toluene

The observed first-order rate constants are in Figs.(3-32) to (3-37). The concentration range of toluene is 0.1-10 mol/m^3. The k_2 values at each temperature are in Table(3-7) and the Arrhenius plots in Fig.(3-38). The reaction rate parameters are in Table(3-8).

In pure alcohol the Arrhenius plot is curved and has a maximum at 318K. Tertiary butanol is a solid at 299K. Therefore the activation energy listed in the table was calculated in the temperature range 300-318K.The composition and temperature dependence of rate constants are similar to those for phenol (Fig. 3-39).

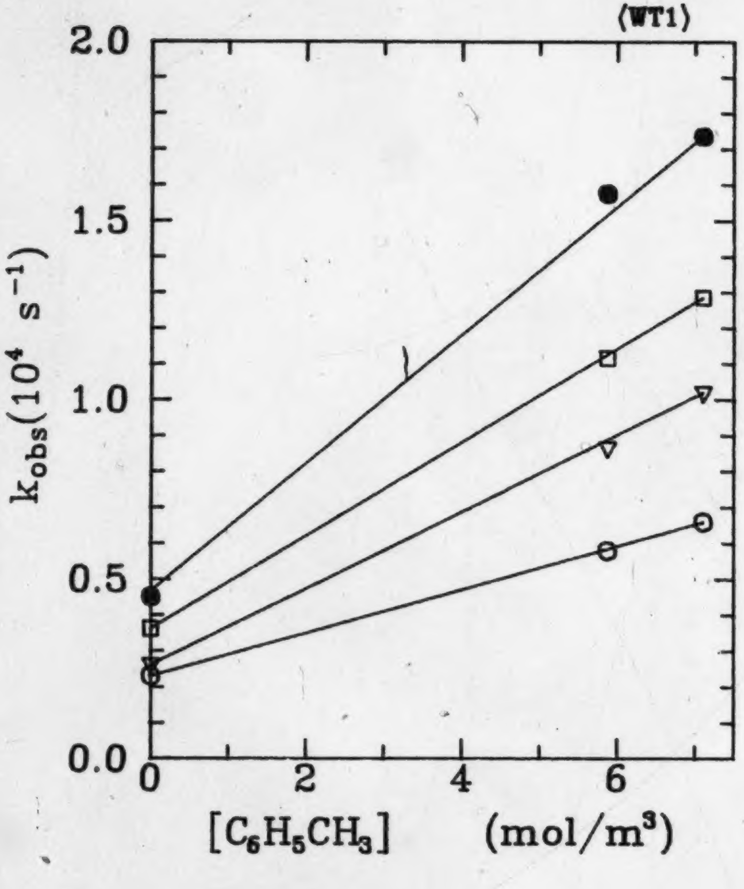

Fig. 3−32: H_2O
○ 275.4K ▽ 296.0K □ 306.6K
● 318.7K

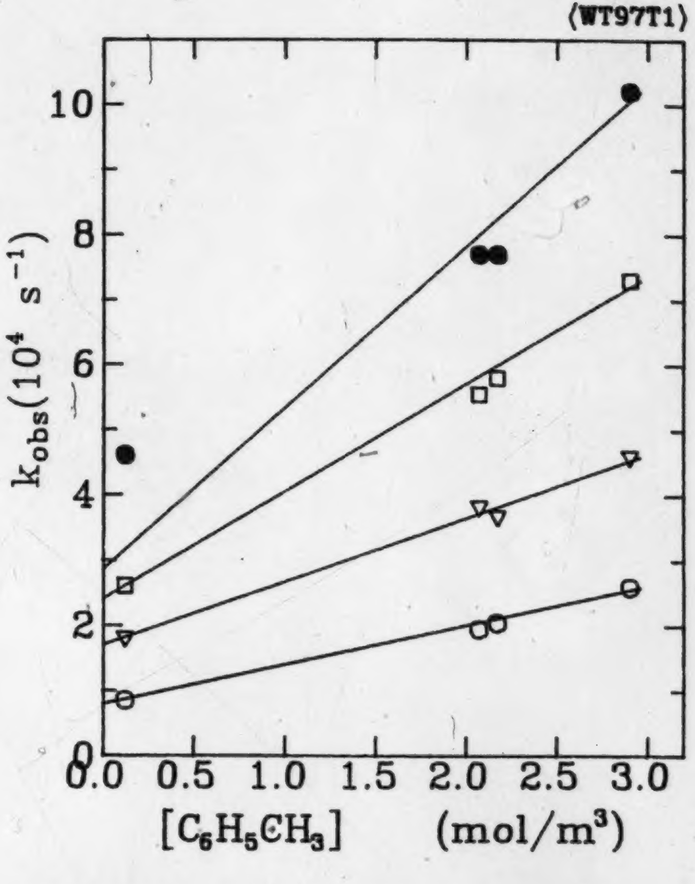

Fig. 3−33: t−BuOH/H_2O:3/97
○ 280.7K ▽ 296.0K □ 316.2K
● 339.6K

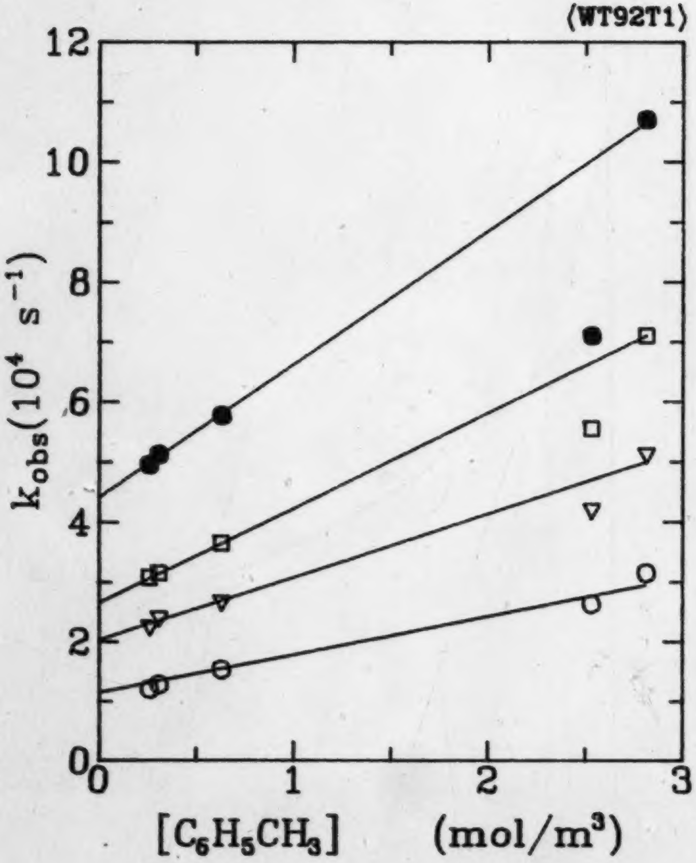

Fig. 3–31: t–BuOH/H_2O:8/92
○ 297.0K ▽ 315.2K □ 330.4K
● 346.3K

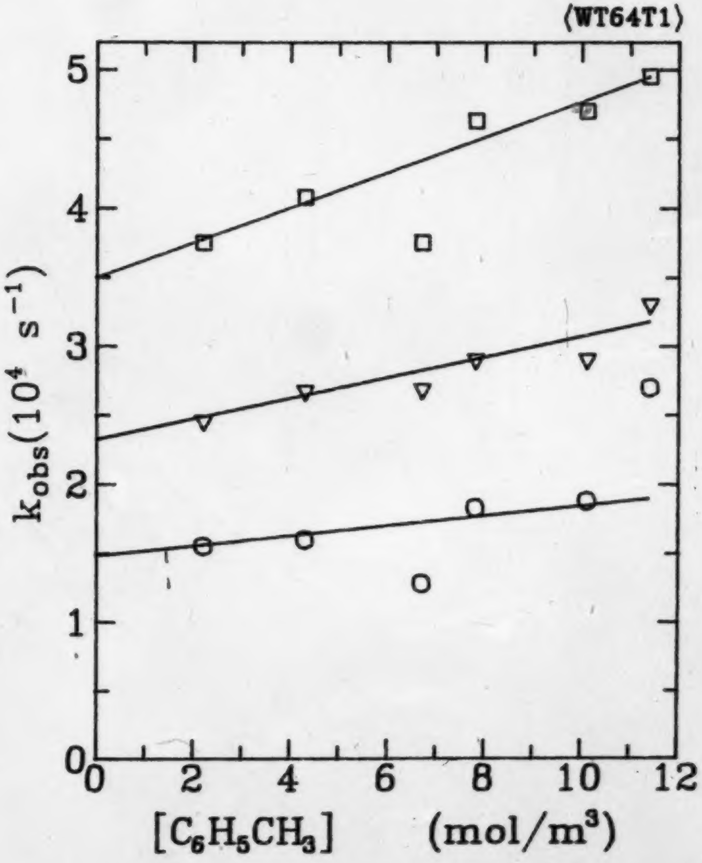

Fig. 3–35a: t–BuOH/H_2O:36/64
○ 295.5K ▽ 319.5K □ 331.9K

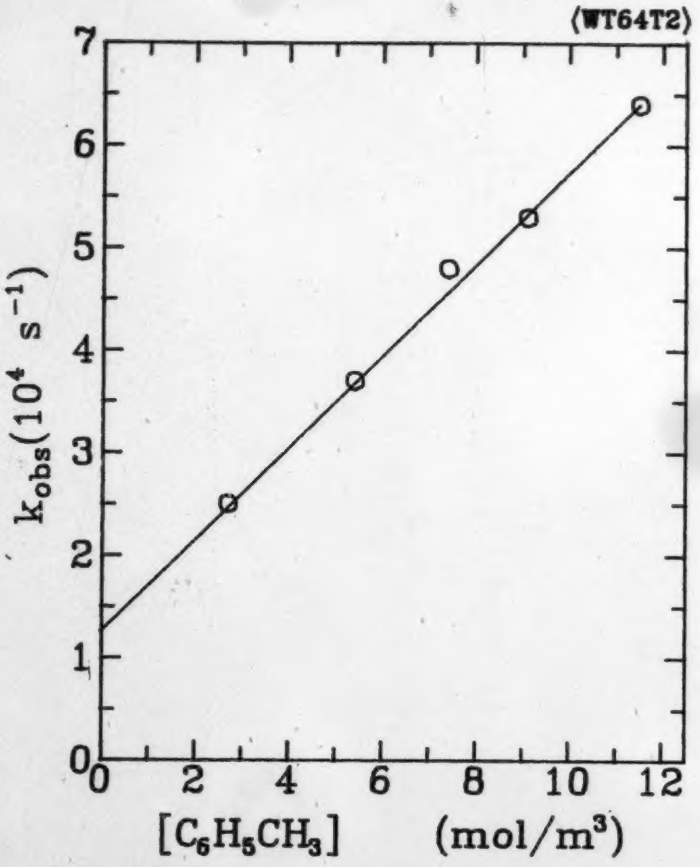

Fig. 3-35 b: t-BuOH/H_2O:36/64
○ 297.6K

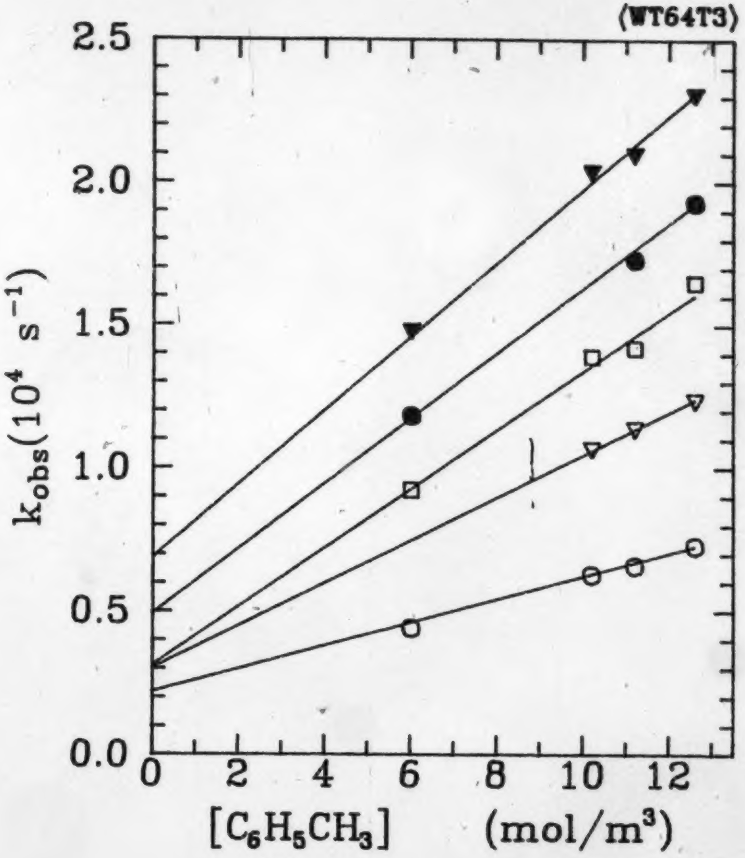

Fig. 3-35c: t-BuOH/H_2O:36/64
○ 296.8K ▽ 313.9K □ 324.2K
● 334.5K ▼ 359.0K

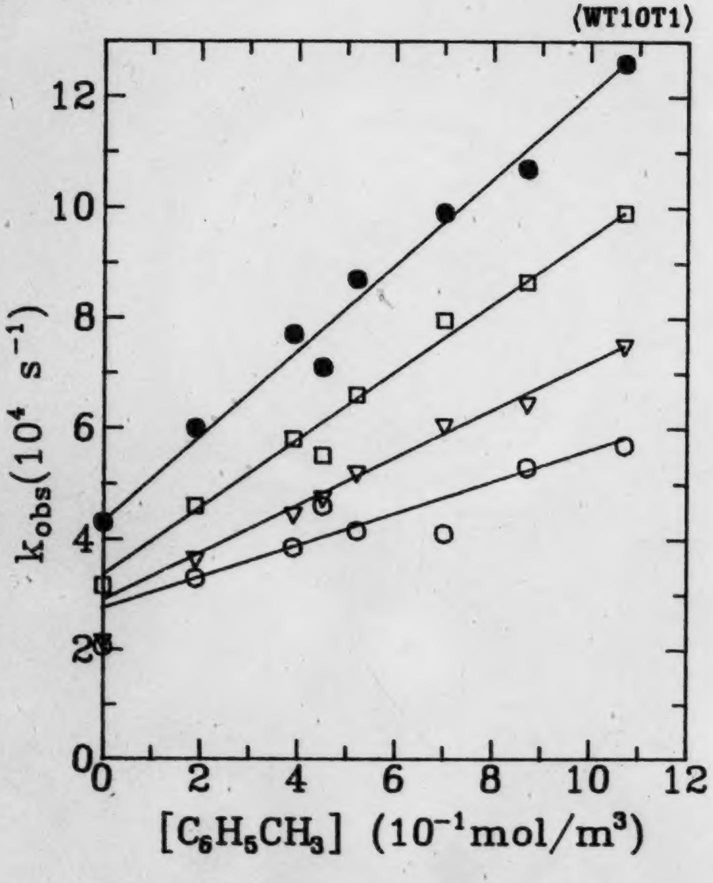

Fig. 3–36: t–BuOH/H_2O:90/10

○ 296.0K ▽ 308.0K □ 318.6K
● 328.8K

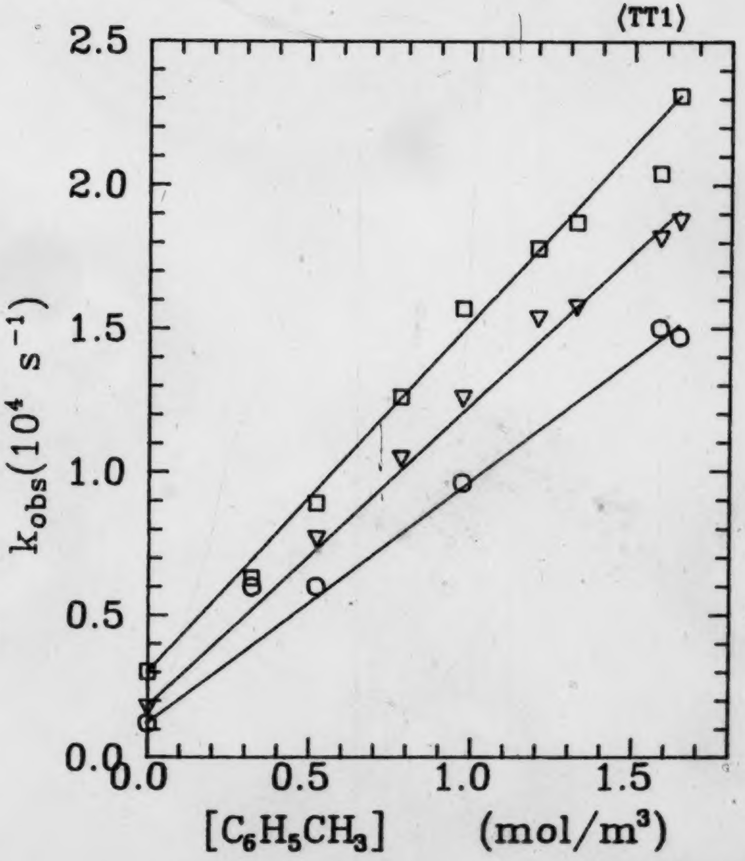

Fig. 3–37a: t–BuOH

○ 300.8K ▽ 307.6K □ 316.9K

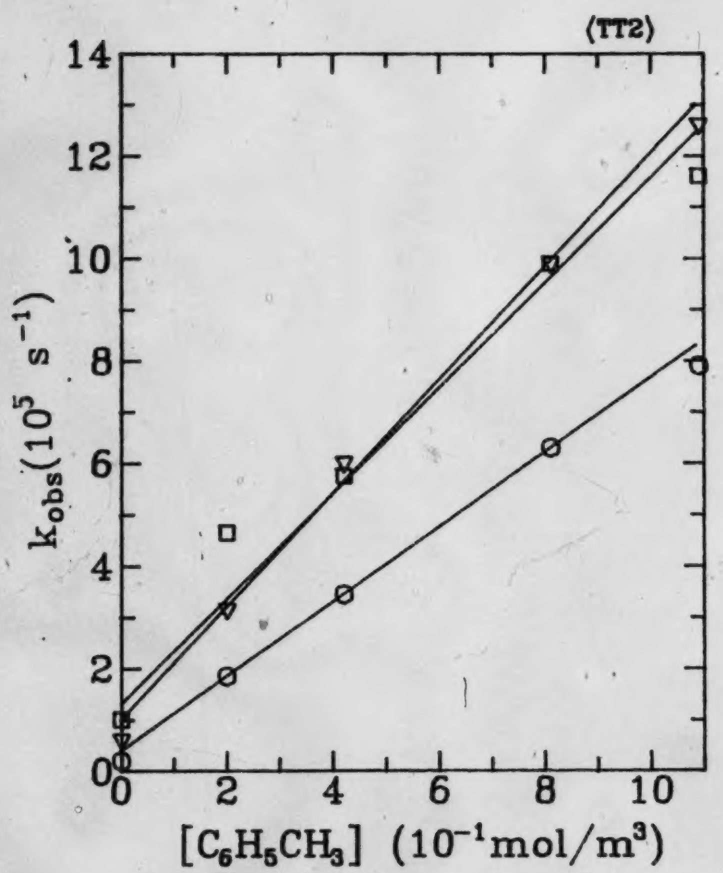

Fig. 3–37b: t–BuOH

○ 299.3K ▽ 313.8K □ 323.1K

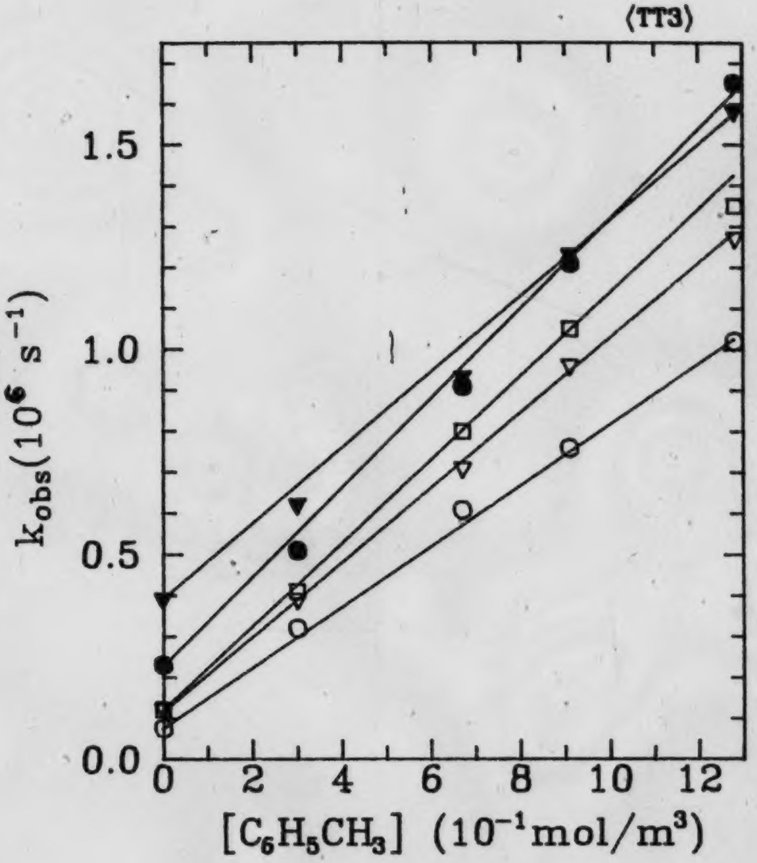

Fig. 3–37c: t–BuOH

○ 301.7K ▽ 306.1K □ 310.7K
● 319.9K ▼ 328.4K

Table 3-7:The values of second order rate constants for toluene in *t*-butanol/water

x_{H_2O}	T (K)	k_2 $10^5(m^3/mol.s)$
0.0	300.8	8.20
	307.6	9.97
	316.9	12.20
0.0	299.3	7.15
	313.8	11.10
	323.1	10.30
0.0	301.7	7.40
	306.1	9.17
	310.7	10.20
	319.9	11.20
	328.4	9.55
0.10	296.0	2.87
	308.0	4.30
	318.6	6.28
	328.8	8.26
0.64	295.5	0.37
	319.5	0.77
	331.9	1.28
0.64	297.6	0.36
0.64	296.8	0.39
	313.9	0.75
	324.2	1.04

	334.5	1.14
	359.0	1.29
0.92	297.0	0.64
	315.2	1.04
	330.4	1.59
	346.3	2.23
0.97	280.7	0.67
	296.0	0.97
	316.2	1.65
	339.6	2.46
1.00	275.4	0.61
	296.0	1.06
	306.6	1.30
	318.7	1.86

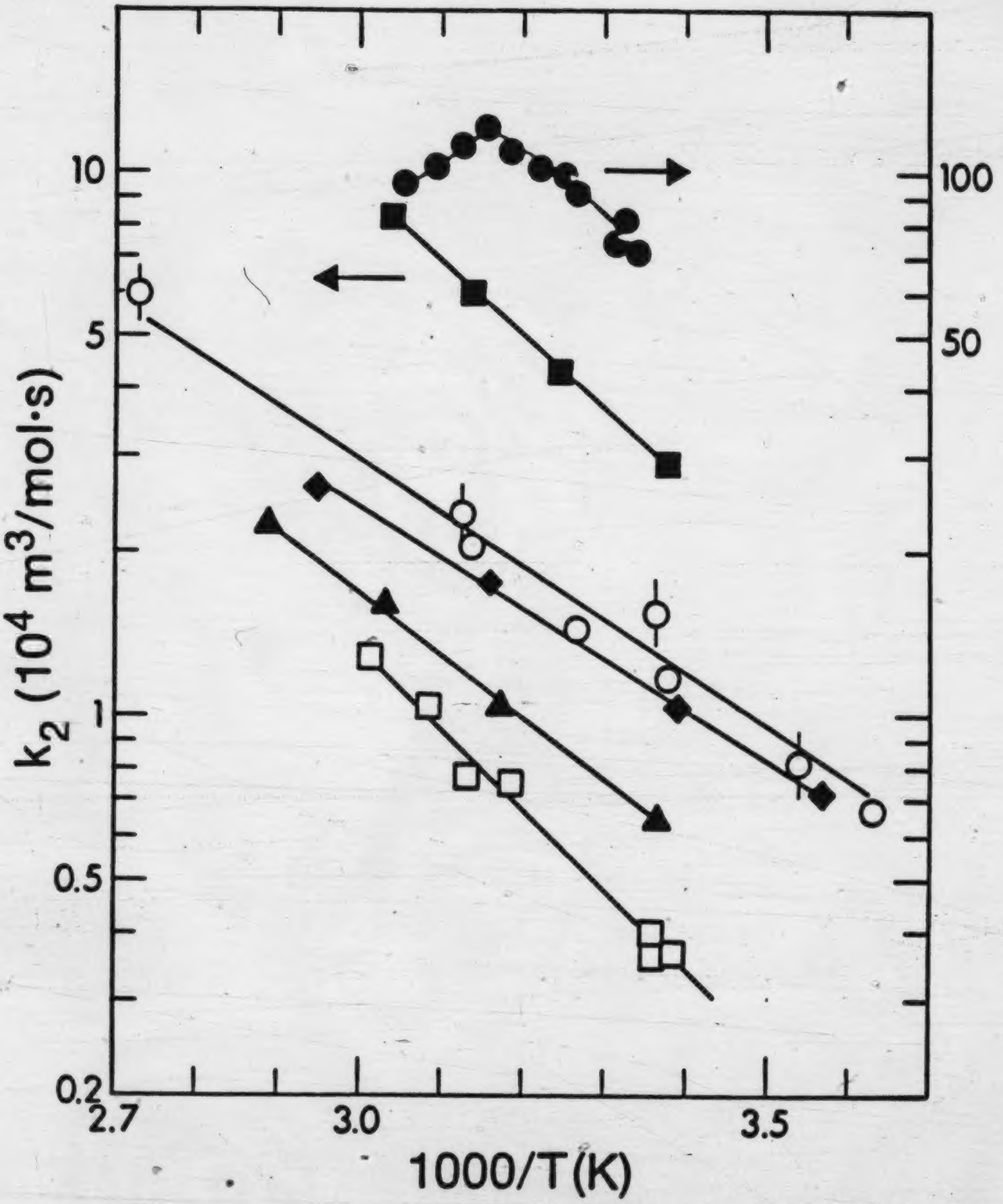

Fig. 3–38: $e_s^- + C_6H_5CH_3$ reaction in t–BuOH/ water mixtures.(Symbols:Fig.3–13)

Table 3-8: Reaction rate parameters for toluene in t-butanol/water

x_{H_2O}	k_2 $10^4 (m^3/mol.s)$	E_2 (J/mol)	log A	$\Delta S_2^{\neq}$ (J/mol.K)
0	67	31	11.08	25
0.10	3.1	26	9.07	
0.64	0.40	28	8.46	-26
0.92	0.66	22	7.65	-41
0.97	1.1	18	7.25	-48
1.00	1.3	19	7.43	-45

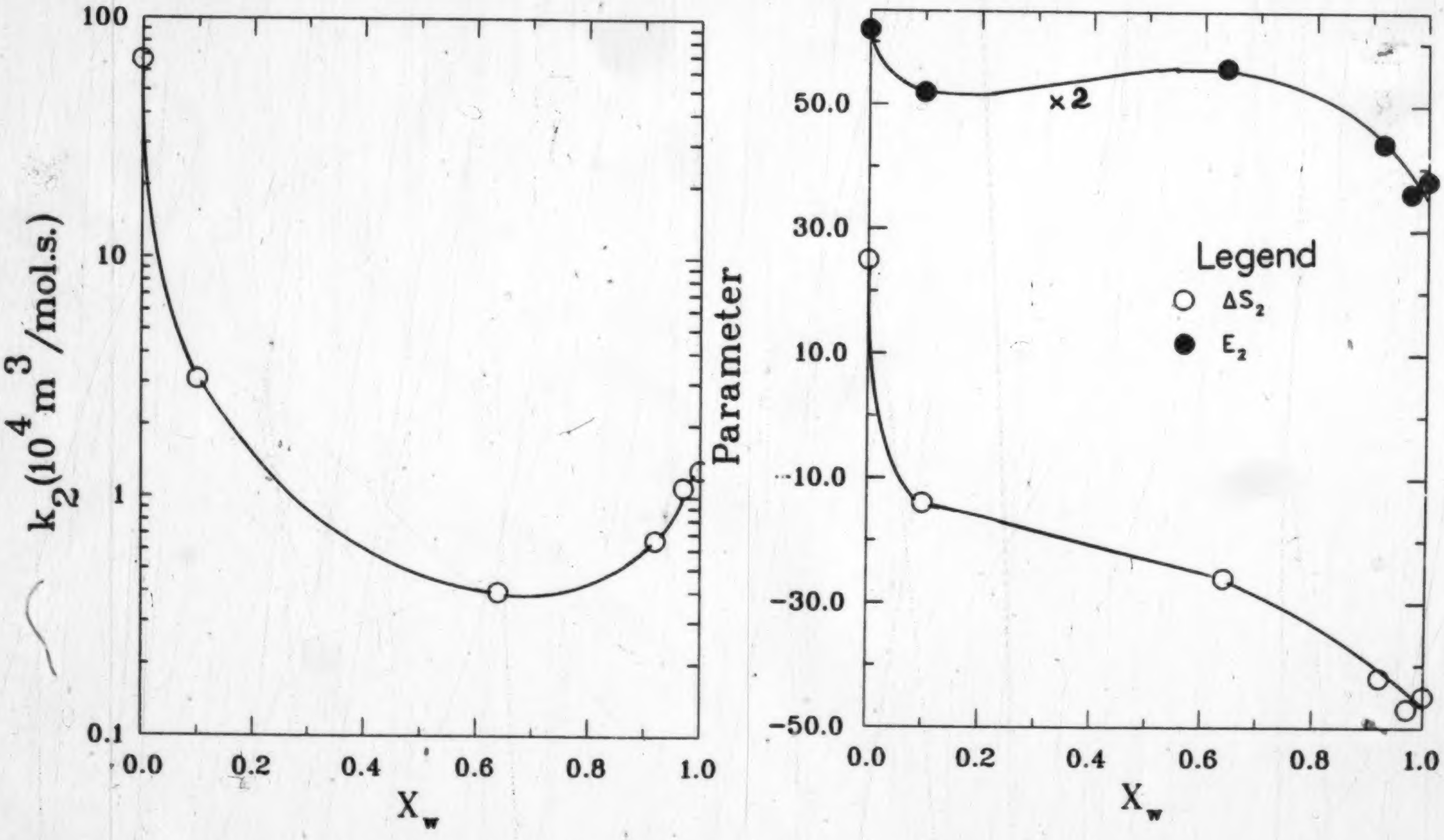

Fig.3–39: k_2, E_2 and ΔS_2 for Toluene in t–BuOH/Water Mixtures.

3.1.2 Iso-butanol/Water and 2-Butanol/Water Mixtures

Both *i*-BuOH and 2-BuOH are only partially miscible with water. Miscibility increases in the order *i*-BuOH < 2-BuOH < *t*-BuOH , with *t*-BuOH being completely miscible with water. Kinetic studies were done only in the miscible regions.

3.1.2(a) Reaction of e_s^- with Nitrobenzene

The mixture compositions for *i*-BuOH /water were: x_{H_2O} = 0, 0.05, 0.10, 0.20, 0.35, 0.45, 0.98, 1.00 whereas for 2-BuOH /water mixtures they were : 0, 0.10, 0.20, 0.35, 0.50, 0.64, 0.68, 0.97, 0.98, 1.00. The regions of immiscibility respectively are x_{H_2O} = 0.45 - 0.98 and x_{H_2O} = 0.68 - 0.97.

The observed first-order rate constants for the *i*-BuOH /water systems are in Figs.(3-40) to (3-47) and for the 2-BuOH /water mixtures they are in Figs.(3-48) to (3-56). The concentration range for both systems are 5-50 $mmol/m^3$. The k_2 values are in Tables(3-9) and (3-10), and the Arrhenius plots in Fig.(3-57). The Arrhenius plots of solvents close to the immiscible regions are slightly curved. This is probably due to micro-phase separation at temperature extremums. The reaction rate parameters for these systems are listed in Table(3-11).

The k_2 values for e_s^- + nitrobenzene reaction in pure alcohol decrease in the order *t*-BuOH > 2-BuOH > *i*-BuOH (Fig. 3-59). When water is added the values of k_2 in primary and secondary alcohols initially increase slightly, and then does not change significantly with the water content. In contrast to these the rate constants in tertiary alcohols initially decrease (Fig. 3-58).The k_2 values at $x_{H_2O} \sim 0.10$ are similar. The rate constants are also similar in water-rich solvents. Differences among the k_2 values in various mixed butanol/water solvents are composition dependent as follows:

(a) $0 < x_{H_2O} < 0.10$, the values of k_2 in pure alcohols or mixed solvents are in the order *t*-BuOH > 2-BuOH > *i*-BuOH .

(b) $0.10 < x_{H_2O} < x_{a,im}$, where $x_{a,im}$ is the mol fraction of water in the alcohol-rich solvent closest to the immiscible region. This value is 0.45 for solvent mixtures of *i*-BuOH and 0.68 for those of 2-BuOH . The order of the k_2 values for the mixed solvents are 2-BuOH > *i*-BuOH > *t*-BuOH .

(c) x_{H_2O} = immiscible region,

(d) $x_{w,im} < x_{H_2O} < 1.00$, where $x_{w,im}$ is the mol fraction of water in the water-rich solvent closest to the immiscible region. This value is 0.98 for solvent mixtures of *i*-BuOH and 0.97 for those of 2-BuOH . In this region the rate constants are similar.

The temperature dependence of the rate constants fit the Arrhenius model. The energies of activation, E_2 , decrease in zone(a), do not change significantly in zone(b), and decrease in zone(c) and (d) (Fig. 3-59). Values of E_2 in different alcohols are in the order *t*-BuOH > 2-BuOH > *i*-BuOH . The extent of change in zone(a) is also in the same order. The composition dependence of the entropies of activation, $\Delta S_2^{\neq}$, are similar to those of E_2 (Fig. 3-60).

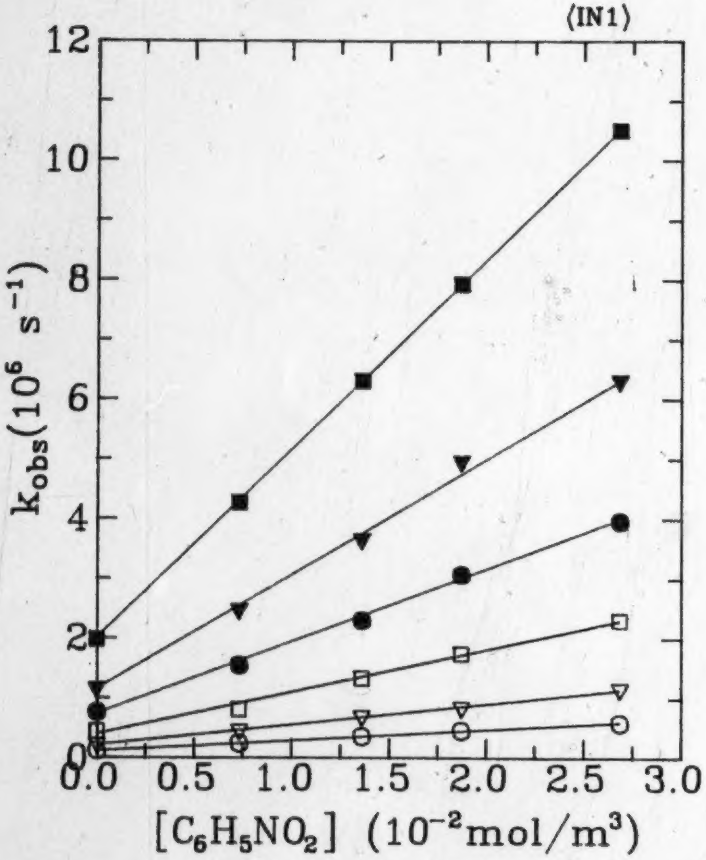

Fig. 3−40: i−BuOH

○ 253.7K ▽ 274.3K □ 297.0K
● 319.0K ▼ 338.1K ■ 362.4K

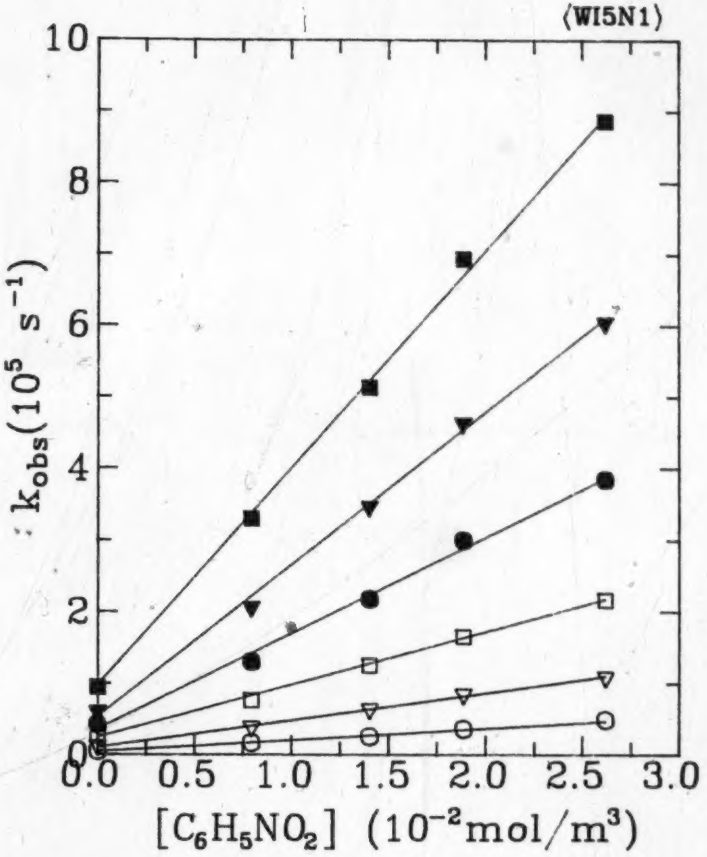

Fig. 3−41: i−BuOH/H_2O:95/5

○ 250.6K ▽ 274.3K □ 296.5K
● 318.9K ▼ 338.1K ■ 362.5K

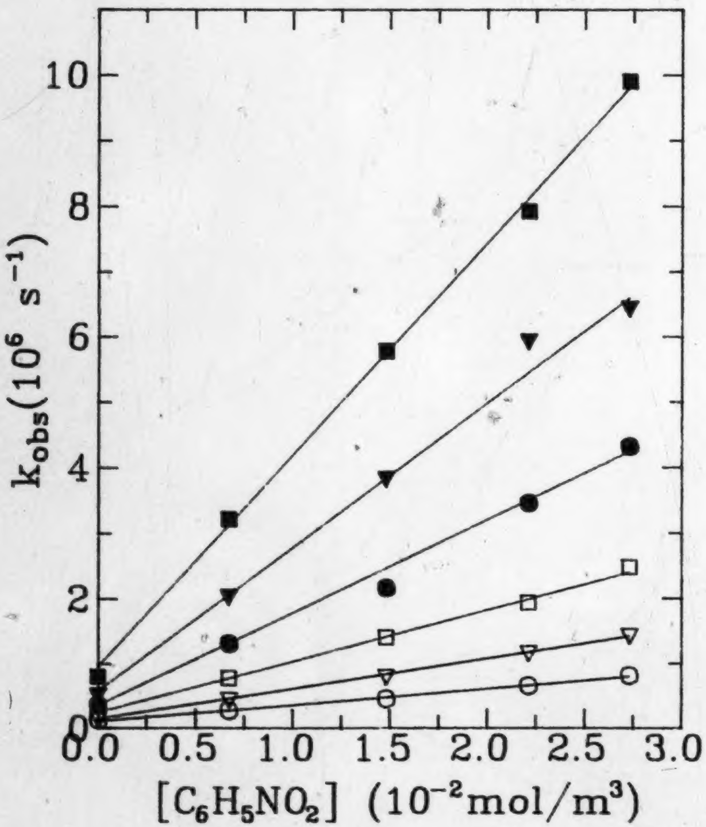

Fig. 3-42: i-BuOH/H_2O:90/10

○ 262.7K ▽ 279.6K □ 296.5K

● 319.0K ▼ 337.6K ■ 362.3K

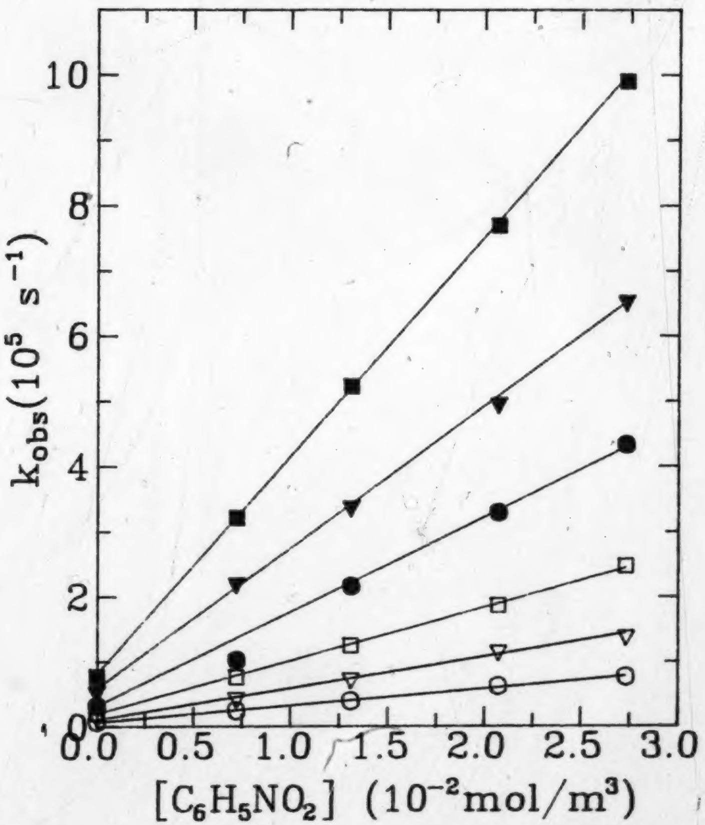

Fig. 3-43: i-BuOH/H_2O:80/20

○ 262.7K ▽ 280.7K □ 296.5K

● 319.0K ▼ 337.8K ■ 362.3K

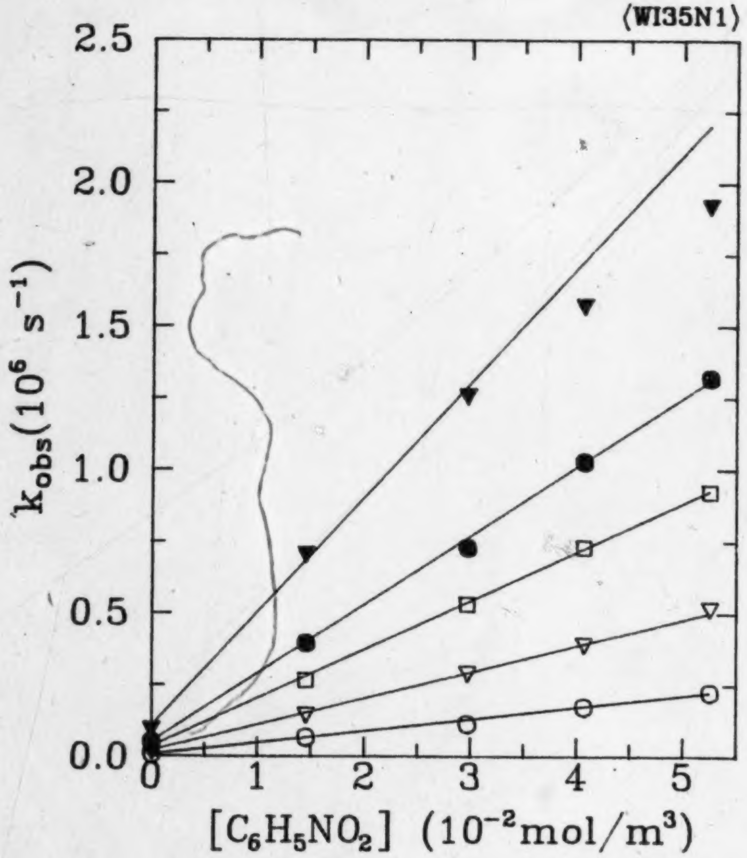

Fig. 3−44: i−BuOH/H_2O:65/35

○ 273.2K ▽ 296.7K □ 320.3K
● 339.1K ▼ 368.5K

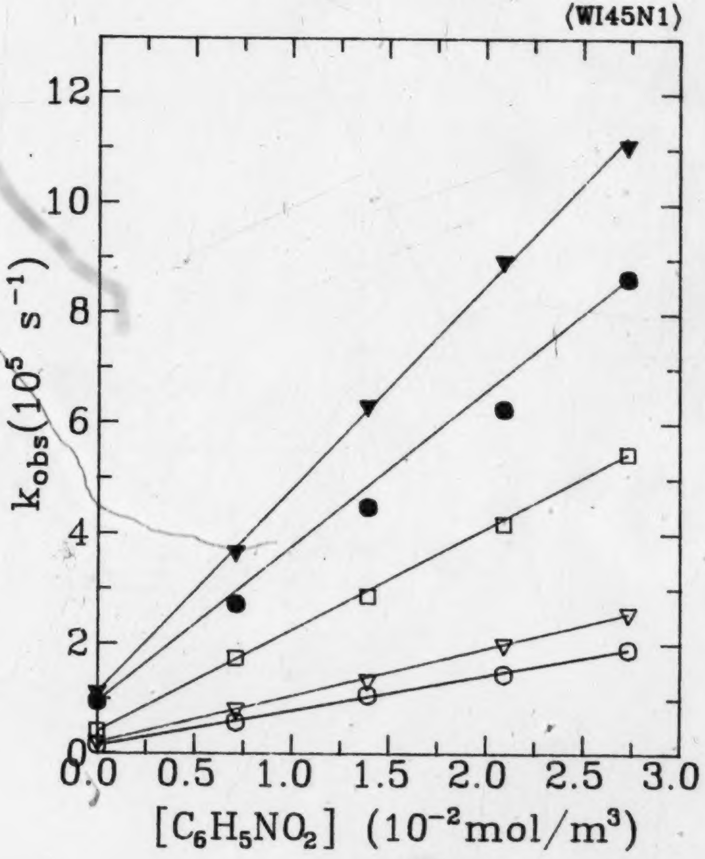

Fig. 3−45: i−BuOH/H_2O:55/45

○ 287.0K ▽ 296.5K □ 323.8K
● 347.2K ▼ 368.0K

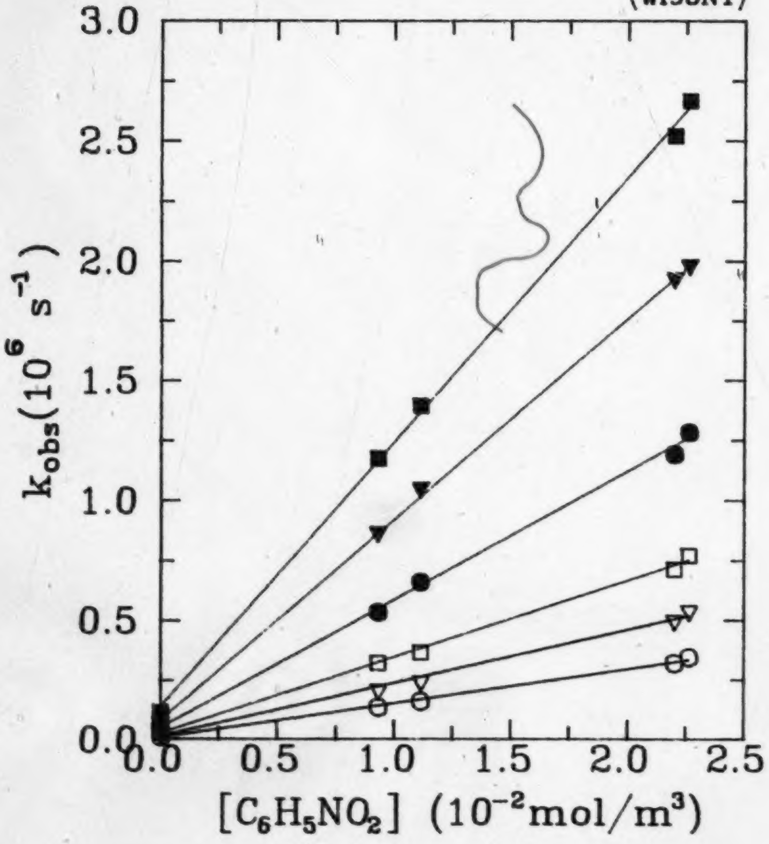

Fig. 3−46: i−BuOH/H_2O:2/98

○ 273.2K ▽ 284.9K □ 296.7K
● 323.3K ▼ 347.0K ■ 366.8K

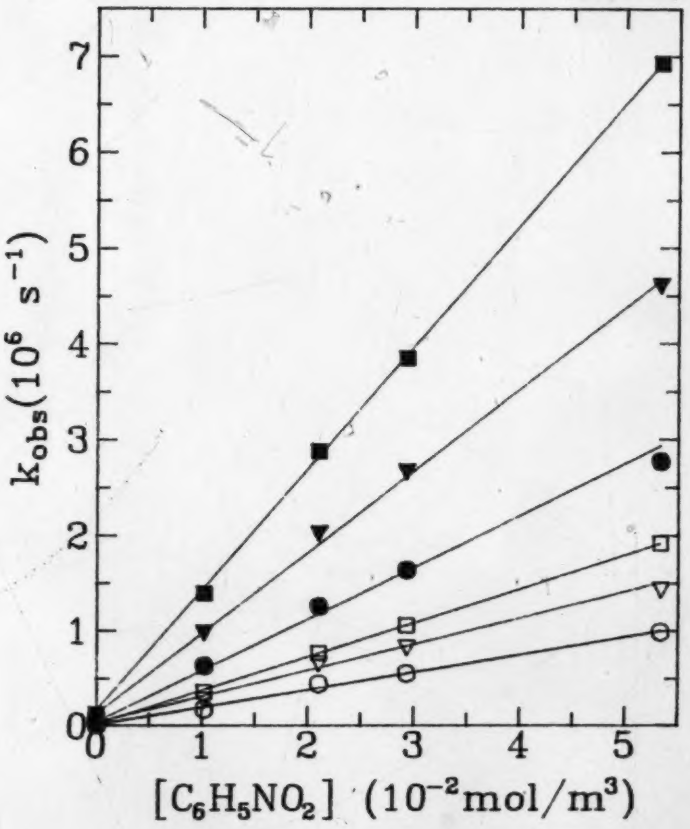

Fig. 3−47: i−BuOH/H_2O:1/99

○ 277.3K ▽ 290.9K □ 296.8K
● 320.2K ▼ 346.6K ■ 372.8K

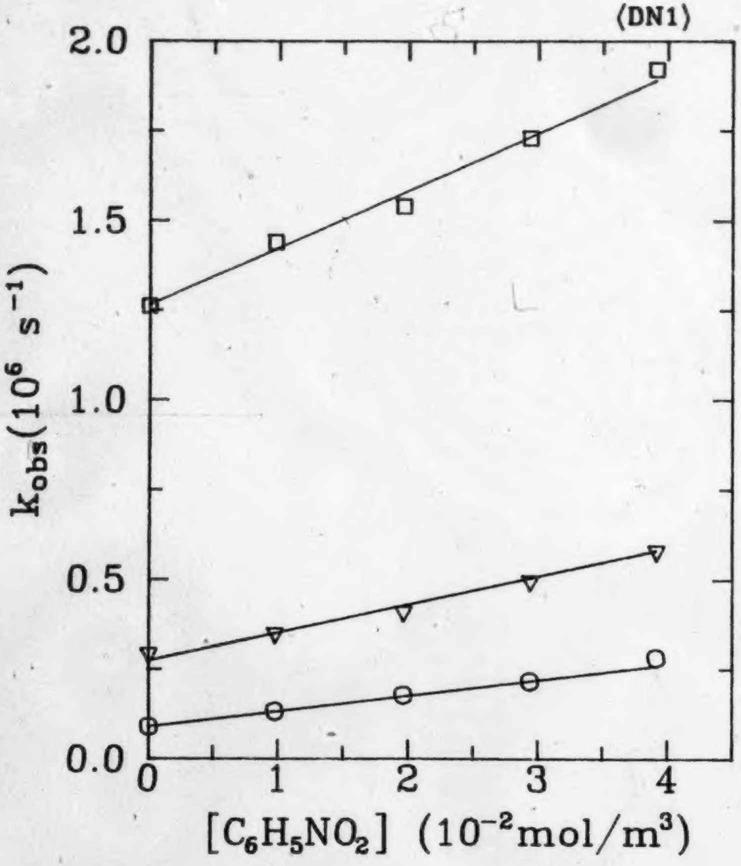

Fig. 3−48a: 2−BuOH

○ 271.8K ▽ 296.8K □ 328.0K

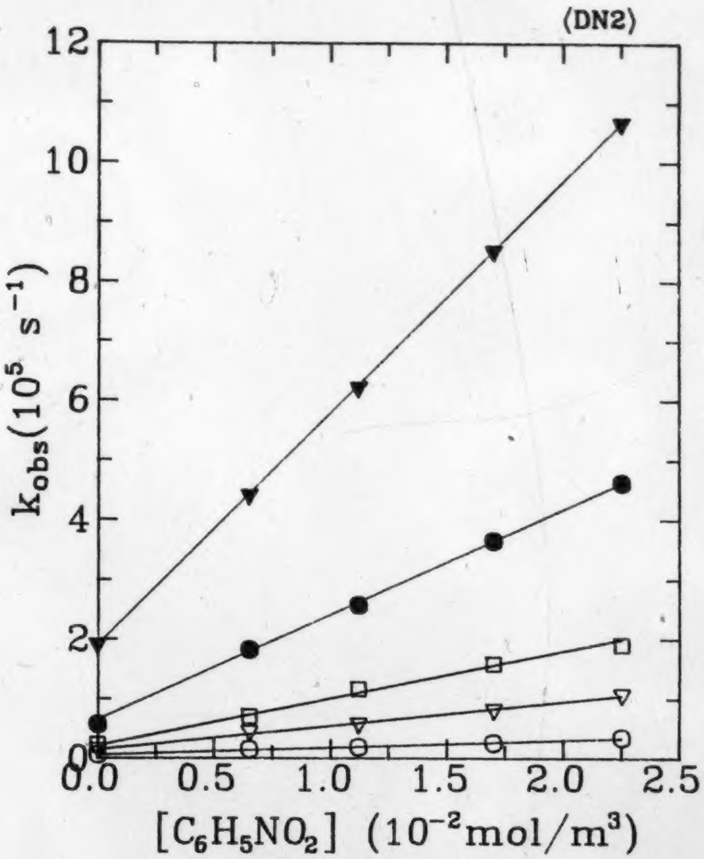

Fig. 3−48b: 2−BuOH

○ 242.9K ▽ 273.4K □ 296.8K
● 328.4K ▼ 362.6K

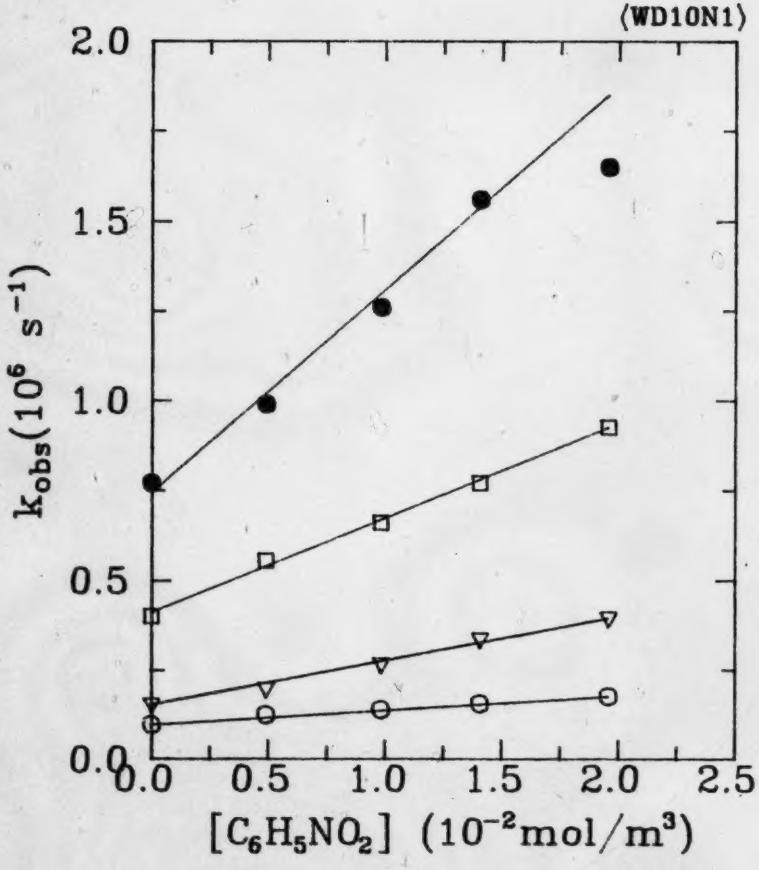

Fig. 3−49a: 2−BuOH/H_2O:90/10

○ 274.9K ▽ 296.1K □ 333.8K
● 368.0K

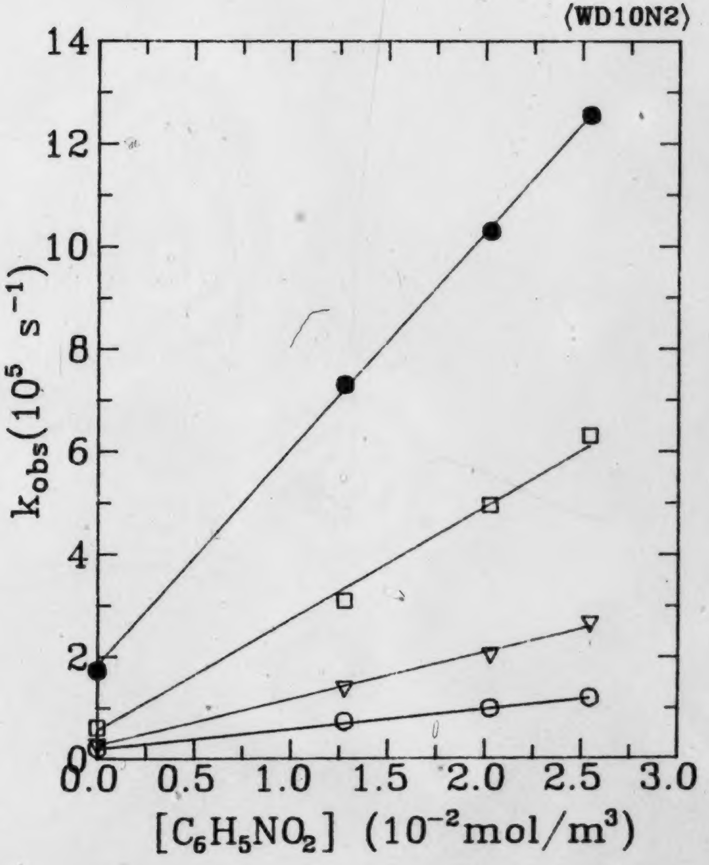

Fig. 3−49b: 2−BuOH/H_2O:90/10

○ 271.9K ▽ 296.7K □ 329.9K
● 368.9K

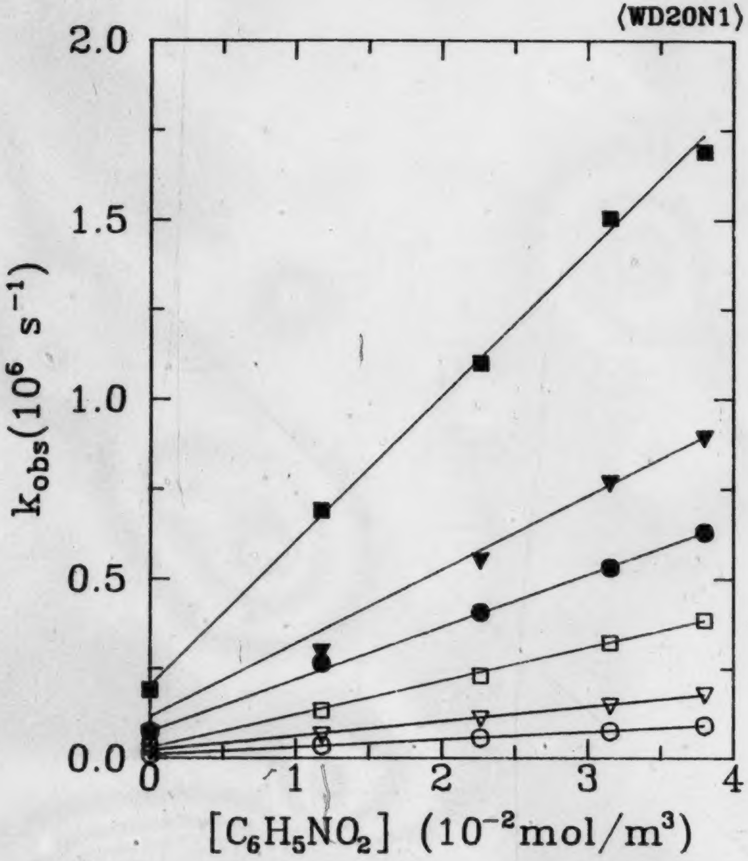

Fig. 3–50: 2–BuOH/H_2O:80/20

○ 256.8K ▽ 271.9K □ 296.5K
● 315.6K ▼ 330.6K ■ 369.3K

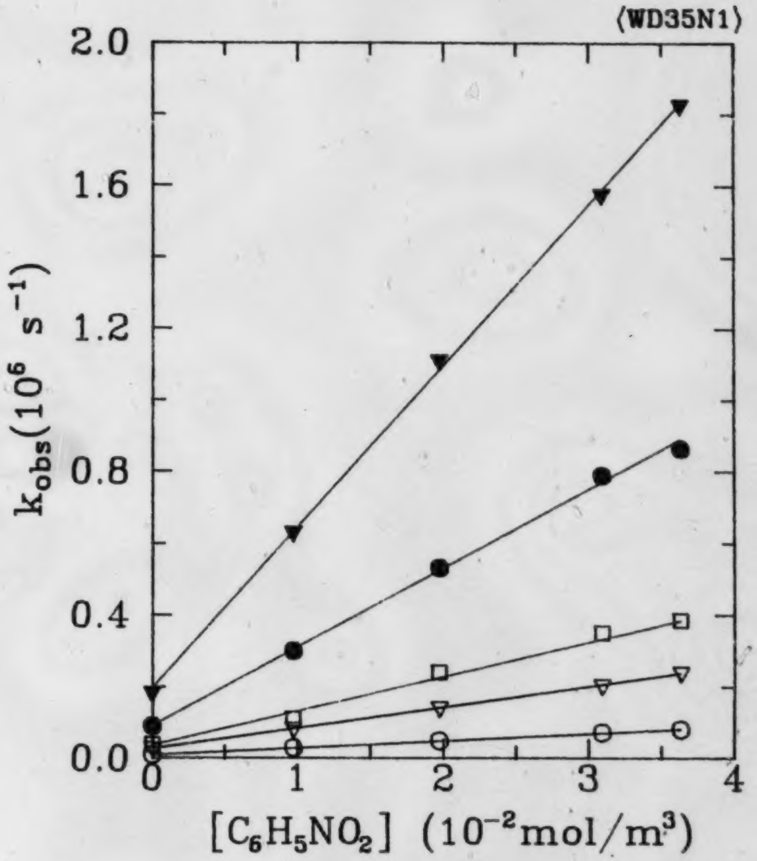

Fig. 3–51: 2–BuOH/H_2O:65/35

○ 256.3K ▽ 280.9K □ 297.0K
● 332.8K ▼ 370.3K

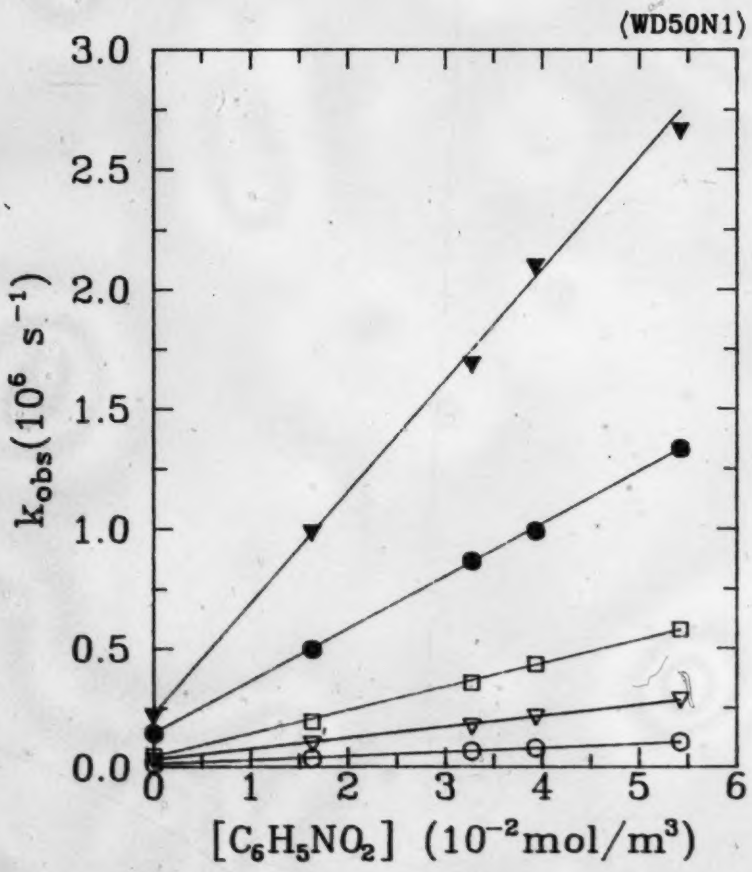

Fig. 3–52: 2–BuOH/H_2O:50/50

○ 255.8K ▽ 278.0K □ 297.0K
● 331.1K ▼ 370.8K

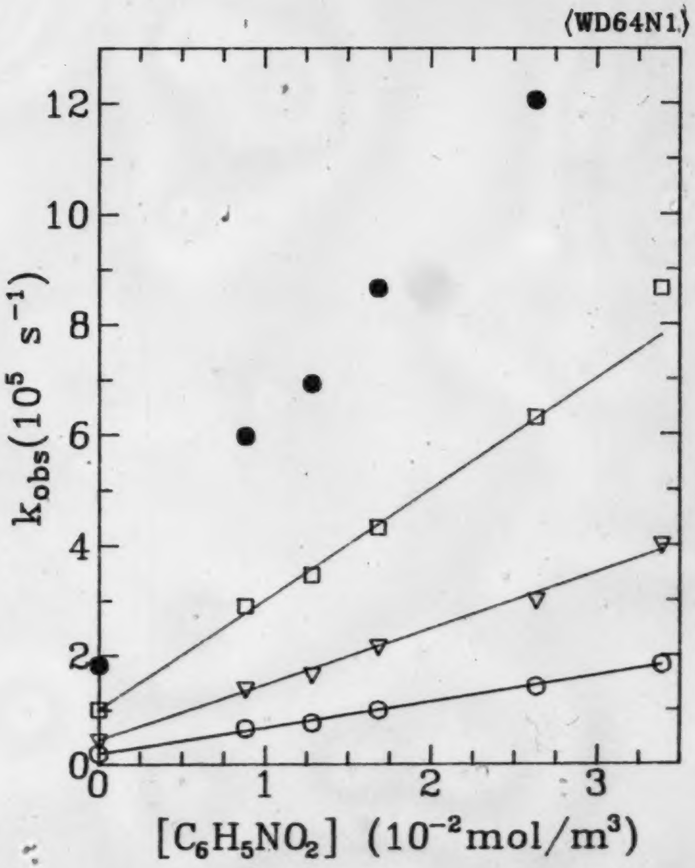

Fig. 3–53: 2–BuOH/H_2O:36/64

○ 275.2K ▽ 295.9K □ 323.5K
● 358.3K

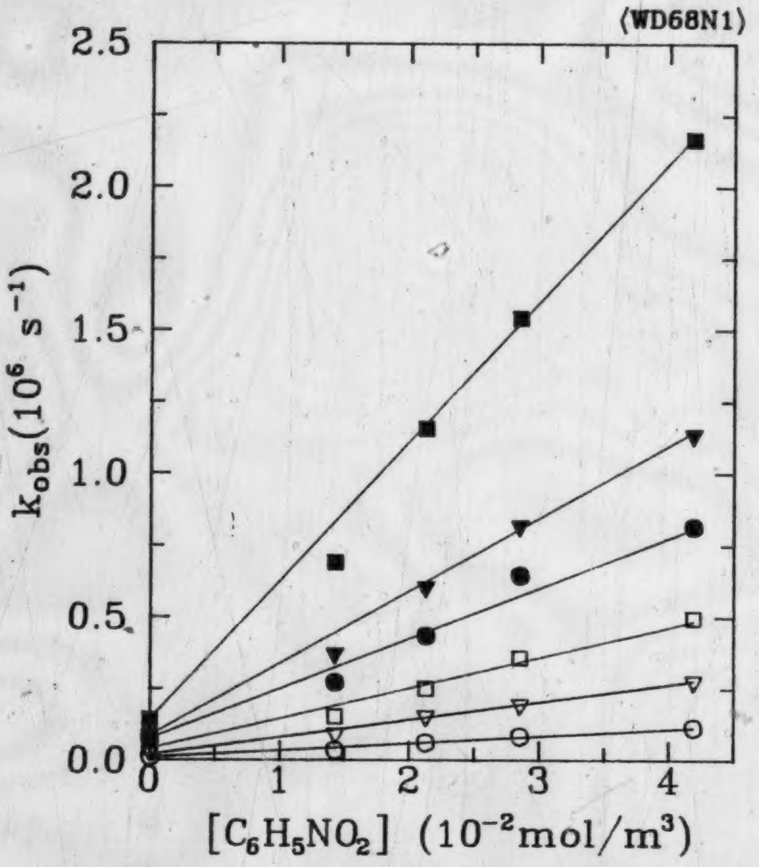

Fig. 3−54: 2−BuOH/H_2O:32/68

○ 262.4K ▽ 280.5K □ 297.1K
● 315.4K ▼ 331.3K ■ 369.0K

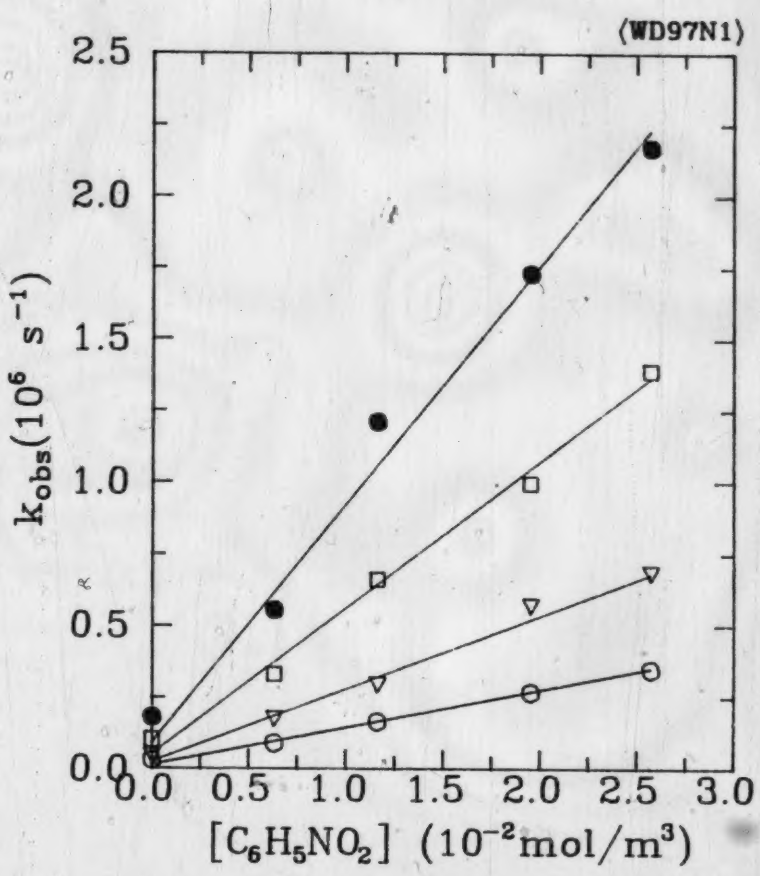

Fig. 3−55: 2−BuOH/H_2O:3/97

○ 275.2K ▽ 296.4K □ 323.3K
● 352.7K

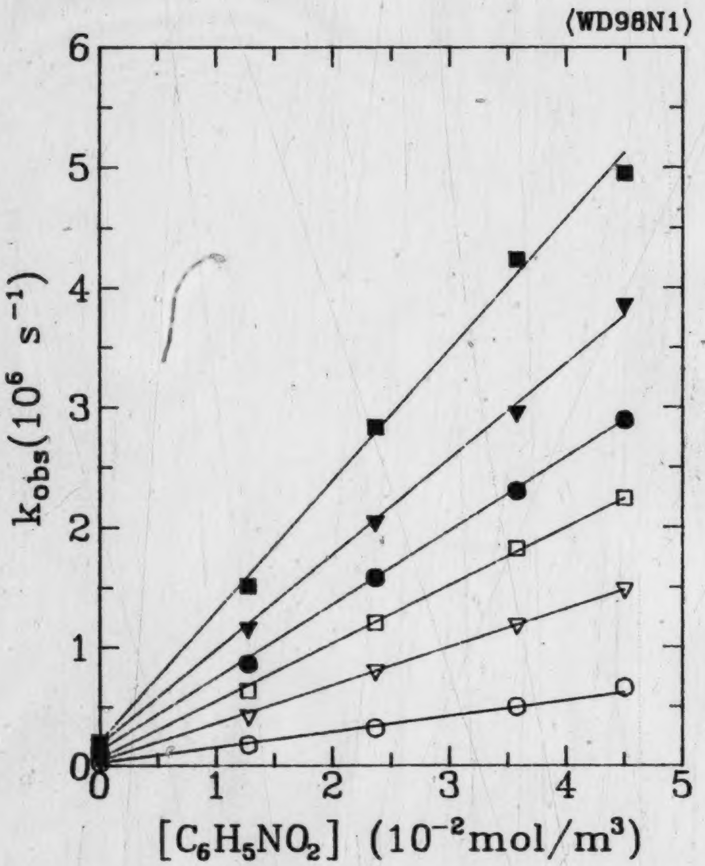

Fig. 3–56: 2–BuOH/H_2O:2/98

○ 272.2K ▽ 297.9K □ 315.6K

● 332.0K ▼ 346.7K ■ 368.6K

Table 3-9:The values of second order rate constants for nitrobenzene in *iso*-butanol/water

x_{H_2O}	T (K)	k_2 $10^7 m^3/mol.s$	x_{H_2O}	T (K)	k_2 $10^7 m^3/mol.s$
0.0	253.7	0.18	0.35	273.2	0.41
	274.3	0.35		296.5	0.92
	297.0	0.71		320.3	1.73
	319.0	1.22		339.1	2.40
	338.1	1.92		368.5	3.97
	362.4	3.17	0.45	287.0	0.64
0.05	250.6	0.17		296.5	0.86
	274.3	0.38		323.8	1.83
	296.5	0.74		347.2	2.91
	318.9	1.35		368.0	3.71
	338.1	2.14	0.98	273.2	1.45
	362.5	3.04		284.9	2.27
0.10	262.7	0.25		296.7	3.25
	279.6	0.46		323.3	5.38
	296.5	0.78		347.0	8.46
	319.0	1.43		366.8	11.10
	337.6	2.21	0.99	277.3	1.86
	362.3	3.23		290.9	2.76
0.20	262.7	0.26		296.8	3.57
	280.7	0.49		320.2	5.41
	296.5	0.82		346.6	8.53
	319.0	1.47		372.8	12.70
	337.8	2.17			
	362.3	3.36			

Table 3-10:The values of second order rate constants for nitrobenzene in 2-butanol/water

x_{H_2O}	T (K)	k_2 $10^7 m^3/mol.s$	x_{H_2O}	T (K)	k_2 $10^7 m^3/mol.s$
0.0	296.8	0.70		370.3	4.51
	328.0	1.68	0.50	255.8	0.17
0.0	242.9	0.13		278.0	0.47
	273.4	0.41		297.0	1.00
	296.8	0.78		331.1	2.19
	328.4	1.77		370.8	4.66
	362.6	3.98	0.64	275.2	0.47
0.10	274.9	0.42		295.9	1.04
	296.1	1.15		323.5	1.98
	333.8	2.62		358.3	3.88
	368.0	5.63	0.68	262.4	0.26
0.10	271.9	0.39		280.5	0.62
	296.7	0.91		297.1	1.06
	329.9	2.19		315.4	1.75
	368.9	4.22		331.3	2.57
0.20	256.8	0.21		369.0	4.92
	271.9	0.41	0.97	275.2	1.31
	296.5	0.93		296.4	2.55
	315.6	1.48		323.3	5.10
	330.6	2.07		352.7	8.28
	369.3	4.03	0.98	272.2	1.36
0.35	256.3	0.20		297.9	3.22

280.9	0.58	315.6	4.93
297.0	0.99	332.0	6.28
332.8	2.20	346.7	8.08
		368.6	11.10

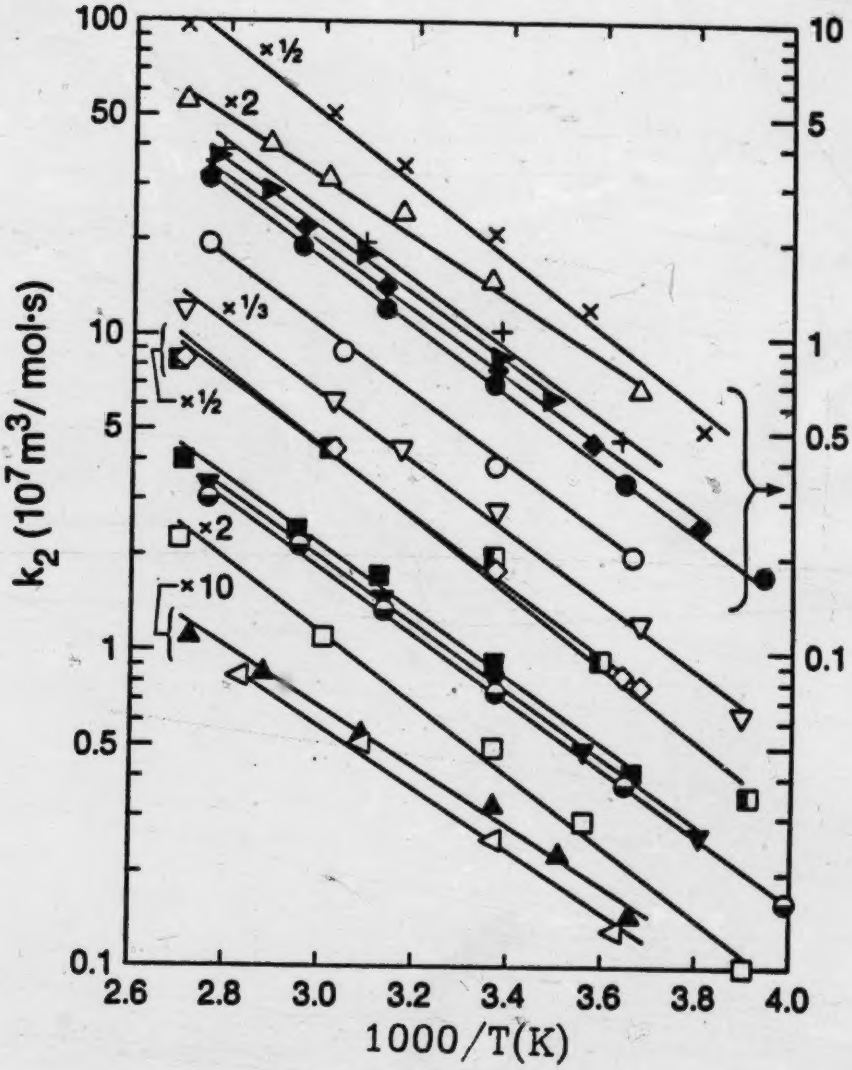

Fig. 3–57: e_s^- + $C_6H_5NO_2$ reaction in i–BuOH
2–BuOH/water mixtures. x_{H_2O} · i–BuOH: ●0.00
◒ 0.05 ◆0.10 ▼0.20 ■0.35 ▶0.45 ▲0.98
2–BuOH: ○0.00 ◇0.10 ▽0.20 □0.35 ◧0.50 +0.64
× 0.68 ◁ 0.97

Table 3-11: Reaction rate parameters for nitrobenzene in *i*-BuOH and 2-BuOH /water

x_{H_2O}	k_2 $10^7 (m^3/mol.s)$	E_2 (J/mol)	log A	$\Delta S_2^{\neq}$ (J/mol.K)
	Solvent: Water in *iso*-butanol			
0	7.1	21	10.52	14
0.10	8.1	20	10.47	13
0.20	8.6	20	10.47	13
0.35	9.6	20	10.49	13
0.45	9.2	20	10.52	14
0.98	31	18	10.66	16
1.00	38	17	10.57	15
	Solvent: Water in 2-butanol			
0	8.4	23	10.88	21
0.10	8.9	21	10.67	17
0.20	9.0	21	10.61	15
0.35	10.0	22	10.79	19
0.50	10.0	22	10.86	20
0.64	11	22	10.86	20
0.68	11	22	10.89	21
0.97	25	20	10.91	21
0.98	32	18	10.68	17
1.00	38	17	10.57	15

Fig.3–58:

k_2 for Nitrobenzene (Open) and Acetone (Closed) in Butanol/Water Mixtures.

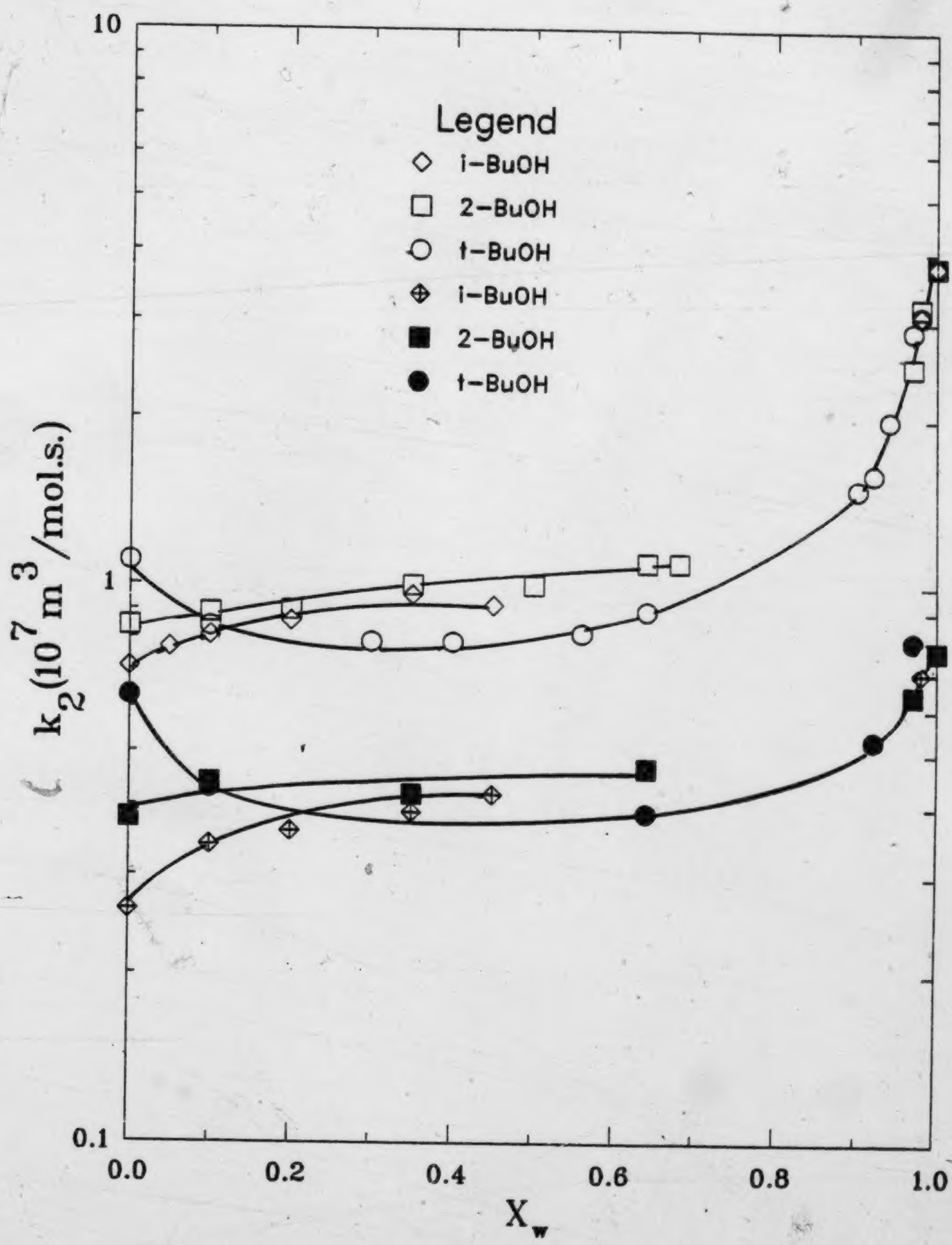

Fig.3–59: E_2 for Nitrobenzene in BuOH/Water Mixtures.

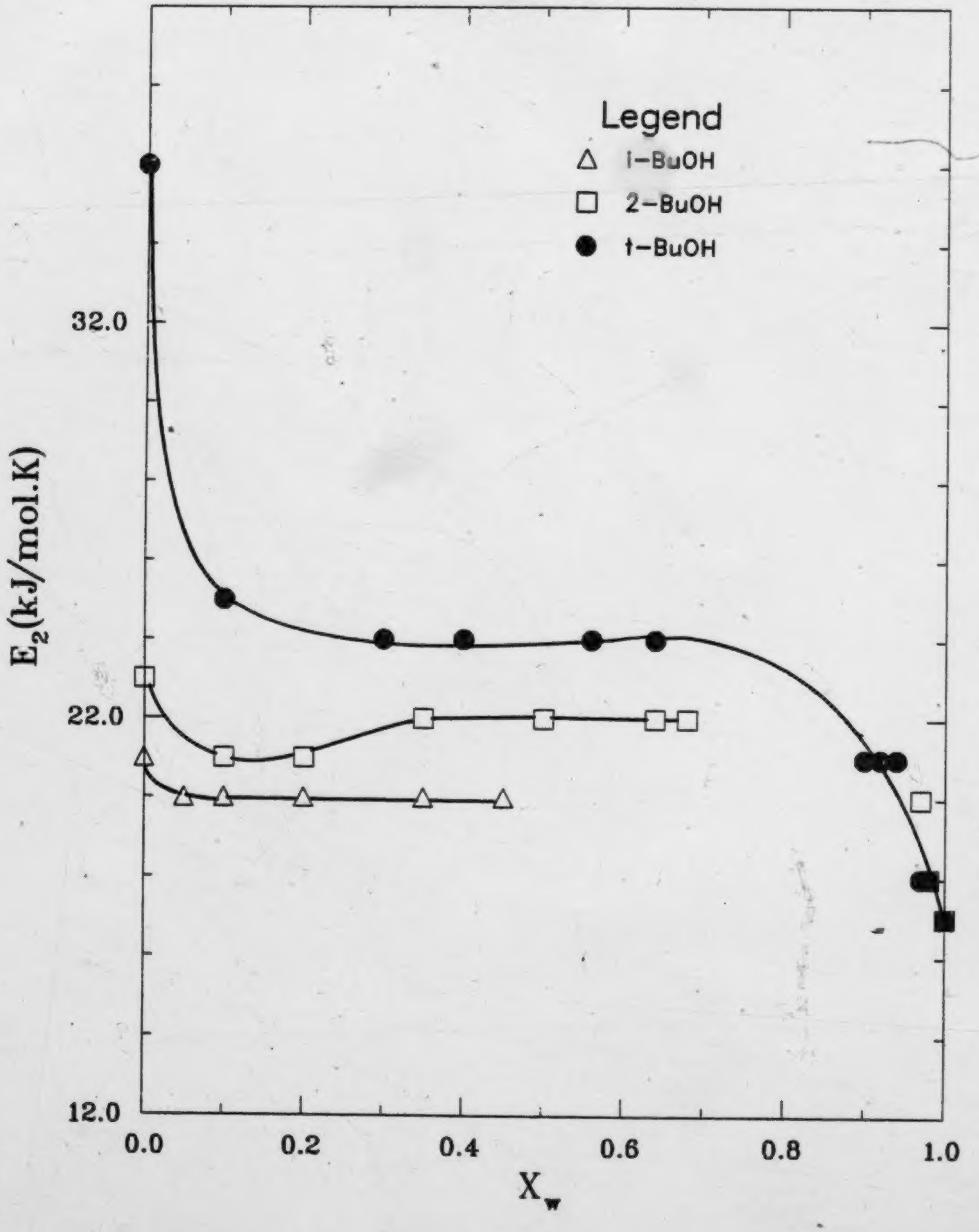

Fig.3—60: ΔS_2 for Nitrobenzenein BuOH/Water Mixtures.

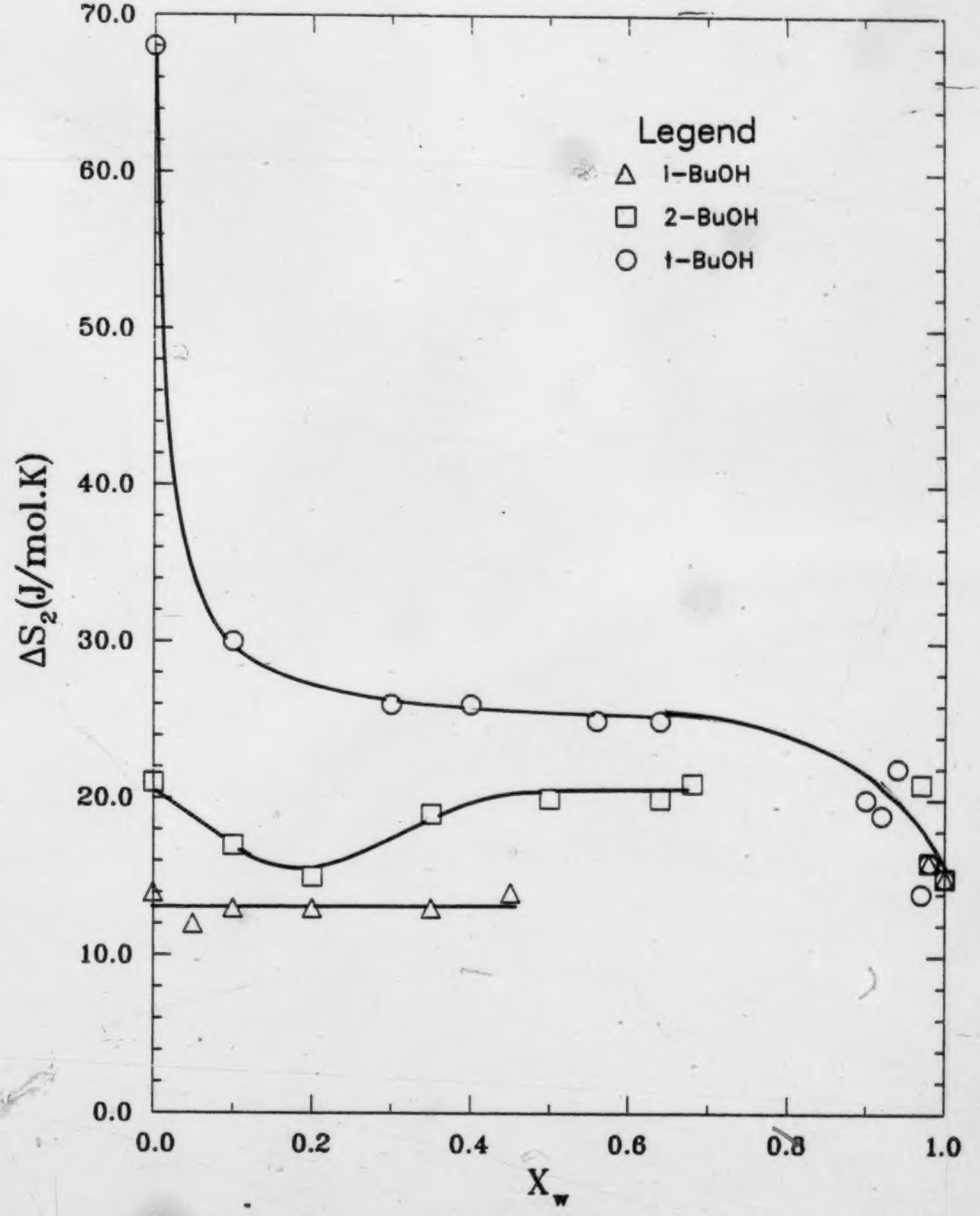

3.1.2(b) Reaction of e_s^- with Acetone

The compositions at which the rate constants were determined in *i*-BuOH /water mixtures were: $x_{H_2O} = 0, 0.10, 0.20, 0.35, 0.45, 0.98, 1.00$ whereas for 2-BuOH /water mixtures they were : $x_{H_2O} = 0, 0.01, 0.35, 0.64, 0.97, 1.00$. The observed first -order rate constants for *i*-BuOH /water solvents are in Figs.(3-61) to (3-66) and those for 2-BuOH /water mixtures are in Figs.(3-67) to (3-71). The concentration range for acetone is 0.02-0.2 mol/m^3. The k_2 values are in Tables(3-12) and (3-13) respectively. The Arrhenius plots are in Fig.(3-72), and the reaction rate parameters are in Table(3-14).

The composition dependence of k_2 is similar to that for the reaction with nitrobenzene(fig 3-58) but the differences among the rate constants are greater in zones (a) and (b). The composition dependence and the extent of changes in energies (Fig. 3-73) and entropies (Fig. 3-74) of activation are also similar to those of nitrobenzene indicating that these two scavengers belong to the same group (efficient scavengers).

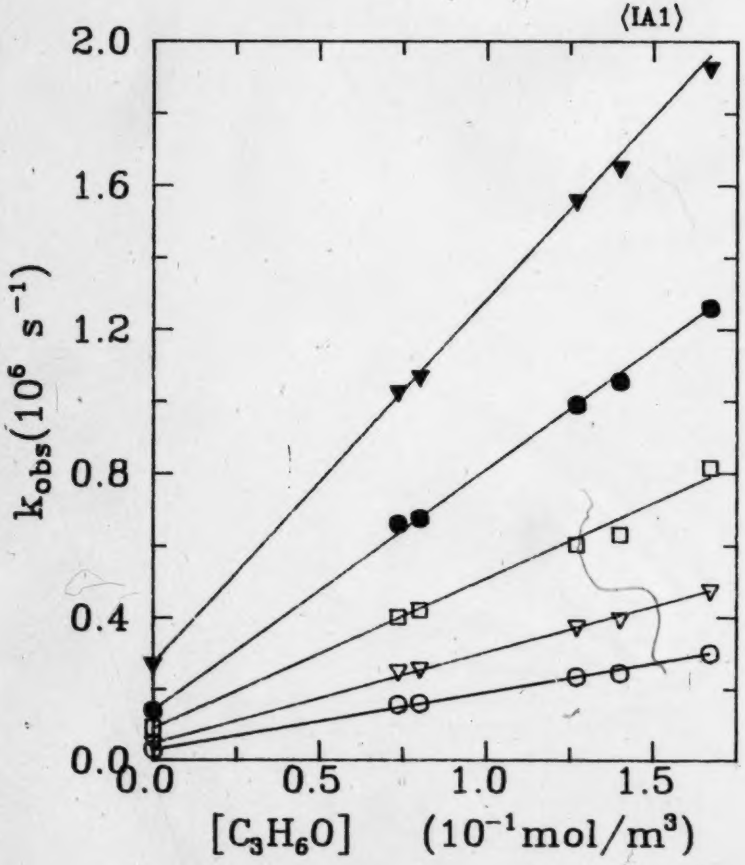

Fig. 3−61: i−BuOH

○ 280.9K ▽ 297.0K □ 318.2K
● 337.7K ▼ 362.5K

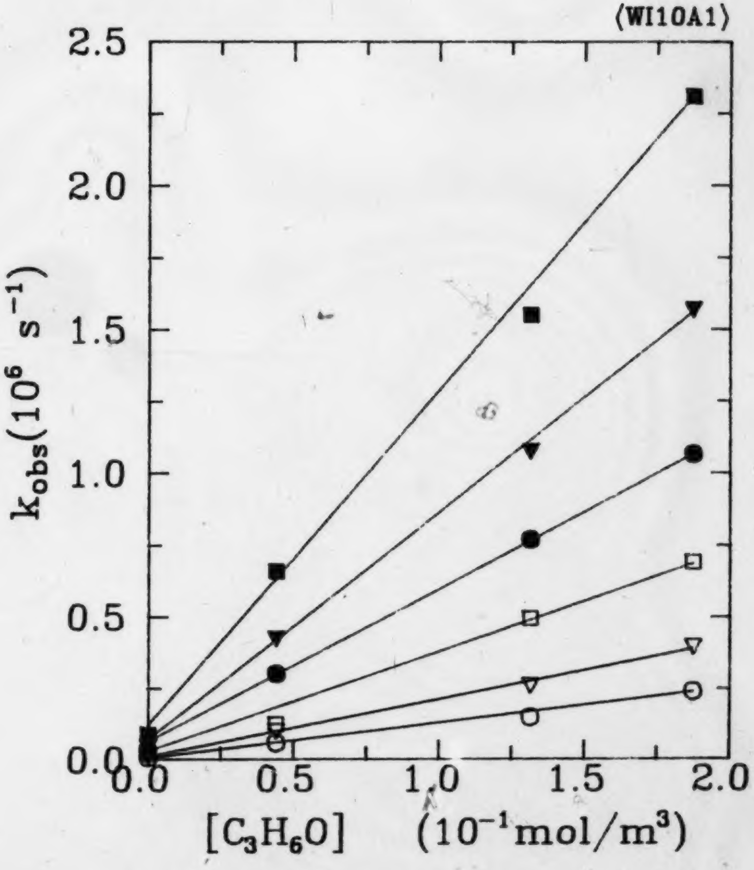

Fig. 3−62: i−BuOH/H_2O:90/10

○ 263.2K ▽ 278.8K □ 296.4K
● 318.2K ▼ 337.8K ■ 362.6K

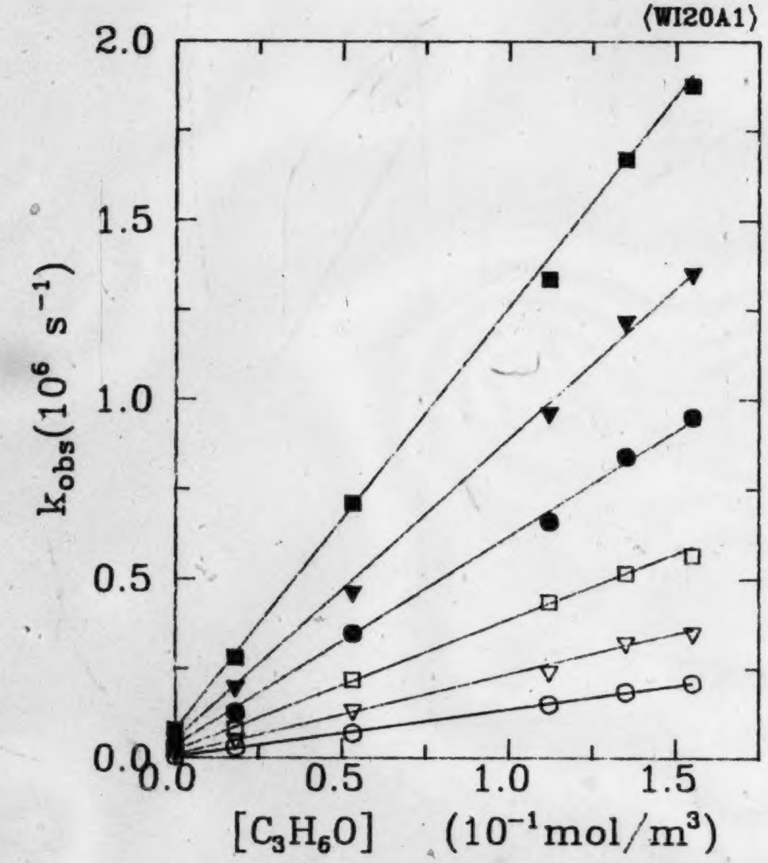

Fig. 3−63: i−BuOH/H_2O:80/20

○ 263.2K ▽ 280.8K □ 297.0K
● 318.1K ▼ 337.6K ■ 362.5K

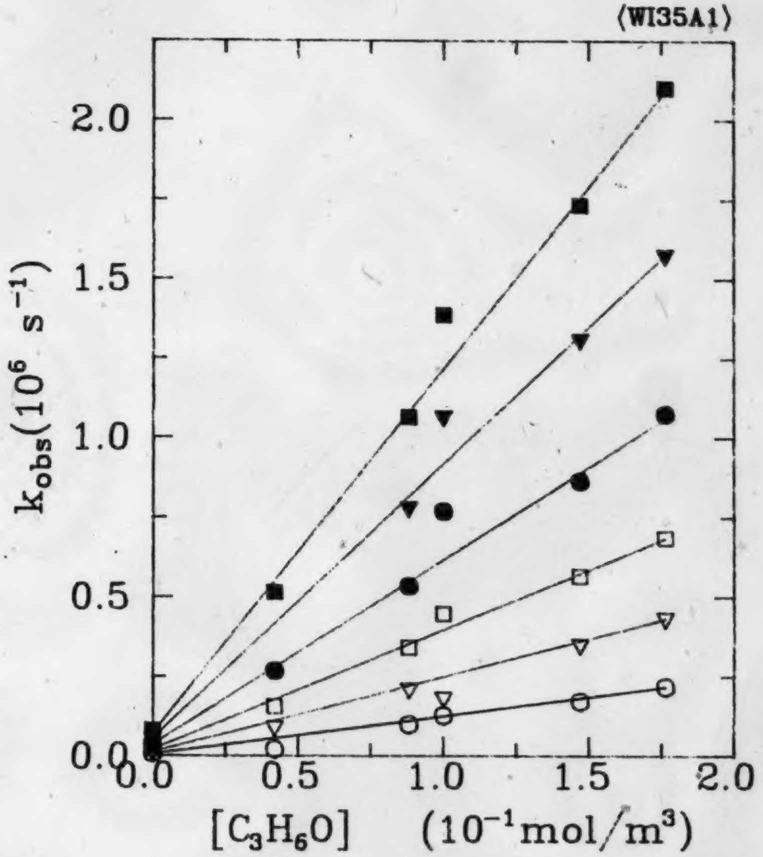

Fig. 3−64: i−BuOH/H_2O:65/35

○ 263.1K ▽ 280.8K □ 297.0K
● 318.1K ▼ 337.8K ■ 362.5K

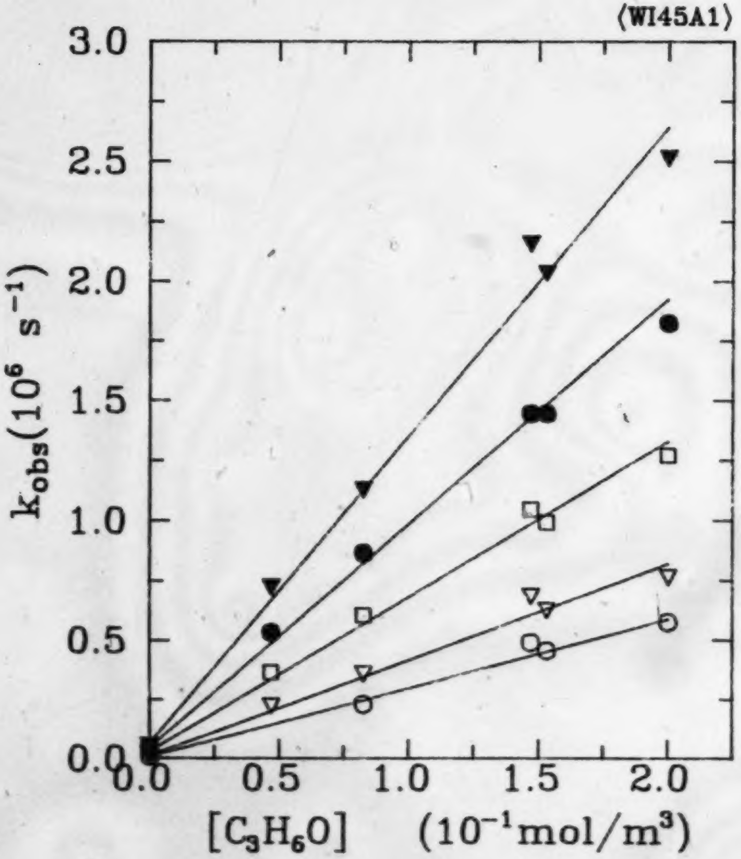

Fig. 3−65: i−BuOH/H_2O:55/45

○ 283.8K ▽ 297.1K □ 318.1K
● 338.7K ▼ 366.2K

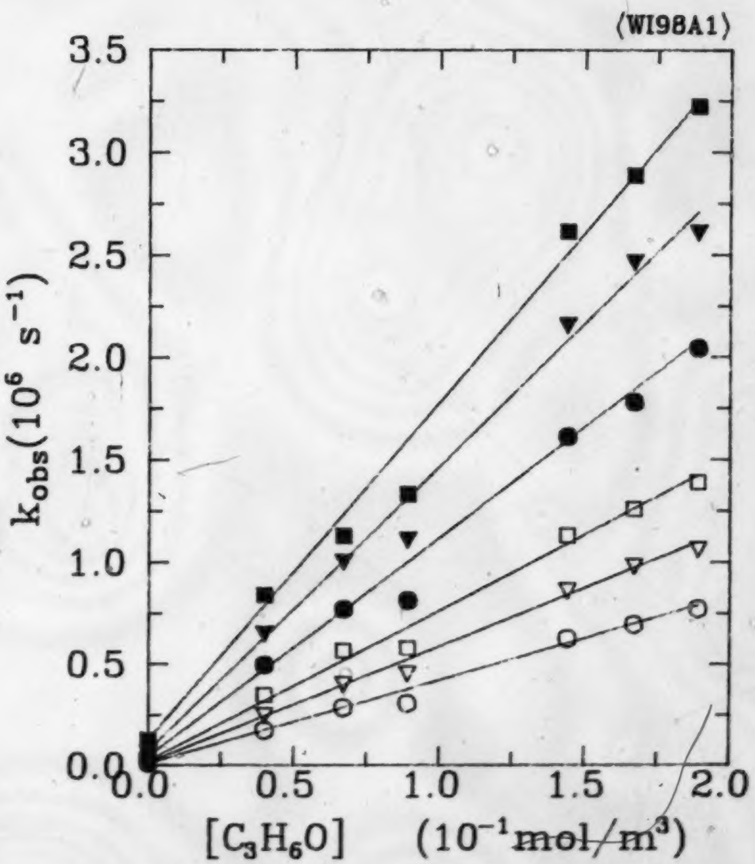

Fig. 3−66: i−BuOH/H_2O:2/98

○ 274.8K ▽ 286.4K □ 297.3K
● 319.5K ▼ 338.2K ■ 359.0K

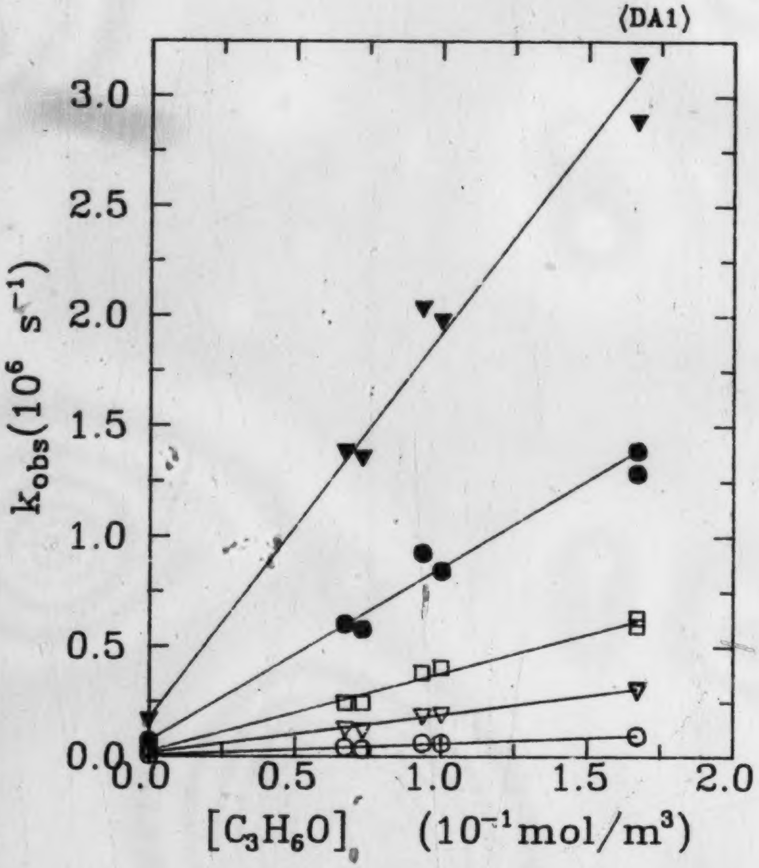

Fig. 3−71: 2−BuOH

○ 244.2K ▽ 274.8K □ 296.7K
● 325.6K ▼ 357.8K

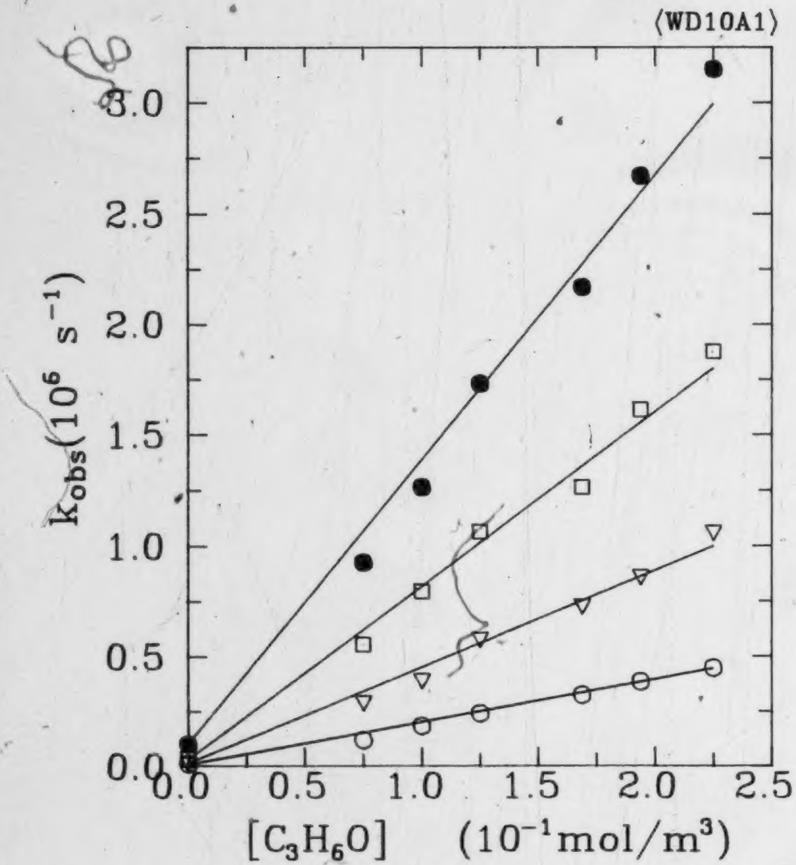

Fig. 3-68: 2-BuOH/H_2O:90/10
○ 268.2K ▽ 296.4K □ 327.0K
● 296.4K

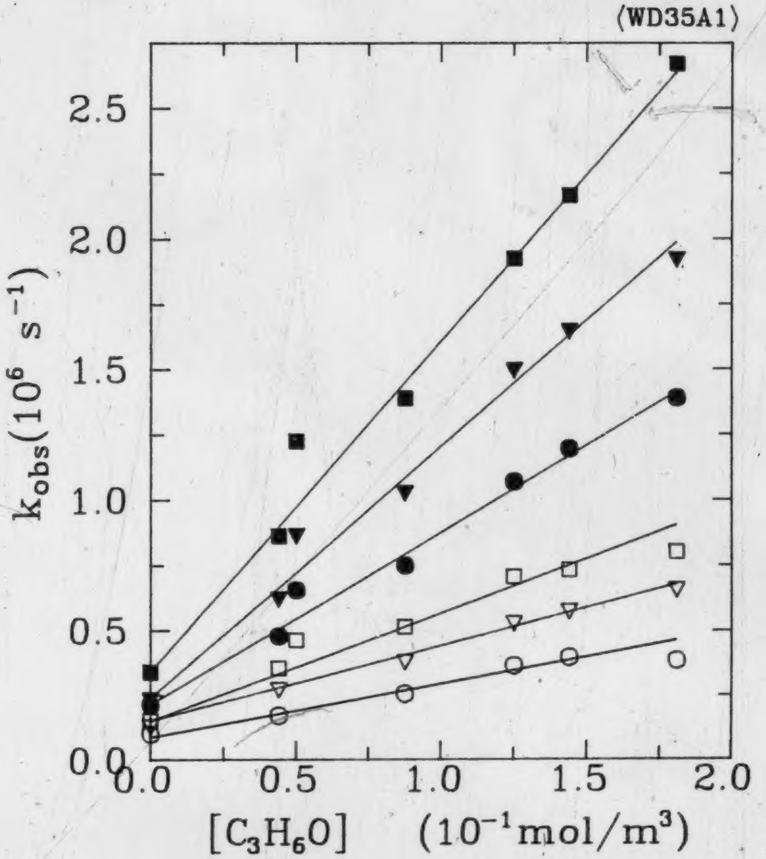

Fig. 3-69: 2-BuOH/H_2O:65/35
○ 270.4K ▽ 286.4K □ 296.7K
● 317.8K ▼ 338.5K ■ 365.4K

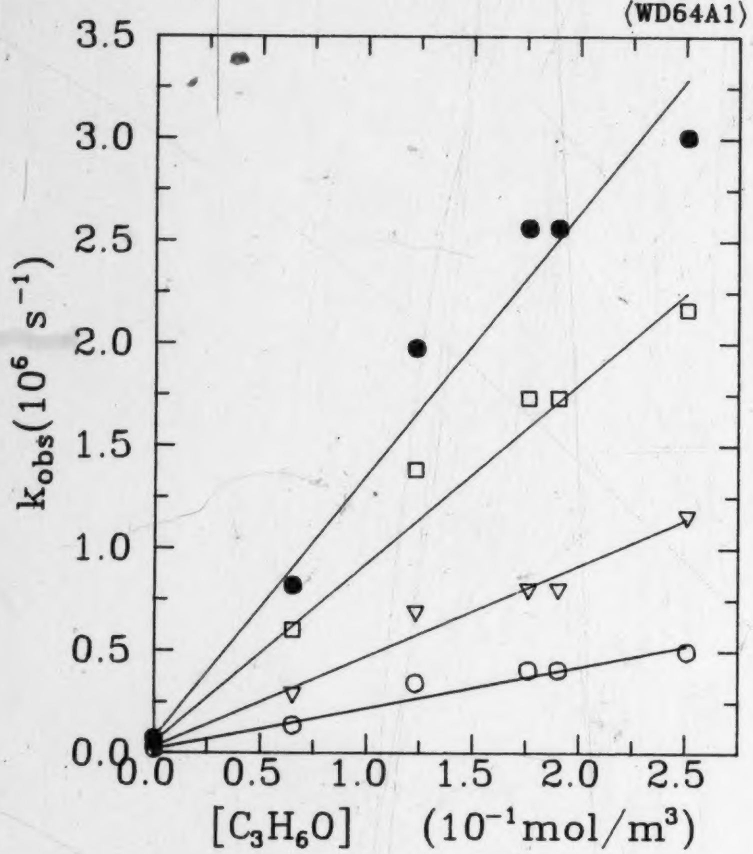

Fig. 3−70: 2−BuOH/H_2O:36/64

○ 272.2K ▽ 296.5K □ 325.7K
● 352.9K

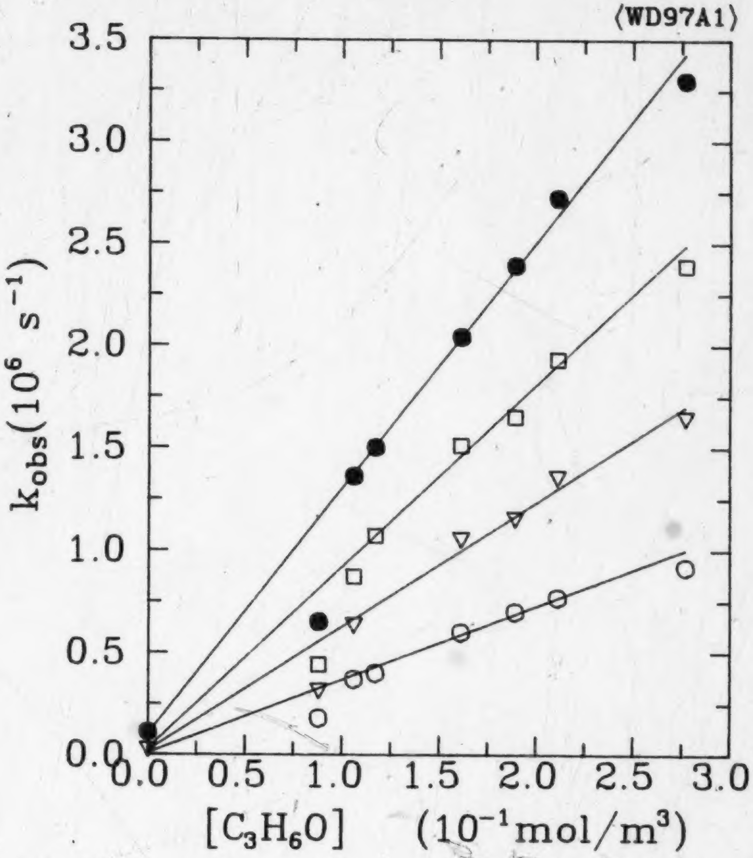

Fig. 3−71: 2−BuOH/H_2O:3/97

○ 275.9K ▽ 296.7K □ 316.1K
● 343.4K

Table 3-12:The values of second order rate constants for acetone in *iso*-butanol/water

x_{H_2O}	T (K)	k_2 $10^6 m^3/mol.s$	x_{H_2O}	T (K)	k_2 $10^7 m^3/mol.s$
0.0	280.9	1.63	0.35	263.1	1.28
	297.0	2.55		280.8	2.50
	318.2	4.22		297.0	3.81
	337.7	6.70		318.1	5.85
	362.5	10.10		337.8	8.66
0.10	263.2	1.25		362.5	11.60
	278.8	2.04	0.45	283.8	2.89
	296.4	3.51		297.1	4.00
	318.2	5.36		318.1	6.42
	337.8	7.96		338.7	9.38
	362.6	11.6		366.2	13.00
0.20	263.2	1.33	0.98	274.8	4.20
	280.8	2.22		286.4	5.77
	297.0	3.67		297.3	7.47
	318.1	5.87		319.5	10.80
	337.6	8.32		338.2	14.00
	362.5	11.80		359.0	16.70

Table 3-13: The second order rate constants for for acetone in 2-butanol/water

x_{H_2O}	T (K)	k_2 $10^6(m^3/mol.s)$
0.0	244.2	0.56
	274.8	1.75
	296.7	3.55
	325.6	7.91
	357.8	17.50
0.10	268.2	1.93
	296.4	4.37
	327.0	7.90
	352.9	12.90
0.35	286.4	3.04
	296.7	1.06
	317.8	6.70
	338.5	9.71
	365.4	12.80
0.64	272.2	2.06
	296.5	4.47
	325.7	8.69
	352.9	12.80
	270.4	2.08
0.97	275.9	3.58
	296.7	5.98
	316.1	8.85
	343.4	12.00

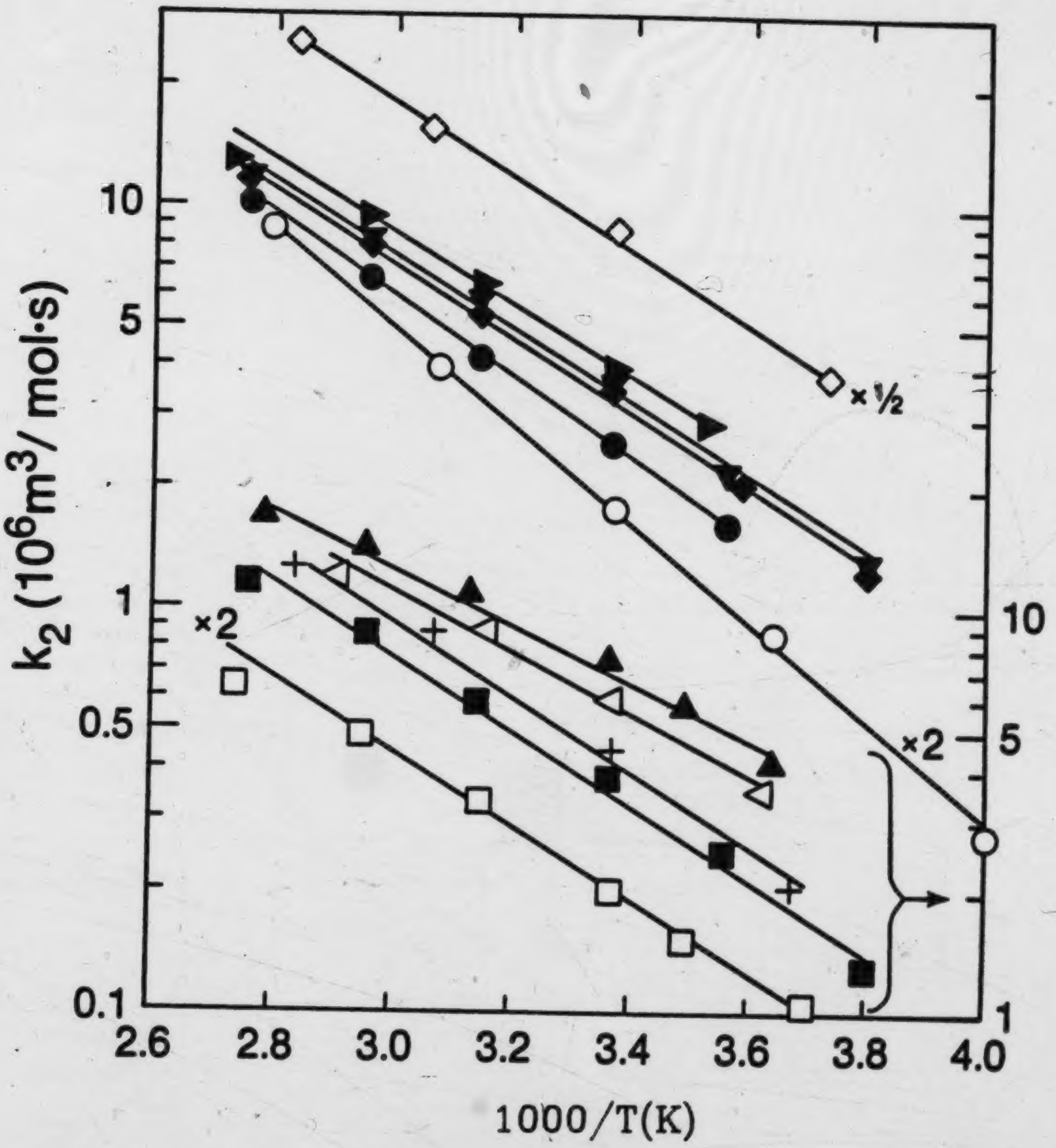

Fig. 3-72: e_s^- + acetone reaction in i-BuOH, 2-BuOH/water mixtures.

x_{H_2O}:
i-BuOH: ●0.00; ◆0.10; ▼0.20; ■0.35; ▶0.45; ▲0.98
2-BuOH: ○ 0.00; ◇ 0.10; □0.35; +0.64; ◁0.97

Table 3-14: Reaction rate parameters for acetone in *i*-BuOH and 2-BuOH water

x_{H_2O}	k_2 $10^6 (m^3/mol.s)$	E_2 (J/mol)	log A	$\Delta S_2^{\neq}$ (J/mol.K)
	Solvent: Water in *iso*-butanol			
0	2.6	19	9.82	0.0
0.10	3.4	18	9.63	-3
0.20	3.6	18	9.63	
0.35	3.9	18	9.63	-3
0.45	4.2	17	9.61	-4
0.98	7.0	14	9.22	-11
1.00	7.7	13	9.08	-14
	Solvent : Water in 2-butanol			
0	3.8	22	10.36	11
0.10	4.4	18	9.72	-1
0.35	4.2	18	9.74	-1
0.64	4.7	18	9.72	-1
0.97	6.4	14	9.32	-9
1.0	7.7	13	9.08	-14

Fig.3–73: E_2 for Acetone in BuOH/Water Mixtures.

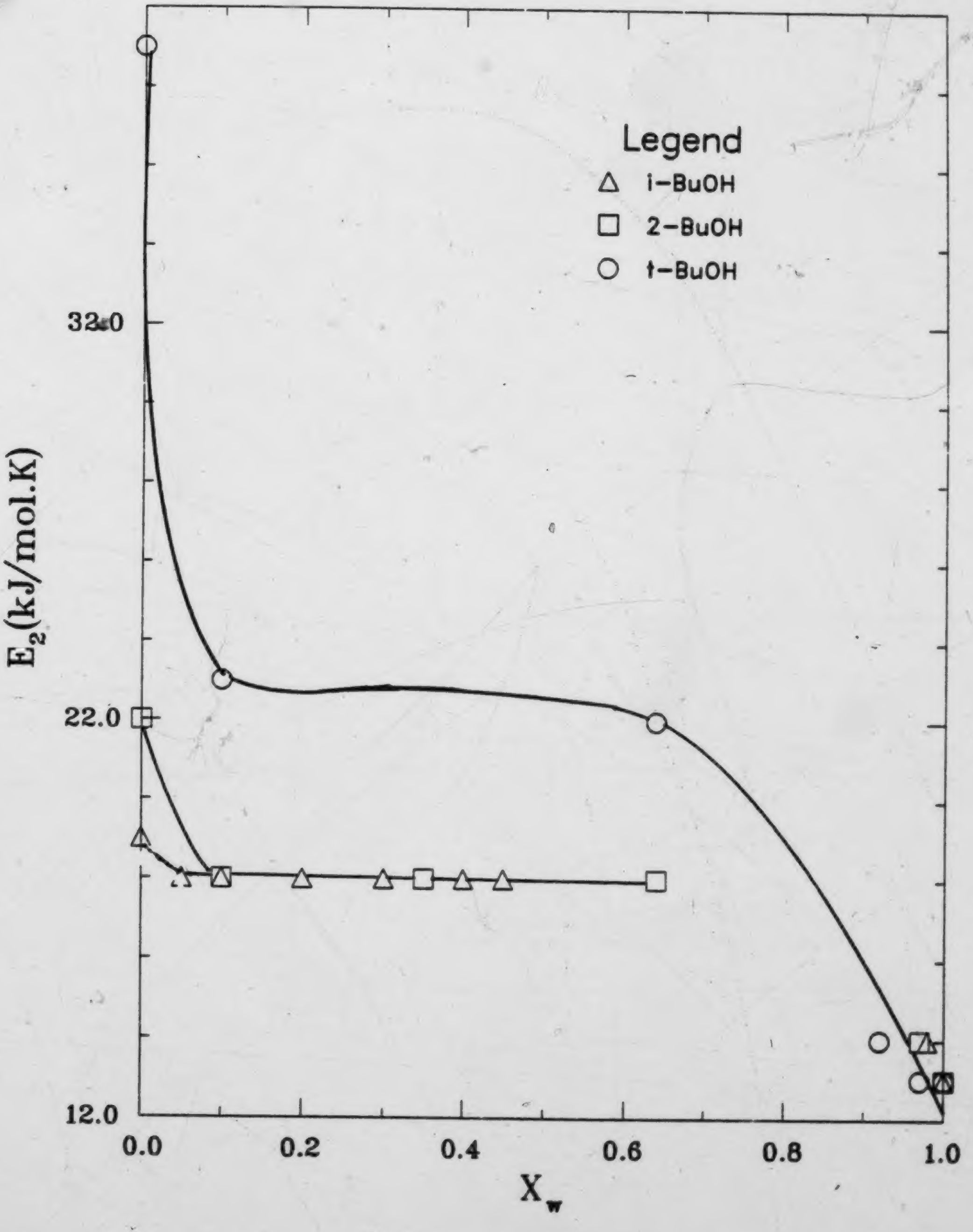

Fig.3–74: ΔS_2 for Acetonein BuOH/Water Mixtures.

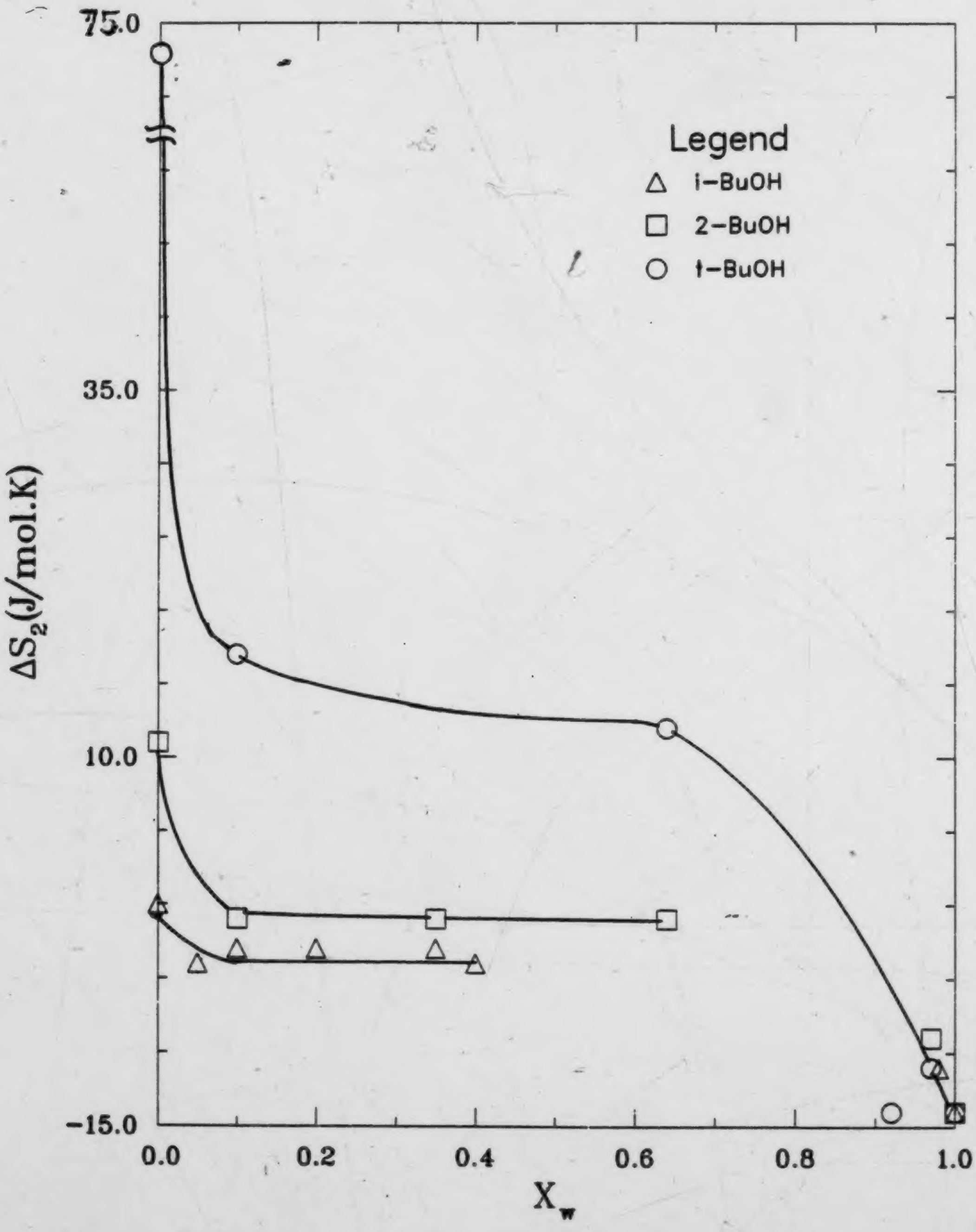

3.1.2(c) Reaction of e_s^- with Phenol

The observed rate constants for *i*-BuOH /water mixtures are in Figs.(3-75) to (3-81), whereas those for 2-BuOH /water mixtures are in Figs.(3-82) to (3-86). The concentration range of phenol is 1 - 20 mol/m^3. The k_2 values for these two systems are listed in Tables(3-15) and (3-16) respectively and the Arrhenius plots in Fig.(3-87). The reaction rate parameters are listed in Table(3-17).

The rate constants for the e_s^- + phenol reaction in pure alcohol are in the same order (*t*-BuOH > 2-BuOH > *i*-BuOH) as for the reaction with nitrobenzene and acetone (Fig. 3-88). The differences between the k_2 values increase with decreasing efficiency of the scavenger. In alcohol/water mixtures the values of k_2 decrease with increasing x_{H_2O} . The differences among the k_2 values of butanol at a fixed composition decrease with greater water content of water, and they become similar in water-rich solvents. The k_2 values for the reaction with phenol display greater composition dependence than for the efficient scavengers (Fig. 3-58). Therefore phenol belongs to a separate group (inefficient scavengers).

The composition dependence of E$_2$ (Fig. 3-89) and $\Delta S_2^{\neq}$ (Fig. 3-90) are similar to those of efficient scavengers. Thus changes in rate constants are due to differences in entropy than that due to energy.

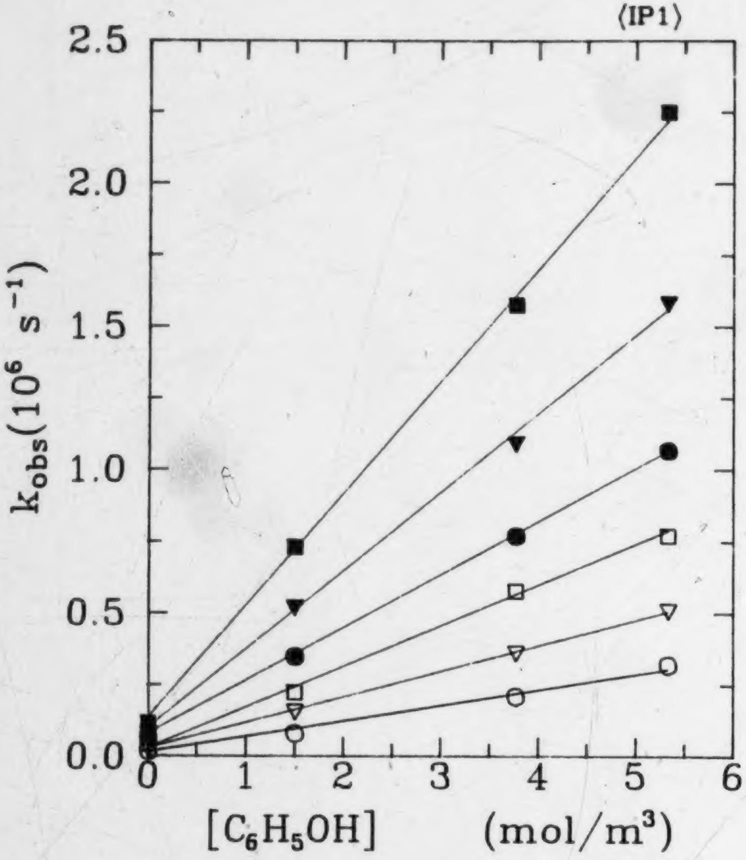

Fig. 3−81: i−BuOH

○ 265.2K ▽ 279.8K □ 296.7K
● 308.9K ▼ 323.4K ■ 335.8K

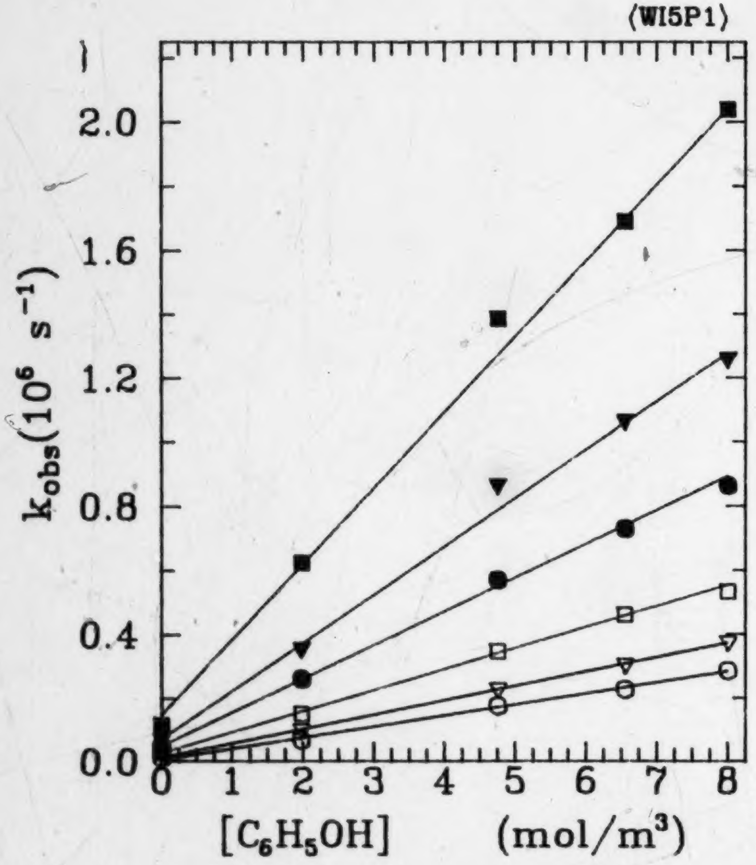

Fig. 3−76: i−BuOH/H_2O:95/5

○ 265.1K ▽ 279.8K □ 296.8K

● 320.0K ▼ 337.8K ■ 359.3K

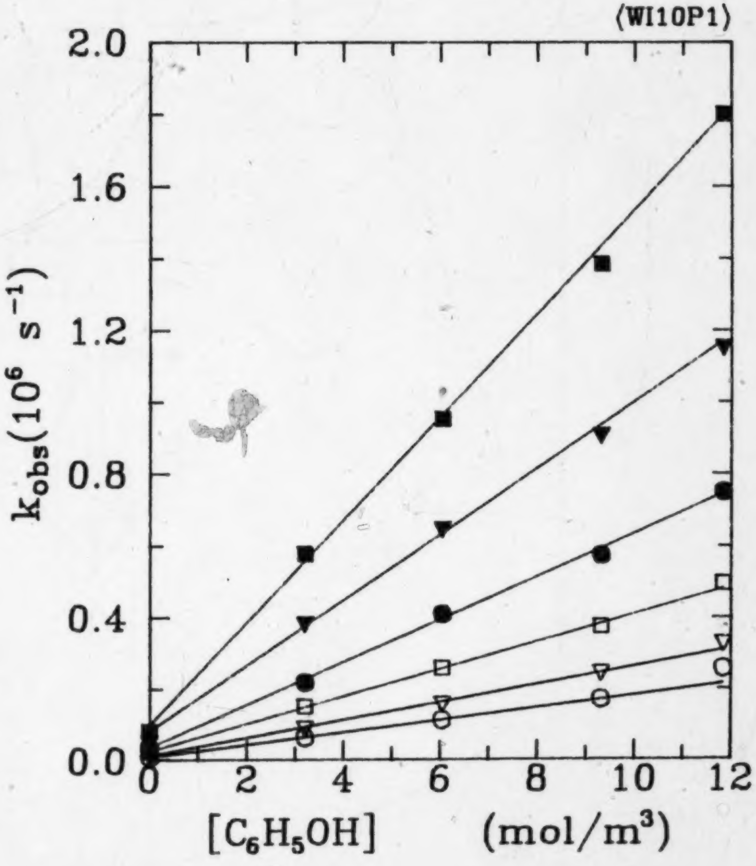

Fig. 3−77: i−BuOH/H_2O:90/10

○ 263.1K ▽ 278.9K □ 297.0K

● 318.1K ▼ 338.8K ■ 362.4K

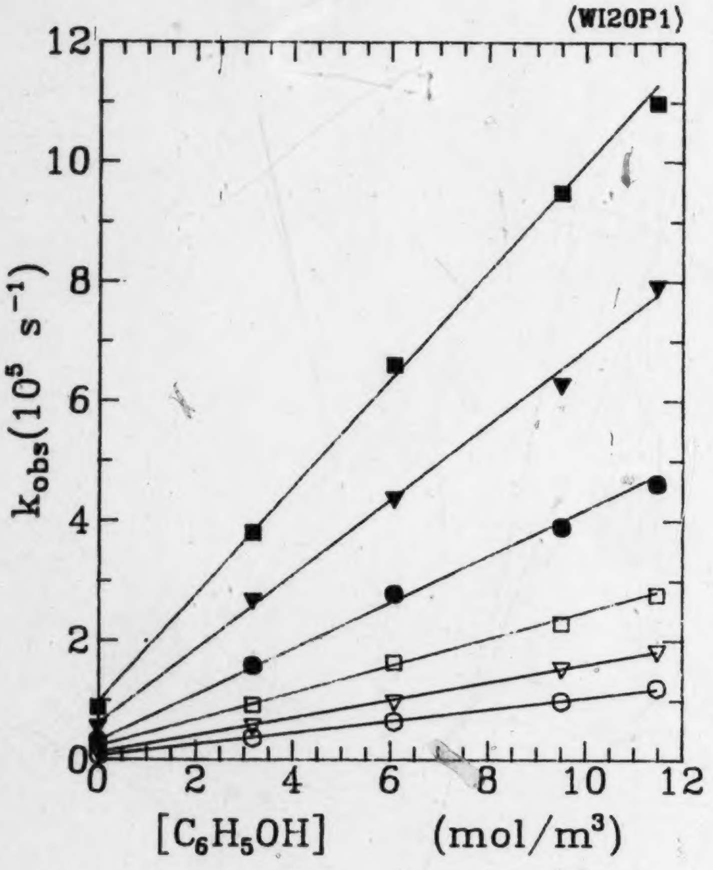

Fig. 3–78: i–BuOH/H_2O:80/20

○ 263.1K ▽ 279.8K □ 297.1K
● 319.0K ▼ 339.7K ■ 363.5K

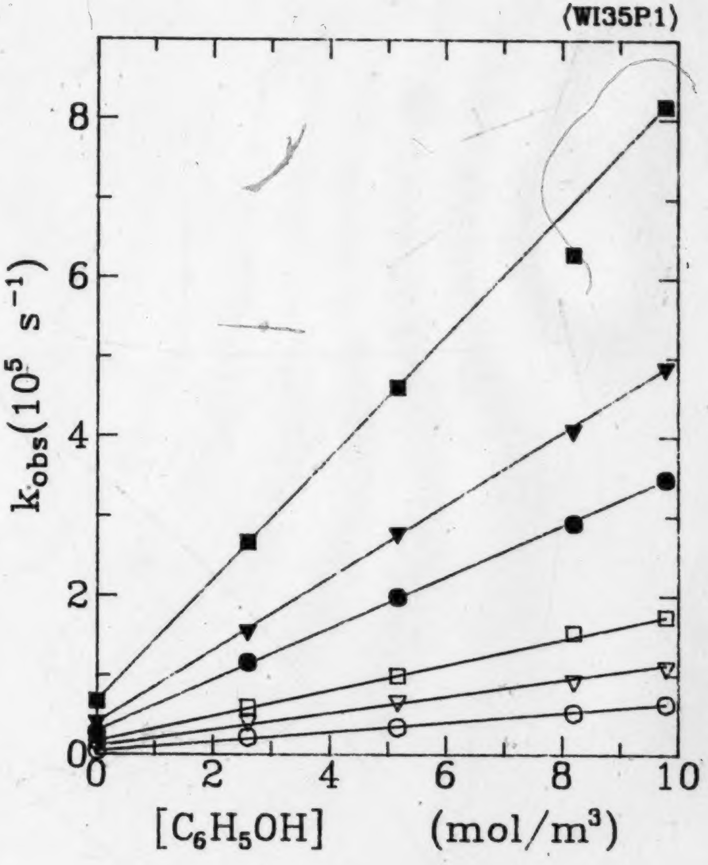

Fig. 3–79: i–BuOH/H_2O:65/35

○ 263.2K ▽ 279.9K □ 296.7K
● 319.9K ▼ 337.6K ■ 364.4K

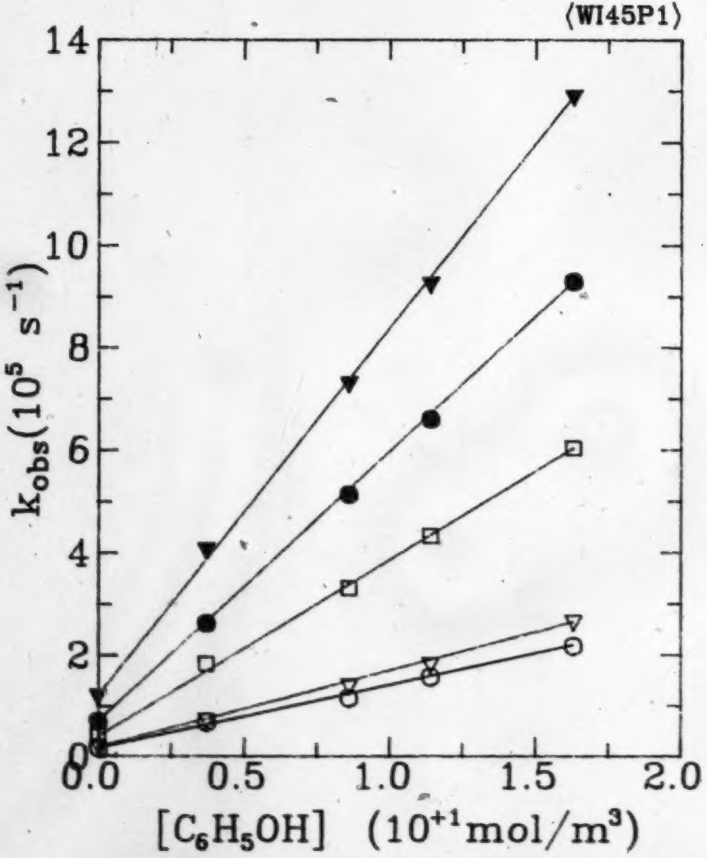

Fig. 3–80: i–BuOH/H_2O:55/45

○ 288.0K ▽ 296.5K □ 323.7K
● 347.4K ▼ 369.1K

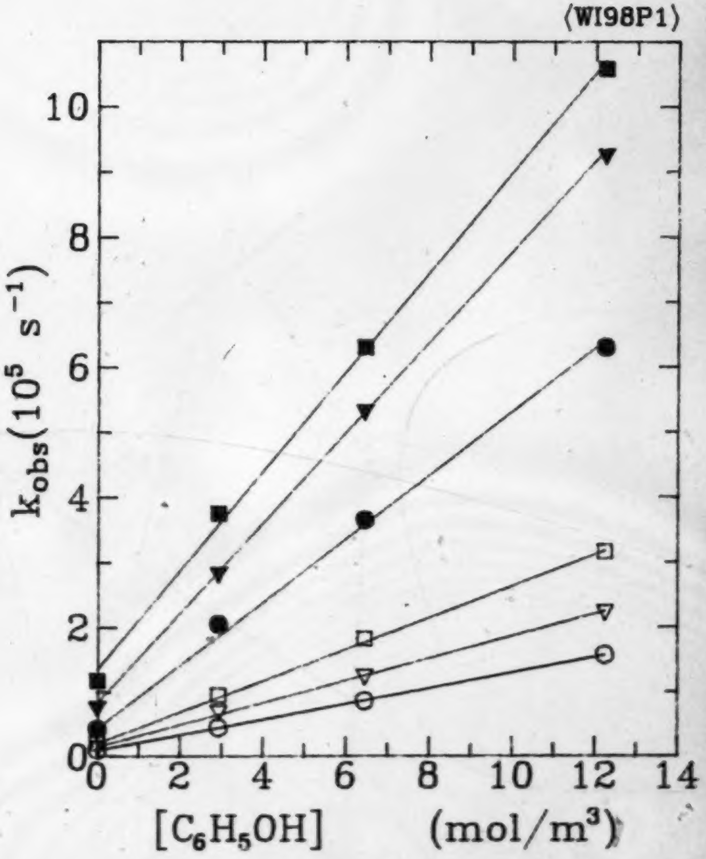

Fig. 3–81: i–BuOH/H_2O:2/98

○ 273.4K ▽ 284.3K □ 297
● 324.2K ▼ 349.7K ■ 370

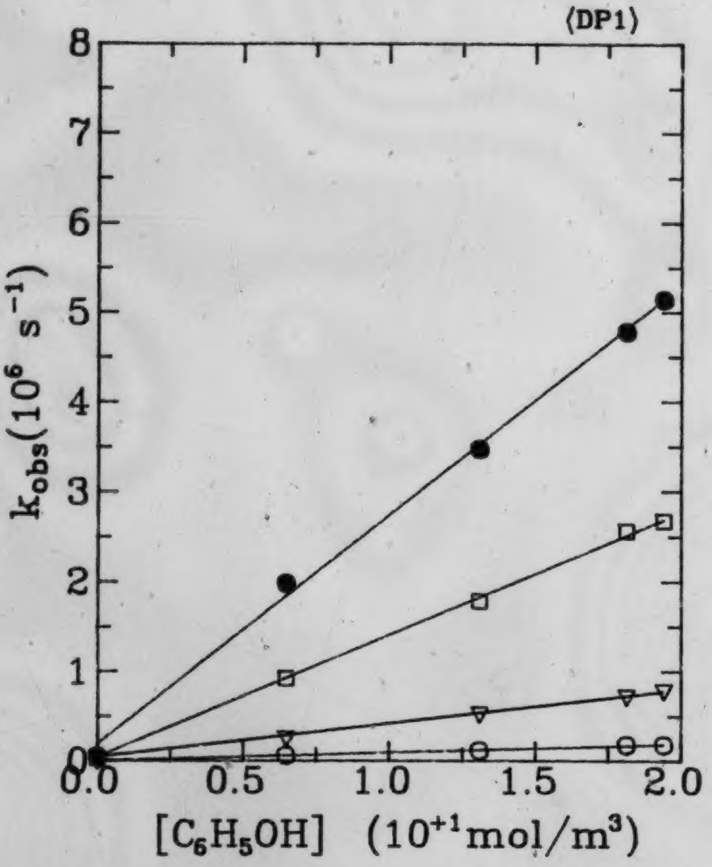

Fig. 3–82: 2–BuOH
○ 220.1K ▽ 244.6K □ 274.5K
● 296.5K

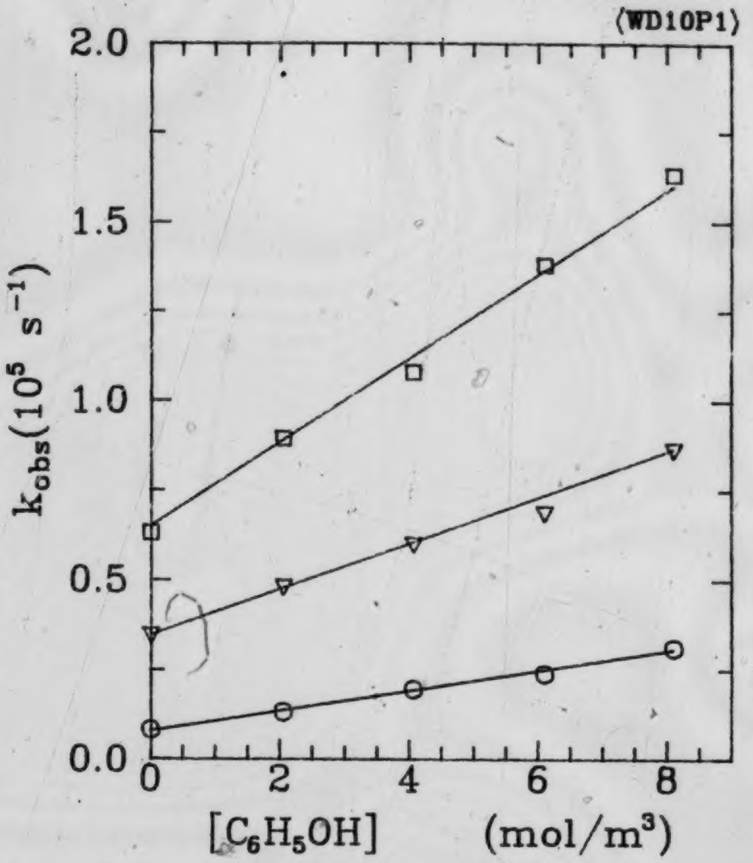

Fig. 3–83a: 2–BuOH/H_2O:90/10
○ 271.5K ▽ 323.2K □ 353.4K

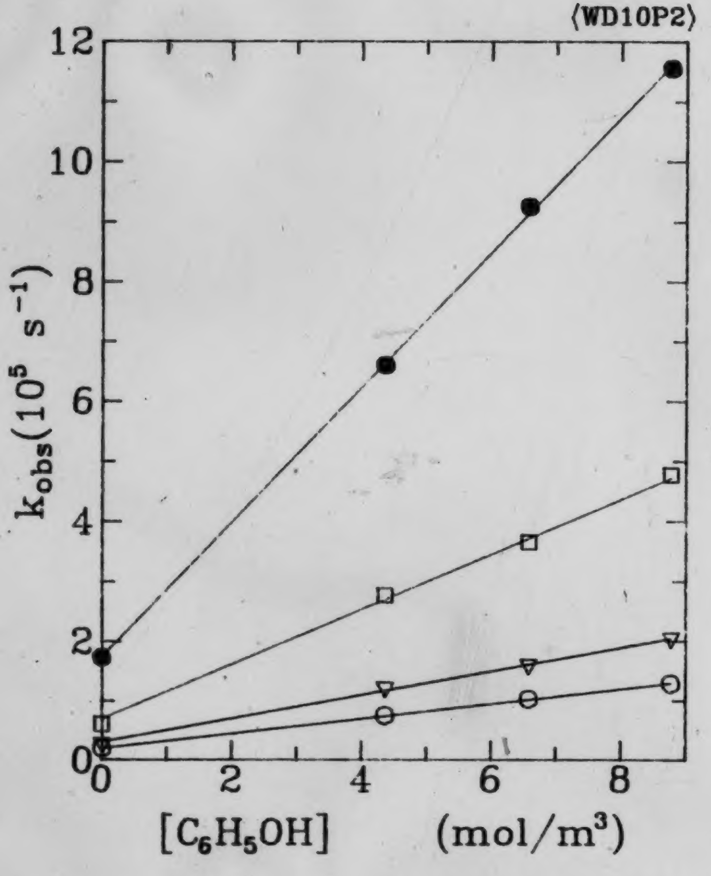

Fig. 3–83b: 2–BuOH/H_2O:90/10
○ 271.0K ▽ 296.7K □ 329.9K
● 368.9K

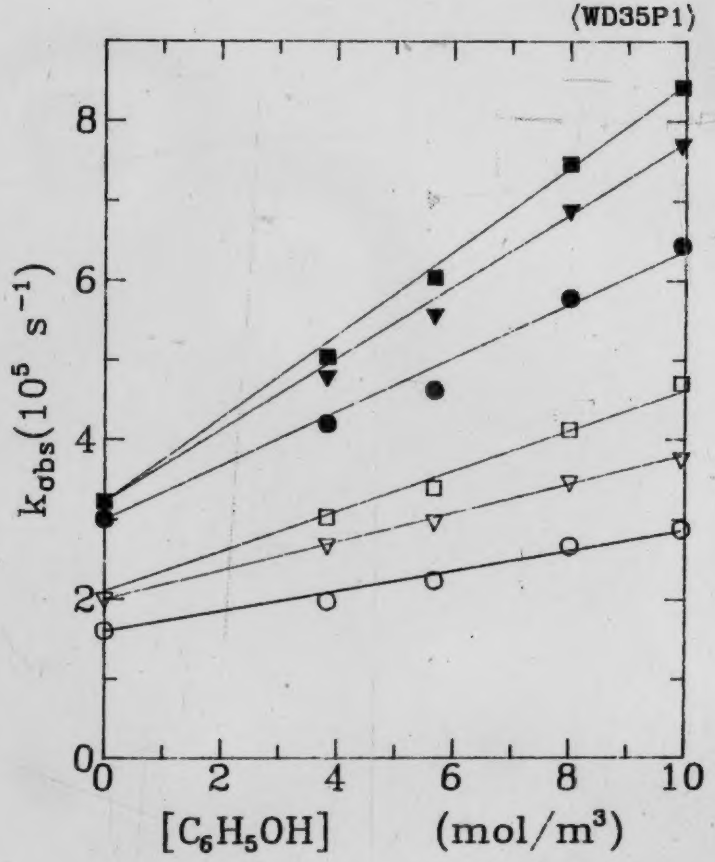

Fig. 3–84: 2–BuOH/H_2O:65/35
○ 296.8K ▽ 310.2K □ 323.8K
● 337.9K ▼ 354.9K ■ 366.3K

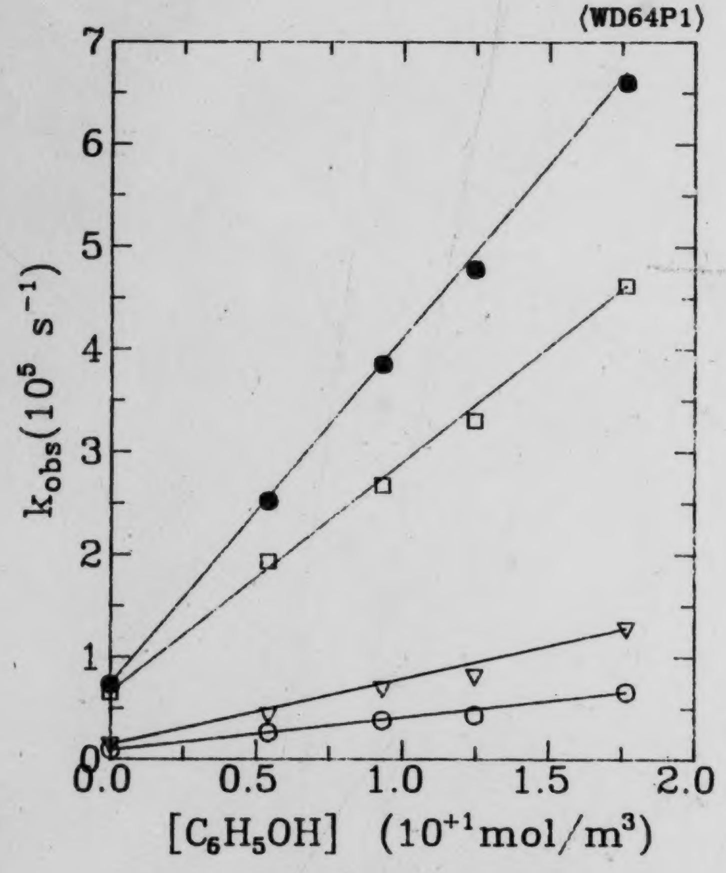

Fig. 3–85: 2–BuOH/H_2O:36/64

○ 272.0K ▽ 296.5K □ 343.4K
● 370.2K

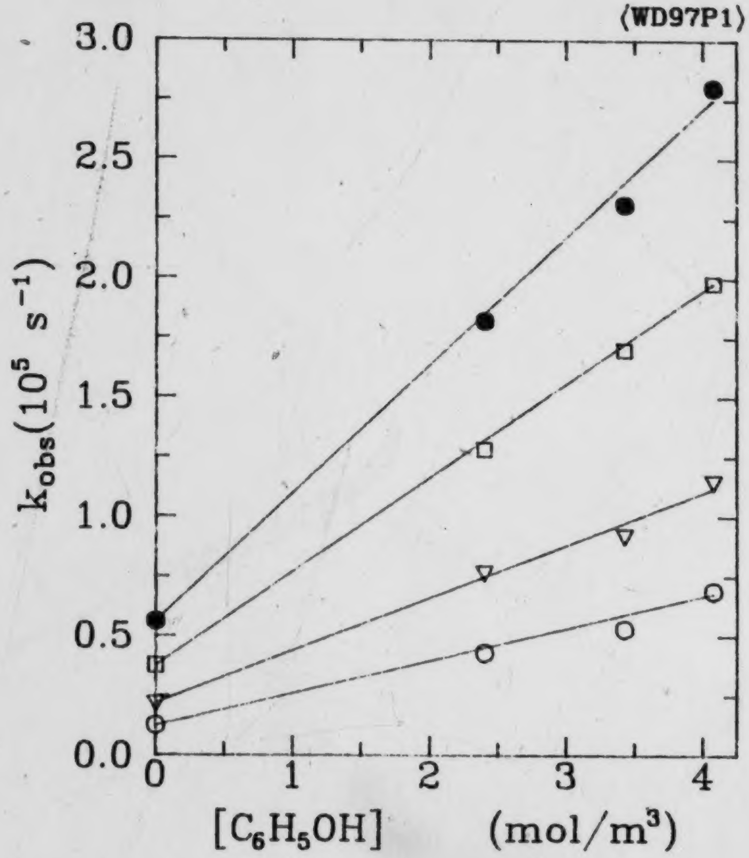

Fig. 3–86: 2–BuOH/H_2O:3/97

○ 274.7K ▽ 296.1K □ 318.6K
● 337.3K

Table 3-15:The values of second order rate constants for phenol in *iso*-butanol/water

x_{H_2O}	T (K)	k_2 $10^4 m^3/mol.s$	x_{H_2O}	T (K)	k_2 $10^4 m^3/mol.s$
0.0	265.2	5.53	0.35	263.2	0.61
	279.8	8.00	0.35	263.2	0.61
	296.7	14.20		296.7	1.61
	308.9	18.80		319.9	3.24
	323.4	27.50		337.6	4.57
	335.8	39.10		364.4	7.67
0.05	265.1	3.46	0.45	288.0	1.28
	279.8	4.48		296.5	1.52
	296.8	6.67		323.7	3.43
	320.0	10.50		347.4	5.24
	337.8	15.20		369.1	8.07
	359.8	23.70	0.98	273.4	1.21
0.10	263.1	1.75		284.3	1.71
	278.9	2.51		297.3	2.42
	297.0	3.89		324.2	4.62
	318.1	6.04		349.7	6.96
	338.8	9.33		370.2	7.65
	362.4	14.50			
0.20	263.1	0.97			
	279.8	1.48			
	297.1	2.26			
	319.0	3.86			
	339.7	6.28			
	363.5	8.98			

Table 3-16:The values of second order rate constants for phenol in 2-butanol/water

x_{H_2O}	T (K)	k_2 $10^4(m^3/mol.s)$
0.0	220.1	0.95
	244.6	3.76
	274.5	15.40
	296.5	25.50
0.10	271.5	2.80
	323.2	6.37
	353.4	11.70
0.10	271.0	2.48
	296.7	3.90
	329.9	9.18
	368.9	12.30
0.64	272.0	0.32
	296.5	0.64
	343.4	2.24
	370.2	3.36
0.97	274.7	1.37
	296.1	2.20
	318.6	3.97
	337.3	5.38

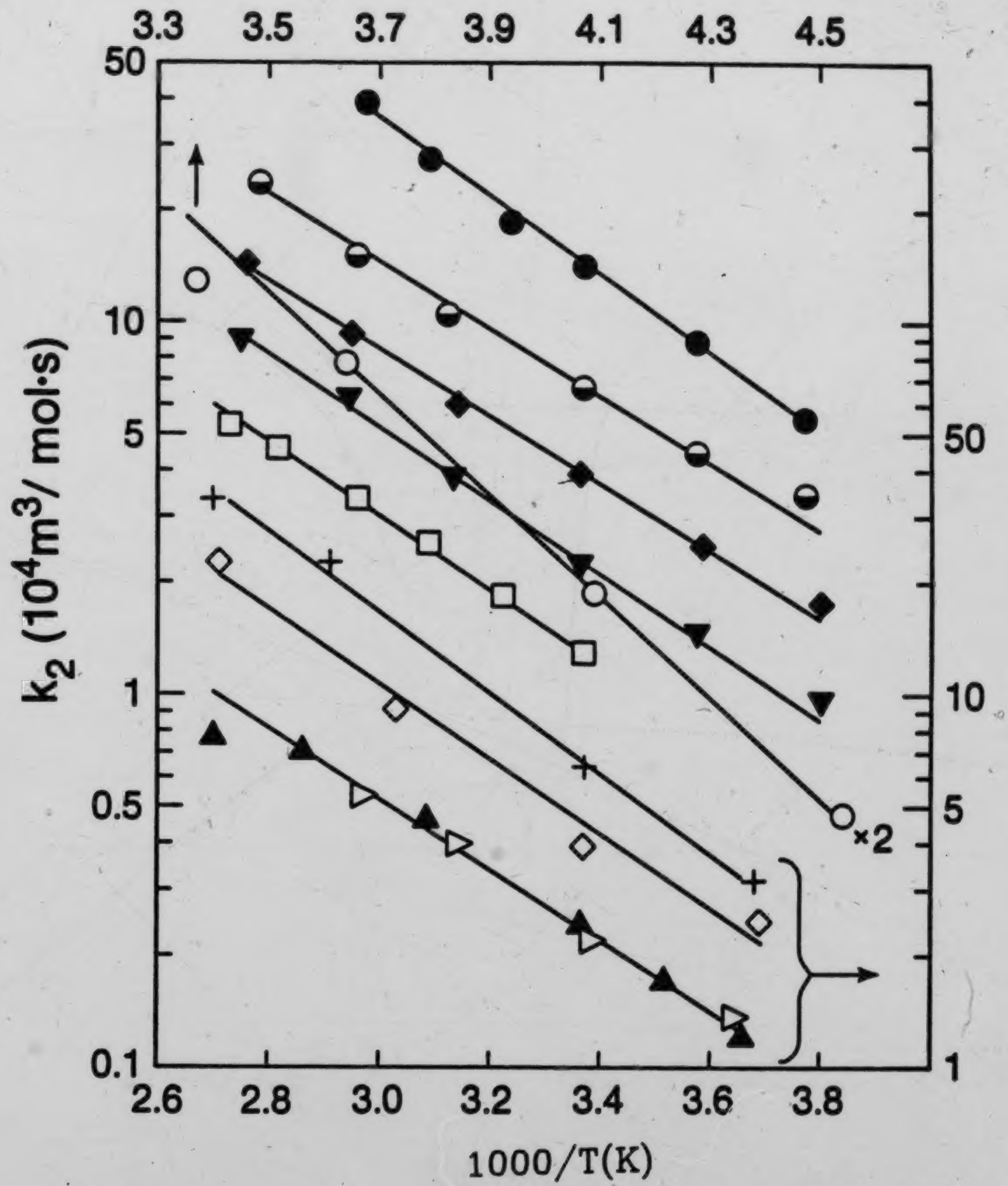

Fig. 3-87: e_s^- + phenol reaction in i-BuOH 2-BuOH/water mixtures.

x_{H_2O}:
i-BuOH: ● 0.00; ◒ 0.05; ◆ 0.10; ▼ 0.20; ■ 0.35; ▶ 0.45;
▲ 0.98; 2-BuOH: ○ 0.00; ◇ 0.10; □ 0.35; + 0.64; ◁ 0.97

Table 3-17: Reaction rate parameters for phenol in *iso*-butanol and 2-butanol/water

x_{H_2O}	k_2 $10^4 m^3/mol.s.$	E_2 (J/mol)	log A	$\Delta S_2^{\neq}$ (J/mol.K)
	Alcohol : *i*-BuOH			
0.0	15.00	20	8.75	-20
0.05	6.90	18	7.92	-36
0.10	4.00	18	7.69	-40
0.20	2.30	18	7.69	-40
0.35	1.80	20	7.77	-39
0.45	1.70	20	7.71	-39
0.98	2.40	18	7.59	-42
1.00	2.60	17	7.41	-45
	Alcohol : 2-BuOH			
0.0	40.00	24	8.89	-17
0.10	4.70	19	8.02	-34
0.35	1.40	19	7.45	-45
0.64	0.69	21	7.45	-45
0.97	2.40	18	7.51	-44
1.00	2.60	17	7.41	-45

Fig.3–88:
k_2 for Toluene (Open) and Phenol (Closed) in Butanol/Water Mixtures.

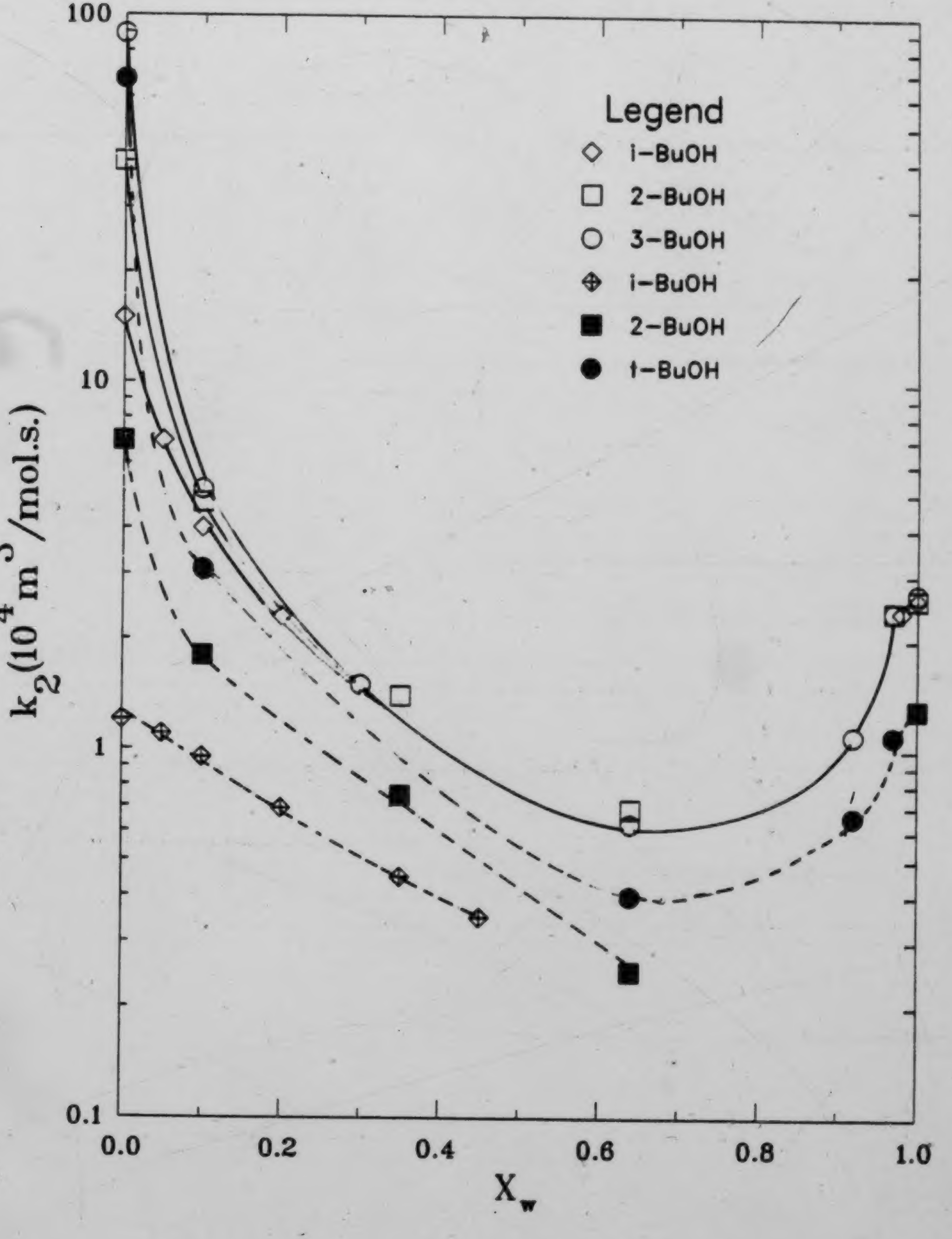

Fig.3-89: E_2 for Phenol in BuOH/Water Mixtures.

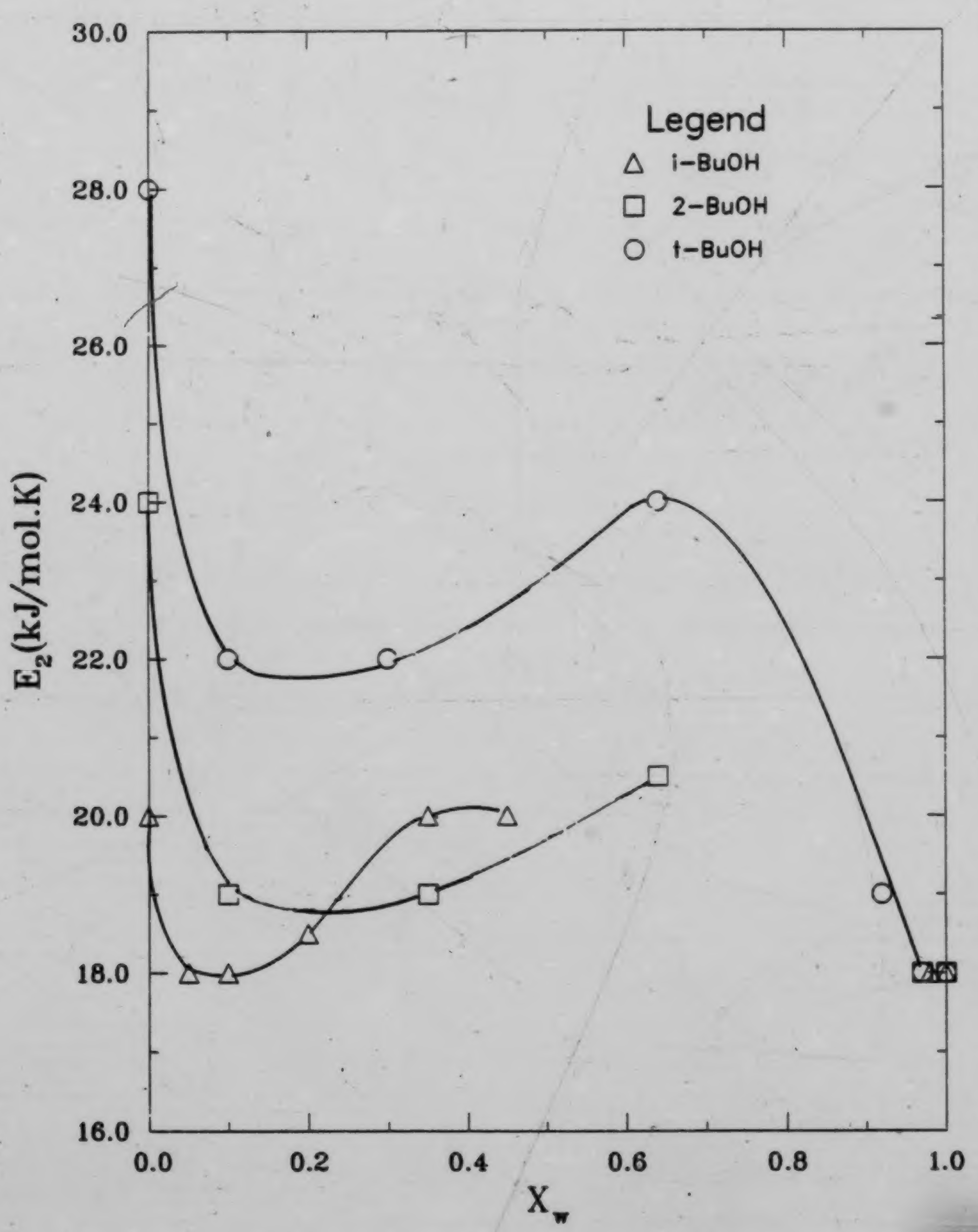

Fig.3–90: ΔS_2 for Phenolin BuOH/Water Mixtures.

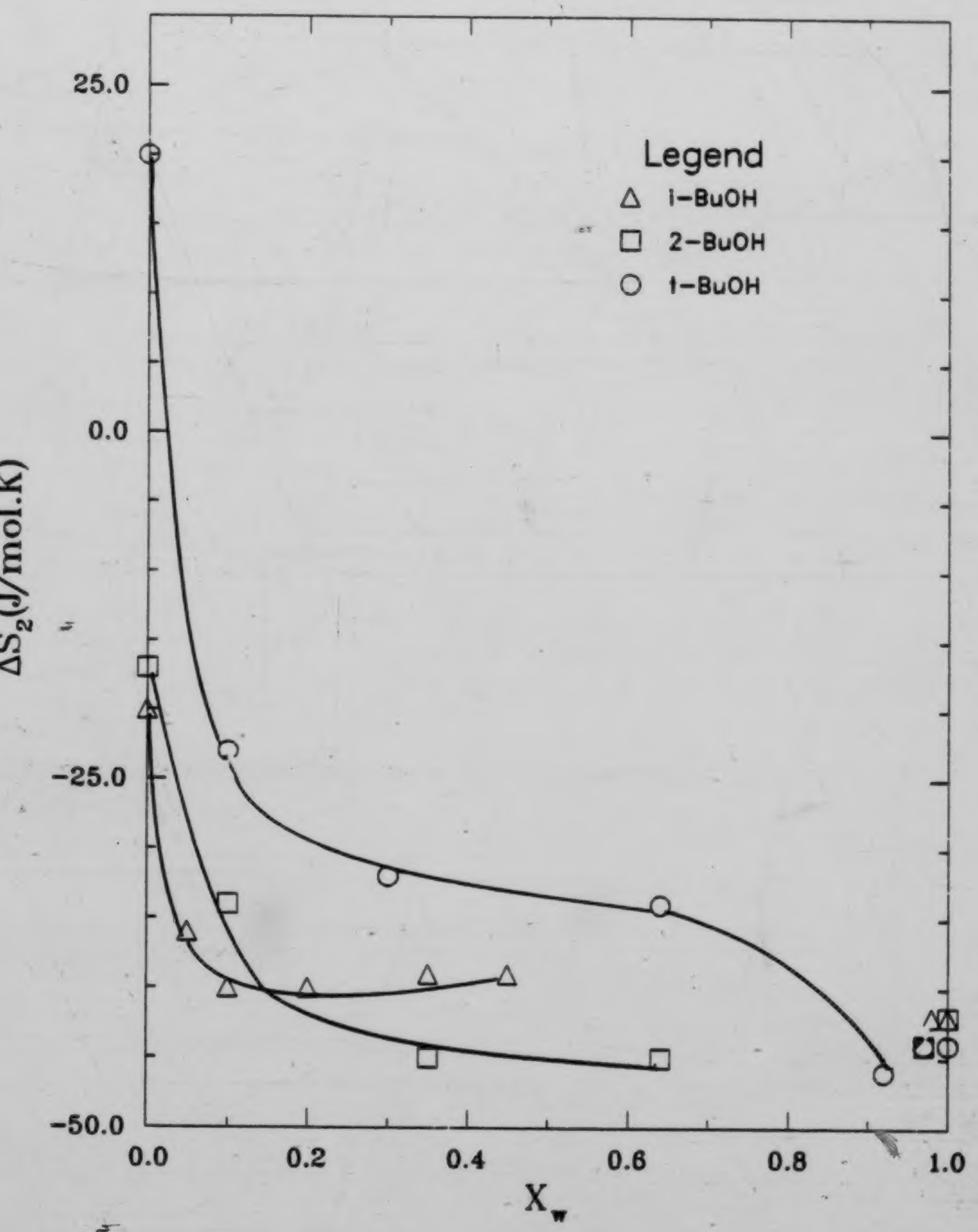

3.1.2(d) Reaction of e_s^- with Toluene

The observed rate constants are in Figs.(3-91) to (3-96) for *i*-BuOH /water mixtures and in Figs.(3-97) to(3-100) for 2-BuOH /water mixtures.The k_2 values are listed in Tables(3-21) and (3-22) respectively.The Arrhenius plots are in Fig.(3-101) and the reaction rate parameters are in Table(3-23).

The k_2 values for the reaction e_s^- + toluene are in the same order as for the other scavengers. The differences among the k_2 values in pure alcohols are greatest for this scavenger since it is the least efficient (Fig. 3-89). In alcohol/water mixtures the rate constants decrease with increasing x_{H_2O} in zones (a) and (b). Unlike the reaction with phenol the k_2 values are always in the order *t*-BuOH > 2-BuOH > *i*-BuOH even in the mid-composition range.

The energies of activation E_2 for e_s^- + toluene reaction in pure *i*-BuOH and pure 2-BuOH are much higher than those for the other scavengers. When a small amount of water is added, E_2 decreases sharply with increasing water content. The energies of activation for the reaction with toluene in alcohol-rich solvents are much higher than that for nitrobenzene in these two alcohols. Therefore the lower rate constants for this reaction are due to changes in the energy of activation more than to entropy changes.

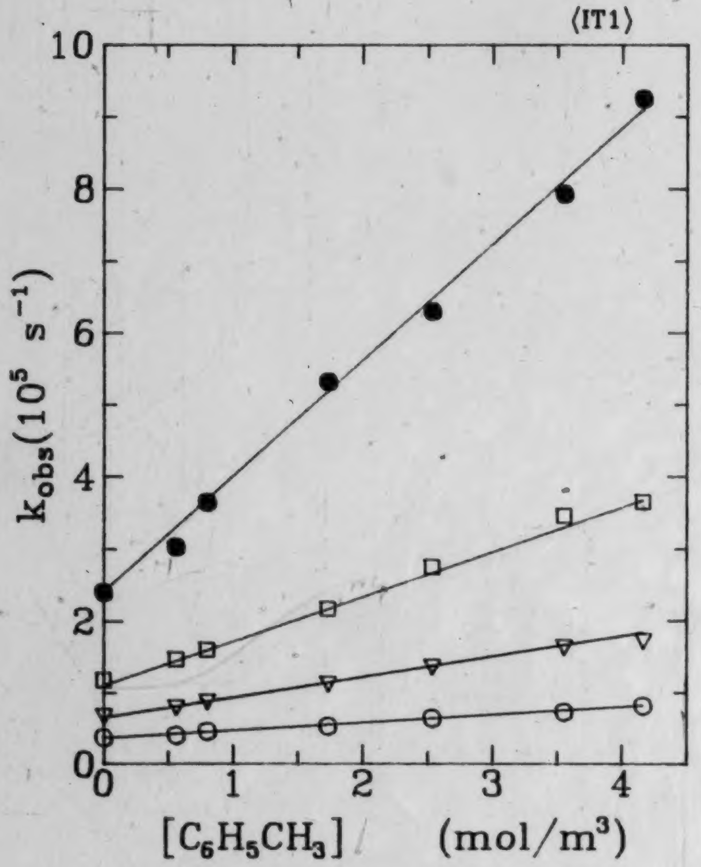

Fig. 3−91: i−BuOH

○ 296.4K ▽ 317.2K □ 337.5K
● 362.3K

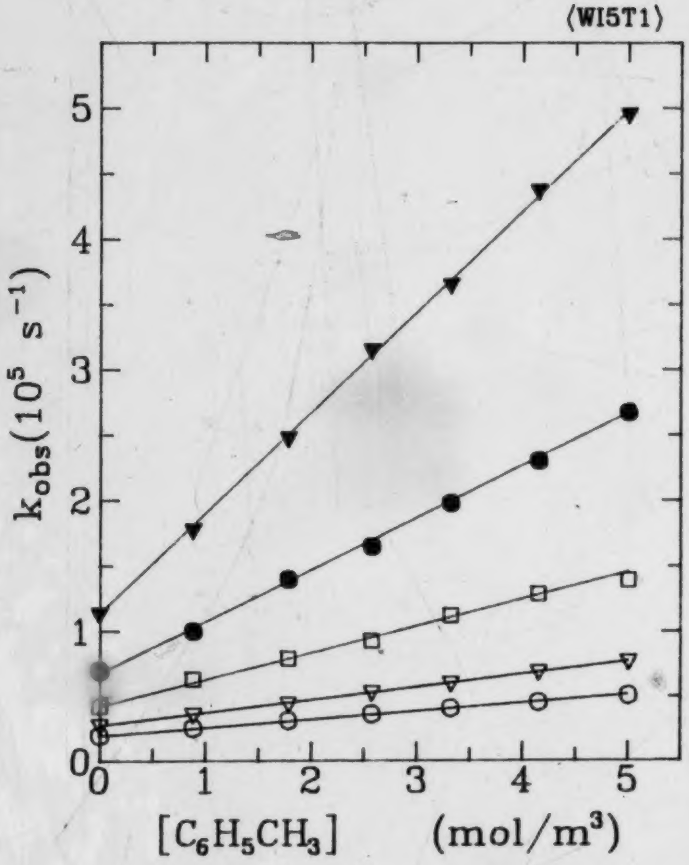

Fig. 3−92: i−BuOH/H_2O:95/5

○ 284.0K ▽ 296.6K □ 317.1K
● 337.8K ▼ 362.2K

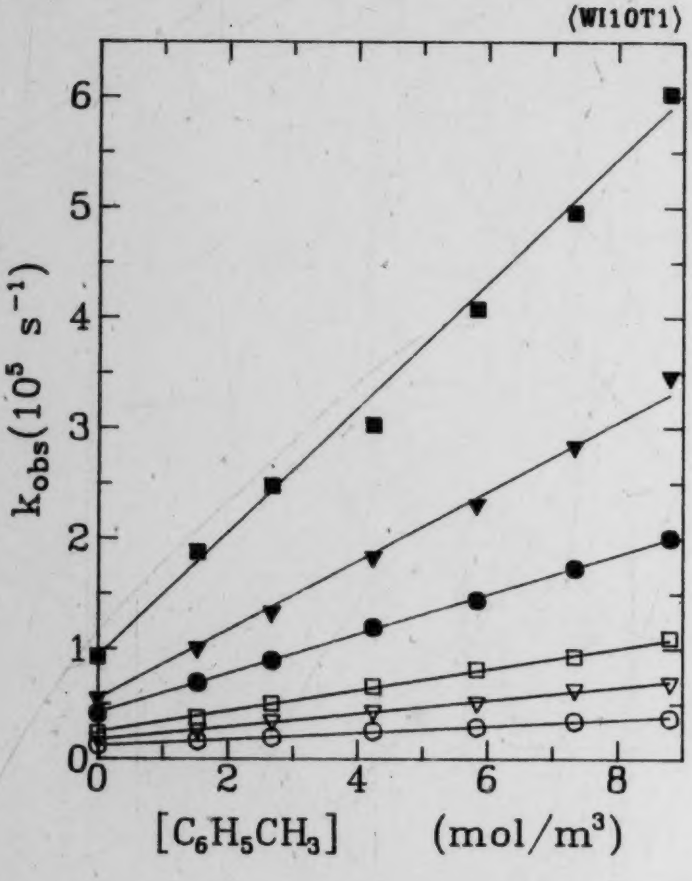

Fig. 3–93: i–BuOH/H_2O:90/10
○ 268.2K ▽ 283.8K □ 297.1K
● 319.0K ▼ 337.5K ■ 364.1K

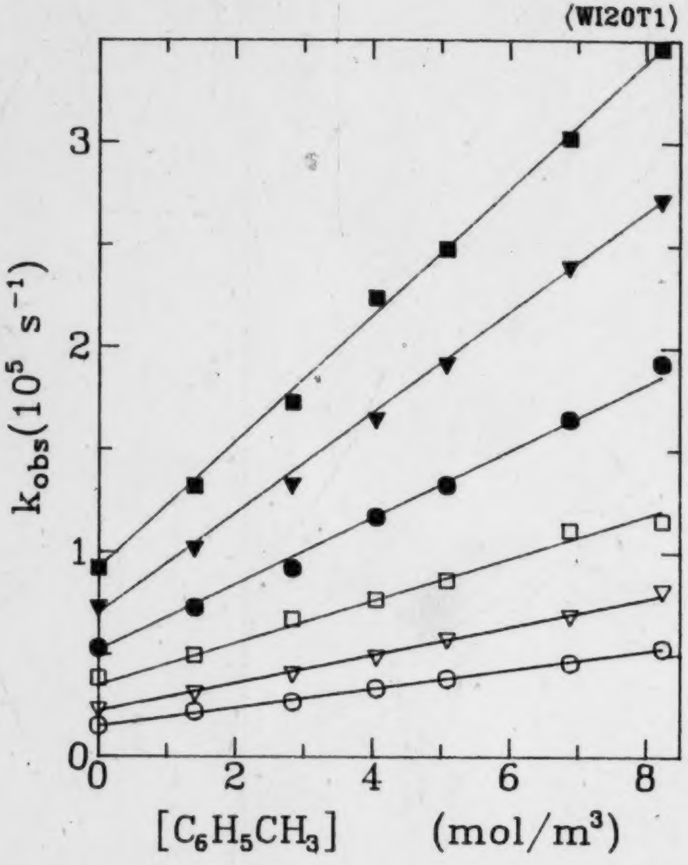

Fig. 3–94: i–BuOH/H_2O:80/20
○ 283.9K ▽ 297.1K □ 313.5K
● 330.2K ▼ 348.9K ■ 364.0K

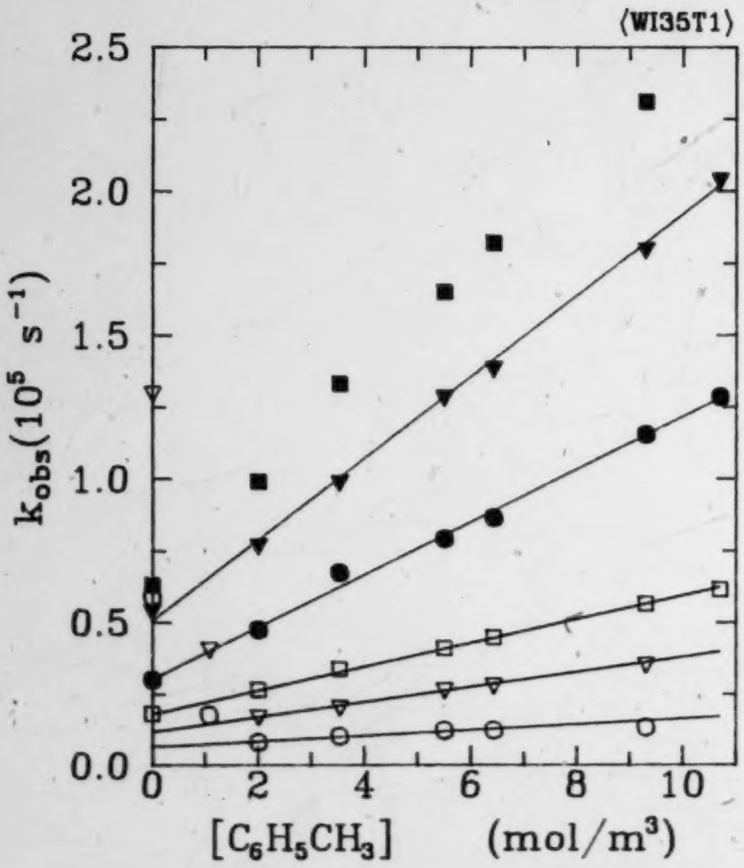

Fig. 3–95: i–BuOH/H_2O:65/35

○ 263.9K ▽ 284.0K □ 296.0K
● 323.1K ▼ 344.2K ■ 363.4K

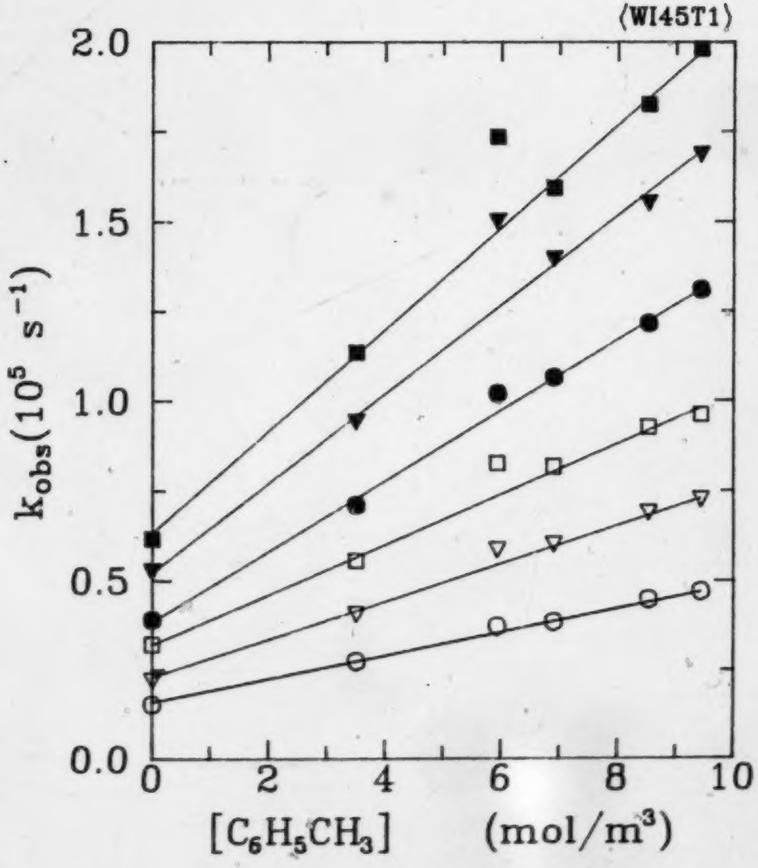

Fig. 3–96: i–BuOH/H_2O:55/45

○ 297.0K ▽ 311.5K □ 326.6K
● 338.6K ▼ 352.9K ■ 366.8K

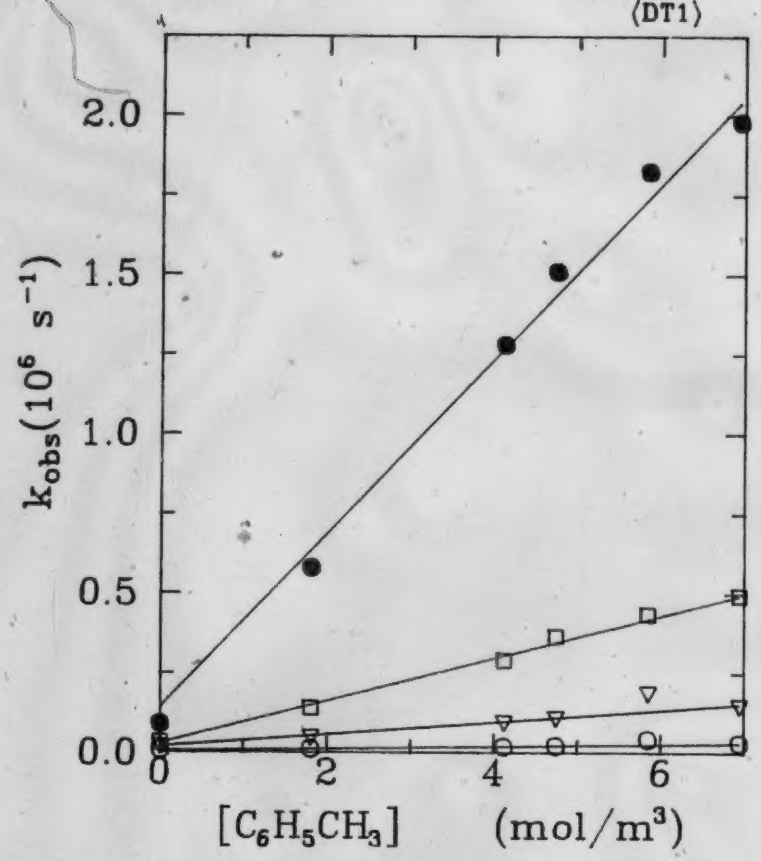

Fig. 3−97: 2−BuOH

○ 246.3K ▽ 275.1K □ 296.3K

● 327.5K

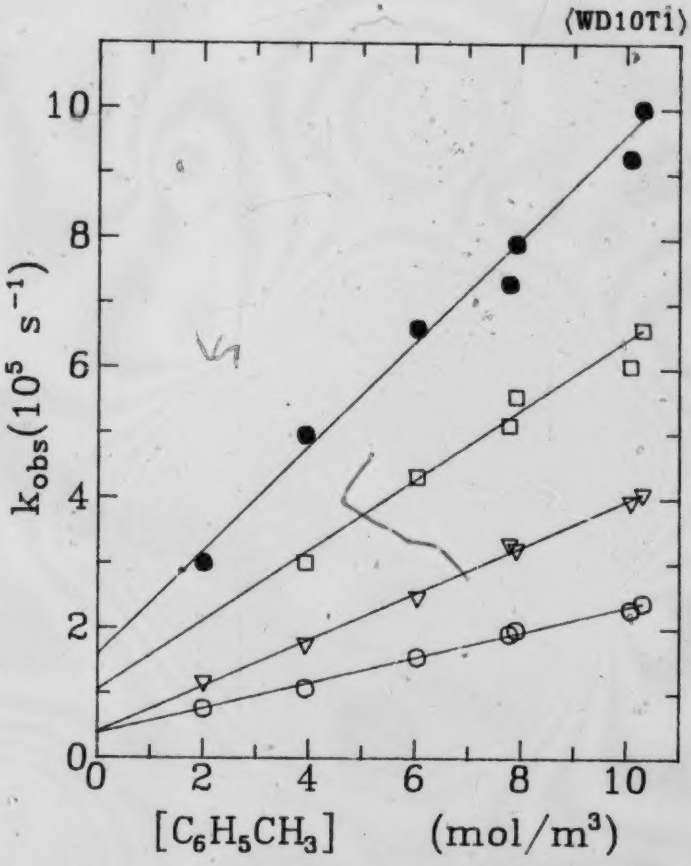

Fig. 3−98: 2−BuOH/H_2O:90/10

○ 296.4K ▽ 314.0K □ 335.3K

● 365.9K

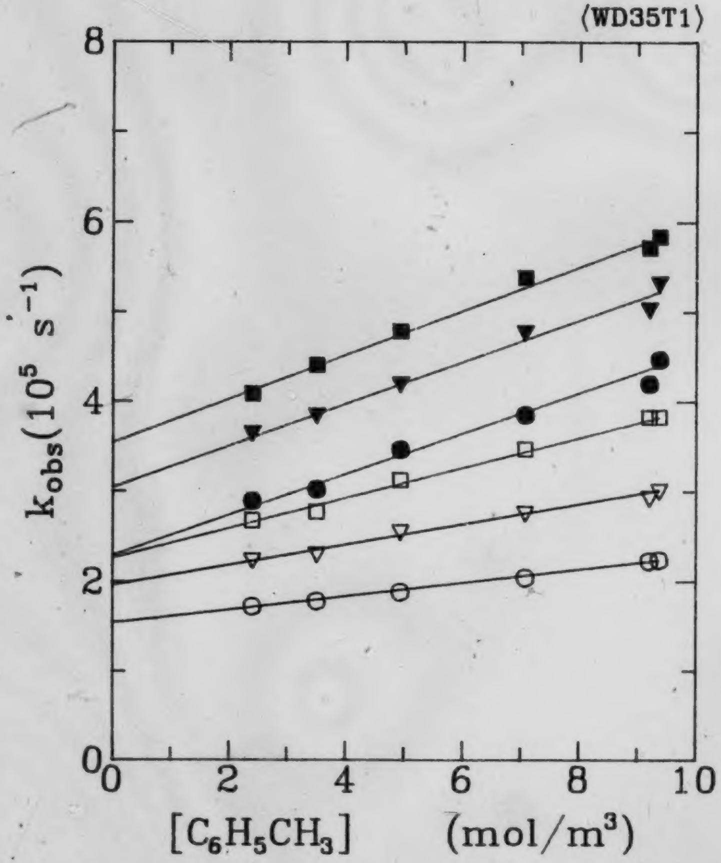

Fig. 3−99: 2−BuOH/H_2O:65/35

○ 295.1K ▽ 310.3K □ 323.9K
● 337.8K ▼ 355.0K ■ 366.4K

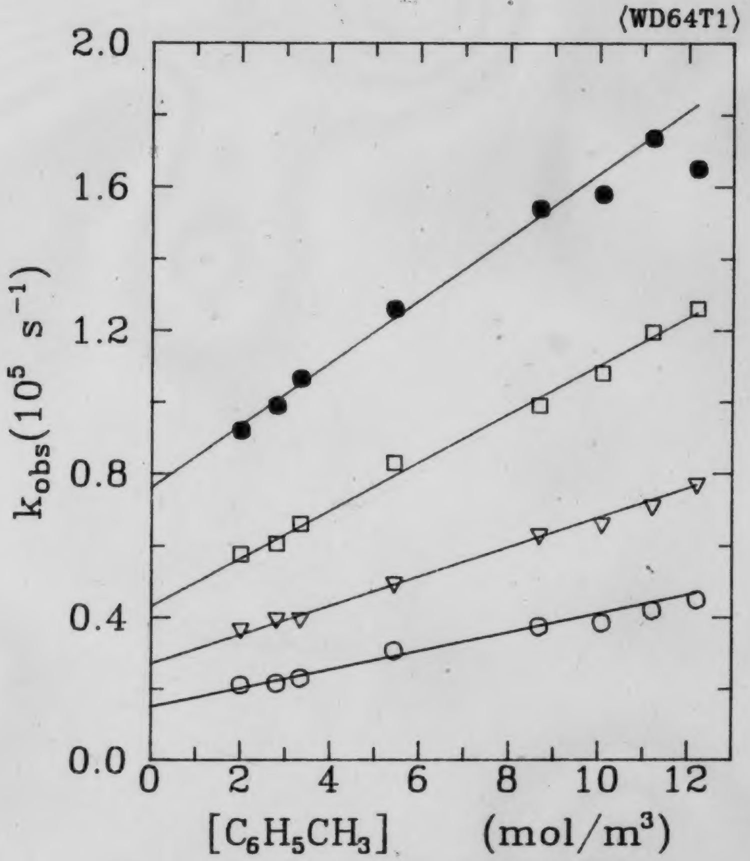

Fig. 3−100: 2−BuOH/H_2O:36/64

○ 295.3K ▽ 314.3K □ 337.6K
● 363.2K

Table 3-18:The values of second order rate constants for toluene in *iso*-butanol/water

x_{H_2O}	T (K)	k_2 $10^4(m^3/mol.s)$
0.0	296.4	1.10
	317.2	2.86
	337.5	6.43
	362.3	16.20
0.05	284.0	0.67
	296.6	1.01
	317.1	2.08
	337.8	3.98
	362.2	7.67
0.10	283.8	0.59
	297.1	0.94
	319.1	1.79
	337.5	3.14
	364.1	5.65
0.20	283.9	0.46
	297.1	0.69
	313.5	1.04
	330.2	1.63
	348.9	2.46
	364.0	3.10
0.35	263.9	0.10
	284.0	0.26

	296.0	0.42
	323.1	0.92
	344.2	1.42
	363.4	1.85
0.45	297.0	0.33
	311.5	0.54
	326.6	0.70
	338.6	0.98
	352.9	1.24
	366.8	1.42

Table 3-19:The values of second order rate constants for toluene in 2-butanol/water

x_{H_2O}	T (K)	k_2 $10^4 (m^3/mol.s)$
0.0	246.3	0.38
	275.1	1.94
	296.3	6.78
	327.5	27.30
0.10	296.4	1.93
	314.0	3.54
	335.3	5.95
	365.9	8.04
0.35	295.1	0.74
	310.3	1.11
	323.9	1.71
	337.8	2.26
	355.0	2.43
	366.4	2.76
0.64	295.3	0.23
	314.3	0.40
	337.6	0.67
	363.2	0.99

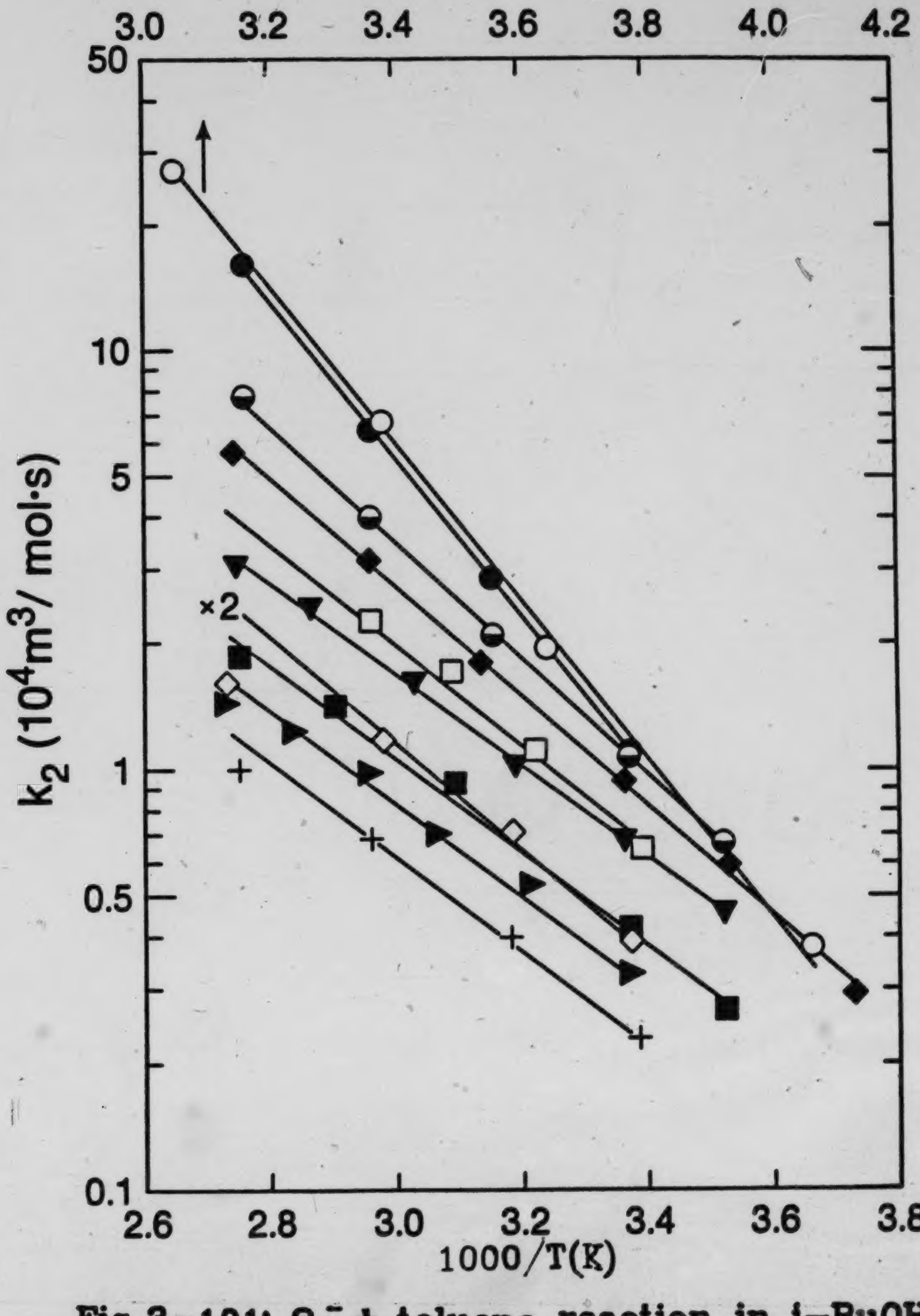

Fig. 3–101: e_s^- + toluene reaction in i–BuOH, 2–BuOH/water mixtures. (Symbols: Fig.3–57)

Table 3-20: Reaction rate parameters for toluene in *iso*-butanol and 2-butanol/water

x_{H_2O}	k_2 $10^4 m^3 mol.s.$	E_2 (J/mol)	log A	$\Delta S_2^{\neq}$ (J/mol.K)
	Solvent : Water in i-BuOH			
0.0	1.20	36	10.43	12
0.05	1.10	26	8.68	-21
0.10	0.95	25	8.33	-28
0.20	0.69	21	7.49	-44
0.35	0.45	21	7.33	-47
0.45	0.35	21	7.33	-50
1.00	1.10	18	7.26	-48
	Solvent : Water in 2-BuOH			
0.0	6.90	35	11.01	23
0.10	1.80	24	8.46	25
0.35	0.75	23	7.81	-38
0.64	0.25	22	7.30	-48
1.00	1.10	18	7.26	-48

Fig.3–102: E_2 for Toluene in BuOH/Water Mixtures.

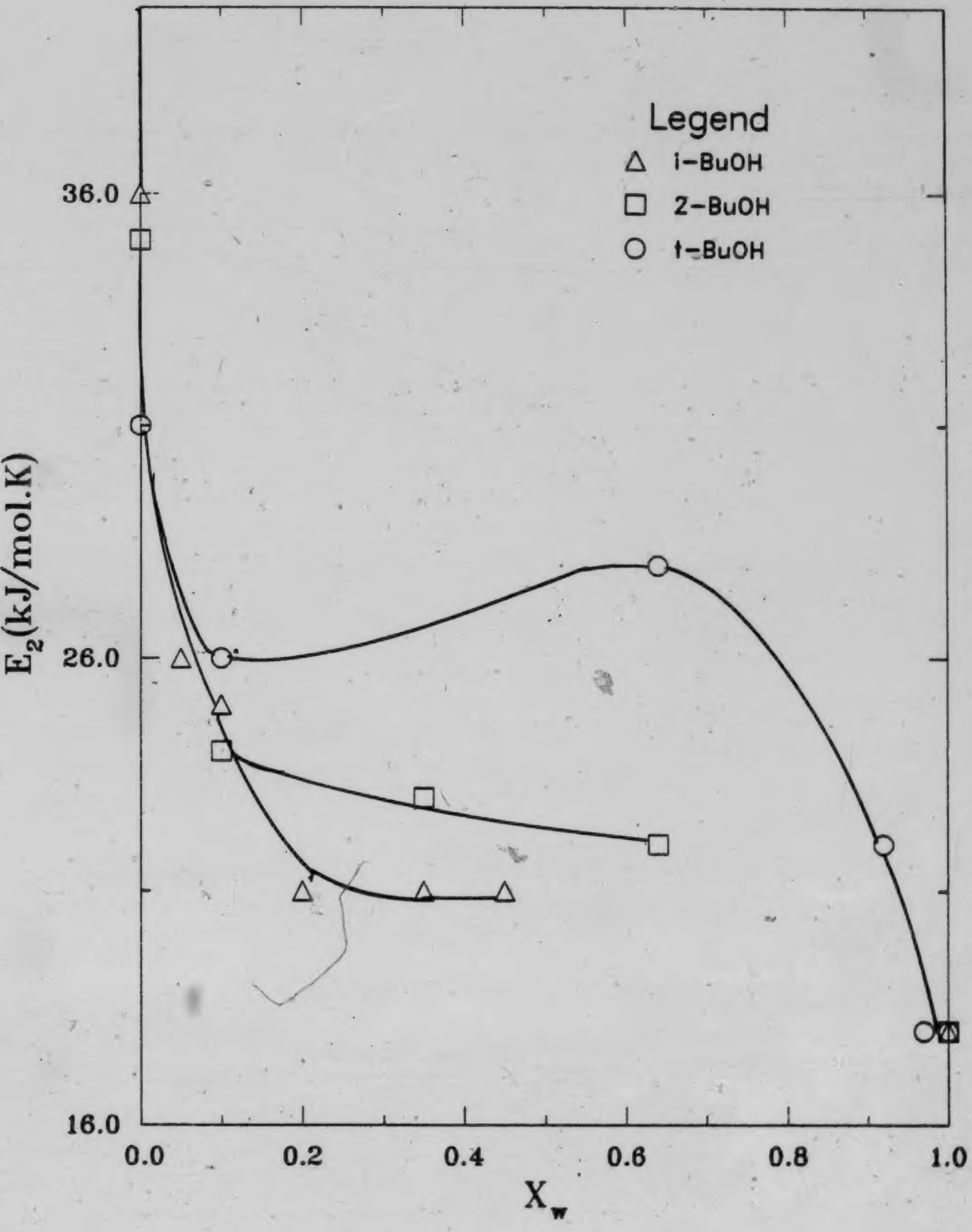

Fig.3–103: $\Delta \bar{S}_2^{\circ}$ for Toluenein BuOH/Water Mixtures.

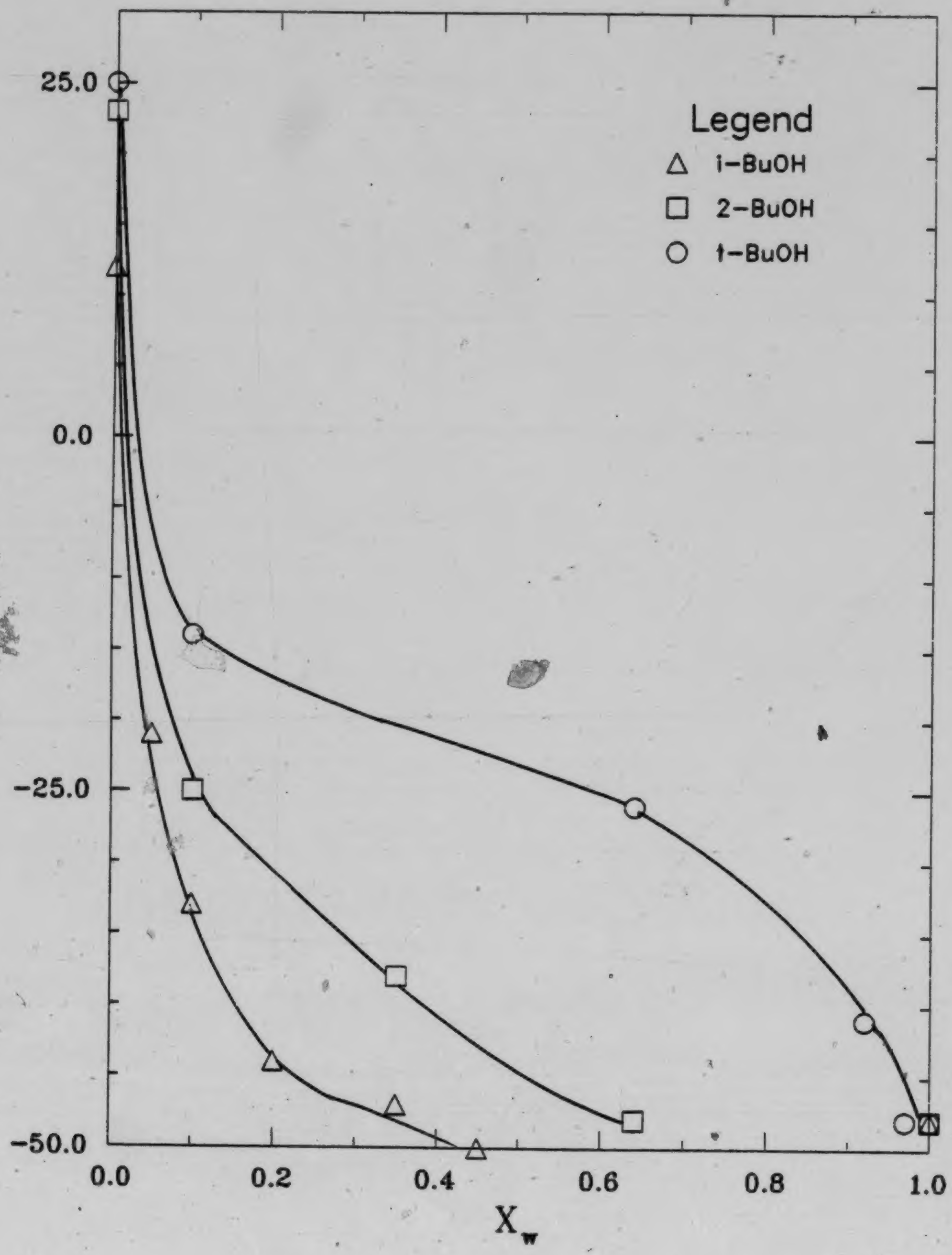

3.2 Inorganic Scavengers

The reactivity of six ions with different charges were studied in *t*-BuOH /water mixtures. The rate constant in water for each of the scavengers is $\sim 10^7 m^3/mol.s.$ and is nearly diffusion controlled.

3.2(a) Reaction of e_s^- with Positive Scavengers

The univalent ion Ag^+ and bivalent ion Cu^{2+} were used. The counter ion for Ag^+ was ClO_4^- and those for Cu^{2+} were ClO_4^- and SO_4^{2-}. Since the rate constants for these counter ions are $< 10^3\ m^3/mol.s.$ (51), the nearly diffusion controlled k_2 values ($10^7\ m^3/mol.s.$) obtained are those of the positive ions.

The solvent compositions for the $e_s^- + AgClO_4$ reaction were: $x_{H_2O} =$ 1.00, 0.98, 0.97, 0.94, 0.90, 0.85, 0.75, 0.64, 0.50, 0.35, 0.10, and 0. The first-order rate constants are in Figs.(3-104) to (3-115). The concentration range of $AgClO_4$ was 0.003 - 0.1 mol/m^3.

For the $e_s^- + CuSO_4$ reaction the compositions were: $x_{H_2O} = 1.00$, 0.98, 0.97, 0.94. Lower water contents were not used because $CuSO_4$ was not sufficiently soluble. The first order rate constants at these compositions are in Figs.(3-116) to (3-120). The concentration range was 0.005 - 0.05 mol/m^3.

The rate constants of this reaction display a temperature dependence different from other scavengers (organic or inorganic), hence the same compositions were studied with $Cu(ClO_4)_2$. These are in Figs.(3-121) to (3-125).

In some water mixed systems the observed rate constants correspond to lower concentrations of the scavenger and give a negative y-intercept in the k_{obs} (y) versus [S] (x) plot. Since the intercept is affected this is probably due to the presence in the water of either a chelating agent or a negative ion that precipitates the positive ion. Since only the intercept is affected (change in the half-life in solvent), there is no effect on the k_2 values.

The second-order rate constants are listed in Table(3-21). The Arrhenius plots for reaction with Ag^+ are in Fig.(3-126) and those for Cu^{2+} are in Fig.(3-127). The Arrhenius plots for Ag^+ display slight curvature in alcohol-rich solvents. Arrhenius parameters in such systems were calculated by drawing an average line through the points. The Arrhenius plot of $Cu(ClO_4)_2$ in water is similar to that of $CuSO_4$ in water. In mixed solvents the ele ctron reaction with Cu^{2+} ion displays complex behaviour.

The k_2 values for the reaction with Ag^+ decrease slightly when up to $x_{H_2O} \approx 0.1$ is added, is relatively constant up to $x_{H_2O} = \approx 0.80$, and then increases sharply until pure water (Fig. 3-128).

Energies and entropies of activation (Fig. 3-128) decrease until $x_{H_2O} \approx 0.1$, is constant $0.1 < x_{H_2O}$ ¡0.85, and decrease until pure water. Those for the $e_s^- + Cu^{2+}$ reaction also display similar behaviour indicating that the complex behaviour for k_2 observed in this system is not due to the energetics of the reaction.

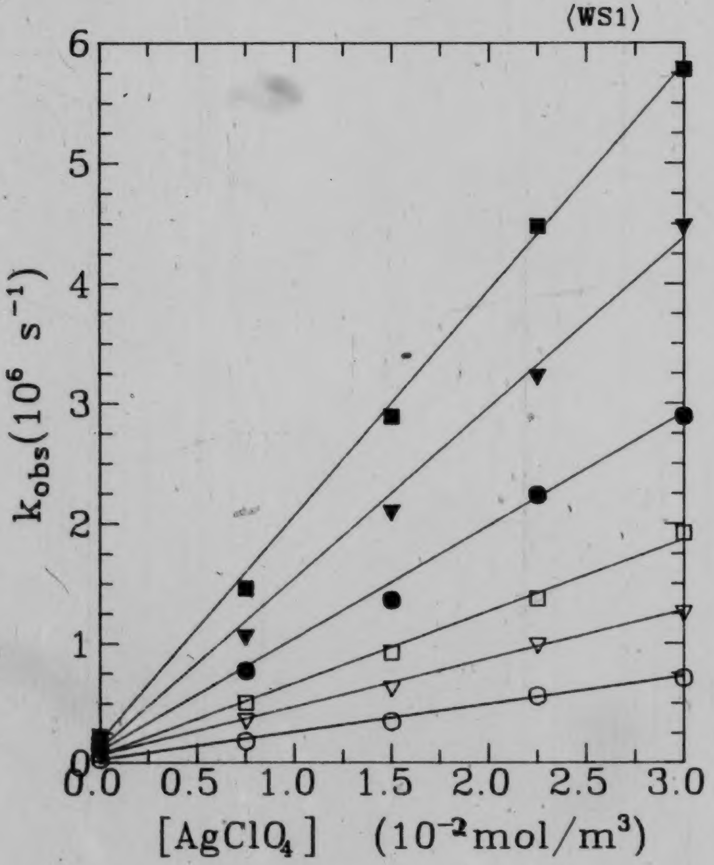

Fig. 3−104a:H_2O

○ 276.8K ▽ 296.8K □ 313.5K
● 333.2K ▼ 354.0K ■ 370.8K

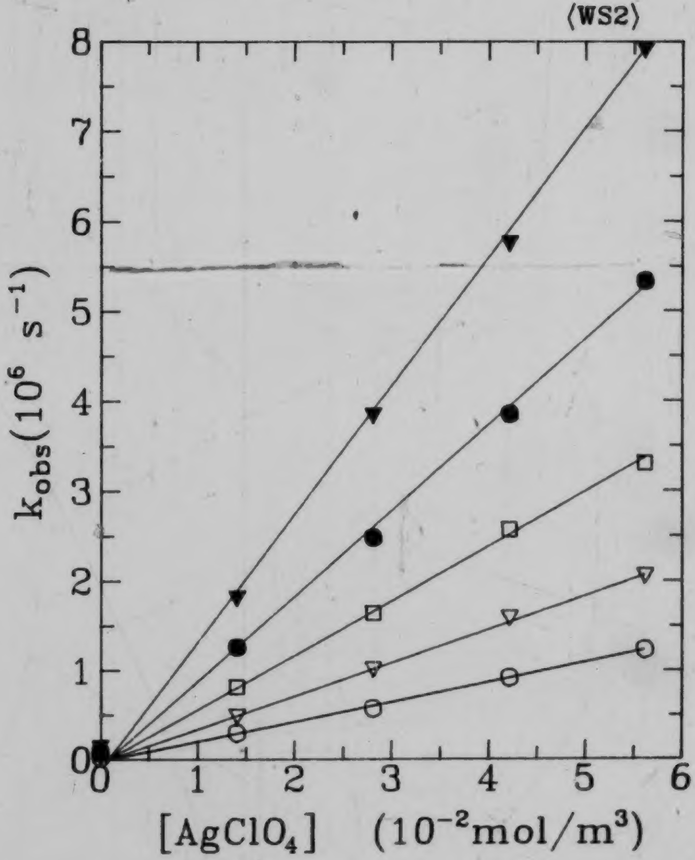

Fig. 3−104b:H_2O

○ 276.2K ▽ 295.1K □ 313.8K
● 333.4K ▼ 354.3K

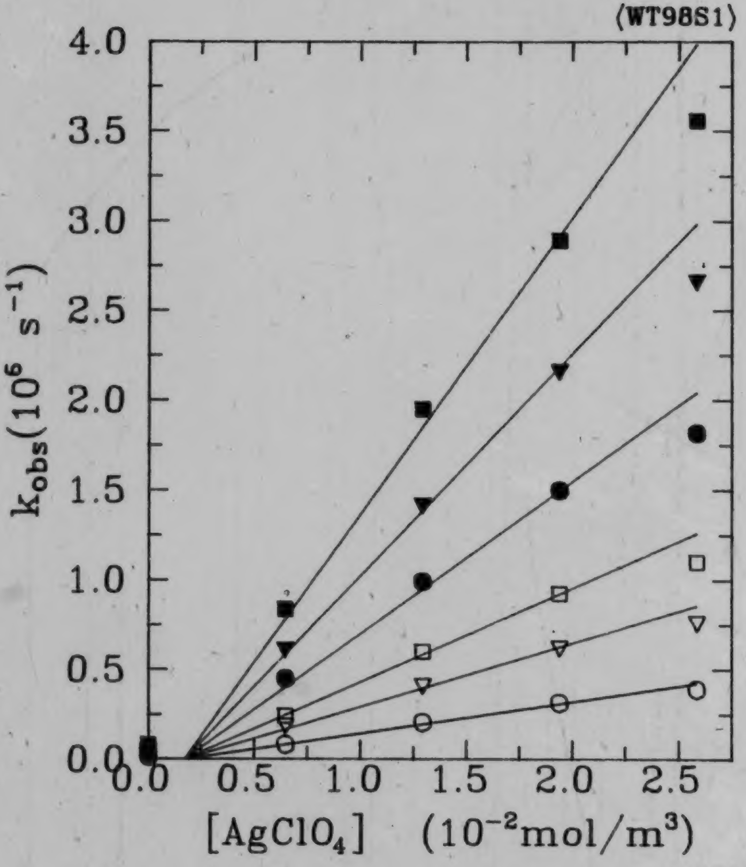

Fig. 3–105: t–BuOH/H_2O:2/98

○ 278.1K ▽ 297.2K □ 313.8K
● 333.3K ▼ 354.1K ■ 370.0K

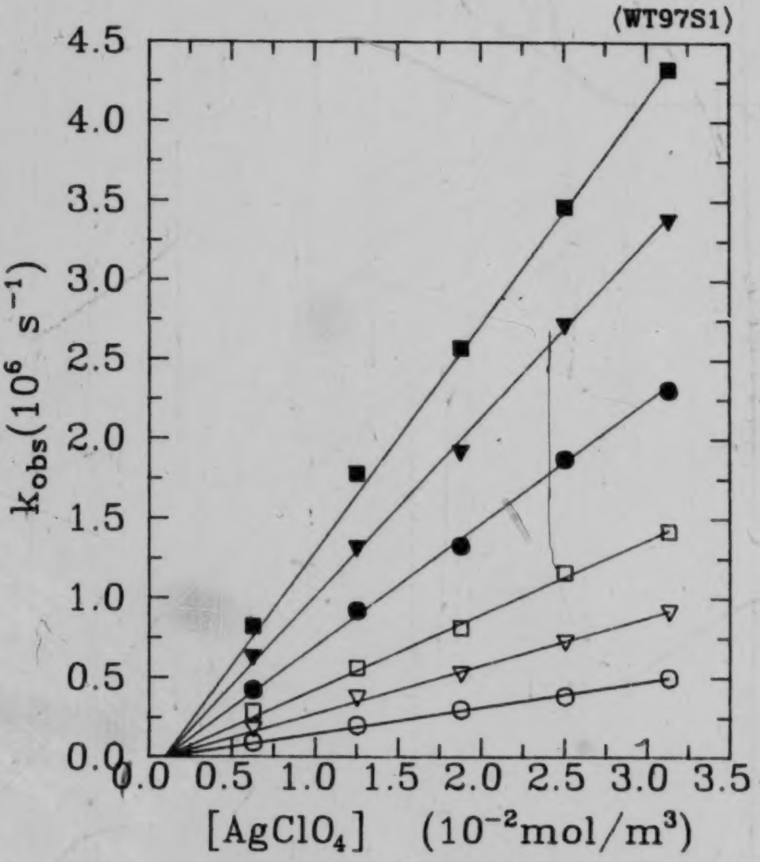

Fig. 3–106: t–BuOH/H_2O:3/97

○ 278.2K ▽ 297.2K □ 313.8K
● 333.3K ▼ 354.1K ■ 368.7K

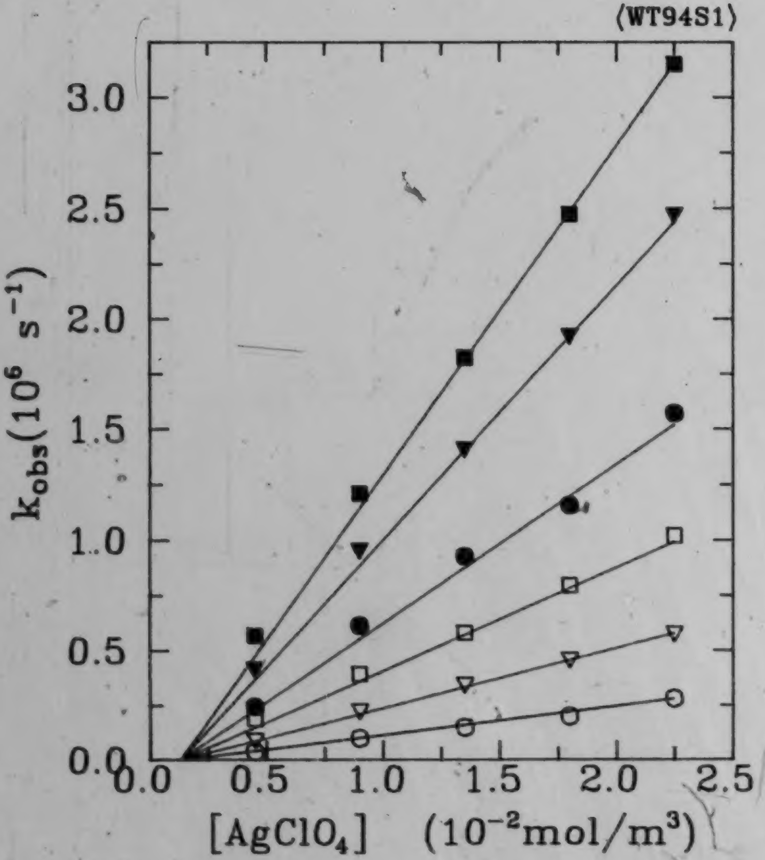

Fig. 3−107: t−BuOH/H_2O:6/94

○ 280.0K ▽ 297.5K □ 313.8K
● 333.4K ▼ 354.1K ■ 368.3K

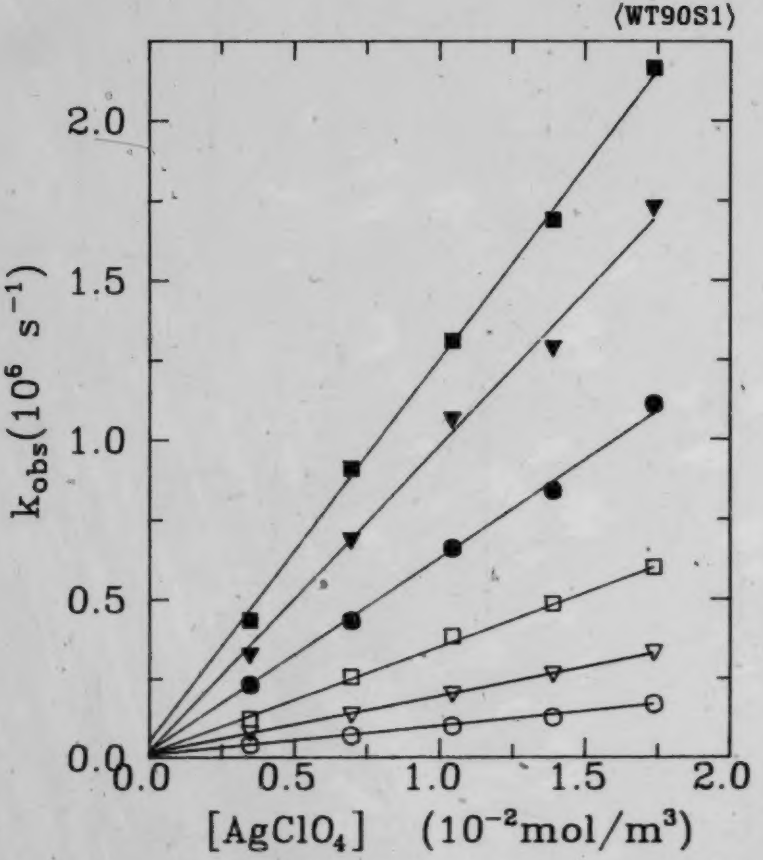

Fig. 3−108: t−BuOH/H_2O:10/90

○ 279.9K ▽ 294.7K □ 313.8K
● 333.4K ▼ 354.3K ■ 368.6K

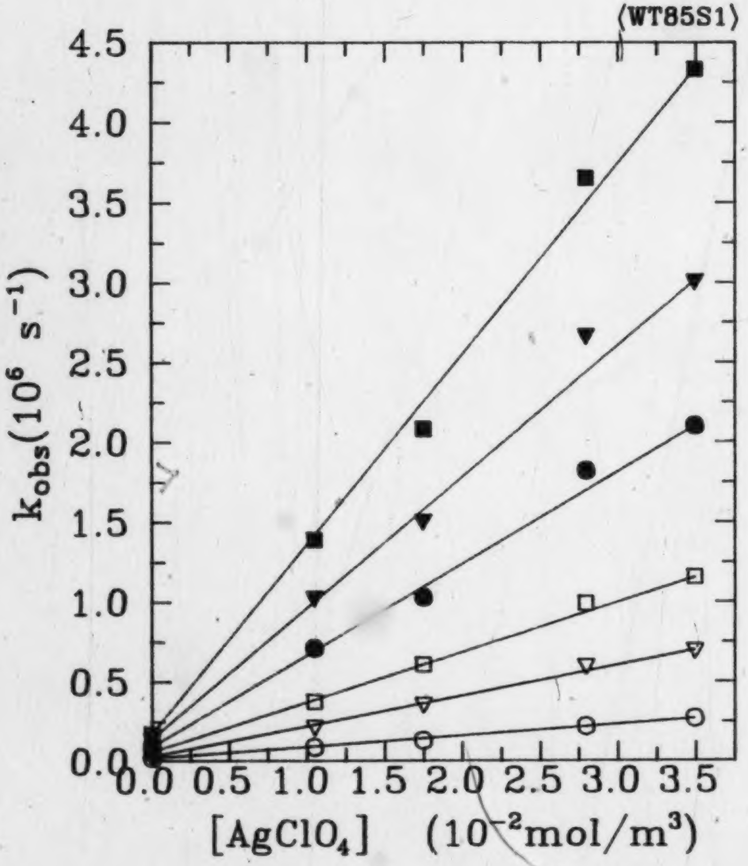

Fig. 3−109: t−BuOH/H_2O:15/85

○ 279.6K ▽ 297.4K □ 313.5K
● 333.1K ▼ 353.1K ■ 368.2K

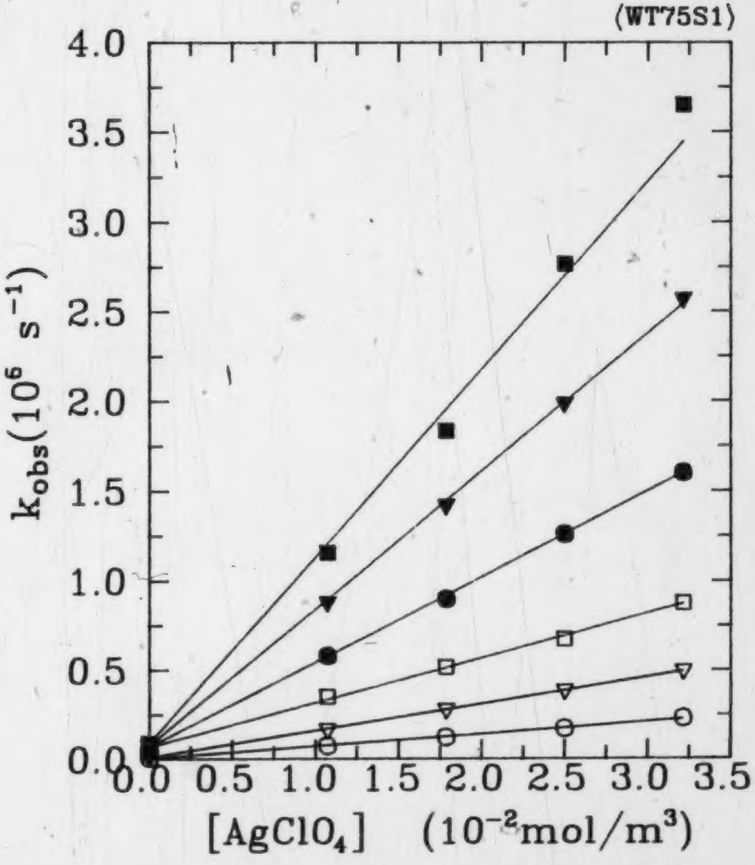

Fig. 3−110: t−BuOH/H_2O:25/75

○ 279.6K ▽ 295.5K □ 313.5K
● 333.2K ▼ 352.9K ■ 367.9K

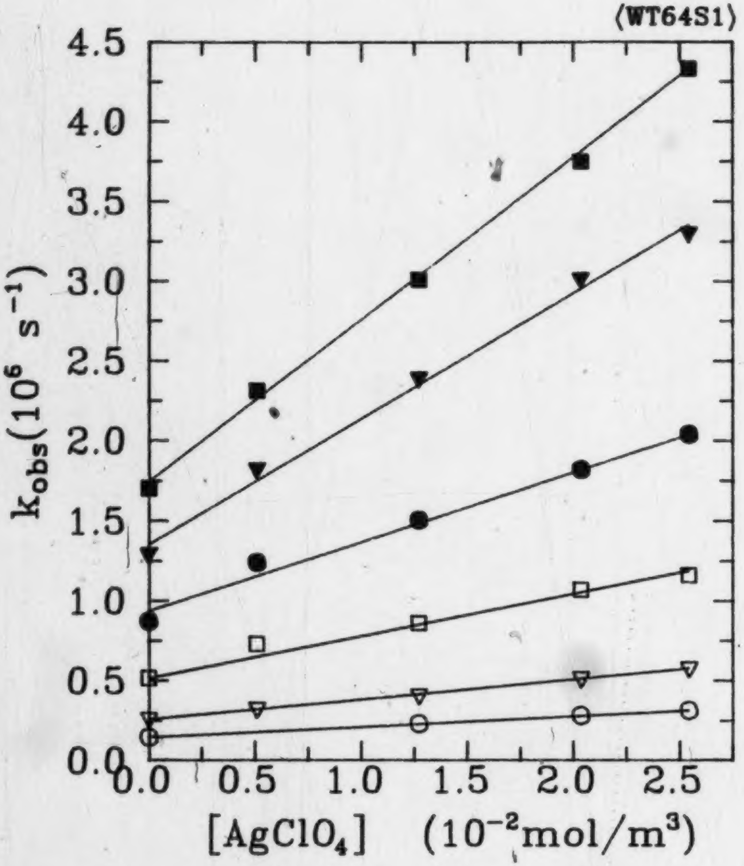

Fig. 3-111: t-BuOH/H_2O:36/64

○ 279.9K ▽ 292.8K □ 313.8K
● 333.4K ▼ 354.4K ■ 367.7K

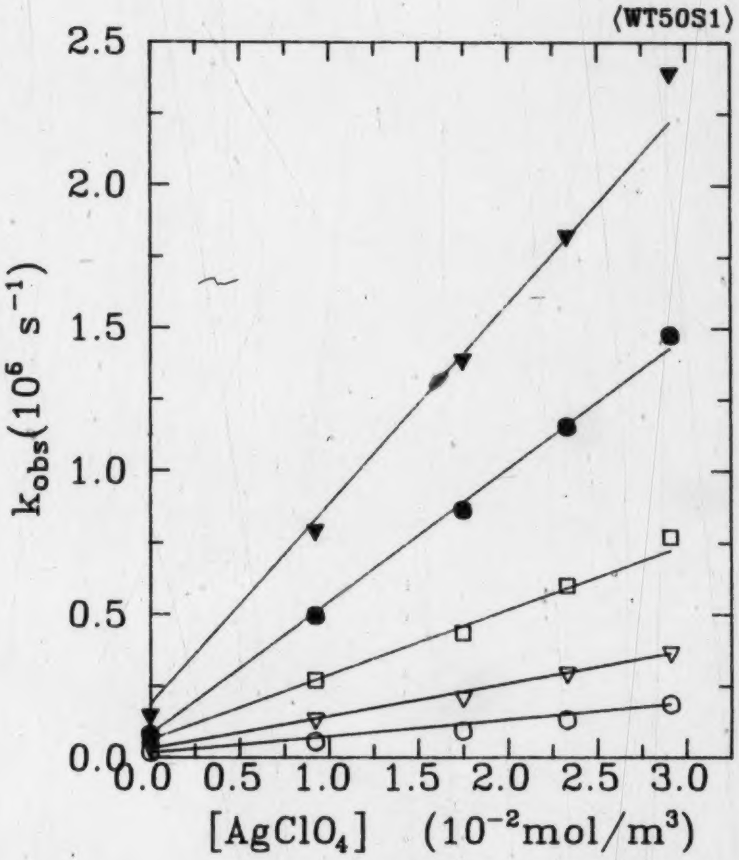

Fig. 3-112: t-BuOH/H_2O:50/50

○ 280.6K ▽ 296.7K □ 313.4K
● 334.2K ▼ 353.6K

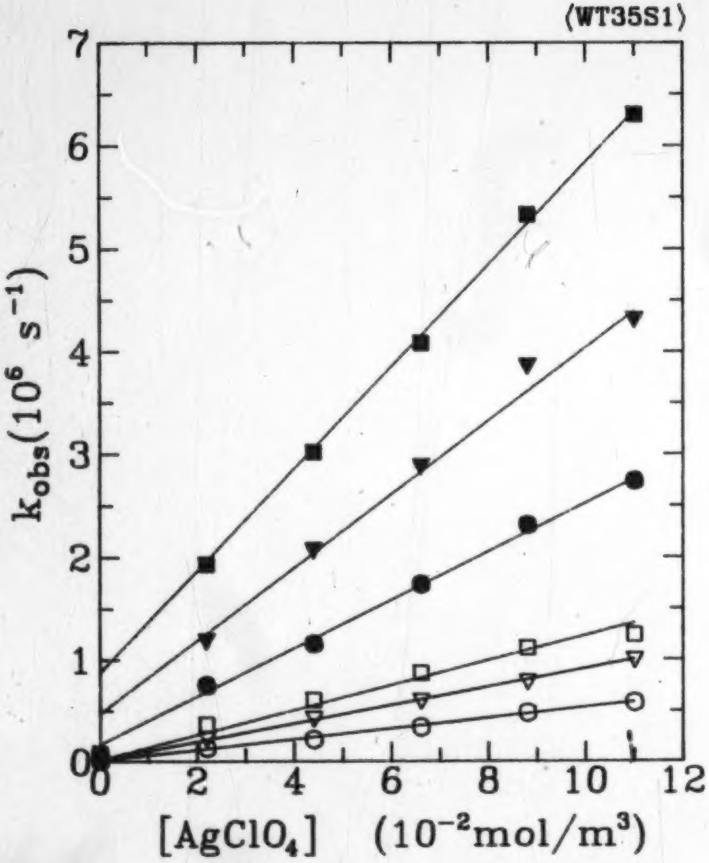

Fig. 3−113: t−BuOH/H_2O:65/35

○ 277.6K ▽ 288.3K □ 296.7K
● 313.4K ▼ 329.3K ■ 343.3K

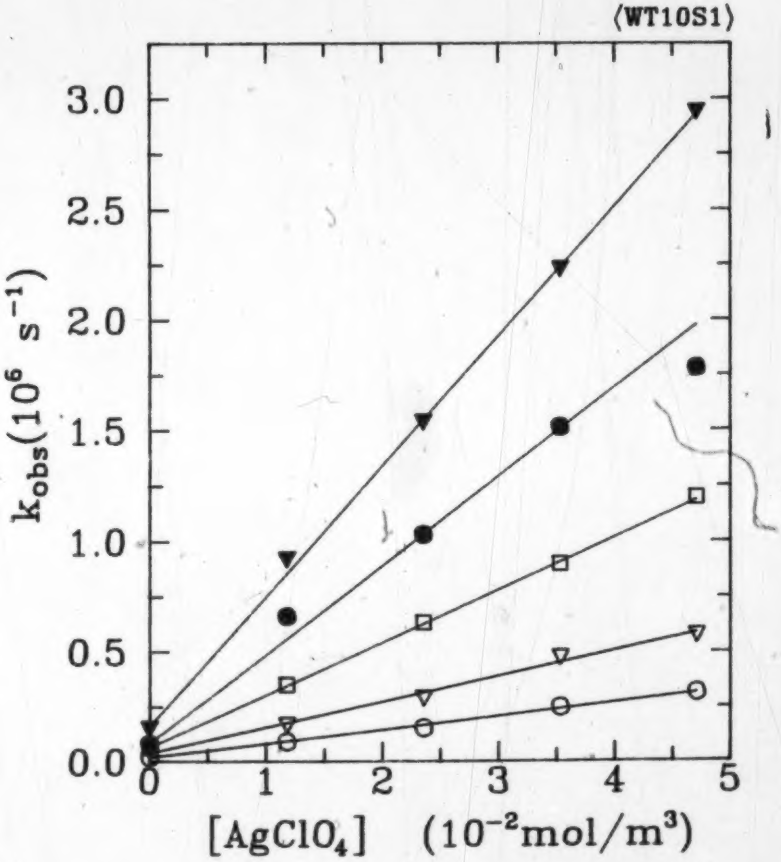

Fig. 3−114: t−BuOH/H_2O:90/10

○ 285.3K ▽ 296.7K □ 313.4K
● 334.0K ▼ 354.0K

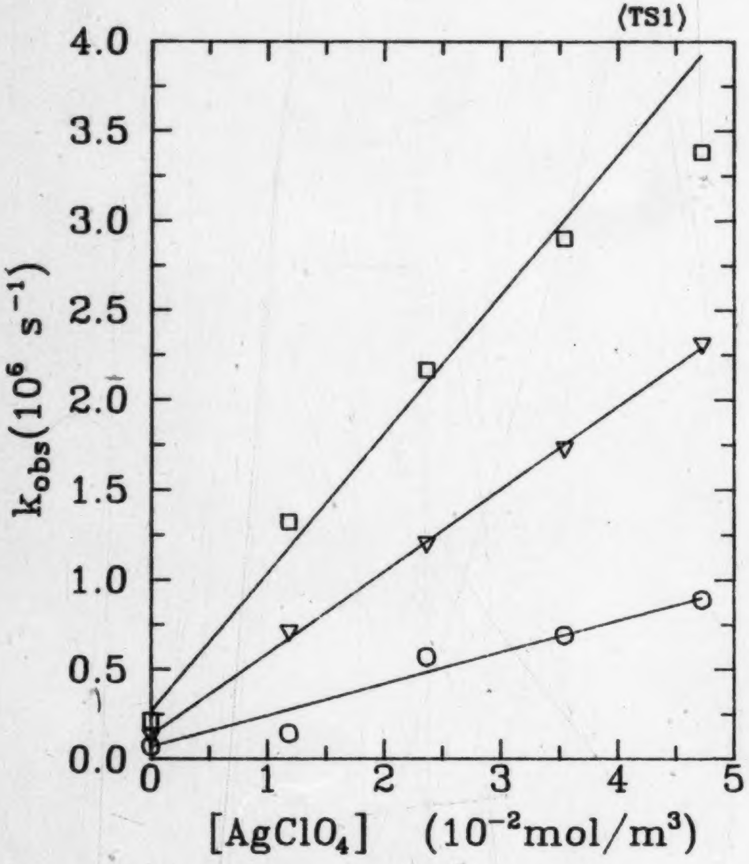

Fig. 3−115: t−BuOH
○ 300.7K ▽ 313.4K □ 324.0K

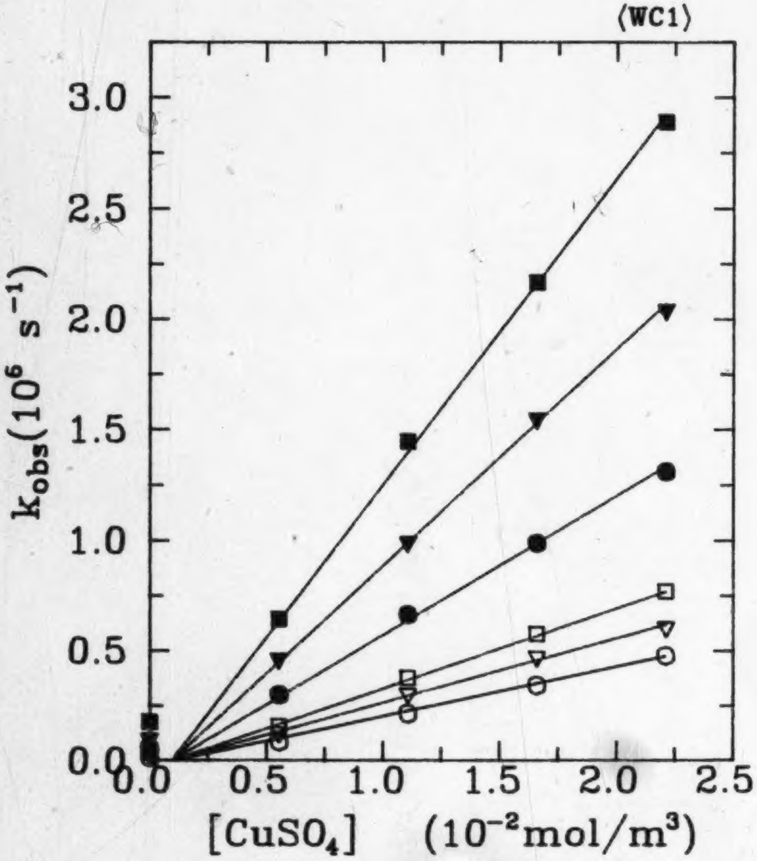

Fig. 3−116a:H_2O

○ 275.9K ▽ 288.5K □ 297.3K
● 323.2K ▼ 347.8K ■ 371.3K

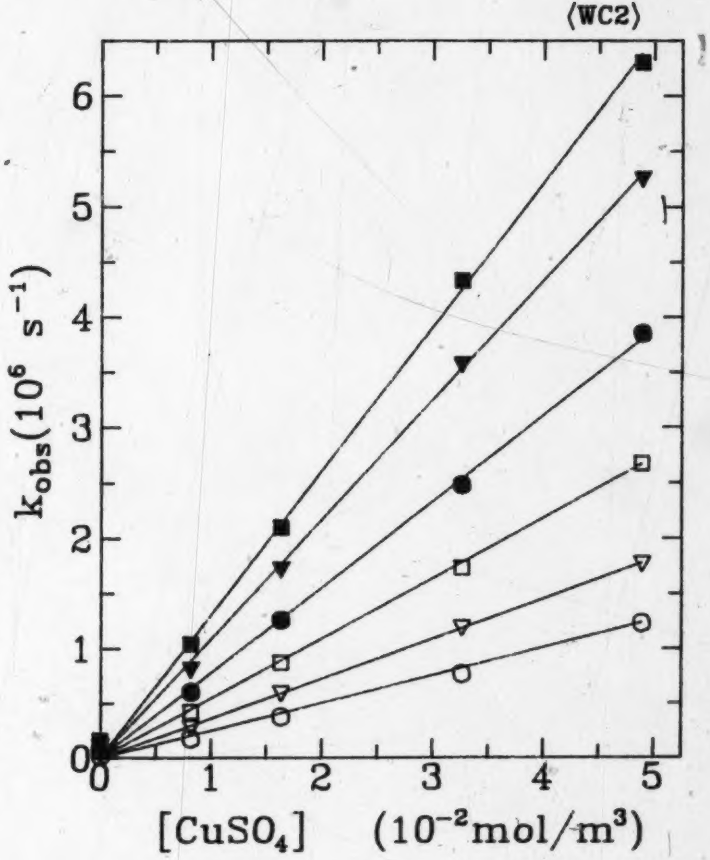

Fig. 3−116b:H_2O

○ 278.2K ▽ 297.0K □ 314.1K
● 333.8K ▼ 354.3K ■ 368.5K

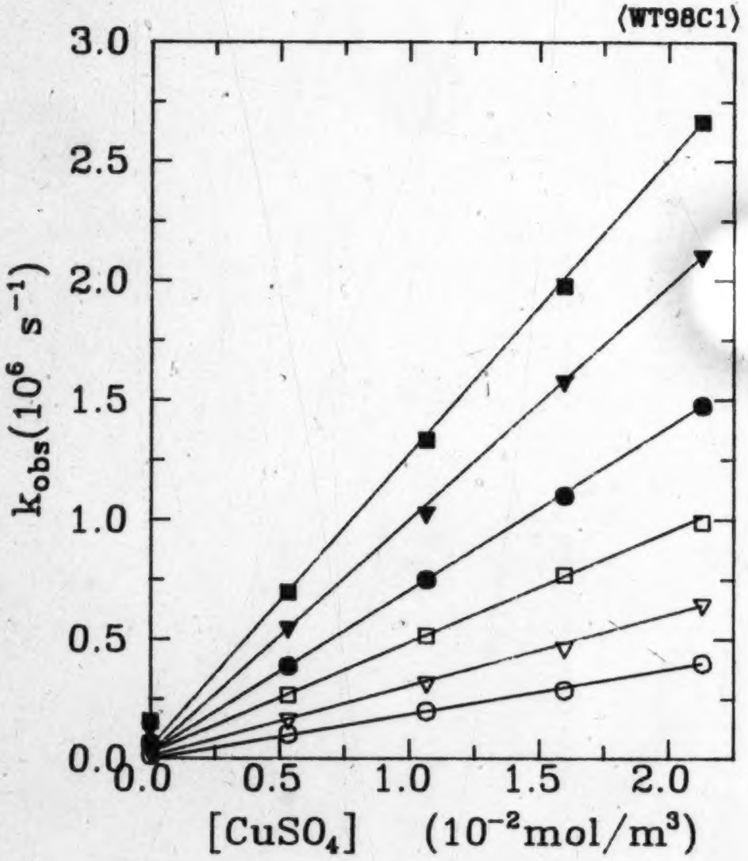

Fig. 3−117: t−BuOH/H_2O:2/98

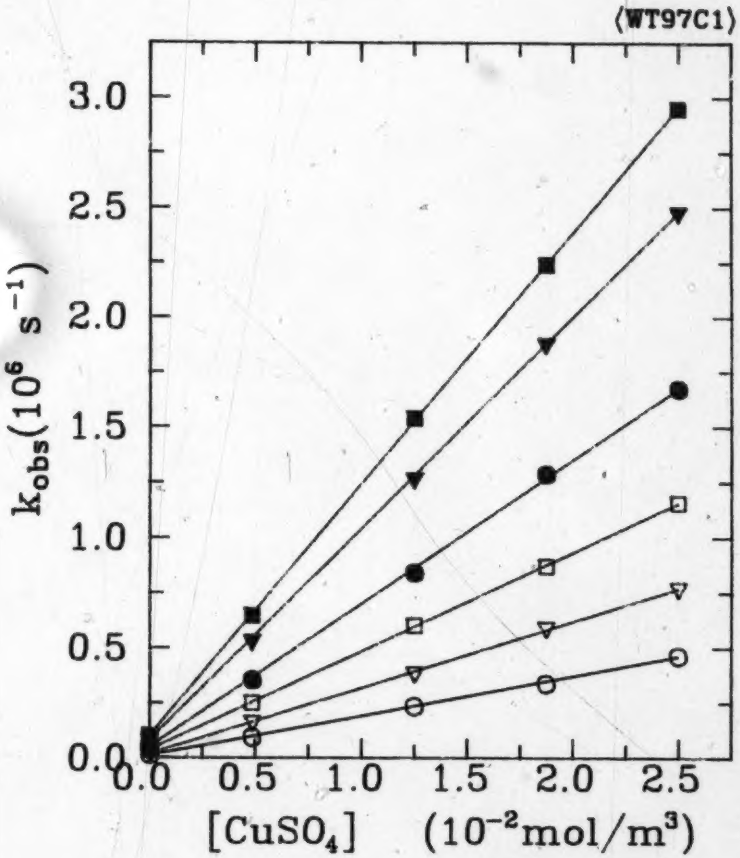

Fig. 3−118: t−BuOH/H_2O:3/97

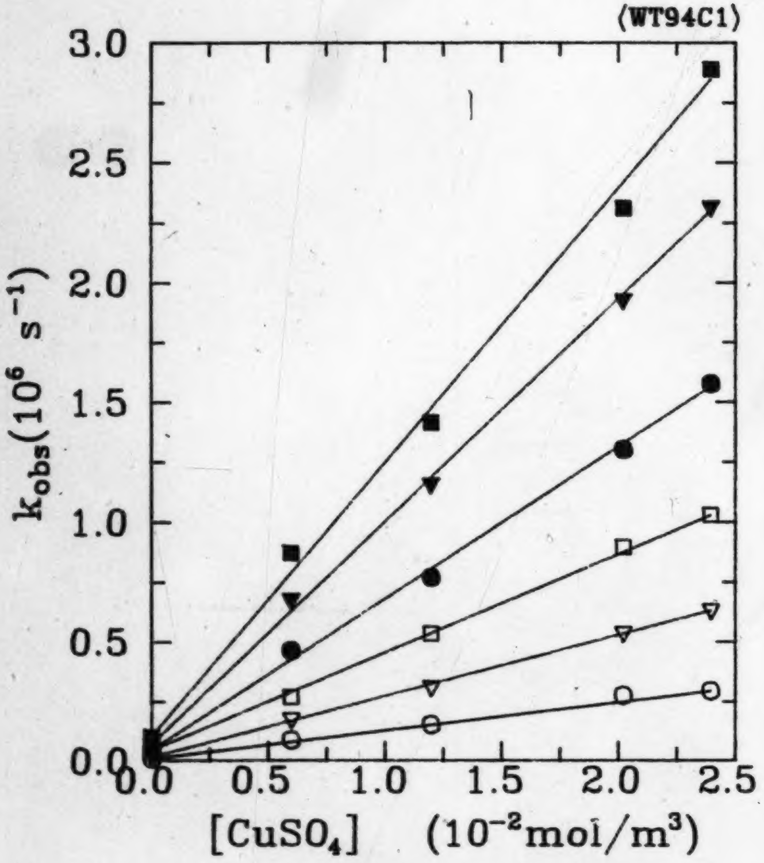

Fig. 3–119: t–BuOH/H$_2$O:6/94

○ 279.2K ▽ 296.6K □ 313.8K
● 333.6K ▼ 353.1K ■ 367.6K

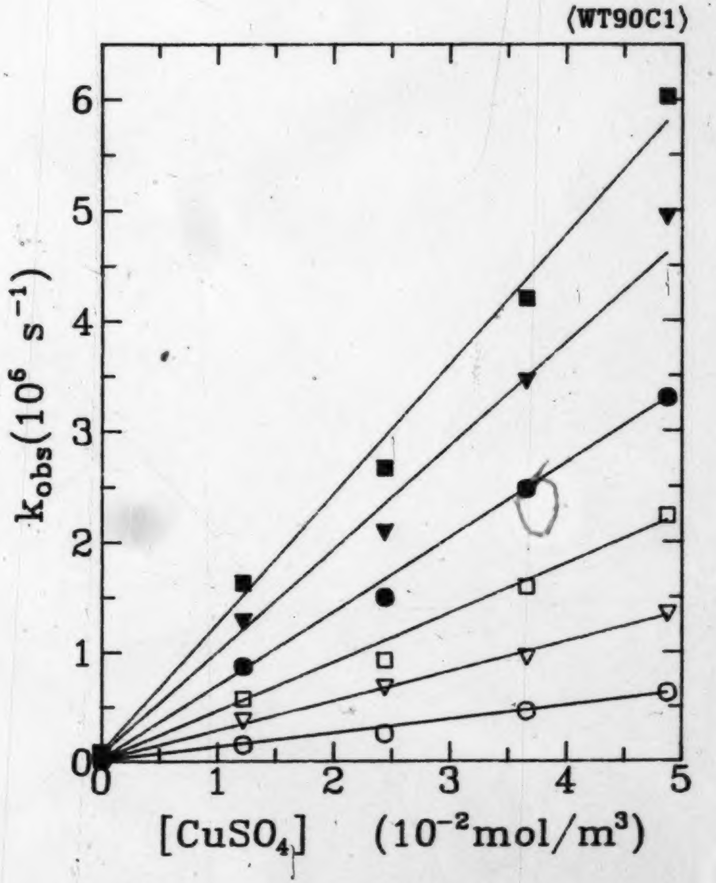

Fig. 3–120: t–BuOH/H$_2$O:10/90

○ 279.3K ▽ 297.1K □ 313.8K
● 333.4K ▼ 354.3K ■ 368.6K

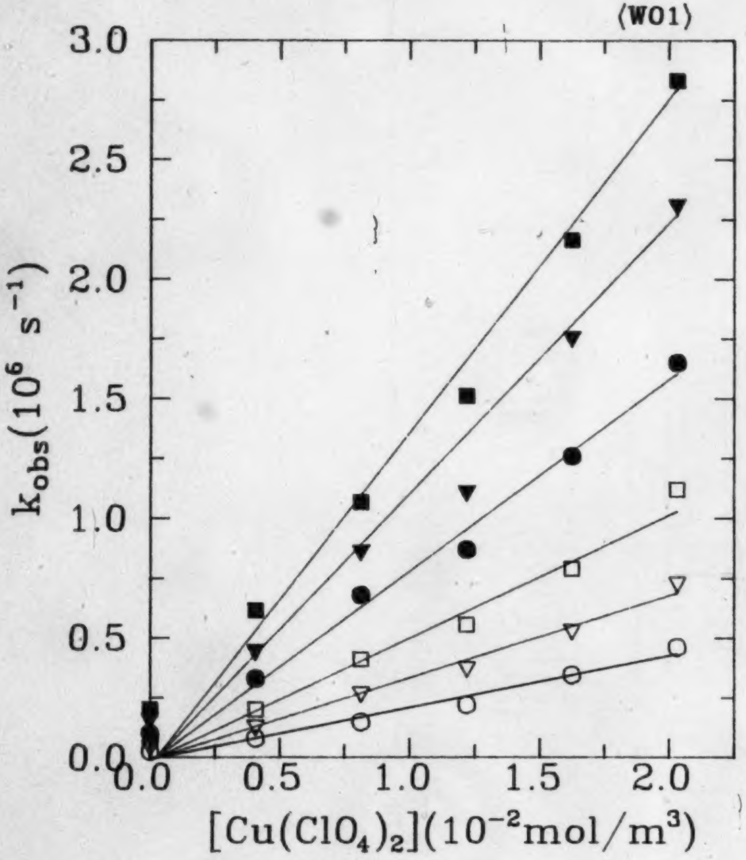

Fig. 3−121: H_2O

○ 276.3K ▽ 293.3K □ 313.4K
● 334.2K ▼ 353.8K ■ 369.6K

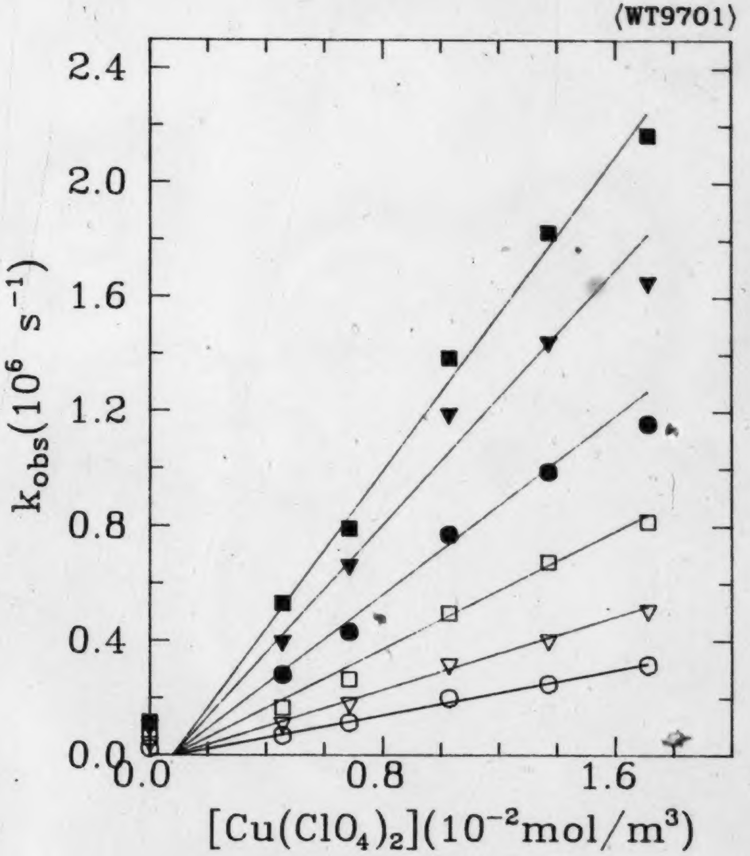

Fig. 3−122: t−BuOH/H_2O:3/97

○ 279.6K ▽ 294.4K □ 313.4K
● 333.4K ▼ 353.9K ■ 369.5K

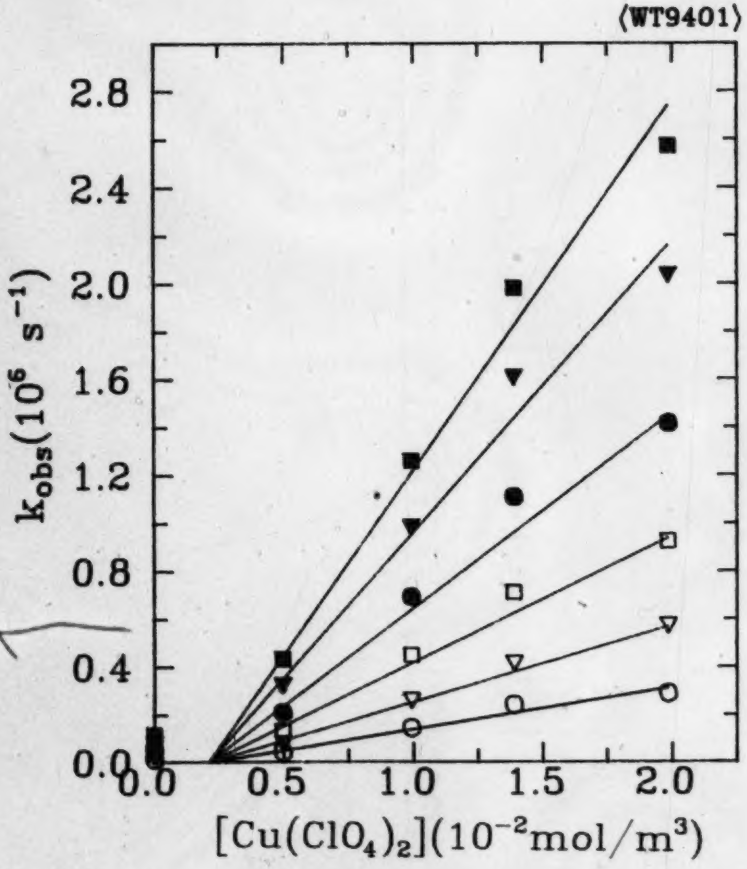

Fig. 3−123: t−BuOH/H_2O:6/94

○ 278.4K ▽ 296.7K □ 313.4K
● 333.4K ▼ 354.1K ■ 367.9K

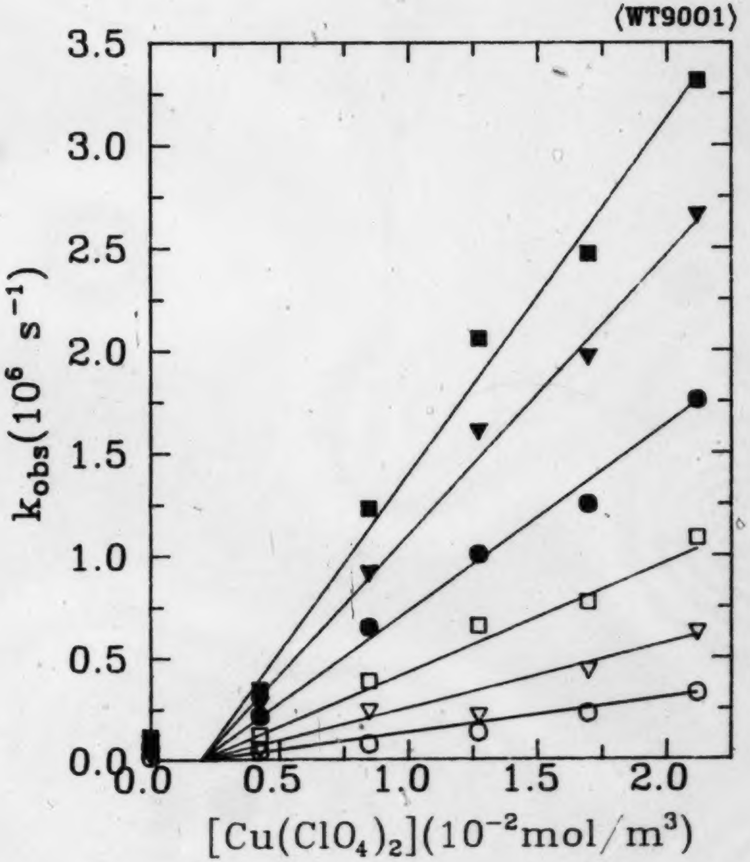

Fig. 3−124: t−BuOH/H_2O:10/90

○ 281.8K ▽ 296.5K □ 313.4K
● 333.3K ▼ 353.7K ■ 369.0K

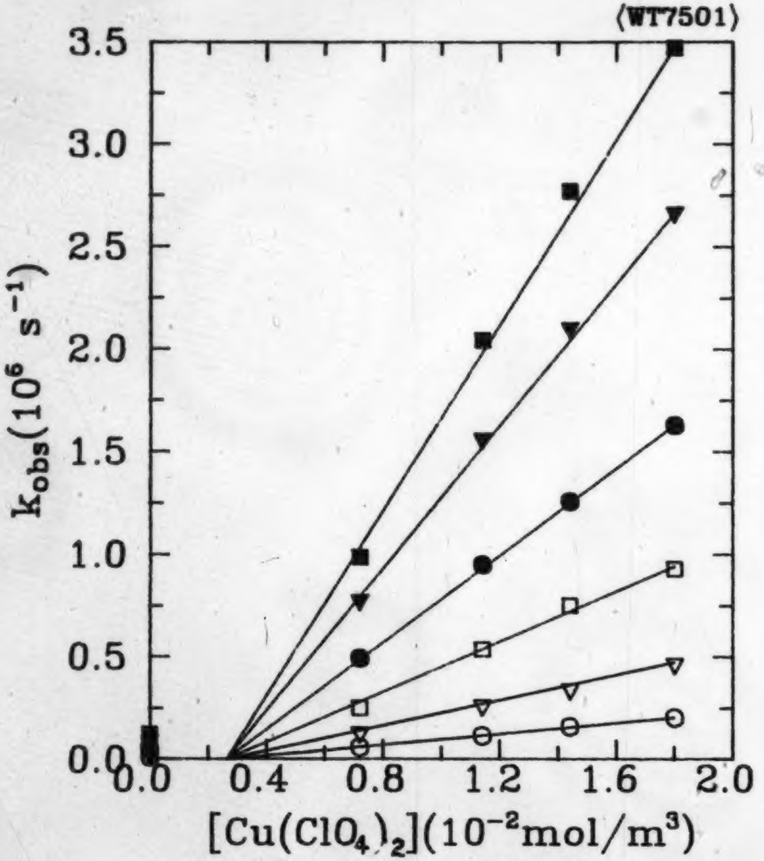

Fig. 3-125: t-BuOH/H_2O:25/75

○ 278.3K ▽ 295.0K □ 313.5K
● 333.9K ▼ 354.0K ■ 367.1K

Table 3-21: The values of k_2 in t-butanol/water mixtures for the reaction of e_s^- with positive scavengers.

x_{H_2O}	T (K)	k_2 $10^7 m^3/mol.s$
Scavenger: $AgClO_4$		
1.00	276.8	2.36
	296.8	4.10
	313.5	6.04
	333.2	9.39
	354.0	14.3
	370.8	18.9
1.00	276.2	2.25
	295.1	3.96
	313.8	6.16
	333.4	9.64
	354.3	14.40
0.98	278.1	1.76
	297.2	3.46
	313.8	5.16
	333.3	8.21
	354.1	12.10
	370.0	16.10
0.97	278.2	1.60
	297.2	2.96
	313.8	4.64
	333.3	7.69
	354.1	11.10

	368.7	14.10
0.94	280.0	1.60
	297.5	2.96
	313.8	4.64
	333.4	7.69
	354.1	11.10
	368.3	14.10
0.90	279.9	0.96
	294.7	1.81
	313.8	3.39
	333.4	6.10
	354.3	9.65
	368.6	12.80
0.85	279.6	0.73
	297.4	1.92
	313.5	3.14
	333.1	5.75
	353.1	8.18
	368.2	12.00
0.75	279.6	0.70
	295.5	1.51
	313.5	2.55
	333.2	4.78
	352.2	7.71
	367.9	10.50
0.64	279.9	0.67

	292.8	1.26
	313.8	2.65
	333.4	4.34
	354.4	7.89
	367.7	10.10
0.50	280.6	0.62
	296.7	1.25
	313.4	2.32
	334.2	4.68
	353.6	7.15
0.35	277.6	0.53
	288.3	0.90
	296.7	1.15
	313.4	2.35
	329.3	3.56
	343.3	4.97
0.10	285.3	0.63
	296.7	1.16
	313.4	2.39
	334.0	4.03
	354.0	5.90
0.0	300.7	1.75
	313.4	4.61
	324.0	6.90

Scavenger: $CuSO_4$

1.00	275.9	2.30

	288.5	2.97
	297.3	3.65
	323.2	6.26
	347.8	9.79
	371.3	13.60
1.00	278.2	2.35
	297.0	3.67
	314.1	5.49
	333.8	7.80
	354.3	11.09
	368.5	13.20
0.98	277.1	1.81
	294.0	2.95
	313.8	4.68
	333.6	6.84
	353.7	9.75
	369.3	12.30
0.97	280.0	1.80
	297.3	3.06
	313.8	4.49
	333.3	6.53
	354.0	9.62
	368.4	11.40
0.94	279.2	1.21
	296.6	2.45
	313.8	4.12

	333.6	6.21
	353.1	9.37
	367.6	11.20
0.90	279.3	1.29
	297.1	2.72
	313.8	4.48
	333.4	6.71
	354.3	10.10
	368.6	12.20
	Scavenger : $Cu(ClO_4)_2$	
1.00	276.3	2.19
	293.3	3.48
	313.4	5.39
	334.2	8.10
	353.8	11.40
	369.6	13.70
0.97	279.6	1.99
	294.4	3.21
	313.4	5.10
	333.4	7.80
	353.9	11.20
	369.5	14.50
0.94	278.4	1.83
	296.7	3.19
	313.4	5.29
	333.4	8.10

	354.1	12.20
	367.9	15.50
0.90	281.8	1.70
	296.5	3.17
	313.4	5.78
	333.3	9.07
	353.7	13.70
	369.0	17.40
0.75	278.3	1.36
	295.0	2.80
	313.5	6.00
	333.9	10.70
	354.0	17.50
	367.1	22.70

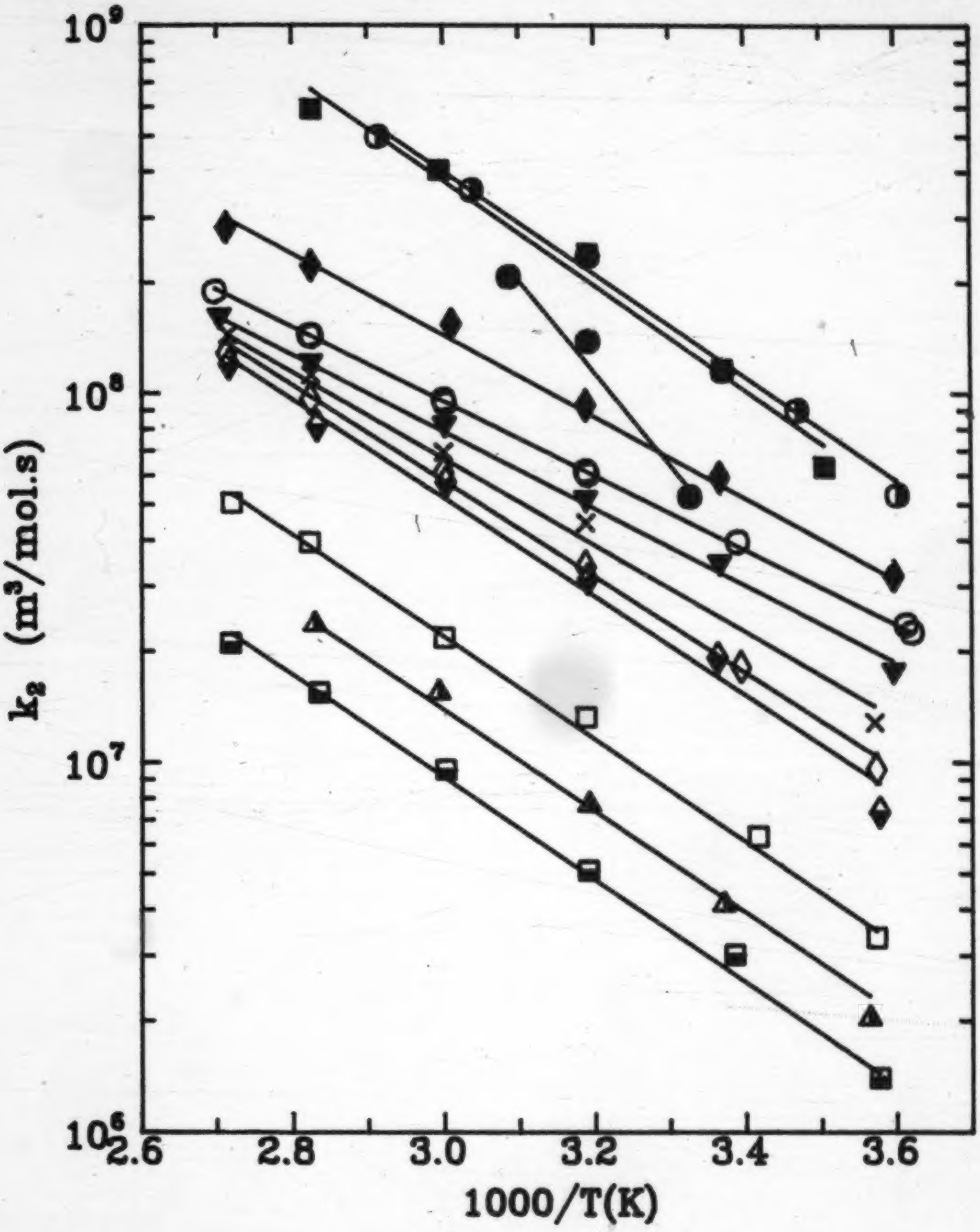

Fig. 3–126: $e_s^- + AgClO_4$ reaction in t–BuOH water mixtures.

x_{H_2O}: ● 0.00 ■ 0.10 ◐ 0.35 ▲ 0.50
□ 0.64 ⊟ 0.75 ◈ 0.85 ◇ 0.90
× 0.94 ◆ 0.97 ▼ 0.98 ○ 1.00

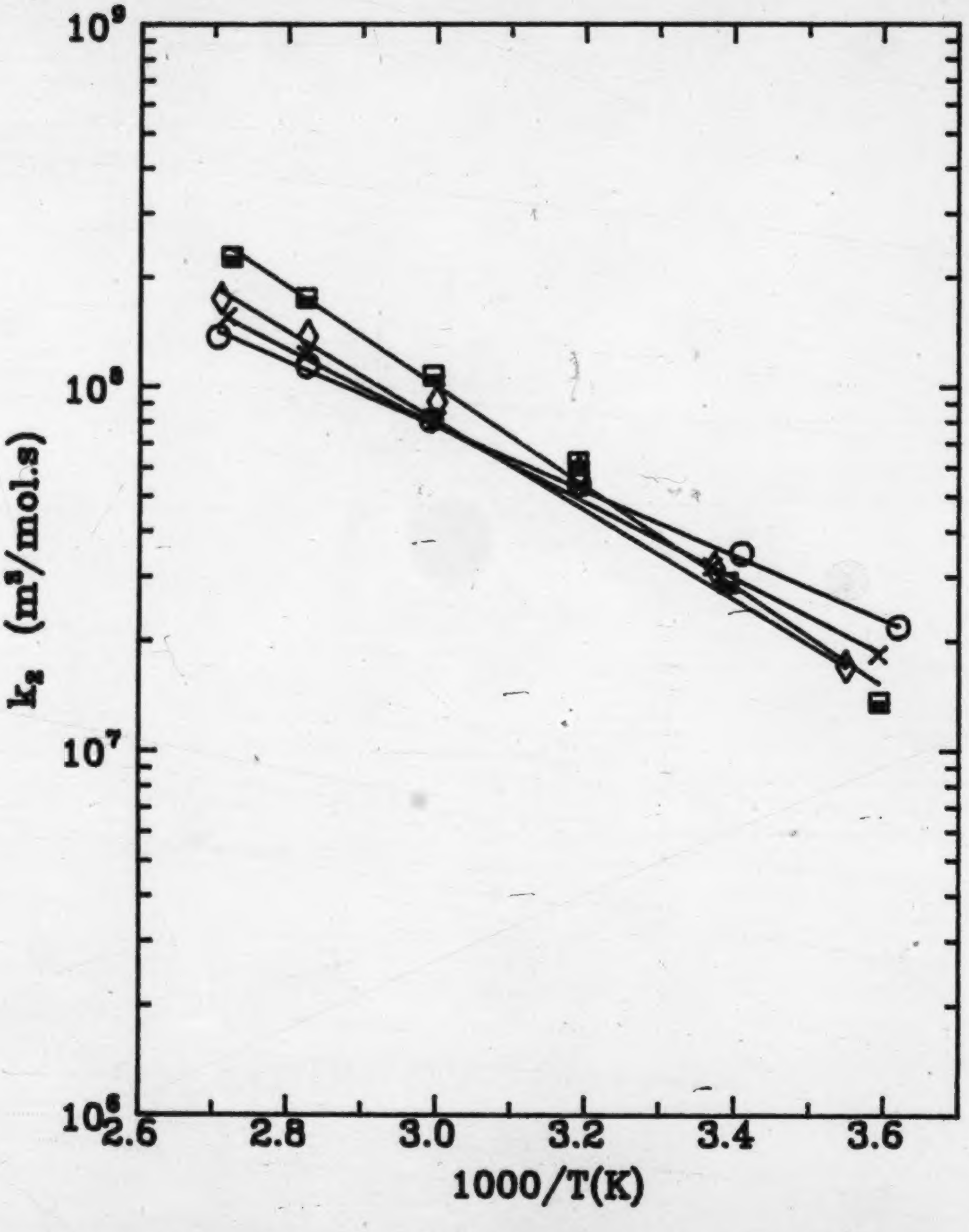

Fig. 3–127a. $e_s^- + Cu(ClO_4)_2$ reaction in t–BuOH water mixtures.

x_{H_2O}: ■ 0.75 ◊ 0.90 × 0.94 ○ 1.00

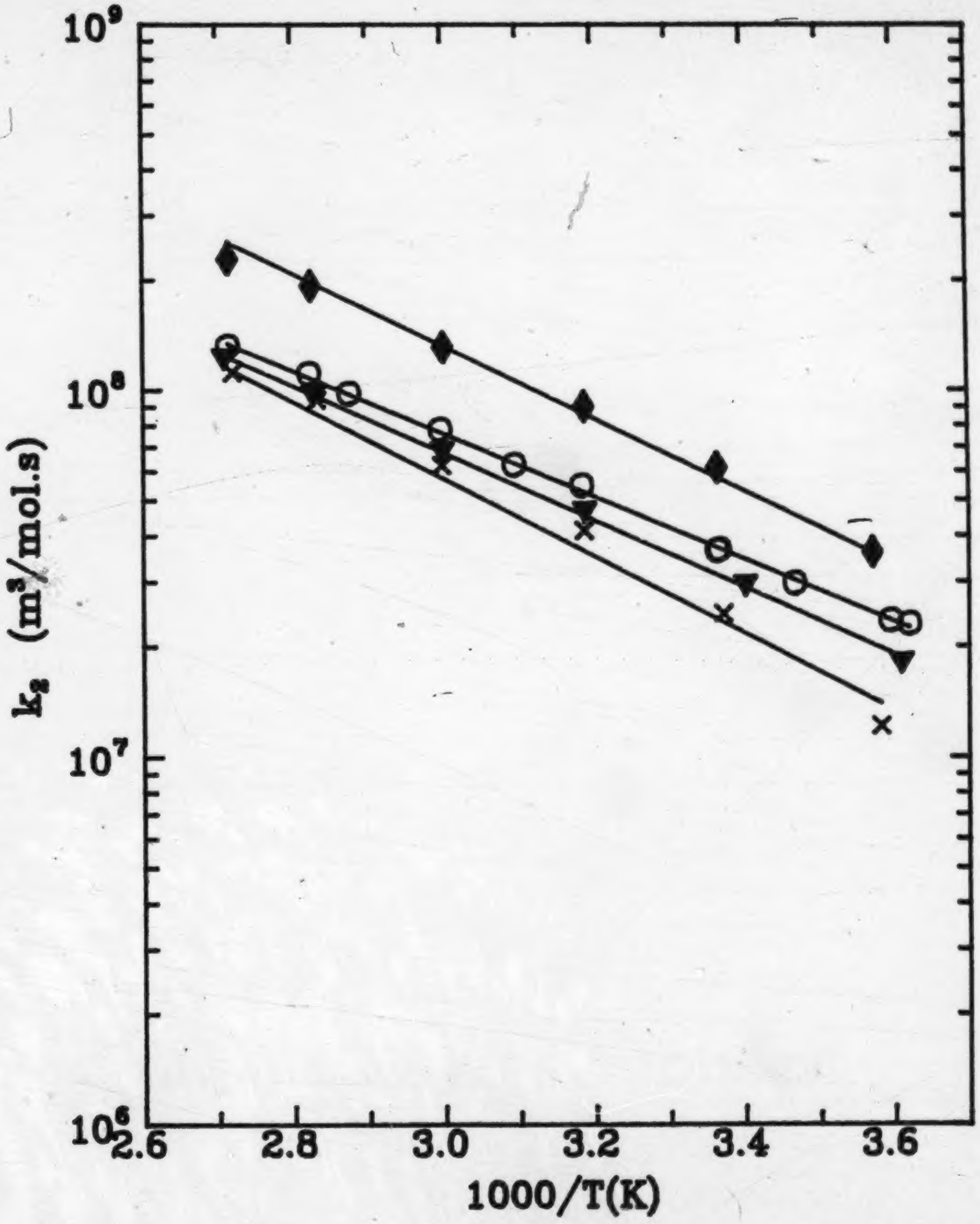

Fig. 3–127b. $e_s^- + CuSO_4$ reaction in t–BuOH water mixtures.

x_{H_2O}: × 0.94 ◆ 0.97 ▼ 0.98 ○ 1.00

Table 3-22: Reaction rate parameters for (+) scavengers in *iso*-butanol and 2-butanol/water

x_{H_2O}	k_2 $10^7 m^3/mol.s.$	E_2 (J/mol)	log A	$\Delta S_2^{\neq}$ (J/mol.K)
Scavenger : $AgClO_4$				
1.00	4.20	19	11.00	23
0.98	3.40	20	11.06	24
0.97	3.00	21	11.16	27
0.94	2.50	23	11.50	32
0.90	2.00	25	11.71	36
0.85	1.80	26	11.77	37
0.75	1.50	26	11.75	37
0.64	1.40	26	11.74	36
0.50	1.35	26	11.69	36
0.35	1.26	26	11.70	36
0.10	1.20	27	11.81	38
0.0	1.50	48		
Scavenger : $CuSO_4$				
1.00	3.80	17	10.47	13
0.98	3.20	18	10.58	15
0.97	2.90	18	10.65	17
0.94	2.50	20	10.98	23
Scavenger : $Cu(ClO_4)_2$				
1.00	3.80	17	10.56	15
0.94	3.30	20	11.09	25
0.90	3.20	23	11.48	32
0.75	3.30	26	12.14	44

Fig.3–128: k_2, E_2 and ΔS_2 for (+)Scavengers in t–BuOH/Water Mixtures.
open points E_2; closed points ΔS_2.

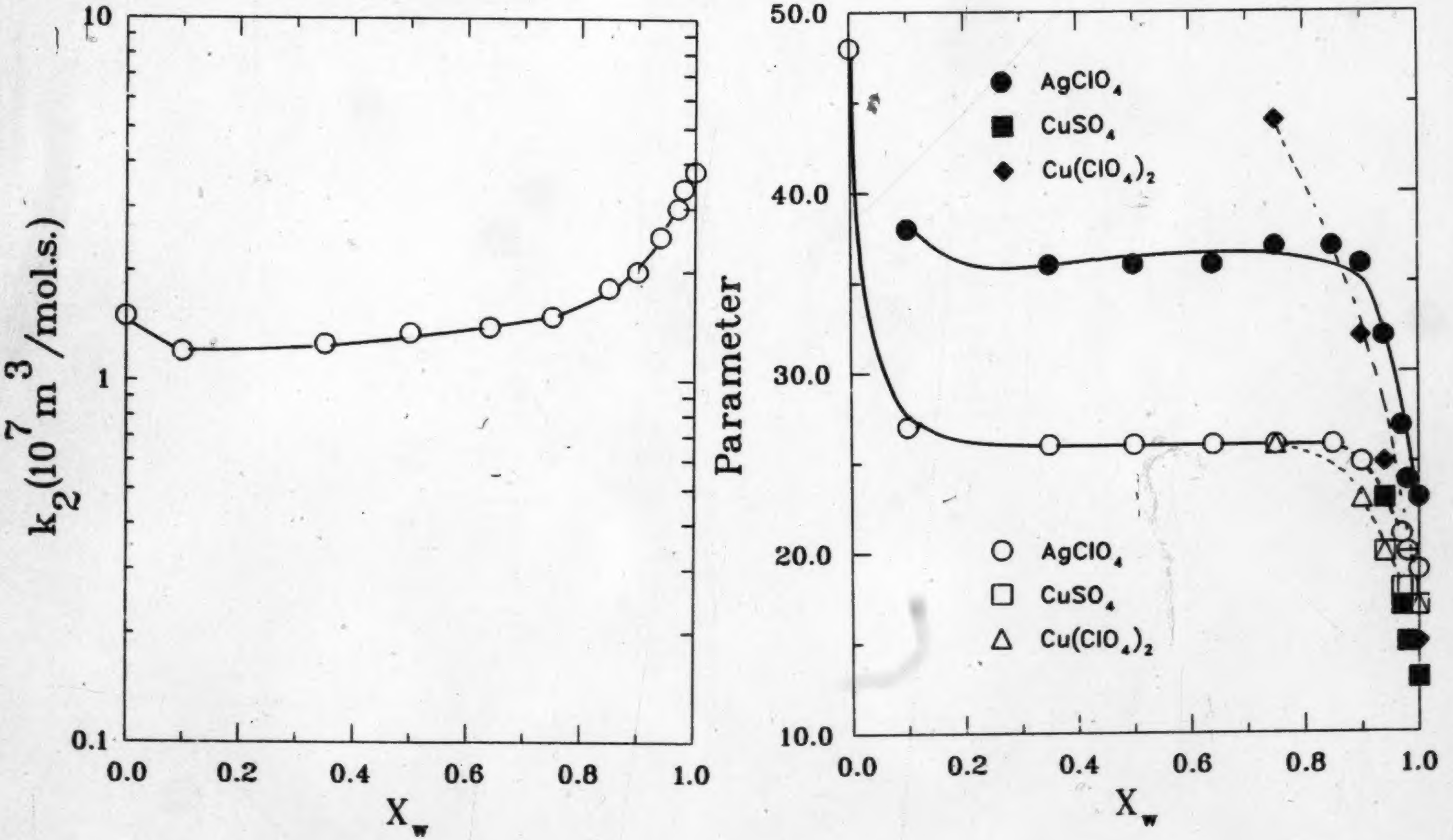

3.2(b) Reaction of e_s^- with Negative Ions

The ions used were NO_3^- and CrO_4^{2-} . The counter ion K^+ has a rate constant $< 10^3 m^3/mol.s.$ (51). Solubility of KNO_3 is quite low in alcohol-rich solvents. Therefore $LiNO_3$ (k_2 value of Li^+ in water $< 10^3 m^3/mol.s.$) was used to measure the rate constants in alcohol-rich solvents and to compare the effect of the positive ion in water-rich solvents.

The compositions of solvents used for reaction with KNO_3 were: $x_{H_2O} =$ 1.00, 0.98, 0.97, 0.94, 0.90, 0.85 and 0.64. The first rate constants are in Figs.(3-129) to (3-135). The concentration range of KNO_3 was 0.005 to 0.15 mol/m^3. To compare these rate constants with that of a bivalent ion, similar compositions with K_2CrO_4 were used. The first order rate constants are in Figs.(3-136) to (3-143). The concentration range of the salt was 0.01 to 0.10 mol/m^3. Since $LiNO_3$ is more soluble than KNO_3, it was used in the alcohol-rich regions: x_{H_2O} = 1.00, 0.94, 0.80, 0.64, 0.50, 0.35, 0.10. The first -order rate constants are in Figs.(3-144) to (3-150). Concentration range of this salt was 0.02-0.5 mol/m^3. The second order rate constants are in Table(3-23). The Arrhenius plots are in Figs.(3-151) to (3-153) for KNO_3, $LiNO_3$ and K_2CrO_4 respectively. The reaction rate parameters for all these systems are listed in Table(3-24).

The k_2 values decrease with the increasing mole fraction of the alcohol (Fig. 154(a)). Values of k_2 for $LiNO_3$ and KNO_3 are the same implying that solubility of KNO_3 was not a problem at the compositions studied. The composition dependence of k_2 values for CrO_4^{2-} ions is similar to that of the NO_3^- ion indicating no charge effect.

Energies and entropies of activation also display similar composition dependence between the two ions (Fig. 3-154(b)). The energies of activation for CrO_4^{2-} ion are consistently higher than that for the NO_3^- ion by about 3 kJ/mol. Therefore the charge effects are displayed in the energetics of the reaction.

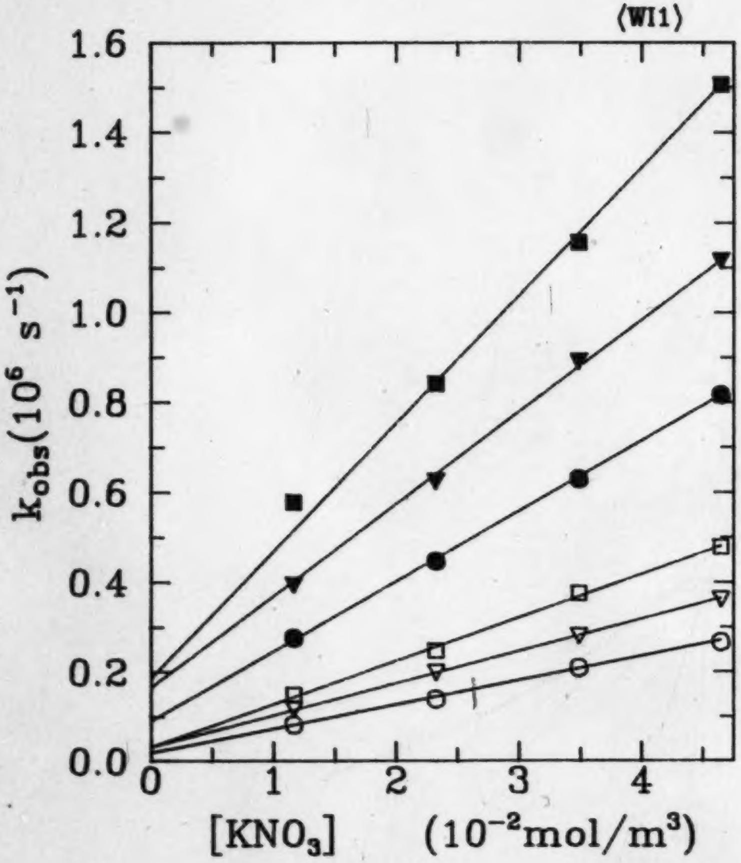

Fig. 3–129: H_2O

○ 275.9K ▽ 287.5K □ 297.5K
● 324.2K ▼ 346.7K ■ 373.3K

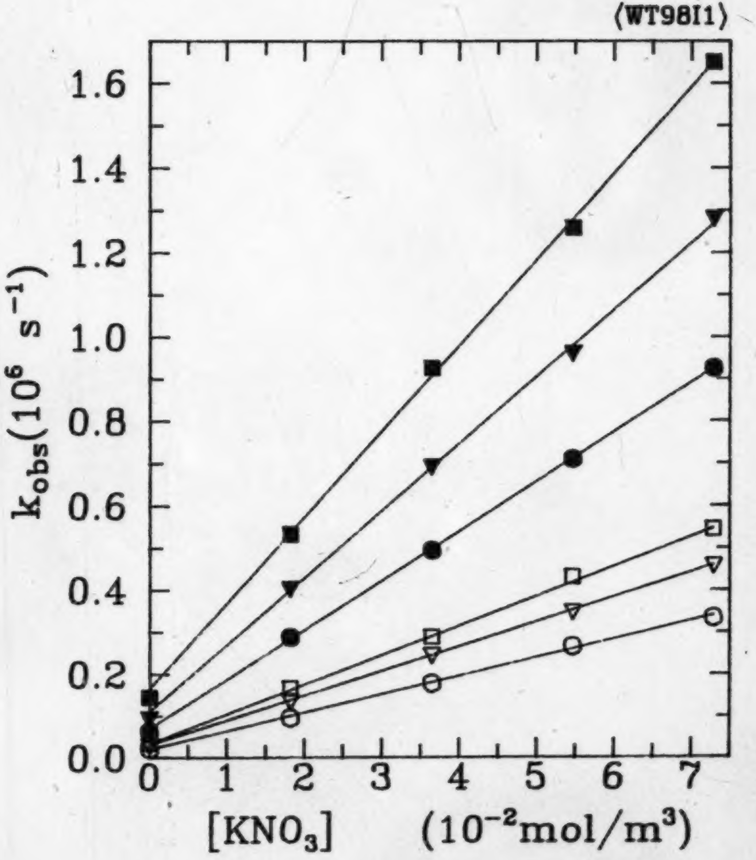

Fig. 3–130: t–BuOH/H_2O:2/98

○ 279.0K ▽ 288.4K □ 297.4K
● 322.3K ▼ 345.8K ■ 368.8K

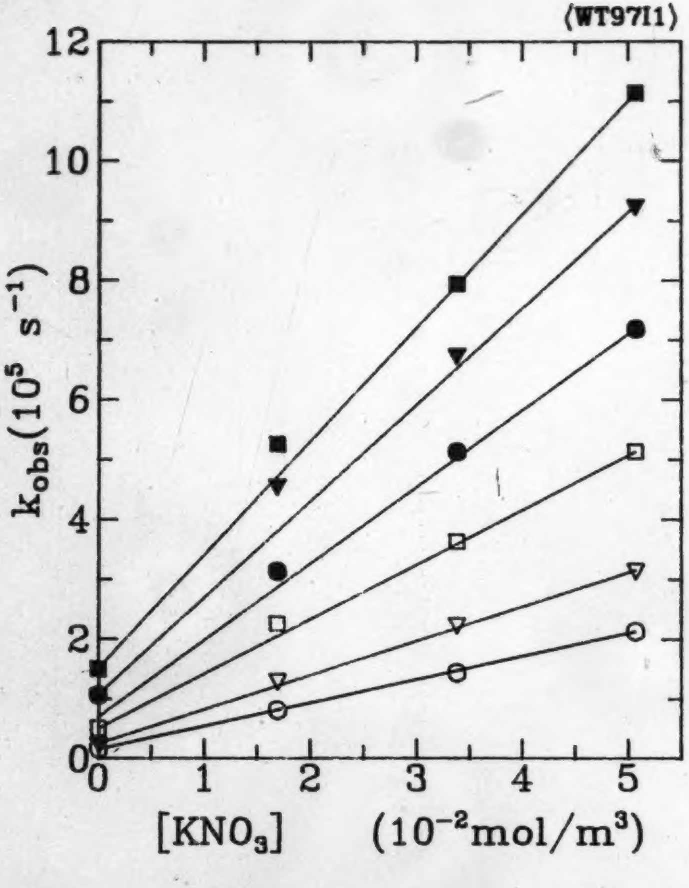

Fig. 3−131: t−BuOH/H_2O:3/97

○ 278.9K ▽ 293.6K □ 313.9K
● 333.4K ▼ 353.5K ■ 368.6K

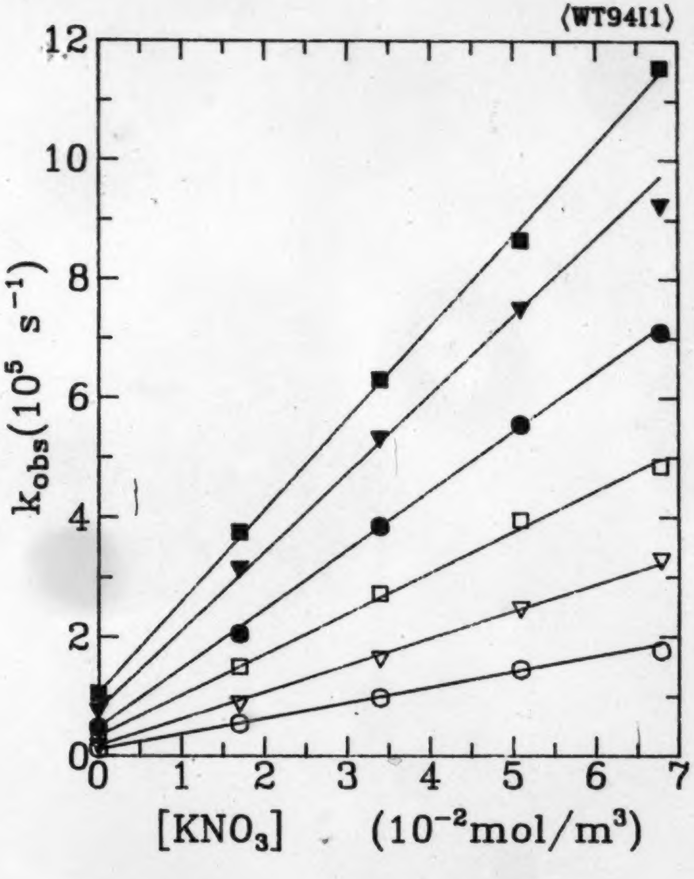

Fig. 3−132: t−BuOH/H_2O:6/94

○ 280.2K ▽ 297.3K □ 314.0K
● 333.5K ▼ 353.4K ■ 368.5K

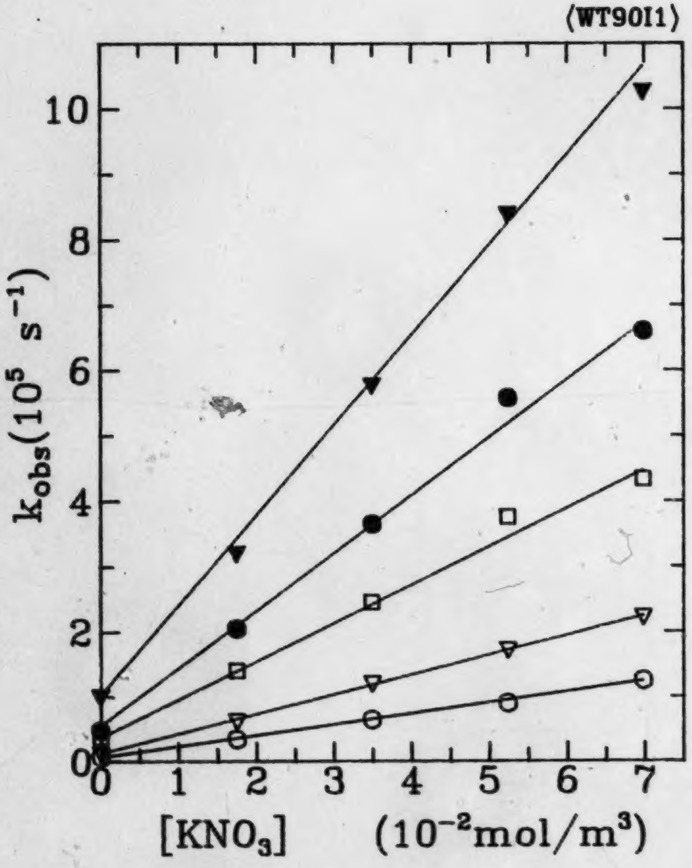

Fig. 3−133a: t−BuOH/H_2O:10/90
○ 279.0K ▽ 293.9K □ 314.0K
● 333.5K ▼ 368.0K

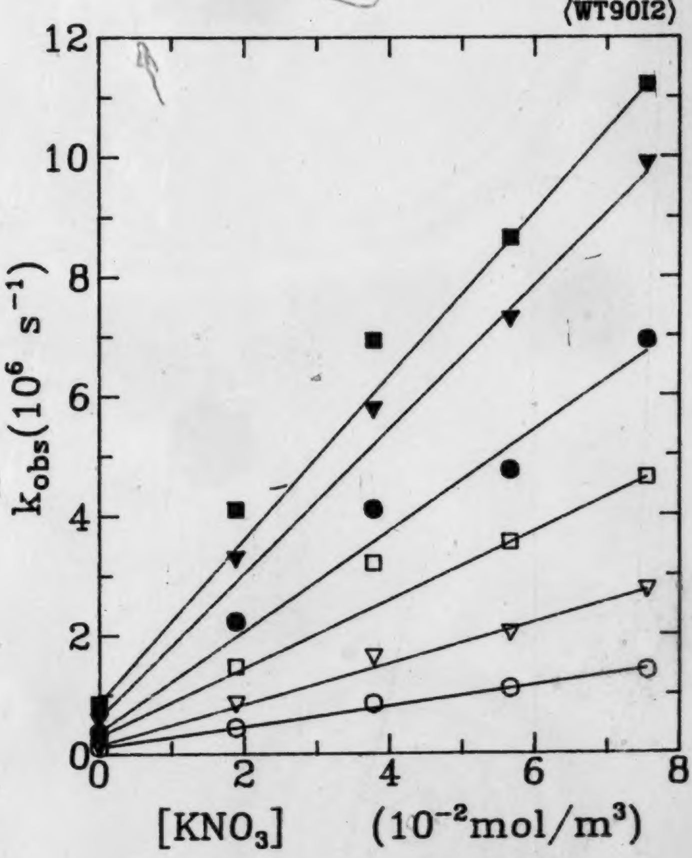

Fig. 3−133b: t−BuOH/H_2O:10/90
○ 279.6K ▽ 296.4K □ 313.5K
● 333.2K ▼ 353.7K ■ 367.7K

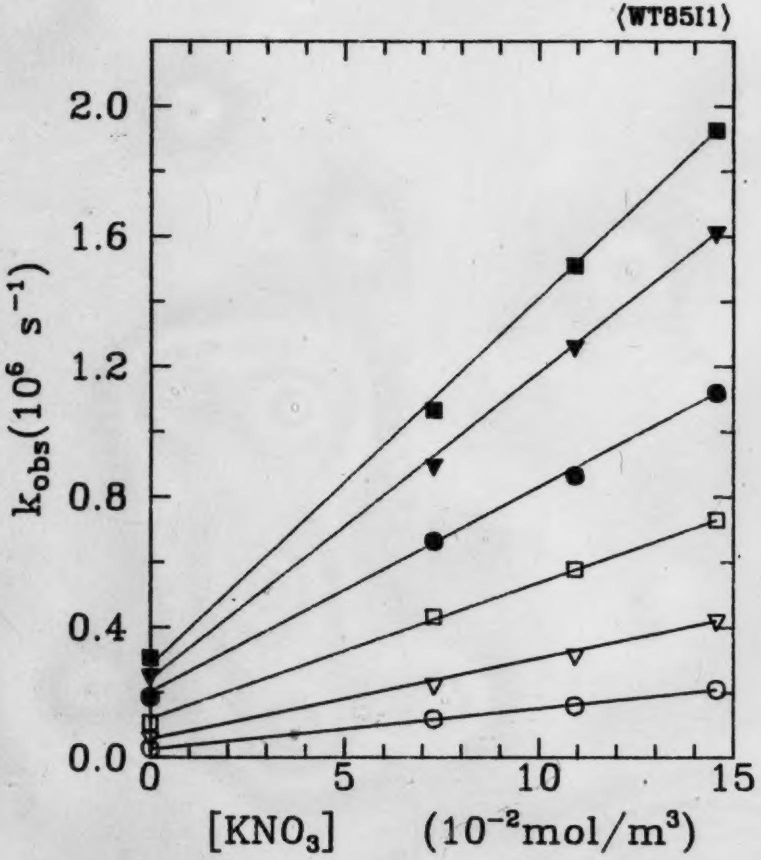

Fig. 3–134: t–BuOH/H_2O:15/85

○ 279.6K ▽ 294.5K □ 313.6K

● 333.2K ▼ 353.0K ■ 368.1K

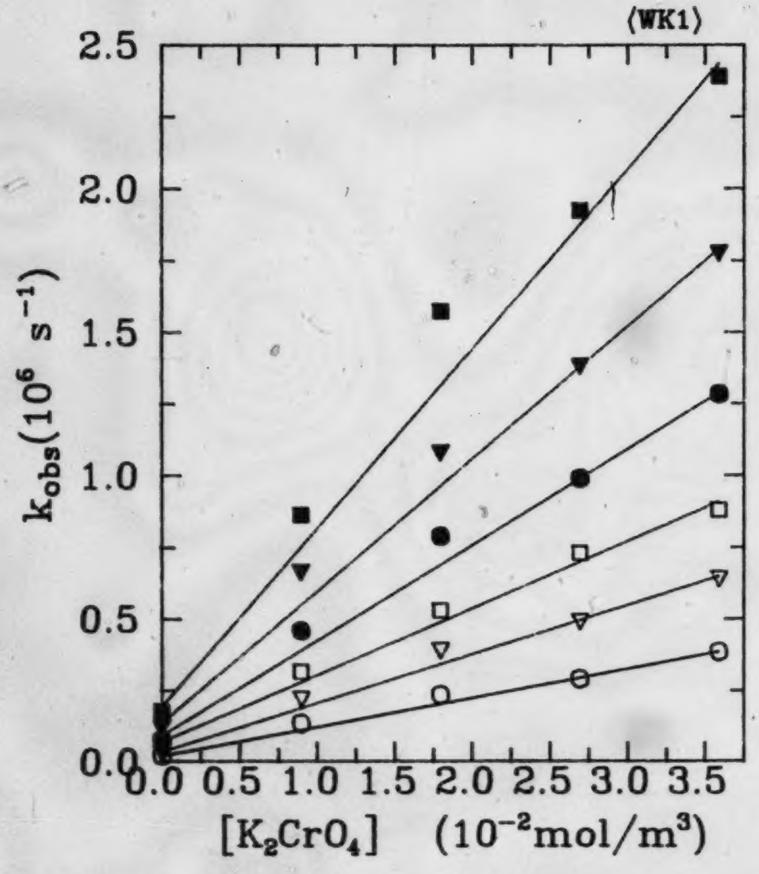

Fig. 3−136: H_2O

○ 277.5K ▽ 298.0K □ 313.6K
● 333.5K ▼ 354.2K ■ 371.4K

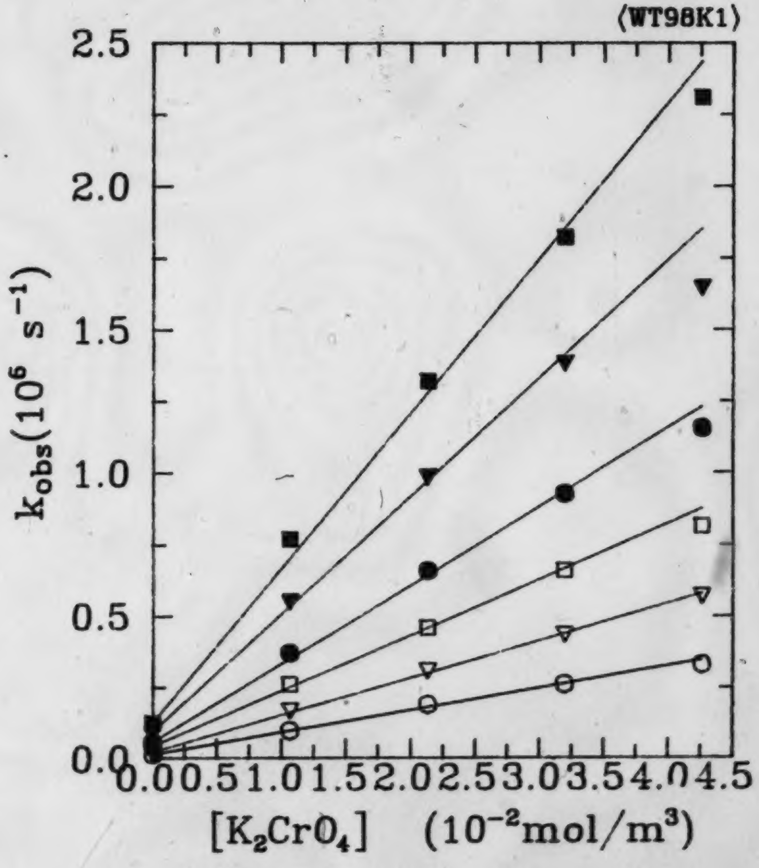

Fig. 3−137: t−BuOH/H_2O:2/98

○ 277.5K ▽ 297.4K □ 313.6K
● 333.4K ▼ 354.0K ■ 370.4K

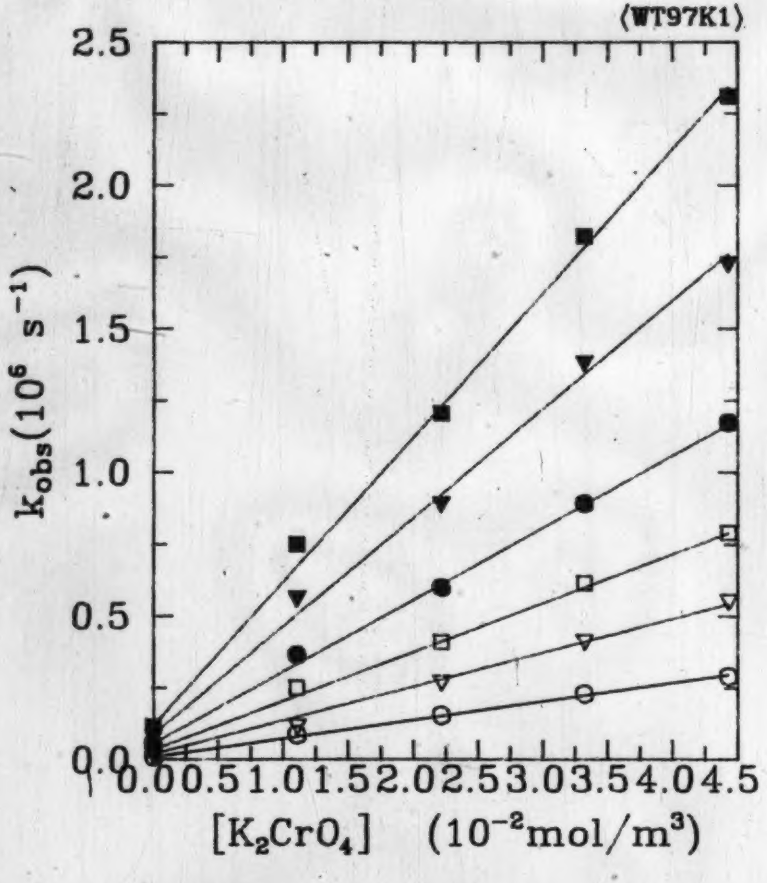

Fig. 3−138: t−BuOH/H_2O:3/97

○ 277.5K ▽ 296.7K □ 314.0K
● 333.2K ▼ 354.0K ■ 370.3K

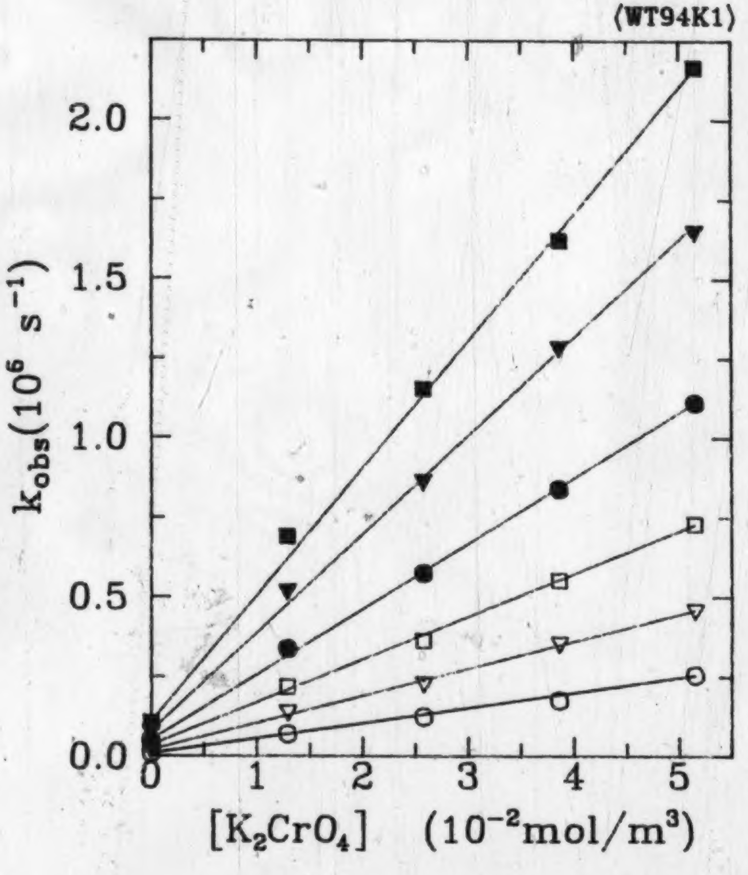

Fig. 3−139: t−BuOH/H_2O:6/94

○ 280.2K ▽ 296.9K □ 314.0K
● 333.3K ▼ 354.0K ■ 369.1K

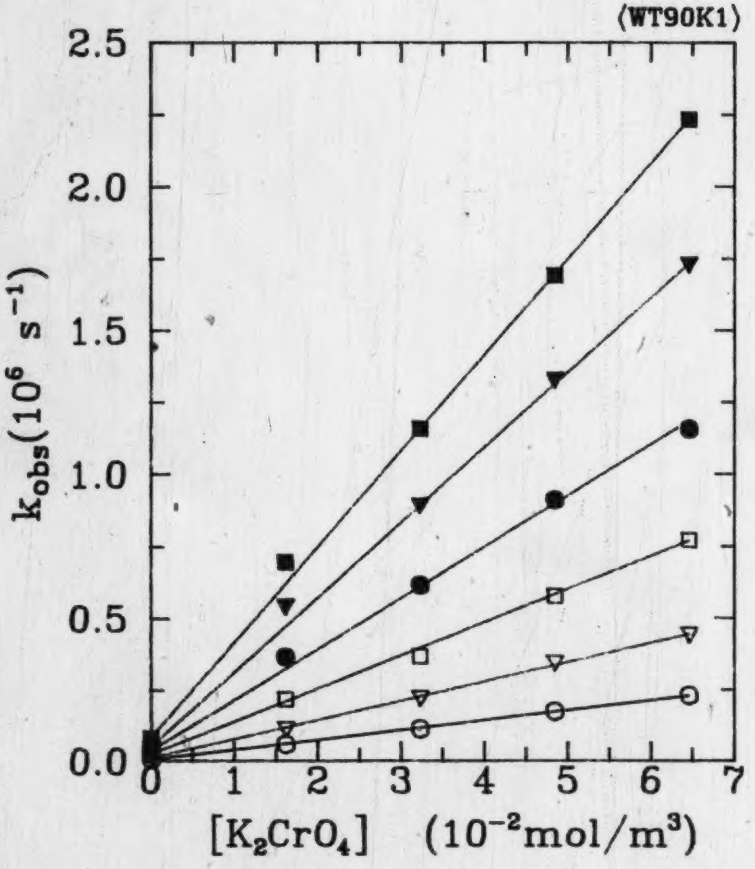

Fig. 3−140: t−BuOH/H_2O:10/90

○ 280.3K ▽ 296.1K □ 313.9K

● 333.3K ▼ 354.2K ■ 368.4K

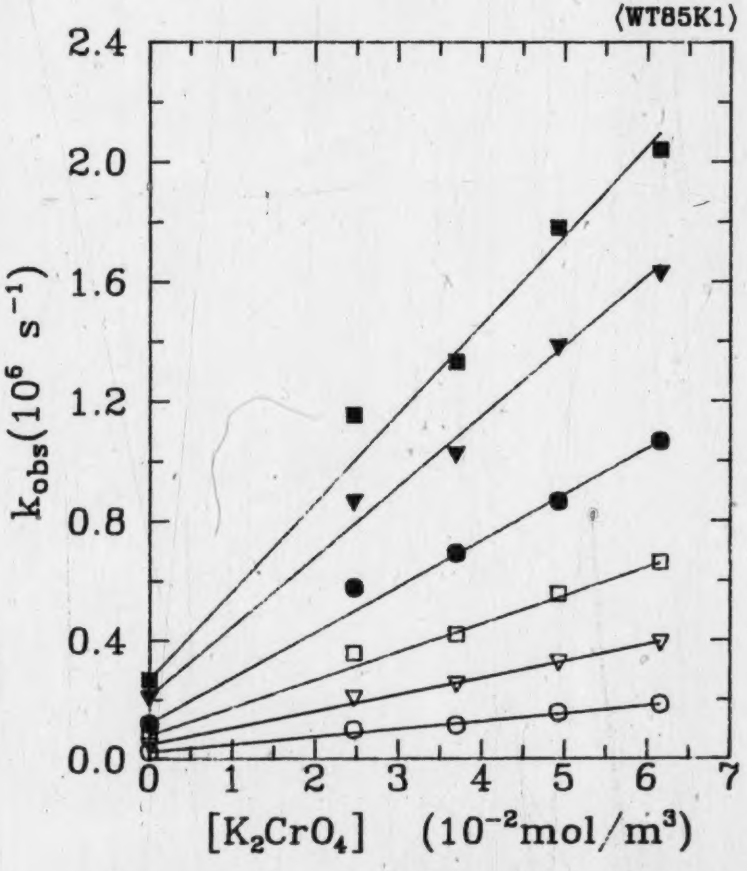

Fig. 3−141: t−BuOH/H_2O:15/85

○ 279.6K ▽ 297.2K □ 313.6K

● 333.2K ▼ 354.0K ■ 368.0K

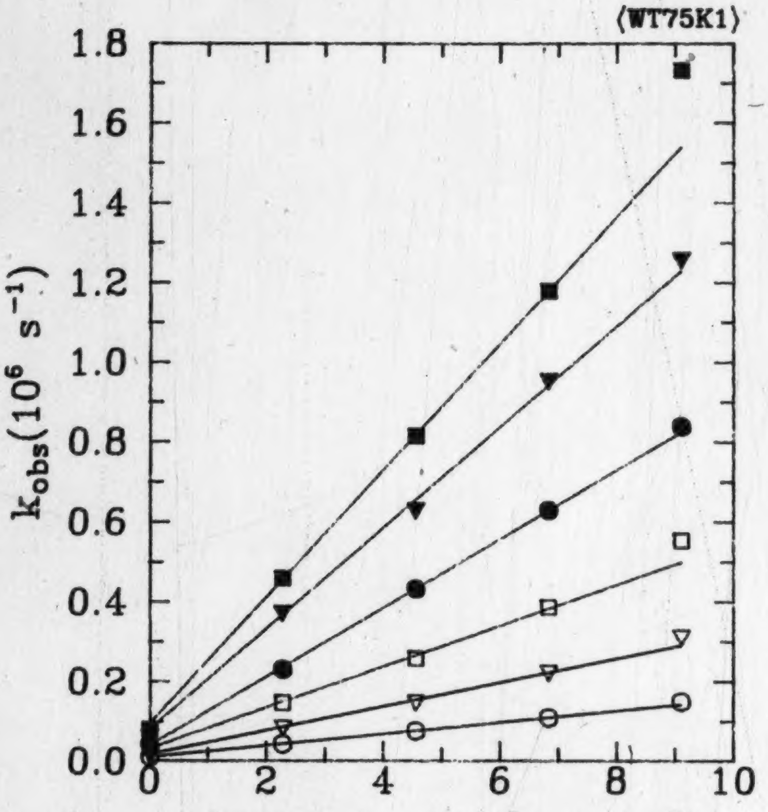

Fig. 3−142: t−BuOH/H_2O:25/75

○ 279.7K ▽ 296.9K □ 313.5K
● 333.2K ▼ 353.0K ■ 368.0K

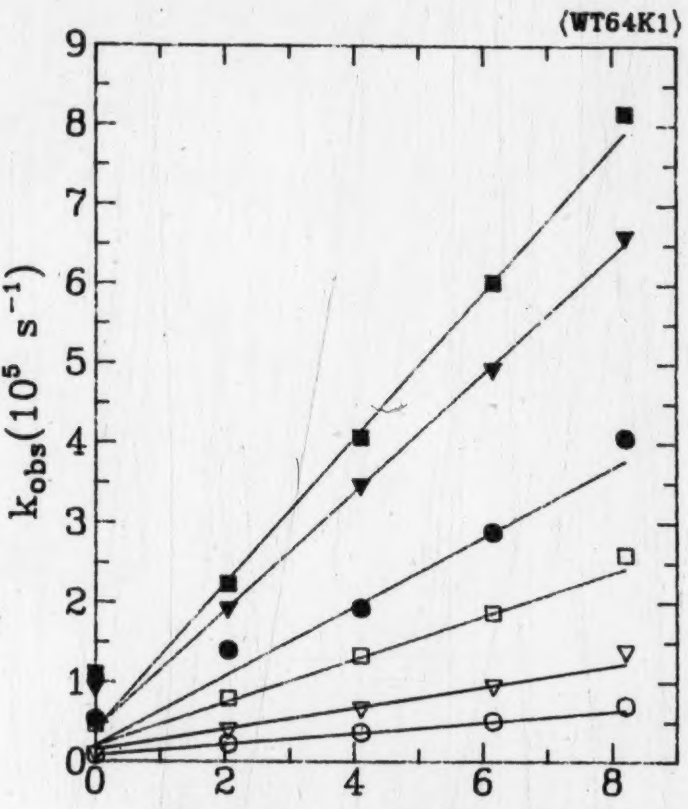

Fig. 3−143: t−BuOH/H_2O:36/64

○ 279.3K ▽ 297.3K □ 314.2K
● 333.3K ▼ 354.1K ■ 368.3K

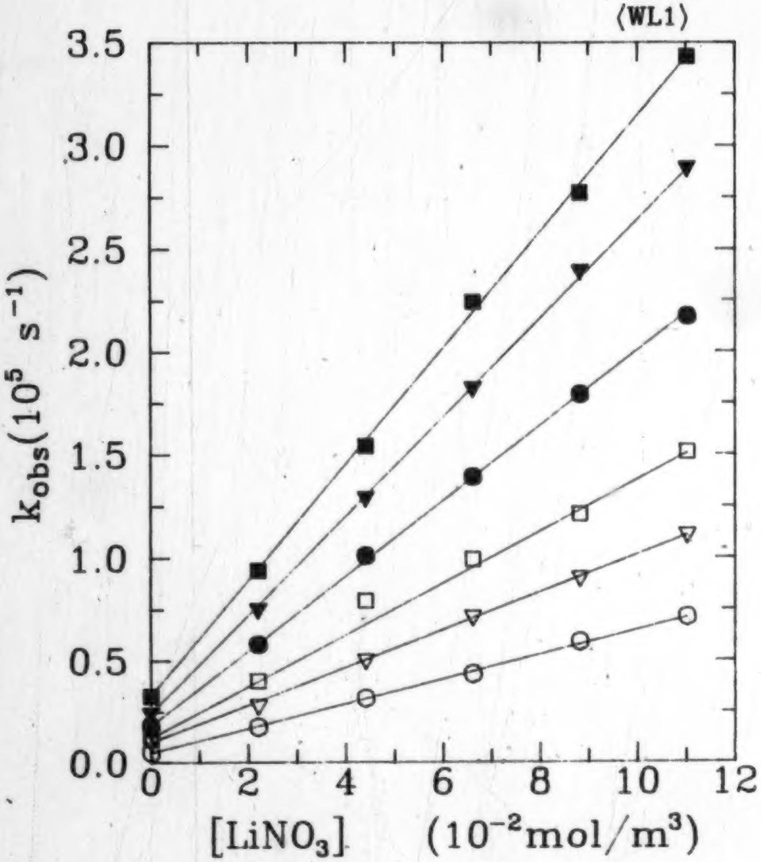

Fig. 3−144: H_2O

○ 279.5K ▽ 296.7K □ 313.3K
● 333.7K ▼ 353.7K ■ 369.7K

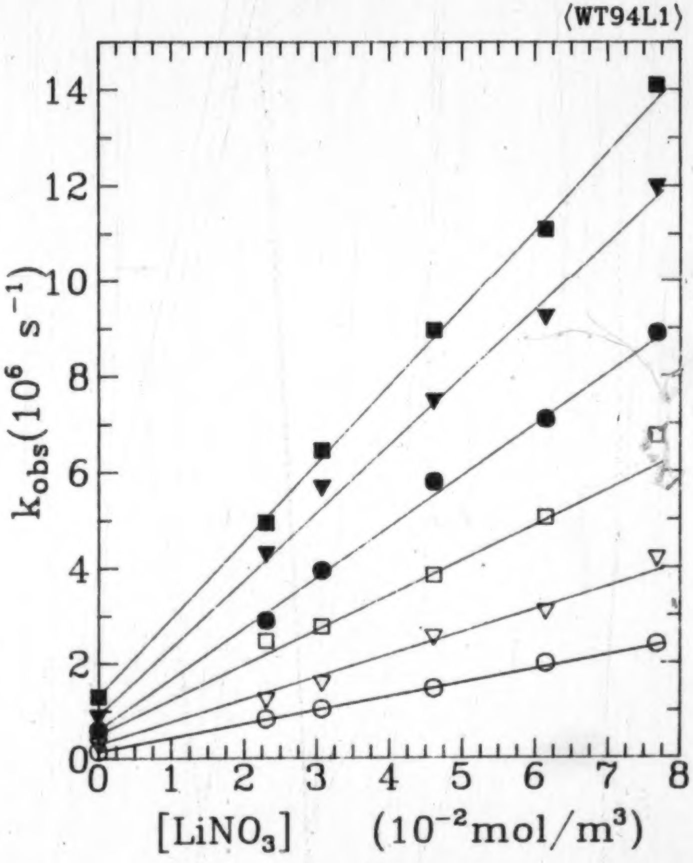

Fig. 3−145: t−BuOH/H_2O:6/94

○ 280.9K ▽ 296.5K □ 313.4K
● 333.4K ▼ 353.8K ■ 368.4K

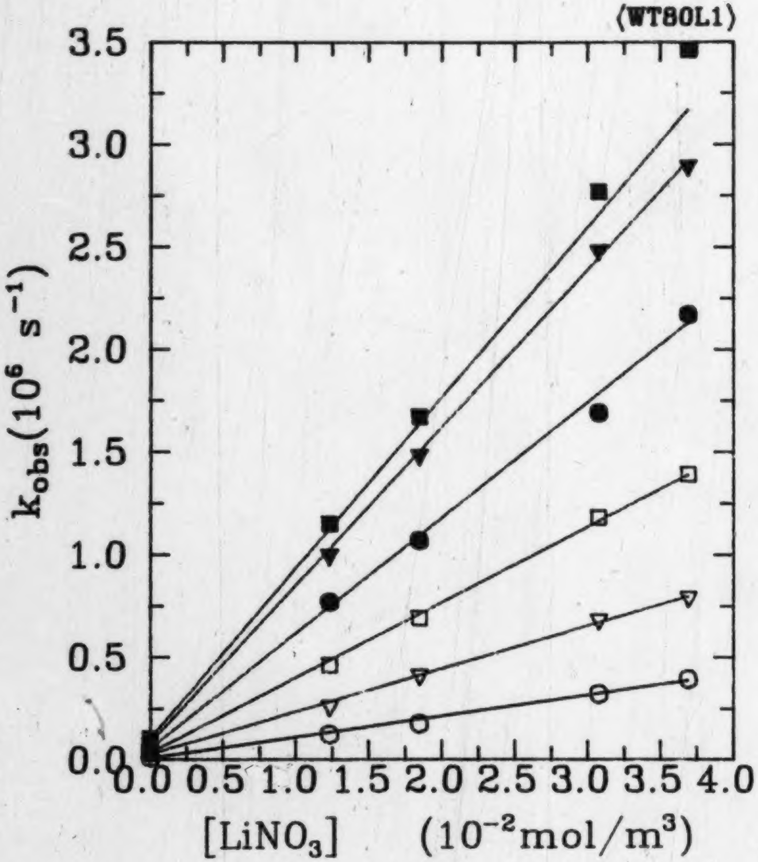

Fig. 3−146: t−BuOH/H_2O:20/80

○ 278.4K ▽ 296.2K □ 313.3K

● 333.0K ▼ 353.9K ■ 368.0K

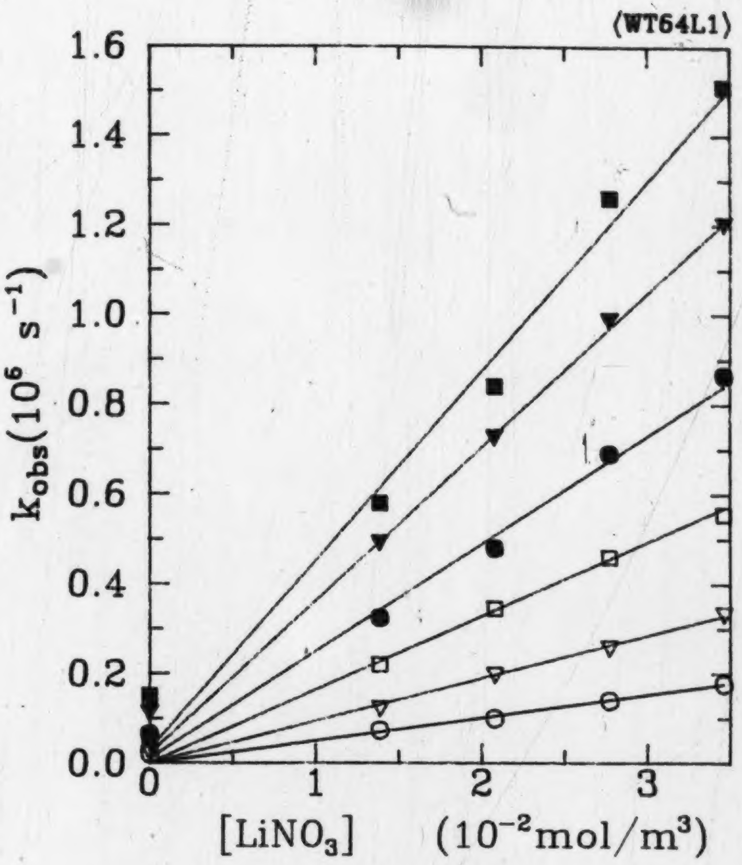

Fig. 3−147: t−BuOH/H_2O:36/64

○ 280.6K ▽ 296.1K □ 313.3K

● 333.0K ▼ 353.9K ■ 368.0K

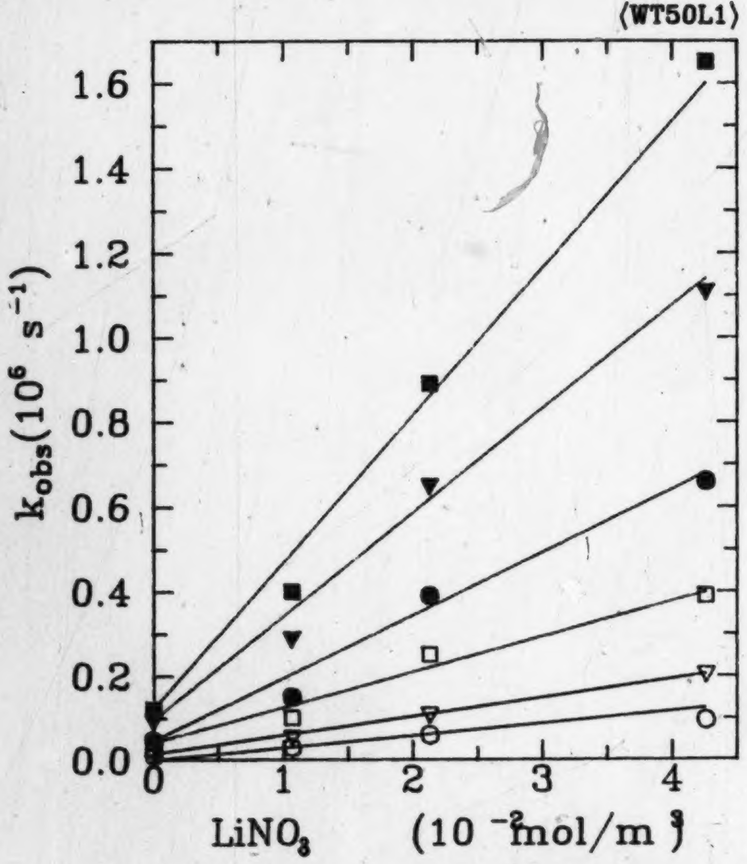

Fig. 3−148: t−BuOH/H_2O:50/50

○ 279.6K ▽ 296.6K □ 313.4K
● 333.0K ▼ 354.0K ■ 368.0K

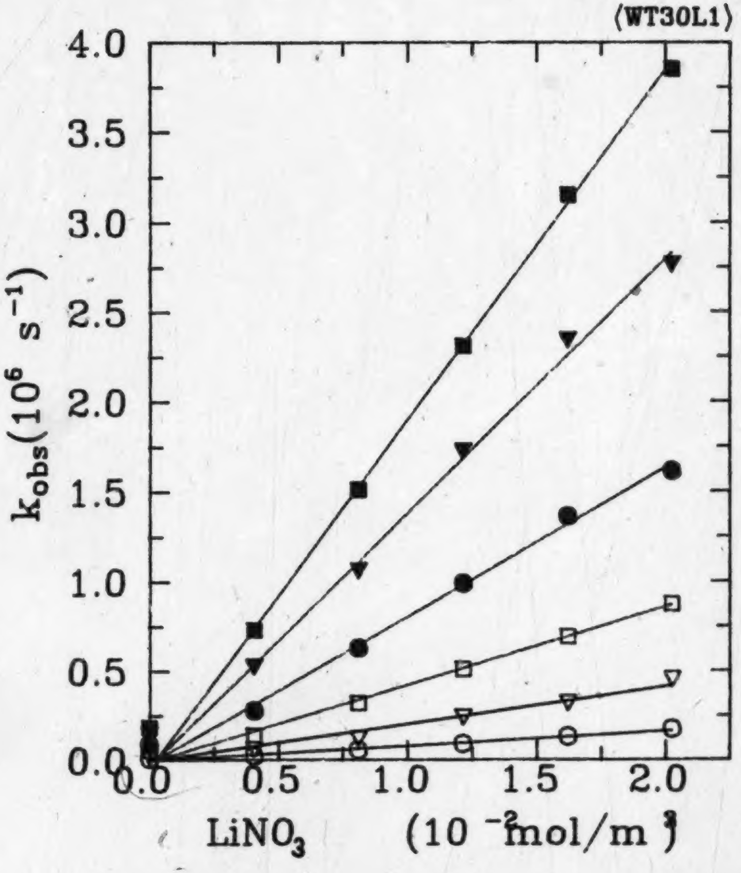

Fig. 3−149: t−BuOH/H_2O:70/30

○ 279.5K ▽ 297.4K □ 313.4K
● 333.0K ▼ 353.9K ■ 368.0K

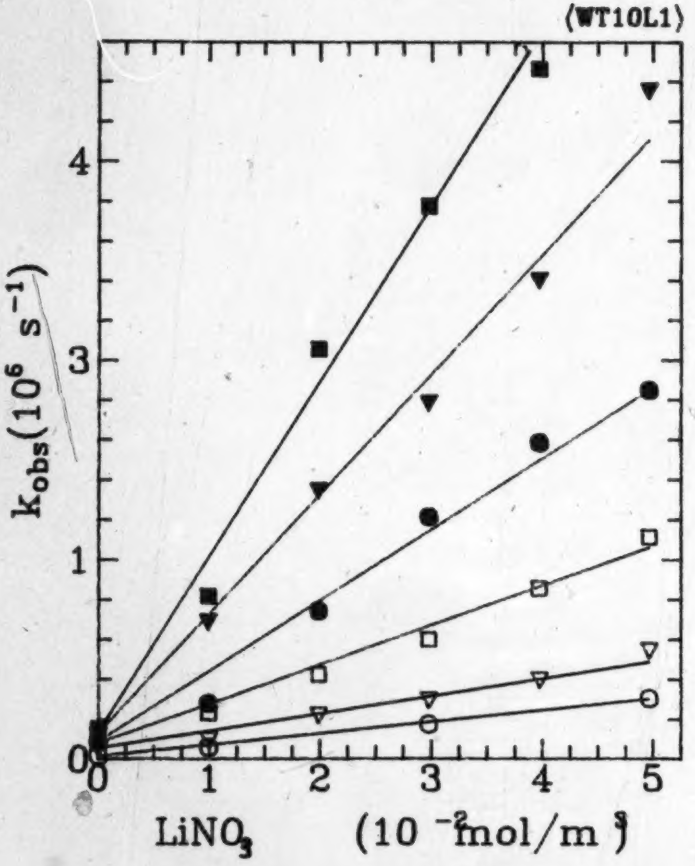

Fig. 3−150: t−BuOH/H_2O:90/10

○ 283.7K ▽ 296.6K □ 313.3K
● 333.0K ▼ 349.1K ■ 363.4K

Table 3-23:The values of second order rate constants for (-) ions in *t*-butanol/water

x_{H_2O}	T (K)	k_2 $10^7(m^3/mol.s)$
	Scavenger: KNO_3	
1.00	275.9	0.55
	287.5	0.72
	297.5	0.98
	324.2	1.57
	346.7	2.17
	373.3	2.84
0.98	279.0	0.44
	288.4	0.59
	297.4	0.71
	322.3	1.18
	345.8	1.60
	368.8	2.04
0.97	278.9	0.38
	293.6	0.58
	313.9	0.90
	333.4	1.30
	353.5	1.62
	368.6	1.88
0.94	280.2	0.26
	297.3	0.45
	314.0	0.69
	333.5	0.99

	353.4	1.31
	368.5	1.53
0.90	279.6	0.18
	296.4	0.35
	313.5	0.57
	333.2	0.85
	353.7	1.21
	367.7	1.37
0.90	279.0	0.17
	293.9	0.31
	314.0	0.59
	333.5	0.89
	368.0	1.39
0.85	279.6	0.13
	294.5	0.25
	313.2	0.62
	333.2	0.62
	353.0	0.94
	368.1	1.12
0.64	297.6	0.10
	314.0	0.16
	334.5	0.24
	334.5	0.24
	353.5	0.32
0.64	279.0	0.05
	297.6	0.93

	313.9	0.15
	333.4	0.25
	353.4	0.37
	368.6	0.43

Scavenger: $LiNO_3$

1.00	279.5	0.60
	296.7	0.92
	313.3	1.26
	333.7	1.82
	353.7	2.40
	369.7	2.82
0.94	280.9	0.29
	296.5	0.48
	313.4	0.80
	333.4	1.08
	353.8	1.56
	368.4	1.65
0.80	278.4	0.10
	296.2	0.21
	313.3	0.37
	333.0	0.56
	353.9	0.37
	368.0	0.83
0.64	280.6	0.50
	296.1	0.96

	313.3	1.64
	333.0	2.38
	353.9	3.42
	368.0	4.23
0.50	279.6	0.31
	296.6	0.45
	313.0	1.46
	354.0	2.72
	368.0	3.49
0.30	279.5	0.09
	297.4	0.21
	313.4	0.44
	333.0	0.77
	353.9	1.42
	368.0	1.95
0.10	283.7	0.62
	296.6	1.09
	313.3	2.30
	333.0	4.43
	349.7	7.48
	363.4	10.70

Scavenger: K_2CrO_4

1.00	277.5	1.02
	298.0	1.72
	313.6	2.33

	333.5	3.35
	354.2	4.61
	371.4	6.25
0.98	277.5	0.80
	297.4	1.30
	313.6	1.96
	333.4	2.74
	354.0	4.14
	370.4	5.43
0.97	277.5	0.65
	296.7	1.17
	314.0	1.70
	333.2	2.51
	354.0	3.80
	370.3	5.03
0.94	280.2	0.47
	296.9	0.87
	314.0	1.37
	333.3	2.05
	354.0	3.10
	369.1	3.96
0.90	280.3	0.36
	296.1	0.68
	313.9	1.15
	333.3	1.78
	354.2	2.62

	368.4	3.35
0.85	279.6	0.27
	297.2	0.57
	313.6	0.96
	333.2	1.52
	354.0	2.41
	368.0	3.02
0.75	279.7	0.15
	296.9	0.30
	313.5	0.52
	333.2	0.87
	353.0	1.27
	368.0	1.59
0.64	279.3	0.07
	297.3	0.14
	314.2	0.27
	333.3	0.44
	354.1	0.75
	368.3	0.92

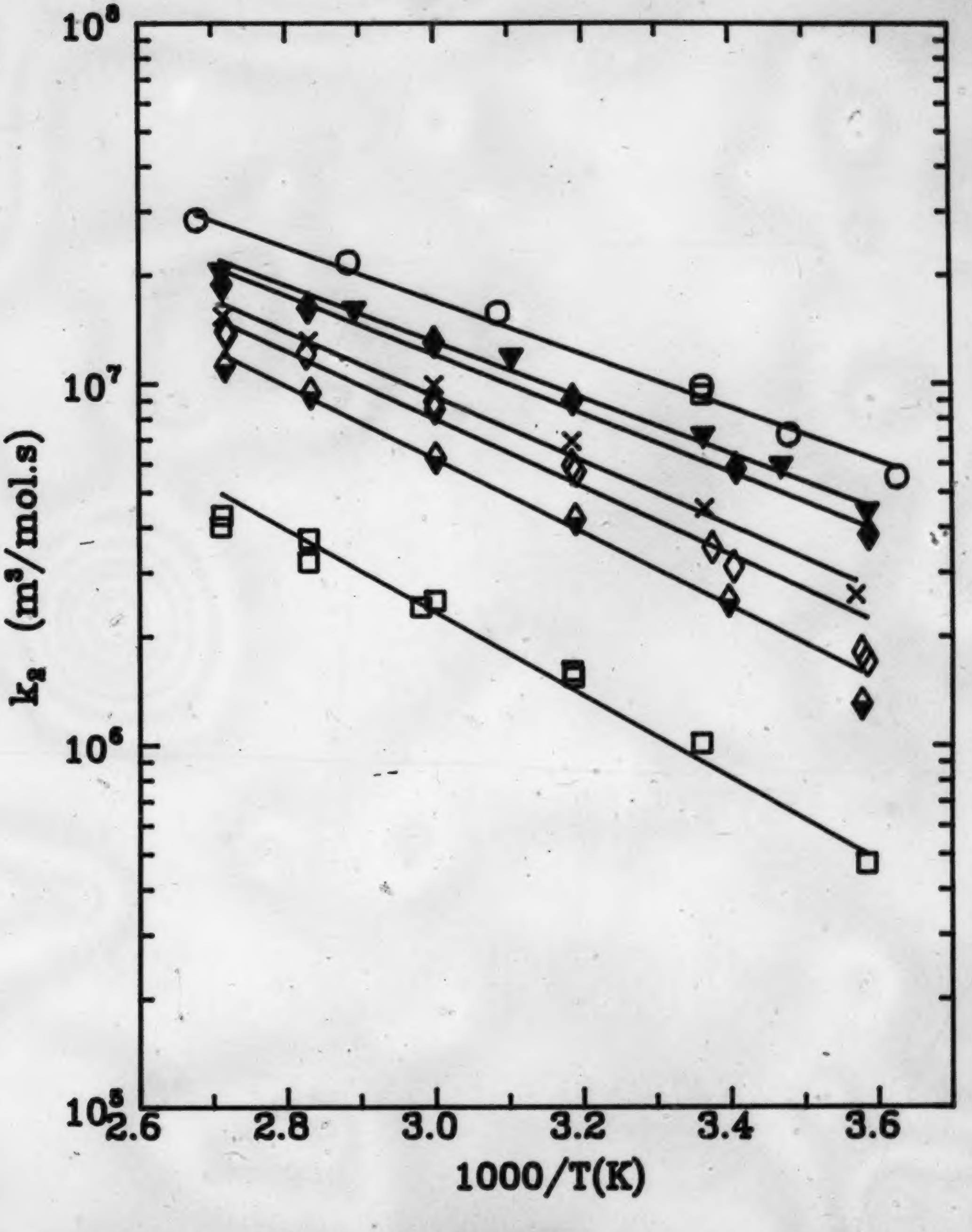

Fig. 3–151: $e_s^- + KNO_3$ reaction in t–BuOH water mixtures.

x_{H_2O}: □ 0.64 ◆ 0.85 ◇ 0.90 × 0.94
◆ 0.97 ▼ 0.98 ○ 1.00

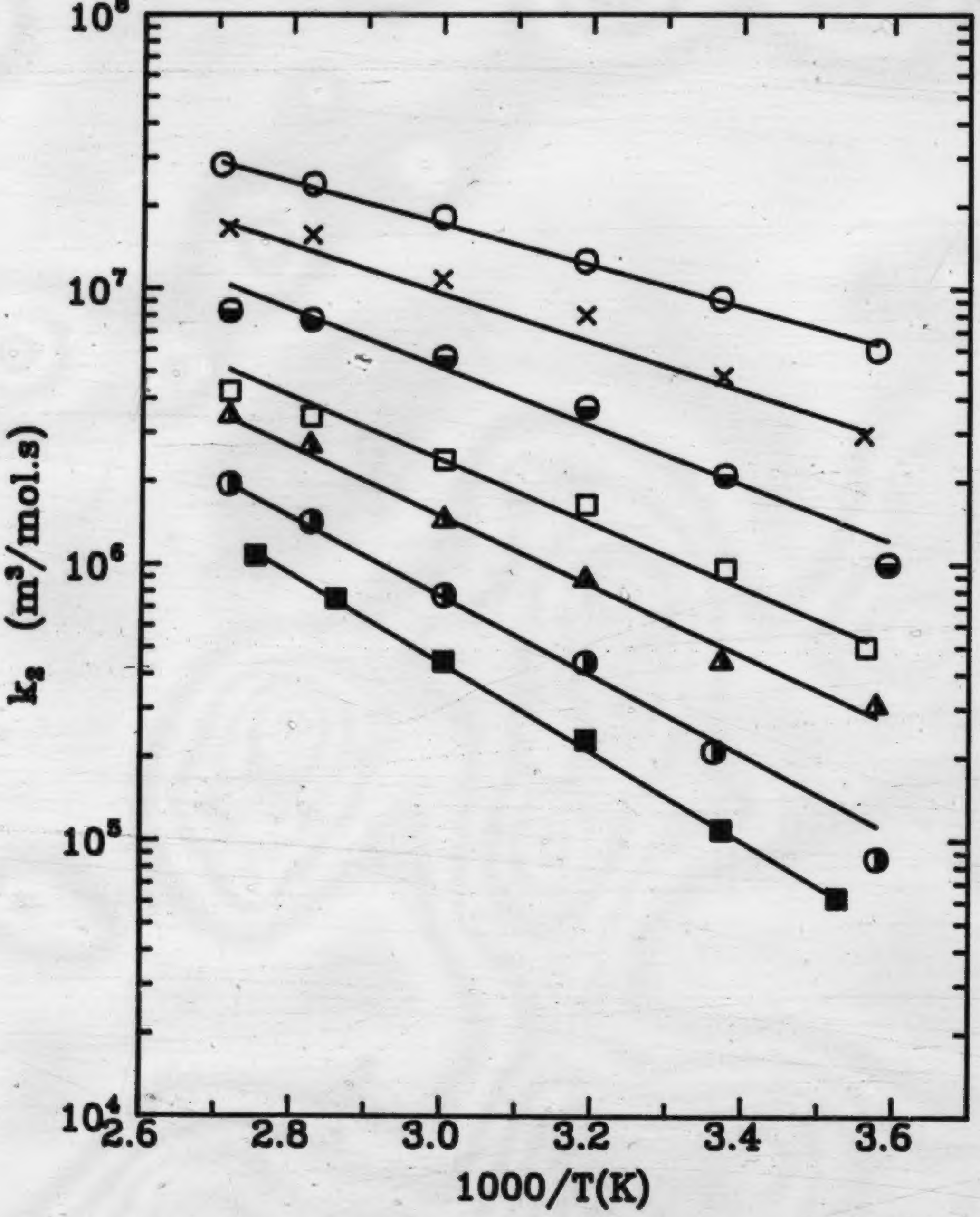

Fig. 3–152: $e_s^- + LiNO_3$ reaction in t–BuOH water mixtures.

x_{H_2O}: ■ 0.10 ◐ 0.35 ▲ 0.50 □ 0.64
⊖ 0.80 × 0.94 ○ 1.00

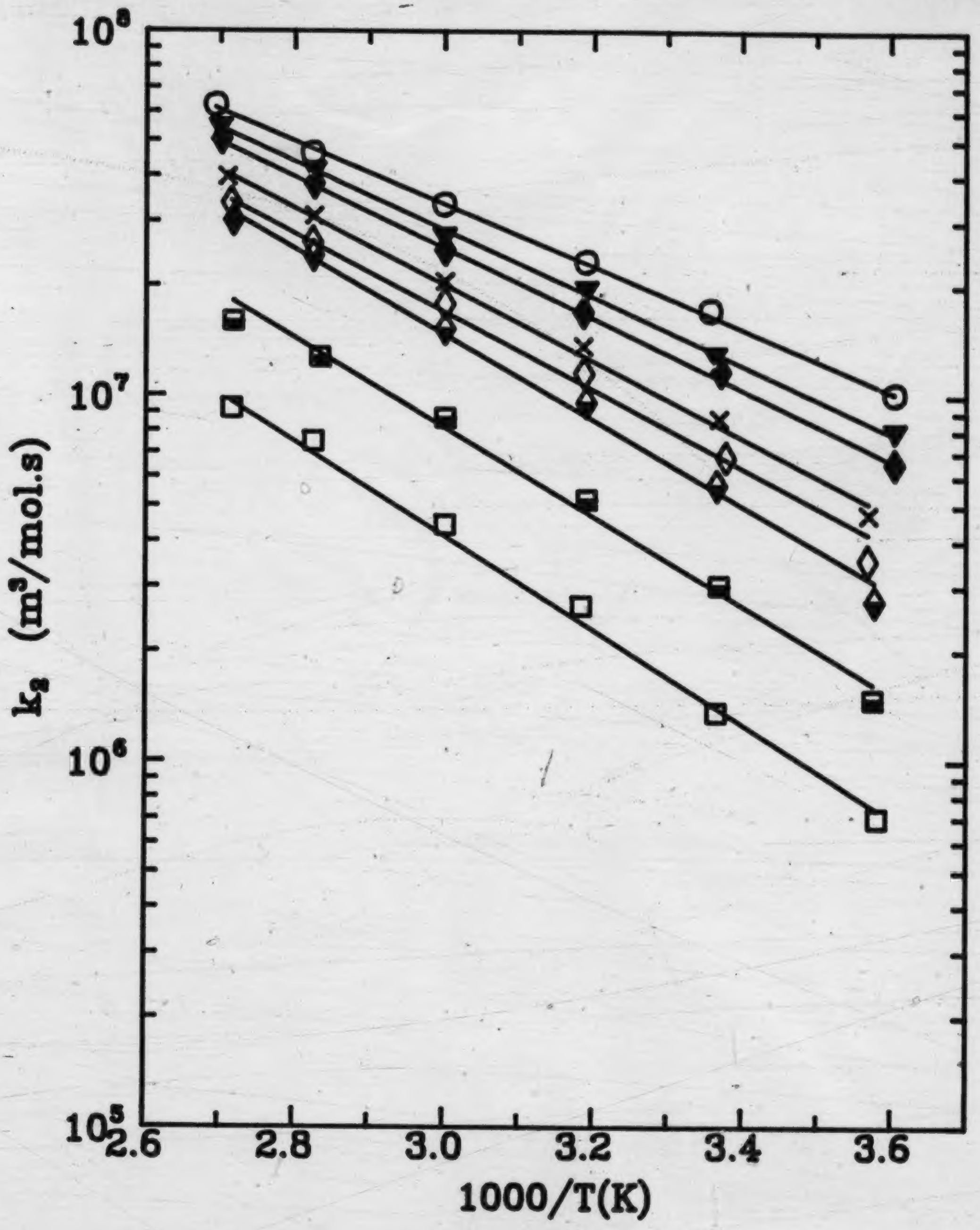

Fig. 3–153: $e_s^- + K_2CrO_4$ reaction in t–BuOH water mixtures.

x_{H_2O}: □ 0.64 ⬓ 0.75 ⬙ 0.85 ◇ 0.90
× 0.94 ◆ 0.97 ▼ 0.98 ○ 1.00

Table 3-24: Reaction rate parameters (-) scavengers in *t*-butanol/water

x_{H_2O}	k_2 $10^6 m^3/mol.s.$	E_2 (J/mol)	log A	$\Delta S_2^{\neq}$ (J/mol.K)
	Scavenger : KNO_3			
1.00	9.30	14	9.40	-8
0.98	7.00	15	9.77	-6
0.97	6.20	16	9.55	-4
0.94	4.50	17	9.63	-4
0.90	3.70	18	9.74	-2
0.85	2.70	20	9.84	0
0.64	0.90	22	9.79	0
	Scavenger : $LiNO_3$			
1.00	9.50	14	9.49	-6
0.94	4.80	17	9.64	-4
0.80	2.10	20	9.84	0
0.64	0.93	22	9.80	0
0.50	0.53	24	9.97	4
0.30	0.24	28	10.22	8
0.10	0.12	31	10.50	13
	Scavenger : K_2CrO_4			
1.00	1.70	16	10.05	6
0.98	1.30	18	10.19	8
0.97	1.20	18	10.28	10
0.94	0.86	20	10.44	11
0.90	0.71	21	10.45	13
0.85	0.56	22	10.60	15
0.75	0.30	23	10.56	15
0.64	0.15	25	10.56	15

Fig.3–154: k_2, E_2 and ΔS_2 for (–)Scavengers in t–BuOH/Water Mixtures. open points E_2; closed points ΔS_2.

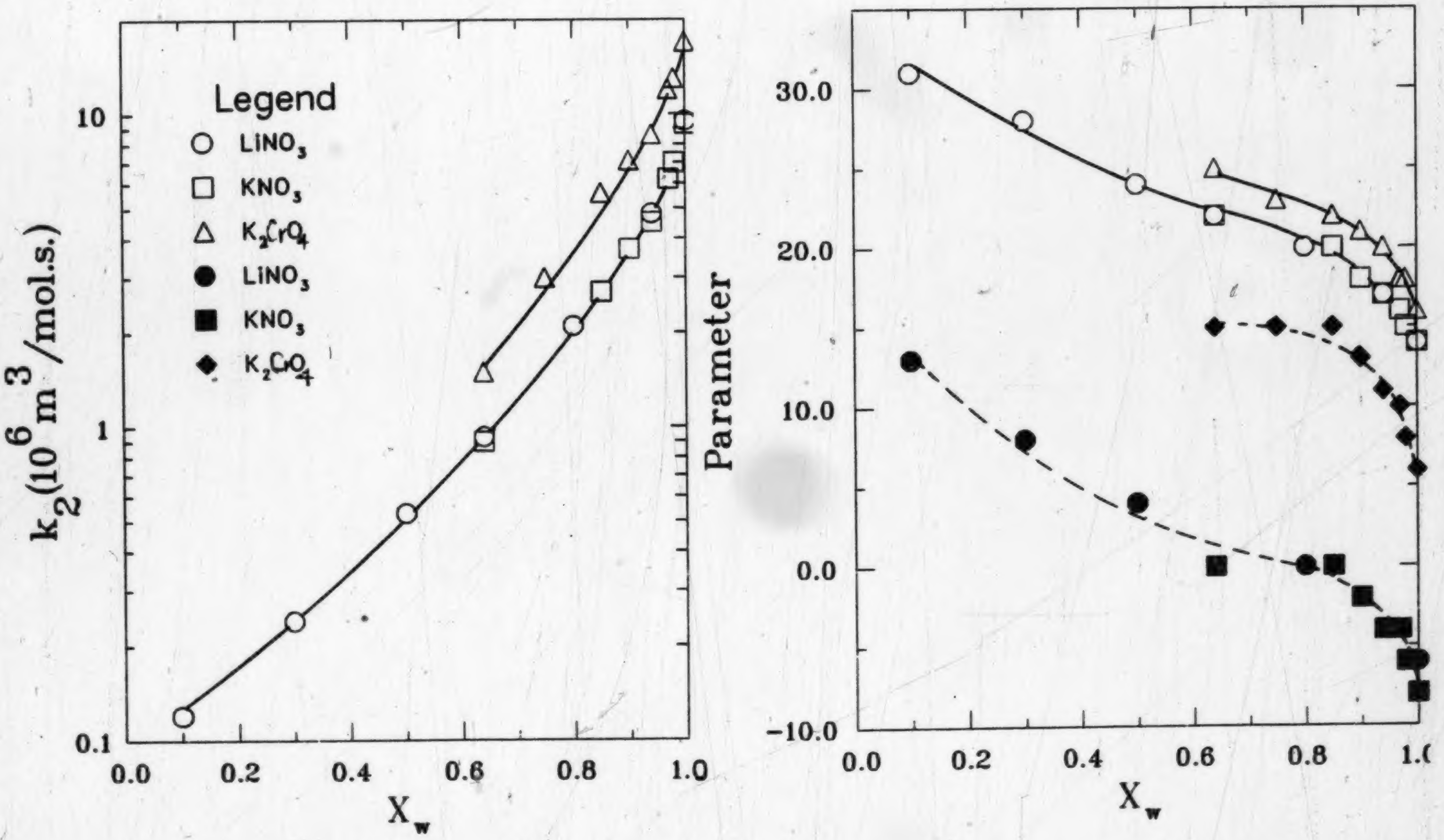

3.3 Densities and Viscosities of Butanol/Water Mixtures

The densities and viscosities were measured as a function of temperature and solvent composition. The values at each composition were fitted with polynomials in temperature. Values of densities and viscosities for the solvents at a given temperature were obtained by interpolation.

3.3.1 Density

The density values, ρ, at a given composition are fitted to the following polynomial:

$$\rho = a_0 + a_1 T + a_2 T^2 \tag{28}$$

The parameters a_i are given in Table(3-26) including the average percent deviation $\Delta_a v$,

$$\Delta_{av} = \frac{100}{n} \Sigma |\Delta_i| \tag{29}$$

The percent deviation Δ_i compares the experimental values to the fitted values.

$$\Delta_i = 100(1 - \frac{fitted}{exp.}) \tag{30}$$

Except for $x_{H_2O} \geq 0.95$, a fit with $\Delta_{av} < 0.1$ % was obtained using $a_2 = 0$. The quadratic term at $x_{H_2O} \geq 0.95$ is due to the curvature of water density towards a maximum at 277.13K.

To compare with literature values these densities at constant temperature were fitted to :

$$\rho(kg/m^3) = \Sigma c_j x_j \tag{31}$$

where x_i is the mole fraction of water. The average deviation among the results, Δ_{av} (eq. 29), average deviation from literature, Δ_{lit} ,

$$\Delta_l = 100(1 - \frac{lit.}{present}) \tag{32}$$

$$\Delta_{lit} = \frac{100}{n}\Sigma|\Delta_l| \tag{33}$$

and constant offset from literature results, Δ_{OS},

$$\Delta_{OS} = \frac{100}{n}\Sigma\Delta_l \tag{34}$$

were also calculated. These numbers are listed in Table(3-27). The results indicate that the composition dependence of the density generated from eq.(3-31) using Table(3-26) parameters are reliable to better than 0.1%.

Table 3-25: Density of butanol/water mixtures as a function of x_{H_2O} and

x_{H_2O}	T (K)	d $10^3 kg/m^3$
Alcohol : *i*-BuOH		
0.0	274.7	0.8149
	283.8	0.8082
	293.7	0.8007
	308.6	0.7893
	322.9	0.7777
	338.2	0.7645
	352.6	0.7521
0.10	274.7	0.8220
	283.5	0.8152
	293.4	0.8024
	308.5	0.7952
	323.4	0.8052
	338.1	0.7923
	344.6	0.7864
0.45	274.7	0.8491
	283.4	0.8453
	293.7	0.8346
	308.8	0.8224
	323.4	0.8103
	338.1	0.7975
	344.6	0.7916
0.99	274.7	0.9935

	283.8	0.9934
	293.7	0.9918
	308.6	0.9872
	322.9	0.9808
	338.2	0.9730
	352.6	0.9646
Alcohol : 2-BuOH		
0.0	283.1	0.8152
	300.0	0.8013
	318.0	0.7857
	333.4	0.7712
	342.5	0.7620
0.10	274.7	0.7994
	285.1	0.7907
	297.9	0.7806
	310.5	0.7694
	324.5	0.7577
	338.7	0.7445
	353.0	0.7304
0.20	283.1	0.8271
	300.0	0.8129
	318.0	0.7968
	333.4	0.7823
	342.5	0.7733
0.30	274.7	0.8402
	285.1	0.8327

	297.9	0.8215
	310.5	0.8106
	324.5	0.7979
	338.7	0.7845
	353.0	0.7713
0.40	274.7	0.8501
	283.9	0.8430
	293.7	0.8349
	308.4	0.8220
	323.8	0.8081
	338.5	0.7944
	353.2	0.7798
0.50	283.1	0.8549
	300.0	0.8549
	318.0	0.8250
	333.4	0.8108
	342.5	0.8021
0.60	283.9	0.8684
	293.7	0.8608
	308.4	0.8486
	323.8	0.8486
	338.5	0.8220
	353.2	0.8076
0.68	274.7	0.8902
	283.9	0.8833
	293.7	0.8753

	308.4	0.8636
	323.8	0.8506
	338.5	0.8376
	353.2	0.8239
0.97	274.7	0.9870
	274.7	0.9870
	283.5	0.9856
	293.4	0.9829
	308.5	0.9767
	323.5	0.9690
	338.1	0.9603
	353.5	0.9502
0.98	274.7	0.9898
	285.1	0.9886
	297.9	0.9858
	297.9	0.9858
	310.5	0.9814
	324.5	0.9748
	338.7	0.9669
	353.0	0.9576
0.99	274.7	0.9940
	285.1	0.9934
	297.9	0.9909
	310.5	0.9869
	324.5	0.9808
	338.7	0.9733

	353.0	0.9648

Alcohol : *t*-BuOH

0.0	301.9	0.7757
	327.7	0.7471
	342.9	0.7293
	353.0	0.7172
0.10	282.6	0.8004
	293.1	0.7909
	307.6	0.7766
	324.0	0.7599
	338.4	0.7444
	348.2	0.7333
0.30	282.6	0.8169
	293.1	0.8072
	307.6	0.7934
	324.0	0.7774
	338.4	0.7628
	348.2	0.7527
0.50	274.7	0.8482
	282.7	0.8417
	293.1	0.8396
	301.9	0.8245
0.60	283.5	0.8570
	293.4	0.8485
	308.5	0.8354
	323.5	0.8217

	338.1	0.8076
	353.5	0.7938
0.65	282.6	0.8688
	293.1	0.8597
	307.6	0.8473
	324.0	0.8325
	338.4	0.8187
	348.2	0.8091
0.75	282.6	0.8938
	282.6	0.8938
	293.2	0.8850
	308.5	0.8722
	323.1	0.8596
	337.9	0.8464
	352.8	0.8364
0.91	282.6	0.9594
	293.2	0.9520
	308.5	0.9410
	337.9	0.9189
	352.8	0.9071
0.95	282.6	0.9780
	293.2	0.9734
	308.5	0.9652
	337.9	0.9458
	352.8	0.9351
1.00	274.7	0.9999

283.6	0.9997
293.7	0.9978
313.4	0.9920
333.3	0.9834
347.9	0.9753

Table 3-26:Parameters for the temperature dependence of density.

x_{H_2O}	a_0	a_1	a_2 10^3	Δ_{av}	Δ_{max}
	Solvent : 2-butanol/water mixtures				
0.0	1069.1	-0.894		0.08	0.12
0.10	1076.3	-0.902		0.10	0.18
0.20	1084.2	-0.906		0.06	0.08
0.30	1085.3	-0.887		0.08	0.10
0.40	1097.4	-0.896		0.09	0.15
0.50	1105.1	-0.880		0.07	0.12
0.60	1117.1	-0.875		0.08	0.14
0.68	1122.4	-0.842		0.07	0.13
0.97	779.3	1.716	-3.489	0.03	0.05
0.98	717.4	2.086	-3.982	0.02	0.03
0.99	708.3	2.147	-4.027	0.03	0.03
1.00	753.6	1.887	-3.594	0.02	0.05
	Solvent : *iso*-butanol/water mixtures				
0.0	1037.0	-0.805		0.07	0.11
0.10	1051.1	-0.831		0.06	0.11
0.20	1056.0	-0.828		0.04	0.05
0.30	1067.9	-0.843		0.07	0.12
0.40	1075.9	-0.839		0.05	0.07
0.45	1089.2	-0.863		0.05	0.12
0.99	713.2	2.117	-3.985	0.04	0.06
	Solvent : *t*-butanol/water mixtures				

0.0	1121.5	-1.144		0.05	0.07
0.10	1101.0	-1.053		0.10	0.15
0.30	1094.3	-0.980		0.04	0.07
0.50	1105.6	-0.933		0.08	0.13
0.60	1115.8	-0.911		0.04	0.06
0.65	1127.2	-0.913		0.16	0.10
0.75	1136.2	-0.857		0.03	0.04
0.91	1170.3	-0.745		0.03	0.05
0.95	915.8	0.892	-2.374	0.02	0.03

Table 3-27 : Parameters for the composition dependence of density in butanol/water mixtures

	t-butanol	2-butanol	t-butanol	2-butanol
T/K	293.1	293.1	298.15	328.15
c_0	786.1	807.0	780.40	775.70
c_1	36.2	14.8	37.20	6.60
c_2	521.8	655.1	582.80	710.20
c_3	-3766.1	-4186.2	-4177.20	-4288.10
c_4	13242.6	13589.8	14364.50	13568.80
c_5	-22545.7	-22087.9	-24023.10	-21848.70
c_6	18628.0	17608.7	19541.30	17394.40
c_7	-5904.8	-5403.7	-6108.80	5333.30
Δ_{av}	0.01	0.03	0.02	0.01
Δ_{lit}	0.13[a],0.09[b]	0.07[c]	0.05[d]	0.05[c]
Δ_{OS}	-0.12[a],-0.05[b]	0.06[c]	-0.02[d]	0.01[c]

a. Ref. 133

b. Ref. 134

c. Ref. 135

d. Ref. 136

3.3.2 Viscosity

Kinematic viscosities as a function of temperature and composition are listed in Table(3-28). To find the extent of deviation from Arrhenius behaviour, the dynamic viscosities at these temperatures were fitted into the following polynomial.

$$ln\eta = b_0 + b_1/T + b_2/T^2 + b_3/T^3 \qquad (35)$$

The parameters of this equation and average deviation between the experimental and the fitted results (eq. 3-30), are in Table(3-29). The viscosities thus obtained are plotted in Fig. (3-154) with literature results for comparison.

The viscosities in pure alcohols are in the order *t*-BuOH > *i*-BuOH > 2-BuOH . When water is added η initially decrease and then slightly increase to come to a maximum at ~ 0.7 The viscosity maximum is a characteristic property of the alcohol/water mixtures. In the other lower alcohols it is in the range $x_{H_2O} \sim 0.70$ - 0.80. Upon further addition of water η decreases until pure water. The change in η in water-rich solvents is much greater than that in alcohol-rich solvents. This implies that a greater change in solvent structure occurs when alcohol is added to water than when water is added to an alcohol.

To compare the energies of activation for electron capture in butanol/water mixtures with the energy of activation for viscous flow, the viscosities were also fitted to the linear form of the polynomial in eq.(3-36) with $b_2, b_3 = 0$. The parameters are $b_1 = E_\eta/R$ and b_0 is related to the entropy of activation. The parameters thus obtained are listed in Table(3-30).

Table 3-28: Experimental flow times (t) and kinematic viscosities (ν) of butanol/water mixtuers as a function of composition and temperature

T	t	ν	d	η
K	s	$10^{-6} m^2/s$	$10^3 kg/m^3$	$10^{-2} Pa.s$
Solvent : 2-butanol/water mixtures				
313.19	267.59	2.7480	0.7847	2.1560
323.45	202.62	2.0760	0.7765	1.6120
333.24	158.77	1.6210	0.7686	1.2460
343.22	126.56	1.2860	0.7605	0.9780
352.88	103.73	1.0460	0.7527	0.7873
363.49	85.29	0.8516	0.7442	0.6338
373.46	72.26	0.7125	0.7362	0.5245
$x_{H_2O} = 0.10$				
298.55	384.46	3.9550	0.8029	3.1750
305.52	311.02	3.1970	0.7971	2.5480
313.66	246.99	2.5350	0.7903	2.0030
323.65	190.32	1.9490	0.7820	1.5240
333.34	150.89	1.5390	0.7739	1.1910
343.29	121.56	1.2230	0.7657	0.9441
353.64	99.23	0.9904	0.7571	0.9441
363.38	83.57	0.8334	0.7490	0.6242
$x_{H_2O} = 0.20$				
298.11	376.60	3.8740	0.8091	3.1340
305.47	301.07	3.0940	0.8030	2.4840
313.57	239.05	2.4530	0.7963	1.9530
323.42	185.08	1.8940	0.7881	1.4930

333.58	145.85	1.4870	0.7797	1.1590
343.47	118.27	1.1990	0.7715	0.9250
353.28	98.06	0.9867	0.7634	0.7532
363.47	82.55	0.8225	0.7550	0.6210

$x_{H_2O} = 0.30$

300.74	344.06	3.5380	0.8143	2.8810
300.33	347.85	3.5770	0.8147	2.9140
306.06	292.05	3.0010	0.8099	2.4310
313.80	234.37	2.4050	0.8033	1.9320
323.33	183.10	1.8740	0.7953	1.4900
333.17	145.52	1.4830	0.7870	1.1670
353.67	97.32	0.9789	0.7697	0.7535
363.32	83.82	0.8360	0.7616	0.6367

$x_{H_2O} = 0.40$

297.76	380.74	3.9170	0.8262	3.2360
305.67	296.49	3.0470	0.8196	2.4970
313.80	234.46	2.4060	0.8128	1.9560
323.32	182.62	1.8690	0.8048	1.5040
333.32	144.39	1.4720	0.7964	1.1720
343.33	116.82	1.1840	0.7880	0.9330
353.58	96.25	0.9676	0.7794	0.7541
363.45	82.16	0.8184	0.7711	0.6311

$x_{H_2O} = 0.45$

298.85	371.40	3.8200	0.8312	3.1750
305.61	298.82	3.0710	0.8254	2.5350
313.52	237.25	2.4350	0.8185	1.9930

323.67	181.58	1.8580	0.8098	1.5050
333.59	143.71	1.4650	0.8012	1.1740
343.18	117.32	1.1890	0.7929	0.9428
353.71	96.18	0.9669	0.7838	0.7579
362.95	83.07	0.8281	0.7759	0.6425

$x_{H_2O} = 0.99$

303.26	330.52	0.9367	0.9887	0.9261
312.99	268.69	0.7586	0.9854	0.7474
323.56	221.34	0.6216	0.9810	0.6097
333.59	188.46	0.5260	0.9760	0.5133
343.32	164.35	0.4553	0.9703	0.4419
353.28	145.40	0.3986	0.9638	0.3843

Solvent : 2-butanol/water mixtures $x_{H_2O} = 0.0$

295.25	413.28	4.2520	0.8051	3.4230
295.45	409.95	4.2180	0.8049	3.3950
304.03	301.08	3.0940	0.7973	2.4670
313.34	221.28	2.2690	0.7889	1.7900
323.29	164.33	1.6790	0.7800	1.3100
333.54	125.21	1.2720	0.7709	0.9806
343.17	100.08	1.0080	0.7623	0.7684
353.34	81.38	0.8100	0.7532	0.6101
362.99	68.66	0.6737	0.7445	0.4989

$x_{H_2O} = 0.10$

296.03	360.89	3.7120	0.8093	3.0040
296.01	361.22	3.7150	0.8093	3.0070

304.92	269.46	2.7680	0.8013	2.2180
313.81	206.12	2.1120	0.7933	1.6750
323.27	158.40	1.6170	0.7847	1.2690
333.22	123.90	1.2580	0.7758	0.9760
343.14	99.64	1.0030	0.7668	0.7691
353.71	81.28	0.8089	0.7573	0.6126
363.35	69.23	0.6799	0.7486	0.5089
	$x_{H_2O} = 0.30$			
296.85	347.52	3.5740	0.8219	2.9370
305.52	262.24	2.6930	0.8142	2.1930
313.87	205.05	2.1010	0.8068	1.6950
323.60	158.45	1.6180	0.7981	1.2910
333.54	125.26	1.2720	0.7893	1.0040
343.47	101.78	1.0260	0.7805	0.8008
353.29	84.91	0.8476	0.7718	0.6542
363.19	72.44	0.7144	0.7630	0.5451
	$x_{H_2O} = 0.40$			
296.86	361.25	3.7160	0.8315	3.0900
306.58	262.37	2.7050	0.8228	2.2260
313.68	212.43	2.1780	0.8164	1.7780
323.34	163.83	1.6740	0.8078	1.3520
333.26	129.16	1.3130	0.7989	1.0490
343.27	104.42	1.0540	0.7899	0.8326
353.28	86.45	0.8640	0.7809	0.6747
363.65	74.59	0.7375	0.7716	0.5691
	$x_{H_2O} = 0.50$			

296.93	374.50	3.8520	0.8438	3.2500
305.19	283.75	2.9150	0.8365	2.4380
313.40	221.00	2.2670	0.8293	1.8800
323.33	168.60	1.7230	0.8205	1.4140
333.06	133.22	1.3550	0.8120	1.1000
343.21	107.15	1.0820	0.8030	0.8688
353.18	88.66	0.8874	0.7943	0.7049
362.97	77.44	0.7680	0.7856	0.6033
$x_{H_2O} = 0.60$				
297.01	386.87	3.9800	0.8579	3.4140
297.15	384.95	3.9600	0.8578	3.4000
305.21	292.47	3.0060	0.8507	1.9460
313.76	225.03	2.3080	0.8432	1.4660
323.65	171.71	1.7560	0.8346	1.1370
333.50	135.28	1.3770	0.8260	0.9039
343.39	109.38	1.1060	0.8173	0.7284
363.11	89.96	0.9011	0.8083	2.5570
$x_{H_2O} = 0.68$				
296.19	405.71	4.1740	0.8730	3.6440
323.41	175.12	1.7910	0.8501	1.5230
328.63	153.78	1.5690	0.8457	1.3270
333.80	136.26	1.3870	0.8414	1.1670
343.27	111.22	1.1250	0.8334	0.9376
353.33	91.92	0.9219	0.8249	0.7605
1.00	1.00	1.0000	1.0000	1.0000
$x_{H_2O} = 0.97$				

303.71	444.92	1.2650	0.9786	1.2390
313.63	345.61	0.9801	0.9743	0.9558
323.18	280.59	0.7930	0.9695	0.7696
333.57	231.56	0.6513	0.9635	0.6282
343.59	197.01	0.5509	0.9570	0.5278
353.64	170.93	0.4747	0.9498	0.4513
	$x_{H_2O} = 0.98$			
302.92	395.48	1.1230	0.9840	1.1050
313.52	307.76	0.8712	0.9801	0.8538
323.73	250.43	0.7059	0.9754	0.6885
333.87	209.92	0.5884	0.9700	0.5707
343.65	180.85	0.5037	0.9641	0.4855
353.62	158.16	0.4371	0.9572	0.4183
	$x_{H_2O} = 0.99$			
303.16	333.24	0.9532	0.9892	0.9429
313.35	269.73	0.7616	0.9858	0.7508
323.66	222.97	0.6263	0.9815	0.6147
333.62	189.93	0.5302	0.9765	0.5177
343.68	164.68	0.4563	0.9706	0.4429
353.77	145.09	0.3985	0.9640	0.3842
	Solvent : *t*-butanol/water mixtures $x_{H_2O} = 0.0$			
303.47	418.03	4.3010	0.7742	3.3300
313.61	261.12	2.6820	0.7627	2.0460
323.51	179.22	1.8340	0.7513	1.3780
333.54	130.76	1.3300	0.7399	0.9841

343.37	101.03	1.0180	0.7286	0.7417
348.47	89.90	0.9005	0.7227	0.6508
353.38	81.15	0.8076	0.7171	0.5788
$x_{H_2O} = 0.10$				
305.54	368.13	3.7870	0.7890	2.9560
313.54	264.52	2.7170	0.7111	2.0980
323.47	185.55	1.8990	0.7610	1.4470
333.38	137.26	1.3970	0.5706	1.0490
343.18	106.28	1.0730	0.7399	0.7939
353.28	85.23	0.8510	0.7286	0.6194
$x_{H_2O} = 0.30$				
303.29	424.60	4.3690	0.7972	3.4830
313.59	281.61	2.8930	0.7871	2.2770
332.55	200.11	2.0500	0.7773	1.5930
333.39	149.30	1.5230	0.7677	1.1690
343.44	115.13	1.1660	0.7579	0.8866
$x_{H_2O} = 0.50$				
303.27	452.92	4.6610	0.8226	3.8340
313.59	303.29	3.1170	0.8130	2.5340
323.44	215.89	2.2140	0.8039	1.7800
333.42	160.77	1.6420	0.7945	1.3050
342.76	126.26	1.2820	0.7858	1.0070
$x_{H_2O} = 0.60$				
303.43	451.57	4.5830	0.8395	3.8470
313.68	304.02	3.0850	0.8302	2.5610
323.72	217.48	2.2050	0.8211	1.8110

333.58	163.24	1.6530	0.8121	1.3420
343.23	127.57	1.2890	0.8033	1.0350
	$x_{H_2O} = 0.65$			
303.46	445.61	4.5860	0.8504	3.9000
313.58	302.45	3.1090	0.8412	2.6150
323.78	316.05	2.2150	0.8320	1.8430
333.73	162.43	1.6590	0.8230	1.3650
343.49	127.24	1.2930	0.8141	1.0530
	$x_{H_2O} = 0.75$			
303.62	410.67	4.2260	0.8761	3.7020
313.65	283.76	2.9150	0.8674	2.5280
323.66	205.70	2.1080	0.8589	1.8110
333.69	156.07	1.5930	0.8503	1.3550
343.49	123.39	1.2530	0.8419	1.0550
353.24	102.23	1.0280	0.8336	0.8569
	$x_{H_2O} = 0.91$			
303.19	912.20	2.6020	0.9446	2.4580
313.49	644.21	1.8360	0.9369	1.7200
323.88	482.43	1.3730	0.9291	1.2760
333.75	328.36	1.0860	0.9218	1.0010
343.63	312.10	0.8837	0.9145	0.8081
	$x_{H_2O} = 0.95$			
302.77	648.09	1.8470	0.9673	1.7870
313.27	467.18	1.3290	0.9608	1.2770
323.02	363.52	1.0320	0.9548	0.9854
333.48	289.86	0.8197	0.9484	0.7774

343.53	240.64	0.6775	0.9422	0.6383
	$x_{H_2O} = 1.00$			
283.15	459.52	1.3070	0.9995	1.3060
288.15	401.39	1.1400	0.9987	1.1390
293.15	353.48	1.0030	0.9977	1.0010
303.29	282.83	0.7994	0.9952	0.7956
313.51	232.43	0.6538	0.9919	0.6485
324.14	194.85	0.5446	0.9877	0.5379
333.69	169.63	0.4708	0.9833	0.4629
343.42	151.57	0.4177	0.9786	0.4088
353.48	133.70	0.3647	0.9719	0.3544

Table 3-29: Parameters for the temperature dependence of viscosity in alcohol/water mixtures.

x_{H_2O}	b_0	b_1 10^{-2}	b_2 10^{-5}	b_3 10^{-8}	Δ_{av}	Δ_{max}
	Solvent : 2-butanol/water mixtures					
0.0	14.16160	-175.96800	60.14050	-5.74516	0.01	0.03
0.10	8.50318	-121.96600	43.54500	-4.12279	0.03	0.08
0.20	-2.98089	-7.35163	5.74238		0.03	0.07
0.30	-2.39655	-10.64170	6.22064		0.04	0.06
0.40	-2.13835	-12.37820	6.55305		0.02	0.04
0.50	-1.97165	-13.41800	6.76191		0.02	0.04
0.60	-1.50166	-16.32201	7.25580		0.06	0.09
0.68	-1.14159	-18.41220	7.58934		0.03	0.06

0.97	-16.70551	142.87900	-47.92830	6.11713	0.03	0.07
0.98	-11.81450	91.34061	-29.84740	3.97164	0.0	0.01
0.99	-14.23320	113.21500	-36.26012	4.53677	0.01	0.02
1.00	-9.24096	62.65074	-19.08150	2.53846	0.04	0.09

Solvent : *iso*-butanol/water mixtures

0.0	4.73580	-91.90840	36.84990	-3.74467	0.03	0.07
0.10	-13.70370	89.39580	-22.37061	2.66483	0.07	0.16
0.20	-4.24979	2.84959	3.94311		0.05	0.11
0.30	-2.88761	-5.87670	5.33538		0.07	0.13
0.40	-3.13074	-4.57166	5.17796		0.03	0.05
0.45	-2.68923	-7.55512	5.69054		0.06	0.13
0.99	-1.41213	-13.14550	5.21390		0.08	0.14

Solvent : *t*-butanol/water mixtures

0.0	-23.00810	218.35600	-80.40421	11.05750	0.02	0.04
0.10	3.71664	-58.17580	15.31610		0.05	0.09
0.30	2.32528	-47.17630	13.31690		0.02	0.04
0.50	1.02506	-37.73540	11.73780		0.10	0.19
0.65	1.88409	-41.96170	12.25170		0.04	0.08
0.75	2.31467	-43.65170	12.32640		0.04	0.07
0.91	-34.52710	323.92896	-109.38200	13.26010	0.0	0.01
0.95	-27.36951	254.76100	-87.21640	10.81080	0.01	0.02

Table (3-30): The energies of activation for the viscous flow E_η (J/mol) in butanol/water mixtures obtained from the linear form of eq.(35).

x_{H_2O}	b_1	E_η
Solvent: *iso*-butanol/water , $\Delta_{av} = 1\%$		
0	1234	23.6
0.10	1199	23.0
0.20	1183	22.6
0.30	1178	22.6
0.40	1193	22.8
0.45	1198	22.9
0.99	816	15.6
Solvent: 2-butanol/water , $\Delta_{av} = 2\%$		
0	1382	26.5
0.10	1246	23.9
0.20	1203	23.0
0.30	1211	23.2
0.40	1257	24.1
0.50	1262	24.2
0.60	1253	24.0
0.68	1253	24.0
0.97	940	18.0
0.98	889	17.0
0.99	824	15.8
Solvent: *t*-butanol/water , $\Delta_{av} = 3\%$		
0	1617	31.0
0.10	1532	29.3
0.30	1540	29.5
0.50	1529	29.3
0.60	1510	28.9
0.65	1482	28.4
0.75	1387	26.6
0.91	1243	23.8
0.95	1140	21.8
0.98	917	17.6
1.00	806	15.4

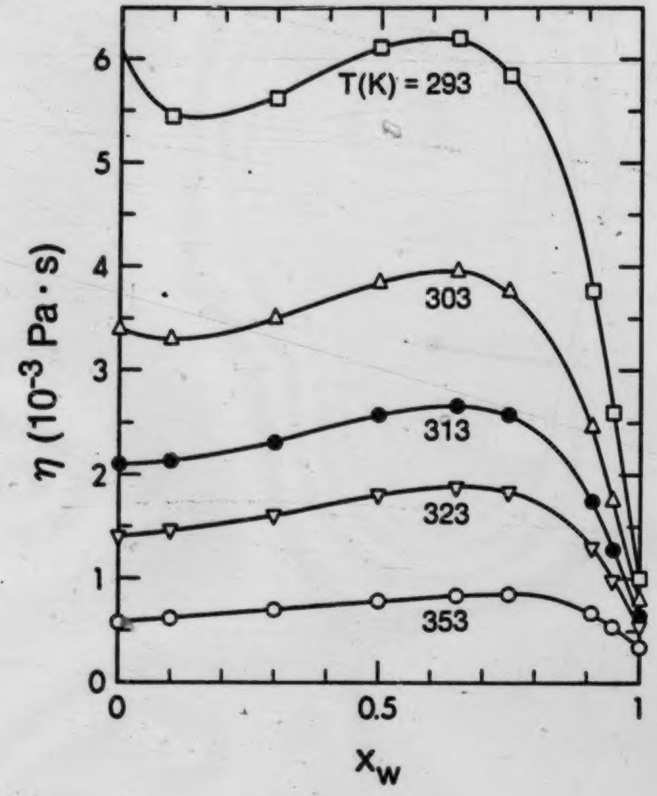

Fig.3-155: Temperature and composition dependence of viscosity of *t*-butanol/water

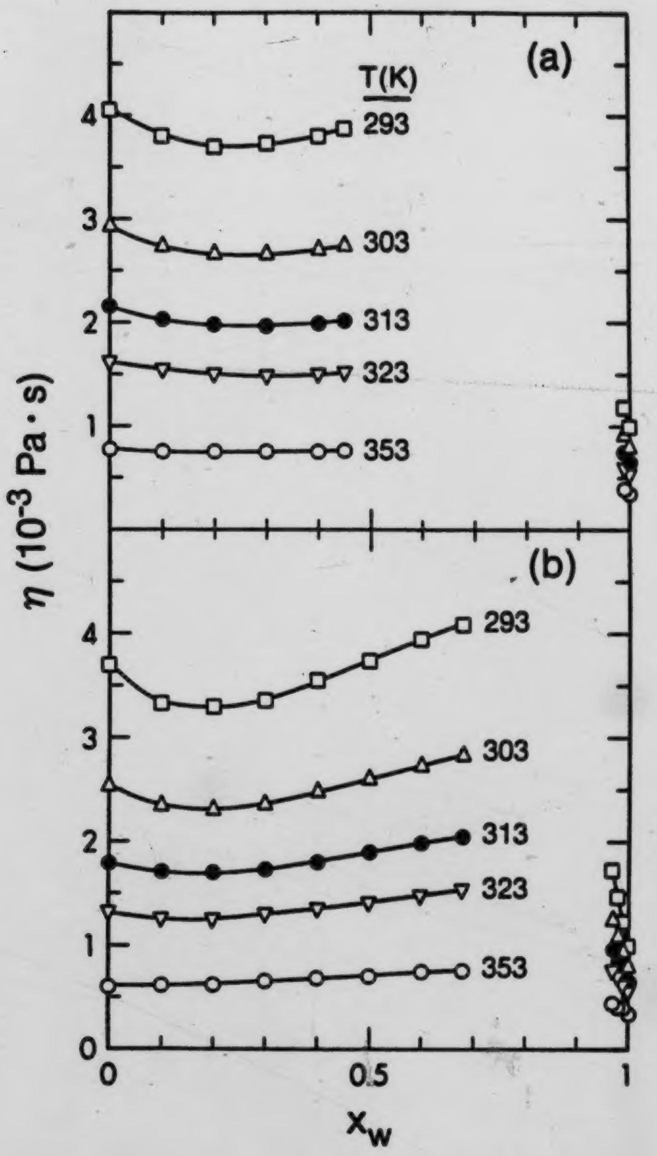

Fig.3-156: Temperature and composition dependence of viscosity of 2-butanol/water and *iso*-butanol/water .

4 DISCUSSION

4.1 Solvent Structure Effects in *t*-Butanol/Water Mixtures

Among the butanols only *t*-butanol is completely miscible with water over the full composition range and the temperature range used in the present study. Hence, *t*-butanol is used as a basis in the study of butanol/water mixtures.

4.1.1 Composition Effects

Rate constants, k_2 , for inefficient scavengers are more dependent on solvent composition than are those for efficient scavengers (Fig. 4-1).

The reactivities of e_s^- with the efficient scavengers are nearly diffusion controlled.

4.1.1.1 Diffusion Controlled Reactions

4.1.1.1(a) Solvent Viscosity Effects

The rate constants for the reaction with nitrobenzene are nearly diffusion controlled, with $k_2 \geq 10^7 m^3/mol.s$. The Smoluchowski (54) equation for diffusion controlled reactions correlates k_2 with the diffusion coefficients D of the reactants:

$$k_2 = 4\pi N_A(D_e + D_S)(R_e + R_S) \tag{36}$$

where N_A is Avogadro's constant, the D's are the diffusion radii, and the R's are reaction radii of the two reactant molecules and $(R_e + R_S)$ is the reaction distance. Subscript e refers to e_s^- and subscript S refers to the scavenger. Application of the Stokes - Einstein (64) equation,

$$D = \frac{k_B T}{6\pi\eta r} \tag{37}$$

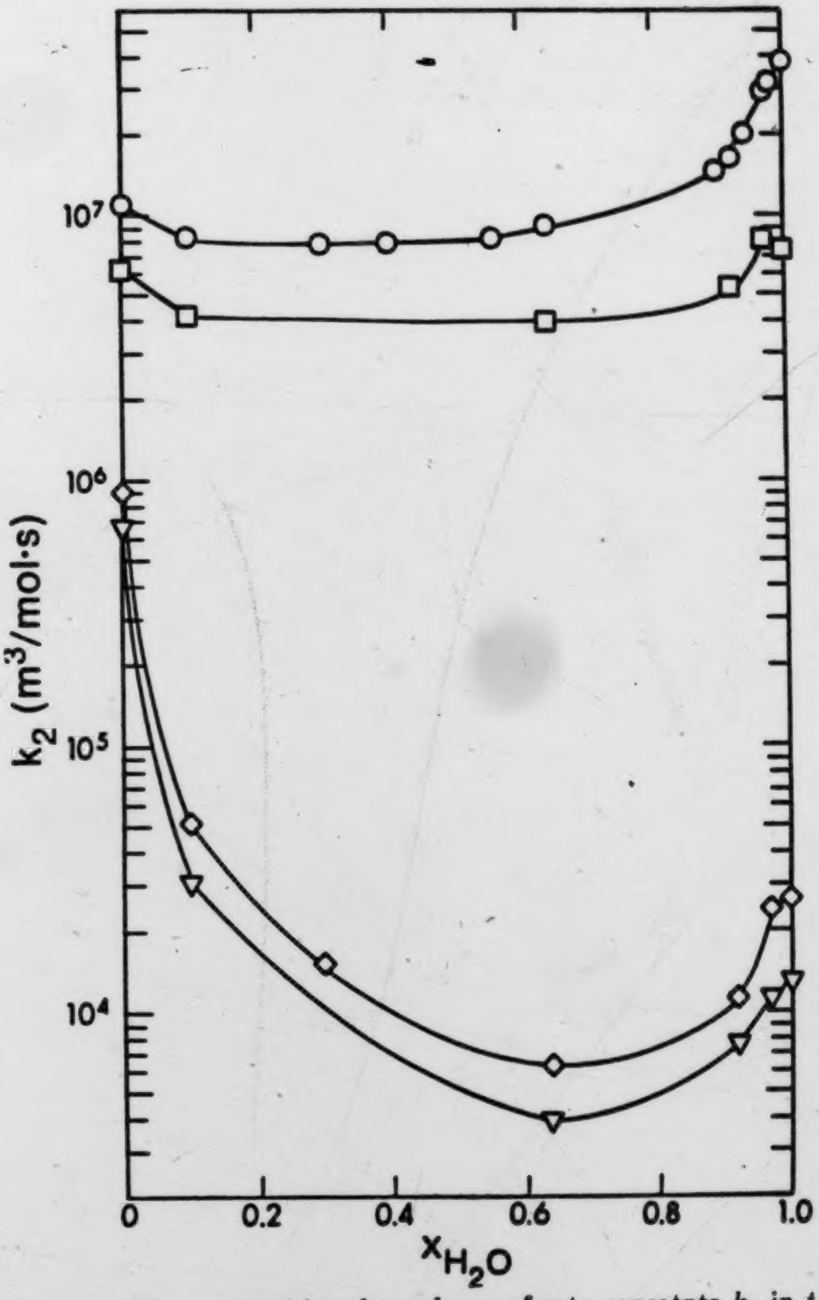

Fig 4-1: The composition dependence of rate consatnts k_2 in *t*-butanol/water mixtures.

Solute: ○, nitrobenzene; □, acetone ; ◇, phenol ; ▽, toluene.

to equation (36) gives the Stokes-Smoluchowski relation :

$$k_2 = \frac{k_B T N_A}{1.5\eta}\left(\frac{1}{r_e} + \frac{1}{r_S}\right)(R_e + R_S) \tag{38}$$

or,

$$k_2 = \frac{constant}{\eta} \tag{39}$$

where k_B is Boltzmann's constant, η is the solvent viscosity and r_x the effective radius of X for diffusion. The deformable e_s^- can diffuse more flexibly through the fluid than can a rigid sphere; the value of the effective radius for diffusion, r_e, is therefore smaller than the molecular radius. In pure water D_e = 4.9 x 10^{-9} m^2/s (63), D_{H_2O} = 2.3 x 10^{-9} m^2/s (147) and η = 8.95 x $10^{-4} Pa.s$ (148) at 298K. This corresponds to Stokes radii of r_e = 0.05 nm and r_{H_2O} = 0.10 nm. Therefore, even though the electron is spread over a diffuse space that covers several water molecules, it diffuses more easily than a single water molecule, and has a correspondingly small *effective* radius for diffusion.

The values of r_e in alcohols, calculated from eq.(40) using the mobility (149 - 152) of e_s^- ,

$$D = \frac{\mu k_B T}{e} \tag{40}$$

where μ is the mobility and e is the charge of the electron, and from eq.(37) using viscosities (153, 154), are not constant. For 296 ± 3K the following values of r_e (nm) are obtained: methanol, 0.28 ; ethanol, 0.28 ; *i*-propanol, 0.09 ; *n*-butanol, 0.04 ; 3-methyl-1-butanol, 0.02. Thus the Stokes - Einstein relation serves only as a framework for discussion in the present work.

Log k_2 for nitrobenzene is plotted against log η in Fig.(4-2).

Equation (39) is obeyed in only one portion of the curve. The curve can be divided into four zones, as had been observed for 1-propanol/water mixtures

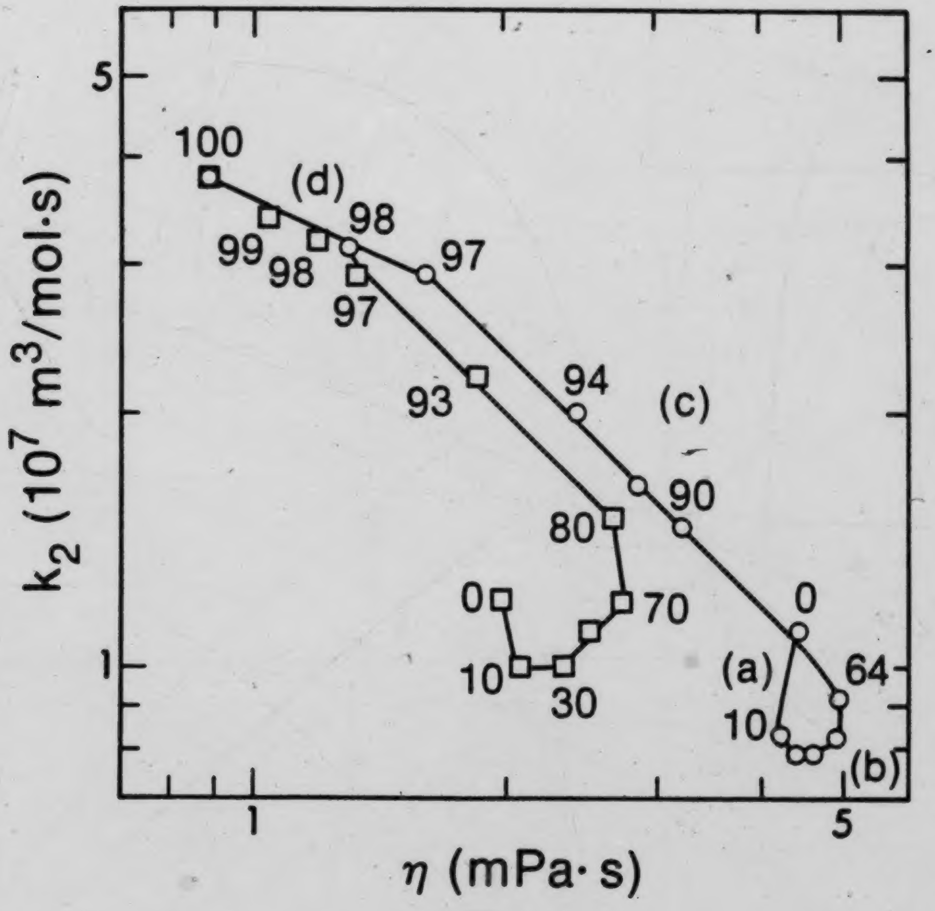

Fig 4-2: The Values of k_2 Against Viscosity η for reaction with nitrobenzene. Solvent:○,*t*-BuOH ;□,*i*-PrOH

(76). The same four zones are also observed in the optical absorption energies of the e_s^- (36, 37), and the freezing point curve of t-BuOH /water mixtures (44, 45). They are:

a. $0 \leq x_{H_2O} \leq 0.10$; k_2 decreases while η decreases slightly,

b. $0.01 < x_{H_2O} < 0.65$; k_2 increases while η increases slightly. The upper limit of this zone corresponds to the maximum viscosity of t-butanol/water mixtures,

c. $0.65 < x_{H_2O} < 0.97$; $k_2 \propto \eta^{-1}$ in accordance with the Stokes-Smoluchowski relation,

d. $0.97 < x_{H_2O} \leq 1.00$; $k_2 \propto \eta^{-0.54}$.

Rate constants in the alcohol rich zones (a) and (b) ($0 \leq x_{H_2O} < x_{\eta_{max}}$) behave in a manner opposite to that predicted by the Stokes-Smoluchowski equation. However, the viscosity changes in these zones are quite small (Fig. 4-3).

The rate constants in the water rich zones (c) and (d) ($x_{\eta_{max}} < x_{H_2O} \leq 1.00$) correlate inversely with η. These zones include a large change in solvent viscosity.

Only zone(c) follows the Stokes-Smoluchowski equation. In this zone the ηk_2 values are constant indicating a constant value throughout the zone for the factor $(\frac{1}{r_e} + \frac{1}{r_S})(R_e + R_S)$. This implies the following in zone (c),

a. either the reaction and diffusion radii increase by the same amount or both decrease by the same amount

b. reaction radii and the diffusion radii remain constant throughout.

The same zone exists in primary alcohol/water mixtures (76). Values of ηk_2 for t-butanol/water ($4.7 \times 10^7 m^3.mPa/mol$) in this zone are consistently higher than those for primary alcohol/water mixtures ($4.0 \times 10^7 m^3.mPa/mol$). This indicates a value 1.2 times greater for the factor $(\frac{1}{r_e} + \frac{1}{r_S})(R_e + R_S)$ in t-butanol/water than in 1-propanol/water mixtures. The larger factor could be due

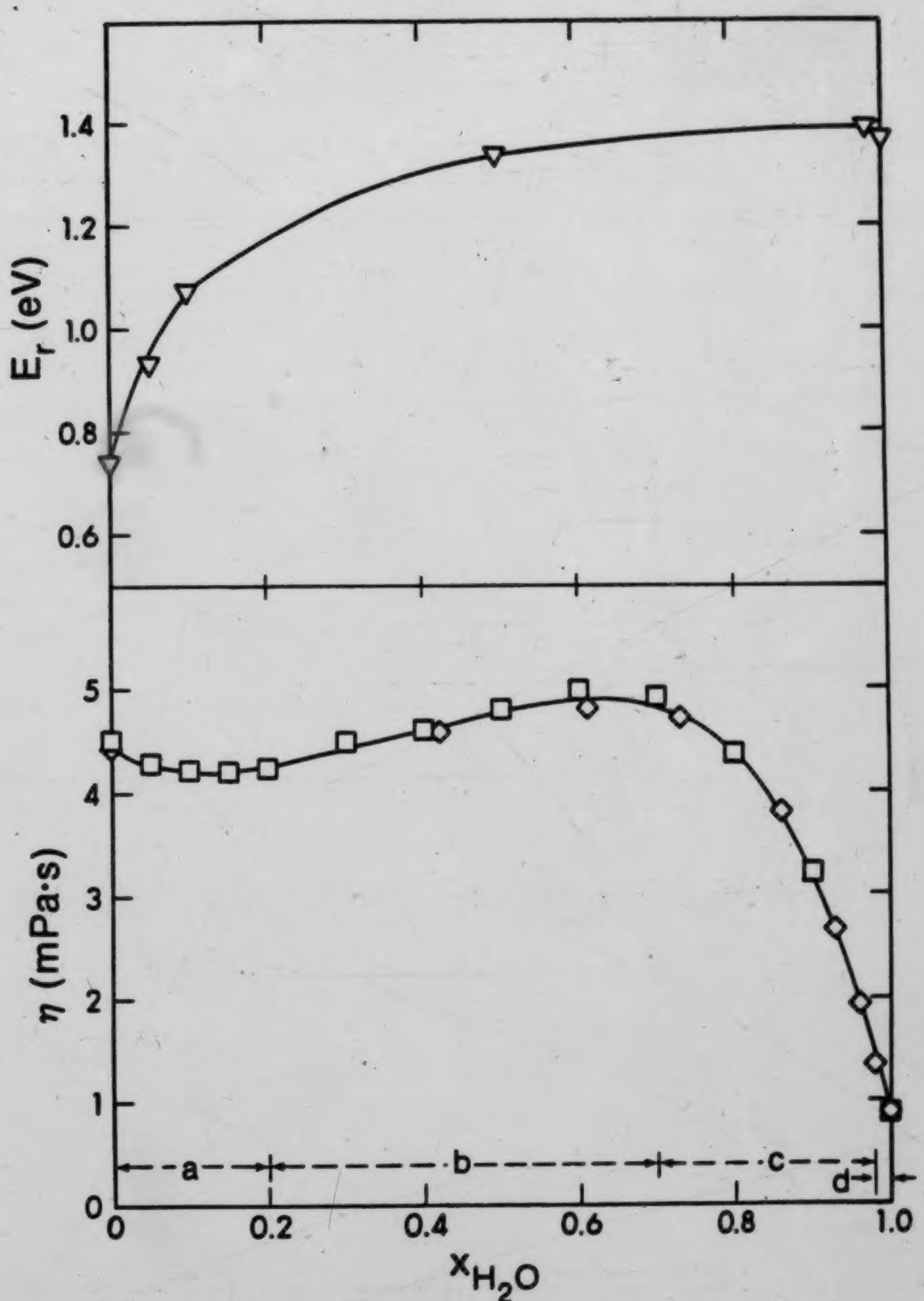

Fig 4-3: Composition dependence of viscosity η and solvation energy of the electron E_r in *t*-butanol/water mixtures. E_r values from ref. 36,37. η values from ref. 138 and 148.

to either an increase in the reaction radius or a decrease in the effective diffusion radii. The difference is probably due to the e_s^- rather than the scavenger. The mean radius of a nitrobenzene molecule is 0.28nm. Assuming $r_e \approx 0.05$ nm for zone (c) (water-rich zone) one obtains effective reaction radii $(R_e + R_S) \approx 0.12$ nm for *t*-butanol/water mixtures and 0.10 nm for 1-propanol/water mixtures. These are smaller than the 0.28 nm physical radius of the nitrobenzene molecule and indicates that the reaction between e_s^- and nitrobenzene does not occur at every diffusive encounter.

Variation of k_2 with η in zone (d) is in the same direction as that predicted by Stokes-Smoluchowski , but has a smaller dependence. Values of ηk_2 in this zone for *t*-butanol/water and 1-propanol/water are approximately the same. The boundary of the zone is approximately 0.97 mol fraction water for both types of alcohol/water mixtures. This composition for *t*-butanol/water is characterized by the maximum structure enhancement of liquid water, which occurs by the hydrophobic *t*-Bu group occupying cavities (154 - 158) in the water lattice.

4.1.1.1(b) Solvent Dielectric Effects

The dielectric properties of the solvent affects the reaction rate constants only if one or more of the participating reactants are ions. The diffusion radius of an ion in a polar solvent depends on the bulk viscosity, the dielectric constant and the dielectric relaxation time of the solvent. The reaction radii depends on the interaction between the ion and the other reactants.

The dipole moment μ of nitrobenzene is 4.2 D (ref.159). The interaction energy between a single charge at a distance of 1 nm from a dipole of the above strength is,

$$|U_{i,d}| = \frac{\mu e}{4\pi\epsilon_0\epsilon r^2} = \frac{2.0}{\epsilon} \times 10^{-18} J \qquad (41)$$

whereas if the dipole is substituted by another single charge it becomes,

$$|U_{i,i}| = \frac{e^2}{4\pi\epsilon_0\epsilon r} = \frac{2.3}{\epsilon} \times 10^{-18} J \qquad (42)$$

The interaction between the electron and the nitrobenzene molecule is comparable to that between the electron and a singly charged ion. Therefore, models that consider the reactivity between two charged reactants also can be applied to the present system.

The modification of Smoluchowski equation by Debye (55) considers the solvent dielectric effect on the reaction radius.

$$k_2 = 4\pi N_A(D_e + D_S)(R_e + R_S)f \qquad (43)$$

where f is a correction factor for the Smoluchowski reaction radius. The factor f is given by,

$$f = \frac{U(R)}{k_B T}\left(\frac{1}{e^{U(R)/k_B T} - 1}\right) \qquad (44)$$

where U(R) is the potential energy between the reactants given by equations (41) and (42). According to this formula the rate constant between two species with an attractive interaction is greater than that if the species are neutral, whereas for a repulsive interaction it is lower.

The rate constant normalized by the correction factor f, k_2/f, (assuming a reaction distance of 0.5 nm) is plotted against η in Fig.(4-4).

The boundaries of zone (d) remain the same whereas those for zone (c) are reduced. Only part of zone (c) ($0.97 > x_{H_2O} > \approx 0.85$) obeys equation (43).

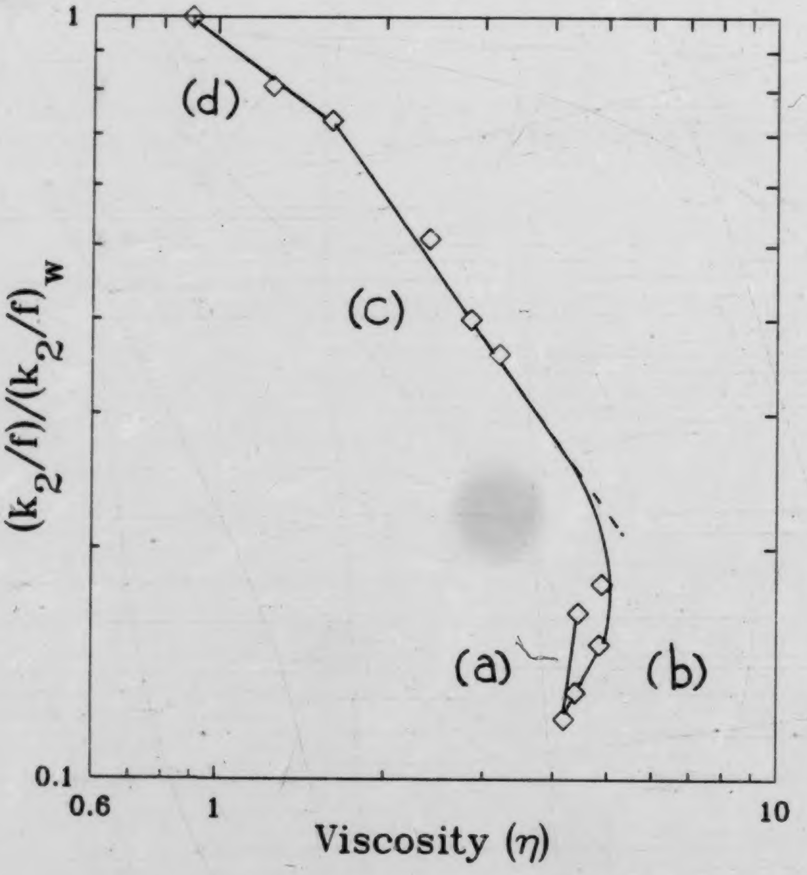

Fig 4-4: Values of k_2 /f for nitrobenzene against viscosity η in *t*-butanol/water.

Since eq.(43) adjusts the reaction radius the constant ηk_2 values in this region indicate that the diffusion radii do not change. But the diffusion radius of an ion (electron) depends on the dielectric properties of the solvent. A constant diffusion radius in this zone is possible only if the electron is solvated in the same environment.

Similar behaviour is observed in the optical absorption energy, E_{Amax}, of the electron. The values of E_{Amax} in this zone are approximately constant and slightly higher than that in water (36,37). Therefore the electron is solvated in a water dominated region throughout this zone.

These results may be interpreted according to the popular clathrate model for alcohol/water micro-structure (108-113). When a small amount of alcohol is added to water, the water molecules order around the alcohol and form oligomers similar to clathrates. With increasing alcohol content micro-phase separation of clathrates and a random mixture of alcohol/water molecules is assumed to occur (109).

Thus the electron in this zone is solvated in the clathrates. Since the compositions in these micro-phases do not change, the environment of the electron remains the same. Hence the trap depth and the diffusion radius of the e_s^- are constant. The affinity of the scavenger molecule to these clathrates is even greater than that of the electron. The clathrate formation of water in the presence of hydrophobic molecules is common to most types of non-electrolytes. Since nitrobenzene has an alkyl group which is hydrophobic, clathrates with this molecule should form. Therefore the reaction rate constants depend only on the viscosity of the solvent since the movement of these micro-phases involves η. If this interpretation is correct it would mean that clathrates exist at much higher alcohol compositions than that for maximum structure stabilization (which for t-BuOH is about 0.97 mole fraction water).

4.1.2 Slow Reactions

The composition dependence of rate constants is greater for the reaction of solvated electron with the scavengers of low electron affinity. Rate constants for phenol and toluene when plotted against viscosity (Fig. 4-5)

display behaviour similar to that for efficient scavengers (Fig. 4-2) only in zones (c) and (d). In these water-rich zones, characterized by large changes of viscosity (Fig. 4-3), k_2 is inversely correlated to η.

The alcohol rich zones (a) and (b) display quite different behaviour from that of efficient scavengers. For the efficient scavengers k_2 decreases slightly in zone (a) and increases slightly in zone (b), whereas for the inefficient scavengers there is a sharp decrease that extends through zones (a) and (b). Viscosity in these two zones changes only slightly. Therefore another effect must be involved.

Low rate constants for inefficient scavengers are due to the low probability of reaction of a (e_s^- + S) encounter pair. When the electron affinity of the scavenger is low, a large solvation energy of the electron decreases the probability that the electron would transfer from the solvent trap to the solute (160, 161). Thus for the inefficient scavengers, the solvation energy of the electron (the depth of the electron potential well or trap depth) is more important than the diffusion.

The electron trap depth in the solvent is related to the optical absorption energy (162). The absorption band is very broad, probably due to a distribution of trap depths. There is no universal agreement as to the cause (42, 163-165) of the broadening. However evidence from the photoionization spectrum suggests that the absorption band includes the bound to bound transitions as well as bound to continuum transitions (20-23).

Whatever the cause, the electrons that have the lowest excitation energies have the greatest reactivity with inefficient scavengers (164). For kinetic

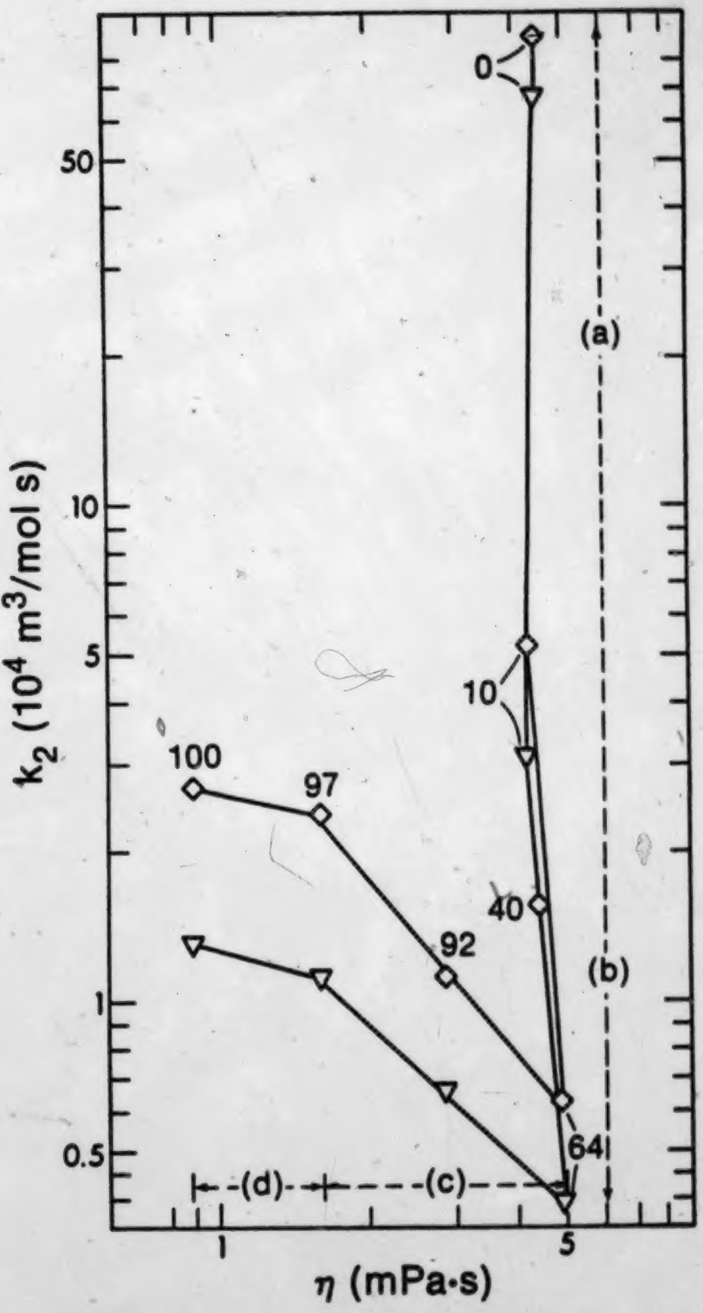

Fig 4-5: Values of k_2 against η for inefficient scavengers in *t*-butanol/water mixtures. Solute:◇, phenol;▽, toluene.

purposes E_r has been chosen as an indicator of reactive shallower trap depths (160) :

$$E_r = E_{Amax} - W_r \quad (45)$$

where E_{Amax} is the energy at maximum absorption and W_r is the width of the band on the low energy side at half-height.

The threshold energy for photoionization E_{th} is related to the shallower trap depths of the solvated electrons. In alcohols E_{th} is slightly greater than the threshold energy for optical absorption and lower than E_r (20, 26, 43). Thus E_r is representative of the depth of the shallower electron traps.

Zones (a) and (b) correspond to a large change in E_r (Fig. 4-3). As E_r increases k_2 decreases. The effect is magnified for inefficient scavengers since trap depth is more important for those. In zones (c) and (d) the change of E_r is very small, but the change in η is large, and k_2 correlates with η.

The rate of reaction for inefficient scavengers is controlled both by the diffusion rate and other factors such as the solvated electron trap depth. Dividing k_2 by the nearly diffusion controlled rate constant k_N of nitrobenzene displays the effects due to other factors. The ratio k_2/k_N is approximately equal to the encounter efficiency of the reaction, taking that with nitrobenzene to be approximately unity. The calculated sum of reaction radii in the previous section was approximately 1/3 of the sum of the physical radii. Thus for nitrobenzene the encounter efficiency is probably $\approx$ 0.3.

The encounter efficiency k_2/k_N is plotted against E_r in Fig.(4-6).

For both phenol and toluene,

$$log(\frac{k_2}{k_N}) \propto \frac{1}{E_r} \quad (46).$$

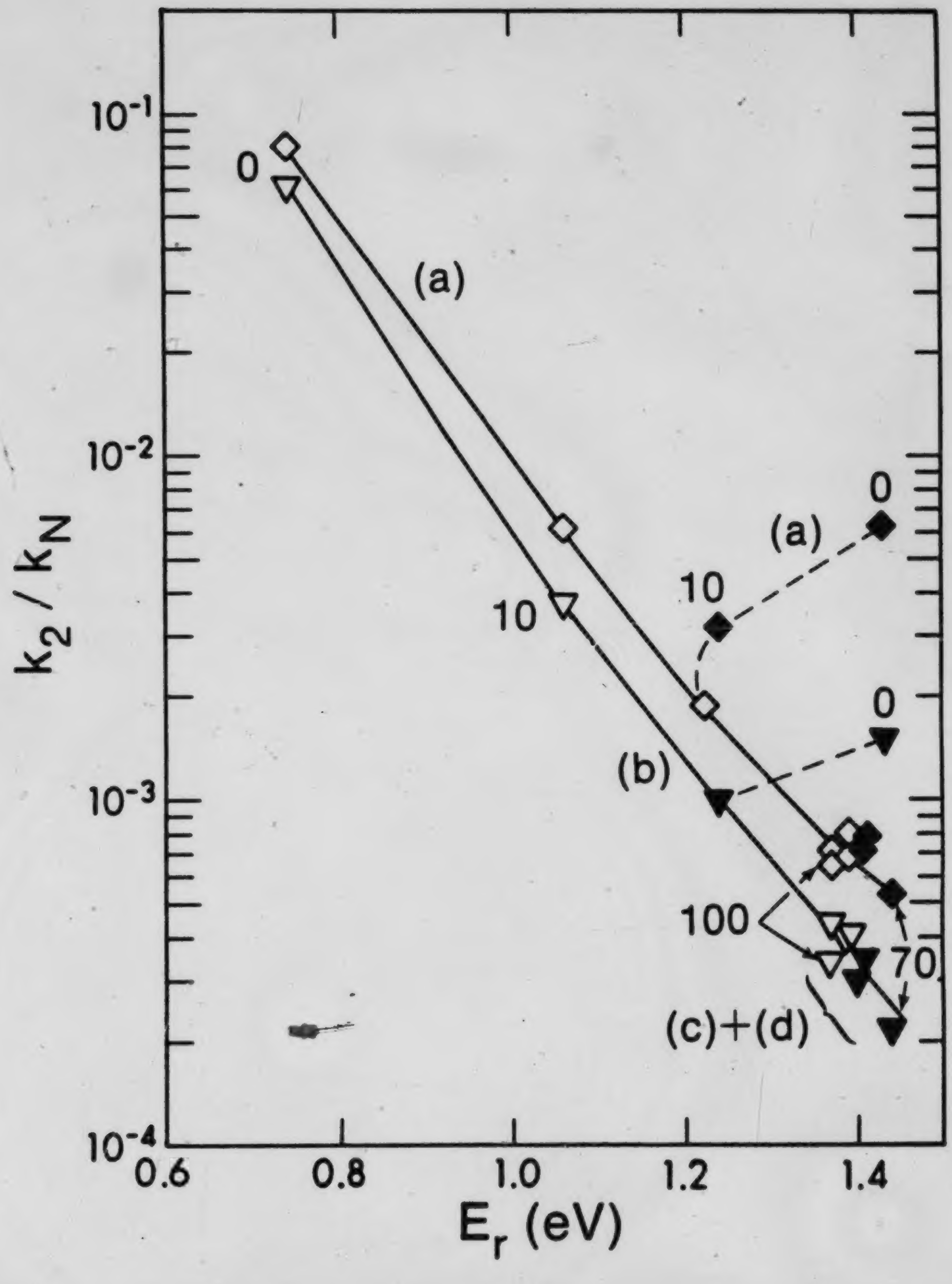

Fig 4-6: Encounter efficiency for inefficient scavengers against solvated electron trap depth in *t*-butanol/water mixtures. Solute: ◇,phenol; ▽,toluene. Solvent:◇▽,*t*-BuOH ,◆▼,i-PrOH.

Therefore rate constants for inefficient scavengers decrease due to the increase of electron trap depths. Values for 1-propanol/water mixtures also agree with the above correlation except in zone (a).

In the primary alcohol/water mixtures a mol fraction of 0.10 of water indicate a minimum in the optical absorption energy of the solvated electron (167). The minimum was explained in terms of a water nucleated hydrogen bonded structure, with the central water molecule bonded to about eight alcohol molecules. This makes the protons of the -OH's less available to the electron. Therefore E_r decreases. These protons are also needed to protonate the S^- of the following two reactions :

$$e_s^- + S \rightleftharpoons S^- \tag{47}$$

$$S^- + ROH \longrightarrow SH + RO_s^- \tag{48}$$

The hydrogen bonded structure makes the protons of the -OH's less accessible to the S^-, thus slowing down reaction (48). Therefore in zone (a) the encounter efficiency of inefficient scavengers for primary alcohol/water mixtures decreases even though the trap depth of the solvated electron decreases.

Deviations from Stokes-Smoluchowski behaviour are displayed for all four scavengers in Fig.(4-7)

by plotting ηk_2 against the mol fraction of water. For all four scavengers ηk_2 decreases in zone (a). It is more intense for the inefficient scavengers due to trap depth dependence. This decrease continues up to $x_{\eta_{max}}$ for the inefficient scavengers, while for efficient scavengers it increases slightly. The value of ηk_2 in zone (c) does not change significantly except in the case of acetone, for which the experimental scatter is greater because of concentration measurement problems. Zone (d) displays a decrease in ηk_2 for all scavengers.

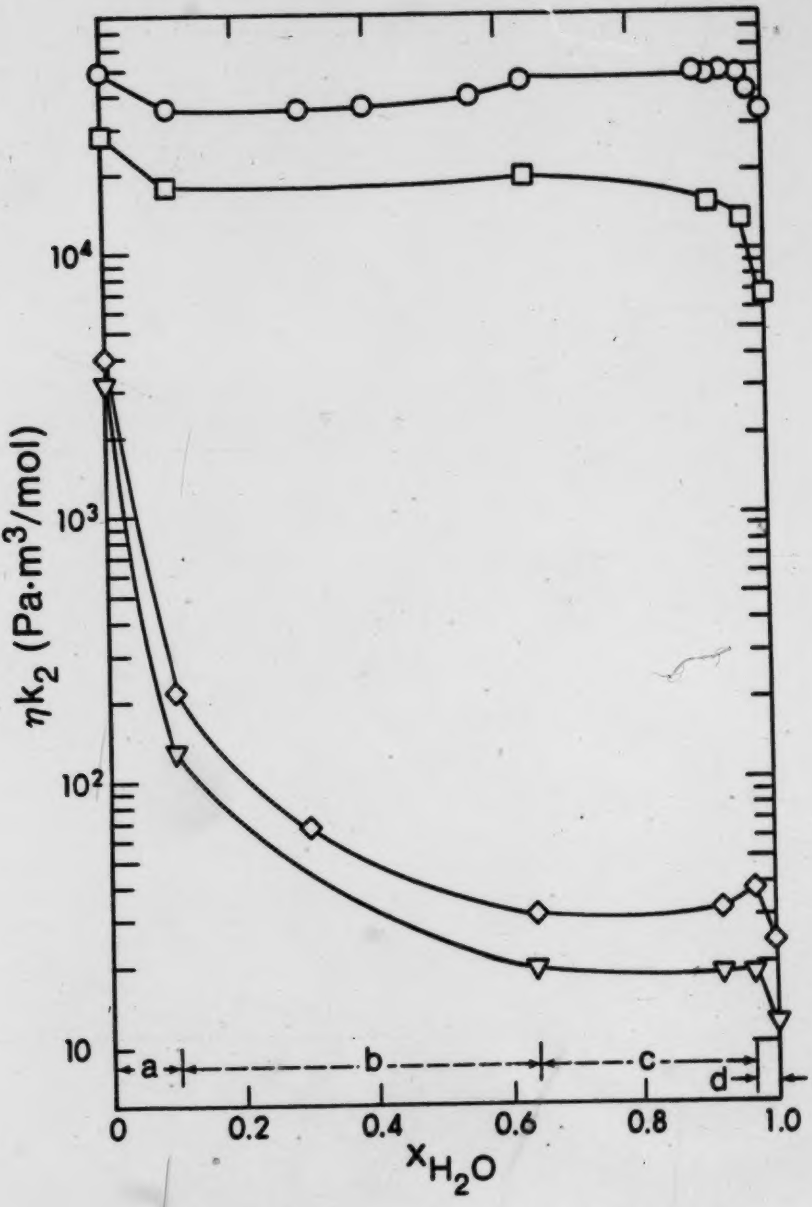

Fig 4-7: The composition dependence of ηk_2 in *t*-butanol/water mixtures. Symbols as same as Fig.(4-1).

Rate constants for all scavengers in the alcohol-rich zones are inversely correlated to η. The similarity between the viscosity dependence of the two types of scavengers arises because in this zone the optical absorption energy does not change significantly. Thus the inefficient scavengers in these zones reflect changes in diffusion. Therefore the increase in ηk_2 when a small amount of alcohol is added to water is probably due to changes in diffusion and reaction radii.

As explained in the previous section, in zone (c) the scavenger and the electron are probably solvated in clathrates. Since clathrates involve water molecules ordered around the non-electrolyte molecules (in the present case alcohol), the microscopic dielectric constant near the electron and the scavenger is lower than in bulk water. The lower dielectric constant leads to a greater potential interaction between the reactant pair which in turn gives a higher rate constant. In zone (d) the electron gets solvated in pure water medium and clathrates until the water structure maximally stabilizes. The local dielectric constant for the encounter pair is lower than in water and the reaction radii higher; the ηk_2 value increases.

4.1.3 Changes for all Alcohols

The alkyl group attached to the -OH in tertiary alcohol is bulkier than in the other three types of alcohols. It is more difficult to orient the molecule around the electron site because a greater disruption of liquid structure is needed. Therefore for the three types of alcohols, the solvation energy of the electron is the lowest in tertiary alcohols. As the mol fraction of water in alcohol increases, the solvation energies in the mixed solvents become more equal. Thus the range of solvation energies in tertiary alcohol/water mixtures is greatest, and the change of k_2 in the alcohol rich zones (a) and (b) is largest for t-BuOH/water mixtures.

On the water rich side, the change of k_2 values is largest for *t*-BuOH because the viscosity change is the greatest. In addition k_2 values are slightly higher in *t*-BuOH , probably due to a larger reaction radius.

4.1.4 Temperature Effects

4.1.4.1 Energies of Activation

Activation energies E_2 of the reaction between e_s^- and scavengers decrease sharply in zone (a) with increasing water content, stay constant in zone (b), then decrease gradually in zones (c) and (d) (Fig. 4-8).

The activation energy for viscous flow E_η displays the same zone behaviour. There is a correlation between E_2 and E_η .

The movement of an ion through a polar medium involves dielectric relaxation (in addition to viscosity) because dipole rotation must occur simultaneously with charge migration. It would be of interest to compare the E_2 values with that for dielectric relaxation E_τ , when the values are available.

Activation energies for the e_s^- reaction with different scavengers (Fig. 4-8) display a slight shift against each other in zones (b) (c) and (d). They are in the order toluene > nitrobenzene > phenol > acetone. The solubility of scavengers in water is in the order acetone $\geq$ phenol > nitrobenzene > toluene. Less soluble scavengers have higher activation energies. This indicates a tendency for the electron to be preferentially solvated by water and the organic solute to be preferentially solvated by the alcohol, creating a small energy barrier for the close approach of the reactants.

4.1.4.2 Entropy Effects

The entropy of activation $\Delta S_2^{\neq}$ also displays zone behaviour similar to E_2 and E_η (Fig. 4-9).

Entropies of activation are negative for less efficient scavengers. The $\Delta S_2^{\neq}$ values for the reaction between e_s^- and inefficient scavengers are about 45 J.mol/K more negative than that for nitrobenzene. The energies of activation

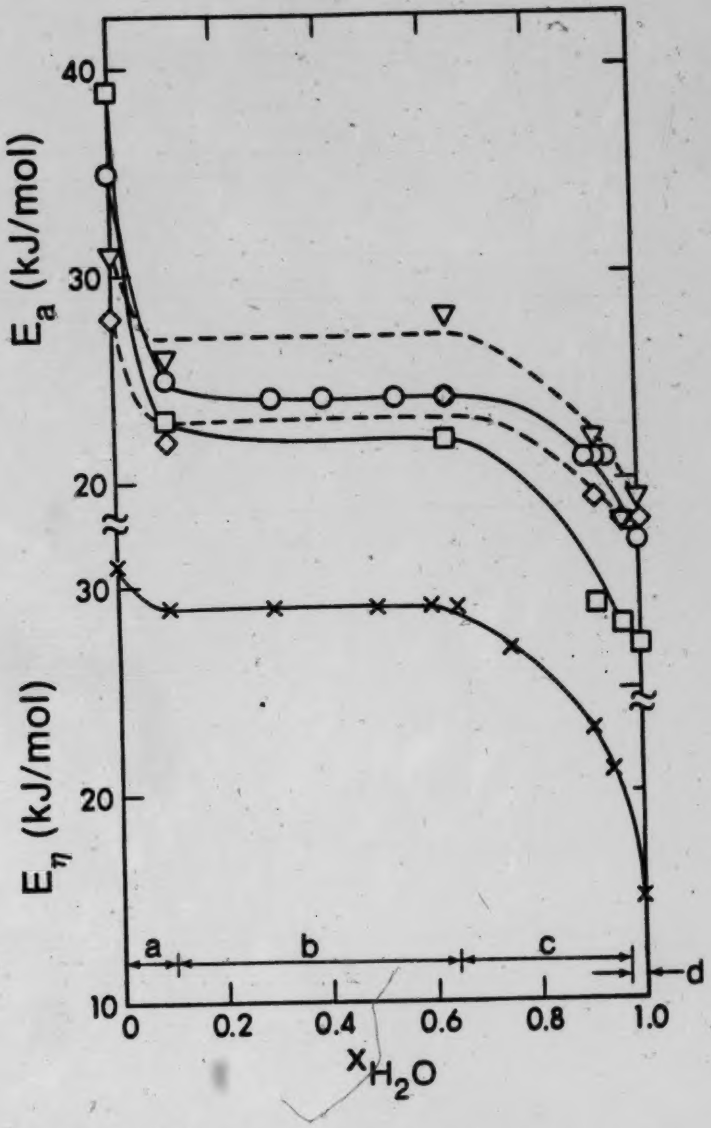

Fig 4-8: The composition dependence of activation energies in *t*-butanol/water

Solute:○,nitrobenzene ;□,acetone ;◇,phenol ;▽,toluene

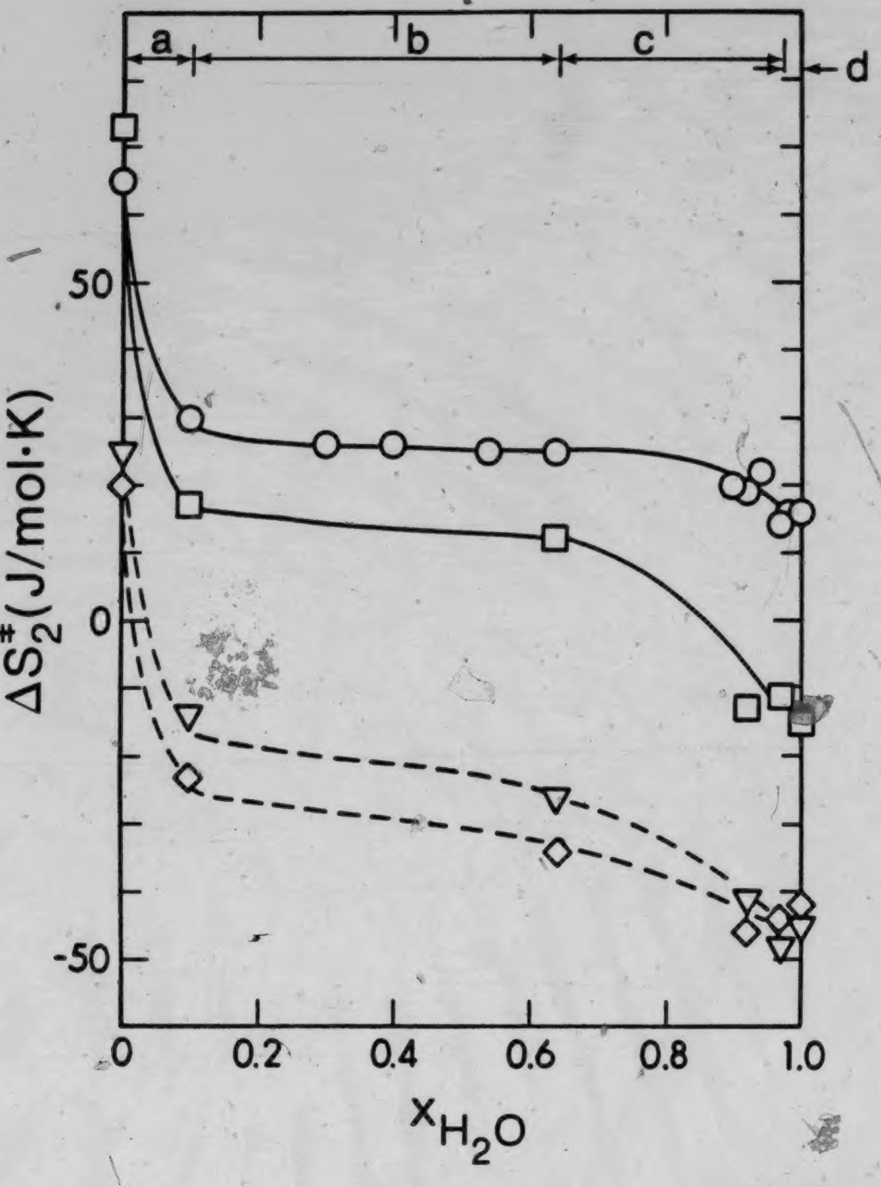

Fig 4-9: The composition dependence of activation entropies in *t*-butanol/water mixt ures. Solute:○nitrobenzene :□,acetone ;◇,phenol ;▽,toluene

for the reactions of inefficient scavengers are within ± 2 kJ/mol of that of nitrobenzene. Therefore, differences of reactivity between efficient and inefficient scavengers are due to changes of entropy rather than of energy. When the electron affinity of the scavenger is low, electron capture depends on a favourable dipole arrangement about the scavenger molecule. A more negative entropy indicates a lower probability of this occurrence.

4.1.4.3 Curved Arrhenius Behaviour

The rate constant for the reaction between e_s^- and toluene in pure *t*-BuOH increases with increasing temperature until 318K and then decreases (Fig. 3-38). Below this temperature the average E_2 = 24 kJ/mol and $\Delta S_2^{\neq}$ = 5 J/mol.K. whereas above it they are -20 kJ/mol and, -135 J/mol.K respectively. A similar change of the rate constant with the temperature was seen for the reaction,

$$2e_S^- \longrightarrow H_2 + 2OH^-$$

in water (161).

The reaction between e_s^- and toluene is a two step process:

$$e_S^- + CH_3C_6H_5 \rightleftharpoons CH_3C_6H_{5,s}^- \tag{49}$$

$$ROH + CH_3C_6H_{5,s}^- \longrightarrow RO_s^- + CH_3C_6H_6 \tag{50}$$

Reaction (50) is probably first order; one of the ROH's in the solvent shell of $CH_3C_6H_{5,s}^-$ protonates the anion. The net rate of decay of the solvated electron is:

$$\frac{-d[e_S^-]}{dt} = k_{obs}[e_S^-][CH_3C_6H_5]$$

where

$$k_{obs} = \frac{k_{49}k_{50}}{(k_{-49} + k_{50})}$$

The reversal of direction of change in the rate constant with increasing temperature can be explained as follows. At lower temperatures,

$$k_{50} \gg k_{-49};\ k_{obs} = k_{49}$$

At higher temperatures,

$$k_{50} \ll k_{-49};\ k_{obs} = \frac{k_{49}k_{50}}{k_{49}}$$

The energy of activation at lower temperatures is,

$$E_{49} = 24kJ/mol$$

and at higher temperatures it is,

$$E_{49} + E_{50} - E_{-49} = -20kJ/mol.$$

Therefore

$$E_{-49} - E_{50} = 44kJ/mol$$

Taking $E_{50} \approx 20kJ/mol$ gives $E_{-49} = 64kJ/mol$, which is quite high. The difference of the entropies of activation,

$$\Delta S^{\neq}_{49} - \Delta S^{\neq}_{50} = 140J/mol.K.$$

If $\Delta S^{\neq}_{49} \approx \Delta S^{\neq}_{-49}$ then $\Delta S^{\neq}_{50} \approx -145J/mol.K.$

Toluene is different from the other scavengers in that it does not hydrogen bond with the solvent. Toluene also has a low electron affinity. The capture of e_s^- by such a scavenger depends upon the occurrence of a favourable configuration of solvent dipoles about the reaction site, so that O-H dipoles are oriented more towards the toluene molecule and less towards the e_s^- site. A favourable reaction configuration increases the solvation energy of the scavenger anion and decreases that of the electron. The same applies for the protonation step.

The net reaction depends on the relative solvation energies of e_s^- , $CH_3C_6H_{5s}^-$ and RO_s^-. The reverse of reaction (49) has $E_{-49} \approx 64kJ/mol$. This large energy is needed to loosen the solvent structure around $CH_3C_6H_{5s}^-$ anion to accomodate the e_s^- when reaction (-49) proceeds. At lower temperatures reaction (50) is sufficiently fast relative to (-49) so that reaction (49) becomes rate determining.

As the temperature is increased there is more thermal agitation in the liquid. This makes it more difficult to have favourable dipole arrangements, which is important to reaction (50). Therefore reaction (-49) becomes more important relative to (50), leading to the second limiting case.

4.2 Solvent Isomer Effects in Butanol/Water Mixtures

The solvent effects in water mixtures of butanol isomers are compared among each other in this section to provide more insight into the study of alcohol/water mixtures as solvents and the effects of these on the reactivity of the e_s^- .

4.2.1 Composition Effects

The rate constants for electron capture by inefficient scavengers in the water mixtures of butanol isomers display greater dependence on solvent composition than do those of efficient scavengers (Fig. 4-10).

4.2.1.1 Efficient Scavengers

The values of k_2 are nearly diffusion controlled and the solvent isomer effects are displayed in four composition zones:

(a) $0 < x_{H_2O} < 0.1$, the k_2 values are in the order : *t*-BuOH > 2-BuOH ≈ 1-BuOH > *i*-BuOH .

(b) $0.1 < x_{H_2O} < x_{a,im}$, the k_2 values are in the order 1-BuOH > 2-BuOH > *i*-BuOH > *t*-BuOH where $x_{a,im}$ is the composition of water at the limit of immiscibility on the alcohol-rich side.

(c) $x_{\eta_{max}} < x_{H_2O} < 0.97$ for *t*-BuOH , for other alcohols this is the immiscible region.

(d) $x_{w,im} < x_{H_2O} < 1.00$, where $x_{w,im}$ is the composition of water at the limit of immiscibility on the water-rich side; the k_2 values are similar.

These differences may arise due to changes in the transport and dielectric properties. Suitably normalized k_2 values should be the same for all isomers of the solvent.

5

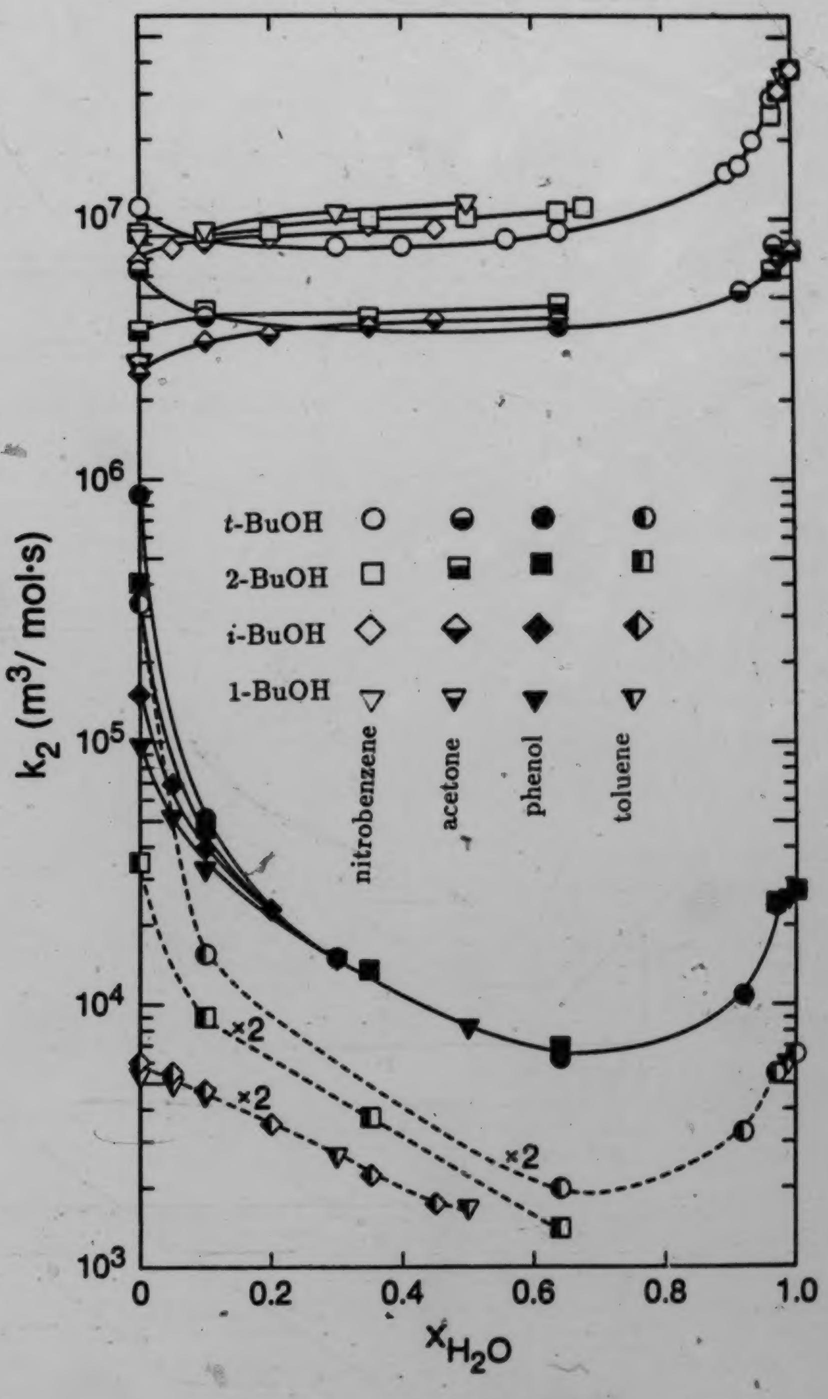

Fig 4-10: Composition dependence of rate constants

4.2.1.1(a) Stokes-Smoluchowski Model

Rate constants k_2 of nearly diffusion controlled reactions between species x and y are compared with solvent viscosity η by inserting the Stokes-Einstein (64) for diffusion coefficients D (eq. 37) into the Smoluchowski (54) relation (eq. 36).

According to the Stokes-Smoluchowski model (54, 64), the isomer effects at a fixed composition may arise due to differences in viscosity η, diffusion radii r, or reaction radii R. In zone (b) the k_2 values in different butanols at a given water content are in the inverse order of viscosities. The ηk_2 values in 1-BuOH , *i*-BuOH and 2-BuOH at a certain composition in zone (b) are the same (Fig. 4-11).

This indicates that at a fixed composition diffusion radii and reaction radii in water mixtures of 1-BuOH , *i*-BuOH and 2-BuOH are the same.

However ηk_2 values in *t*-butanol/water mixtures are different from those of the other alcohol/water mixtures. The above model is sufficient to explain the isomer effects of primary and secondary butanol/water mixtures, but is not adequate to explain the difference in *t*-BuOH /water.

4.2.1.1(b) Debye Model

The Debye modification (55) of the Smoluchowski relation considers the change of the reaction radius due to potential differences between the reactants (eq. 42-44). As seen in section 4.1 this relation is applicable to reactions between an ion and a highly polar molecule. Both scavengers nitrobenzene and acetone are molecules of high dipole moment. Assuming $R = 0.5$nm, the correction factor f for the reaction radius in eq.43 is calculated and the rate constants corrected for this effect and, solvent viscosity are plotted in Fig.(4-12).

These look similar to the plots of ηk_2 in Fig.(4-11); the *t*-BuOH curve remains higher than others.

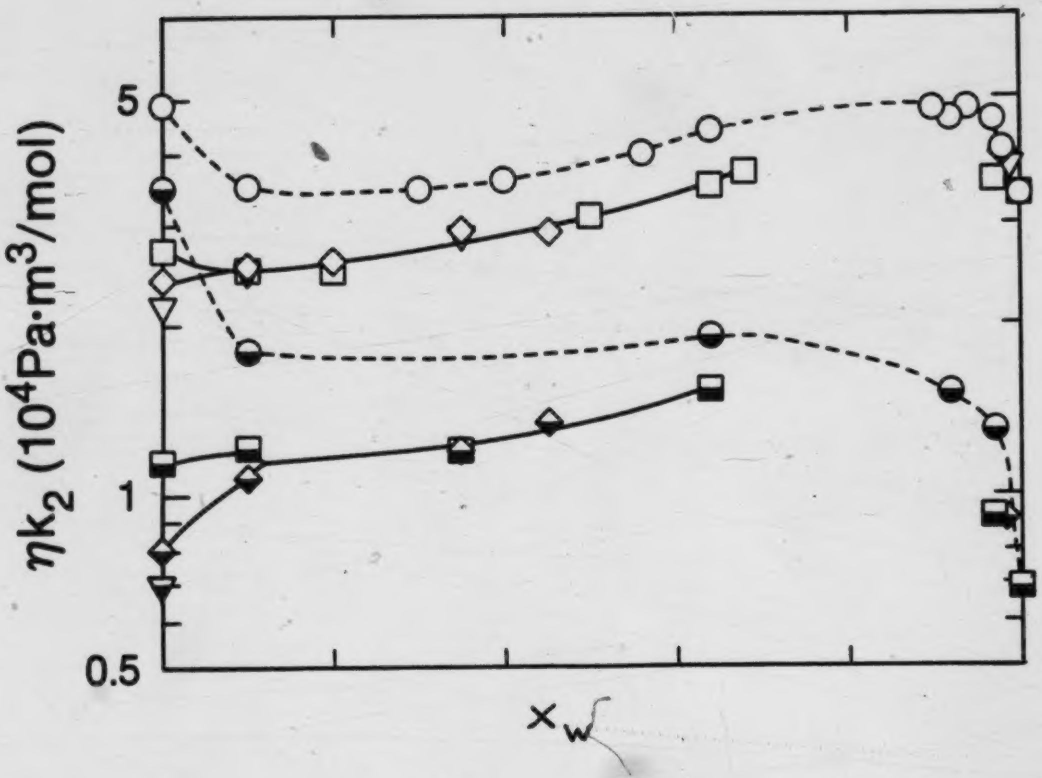

Fig 4-11: Composition dependence of viscosity normalized rate constants

	t-BuOH	2-BuOH	*i*-BuOH	1-BuOH
nitrobenzene	○	□	◇	▽
acetone	◒	⬓	⬙	▼

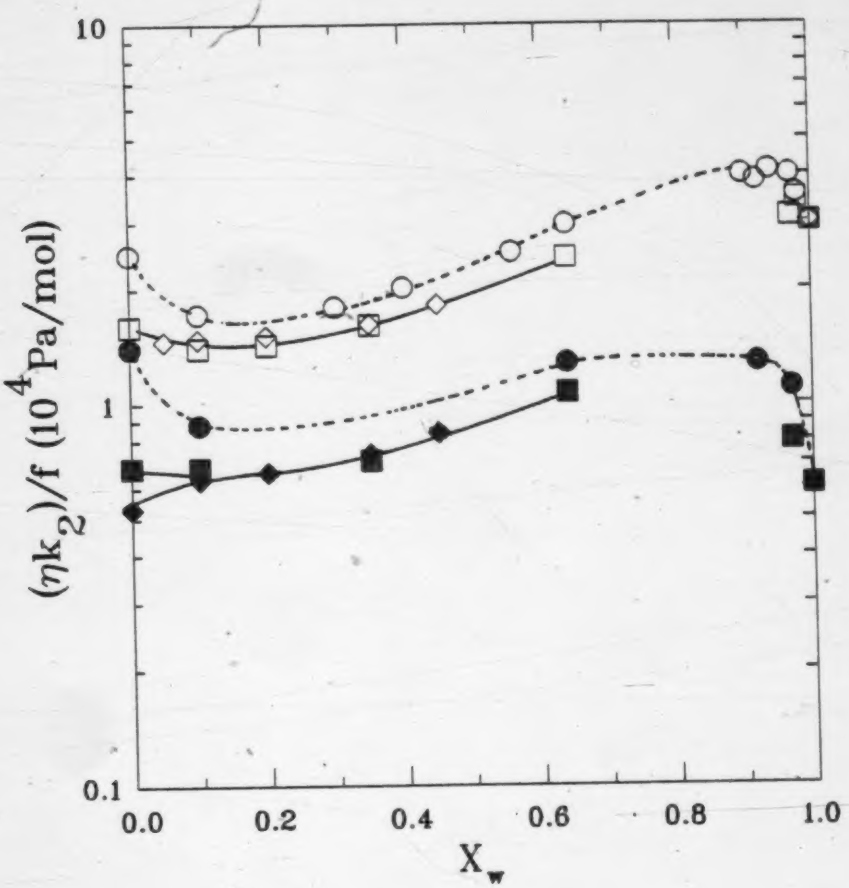

Fig 4-12: Values of $(\overline{k_2}/f)$ normalized with η

(values of ϵ from ref. 168, 169).

	t-BuOH	2-BuOH	*i*-BuOH	1-BuOH
nitrobenzene	○	□	◇	
acetone	●	■	◆	

Both Smoluchowski and Debye models consider the viscosity of the bulk solvent . This probably is different from the microscopic viscosity felt by the diffusing reactants. The microscopic viscosity around a charged species depends on the bulk viscosity, the dielectric constant and the dielectric relaxation of the solvent molecules. In the Smoluchowski and Debye formulations these effects are absorbed in the effective diffusion radius of the reactants.

There are many theories used to calculate the effective diffusion radius of a diffusing species, and the Hubbard-Onsager theory (71) which calculates it as a function of solvent viscosity, dielectric constant and dielectric relaxation time gives the best agreement with experimental results in alcohol/water mixtures (72). The Hubbard-Onsager diffusion radius of a univalent ion in ethanol/water mixtures decreases 3 fold on going from pure alcohol to pure water. A decrease of the diffusion radius corresponds to an increase in the $\eta k_2/f$ values as seen for butanol/water mixtures (Fig 4-11 and 4-12).

The values of $\eta k_2/f$ in alcohol/water mixtures decrease in zone (a), increase in zones (b), (c) and slightly decrease in zone (d). The increase in the above normalized rate constants corresponds to a decrease in the diffusion radii (changes in zone (a) will be explained later) but the extent of change is slightly less than that predicted by the Hubbard-Onsager theory. Therefore the dependence of the reactivity on the dielectric constant is slightly greater than that given by the Debye relation.

The differences among the normalized k_2 values in different butanols at a fixed composition indicate that values of *t*-BuOH are consistently higher. Tertiary butanols are different from the other alcohols in that the dielectric constant is lower than that in the other alcohols (in which it is approximately equal). Therefore the larger values in *t*-butanol/water implicate that the isomer effects arise mainly due to the effect of dielectric constant on the diffusion radius.

The viscosity and dielectric constant normalized rate constants in butanols are the same for all isomeric butanol/water mixtures at a given composition (Fig. 4-13).

This formulation considers the total effect of dielectric constant on the diffusion radii and reaction radii to be proportional to ϵ while that in Debye is is proportional to ϵ^x where x < 1, and in Smoluchowski it is independent of ϵ.

4.2.1.1(c) Trap-depth Model

Neither the Smoluchowski nor the Debye model for nearly diffusion controlled reactions explains the diffrences of rate constants in zone (a).

The values of $\epsilon\eta k_2$ are greatest in tertiary and lowest in primary alcohols. The differences among these increase as the efficiency of the scavenger decreases. The rate constants for the inefficient scavengers depend on the solvation energy of the electron (section 4-1).

The present values of $\epsilon\eta k_2$ in all butanols are inversely related to E_r (Fig. 4-14).

There is greater dependency for scavengers that have lower efficiency of electron capture. It is concluded that for a completely diffusion controlled reaction k_2 would be independent of E_r .

4.2.1.2 Inefficient Scavengers

The reactivity of the solvated electron in the same alcohol is related to the efficiency of the scavenger (Fig. 4-15).

As the efficiency decreases the differences among the rate constants in different alcohols increase. Thus effects other than diffusion are involved in the reactivities of inefficient scavengers.

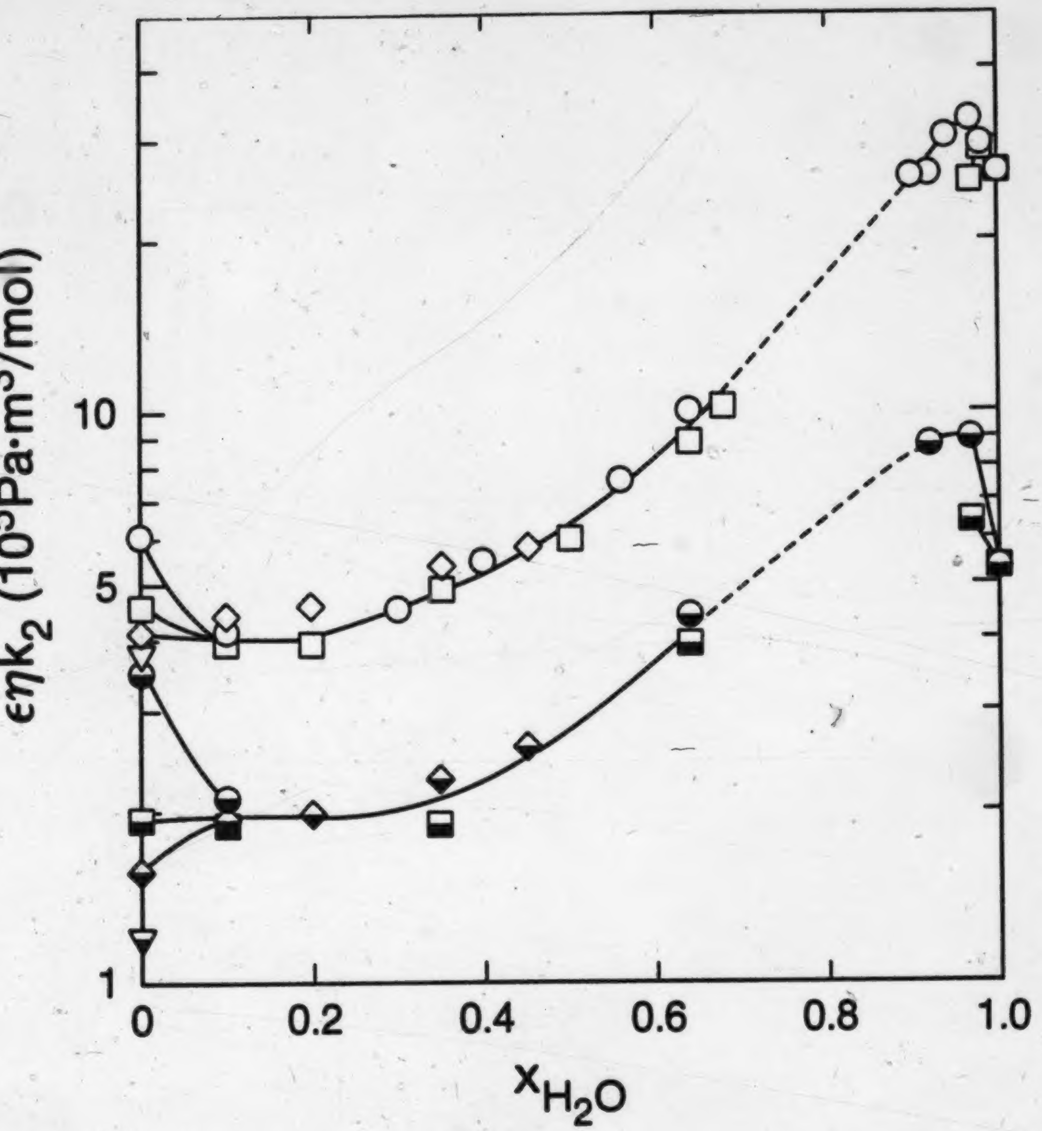

Fig 4-13: Composition dependence of $\epsilon\eta k_2$

	t-BuOH	2-BuOH	*i*-BuOH	1-BuOH
nitrobenzene	○	□	◇	▽
acetone	◒	⬓	⬙	▼

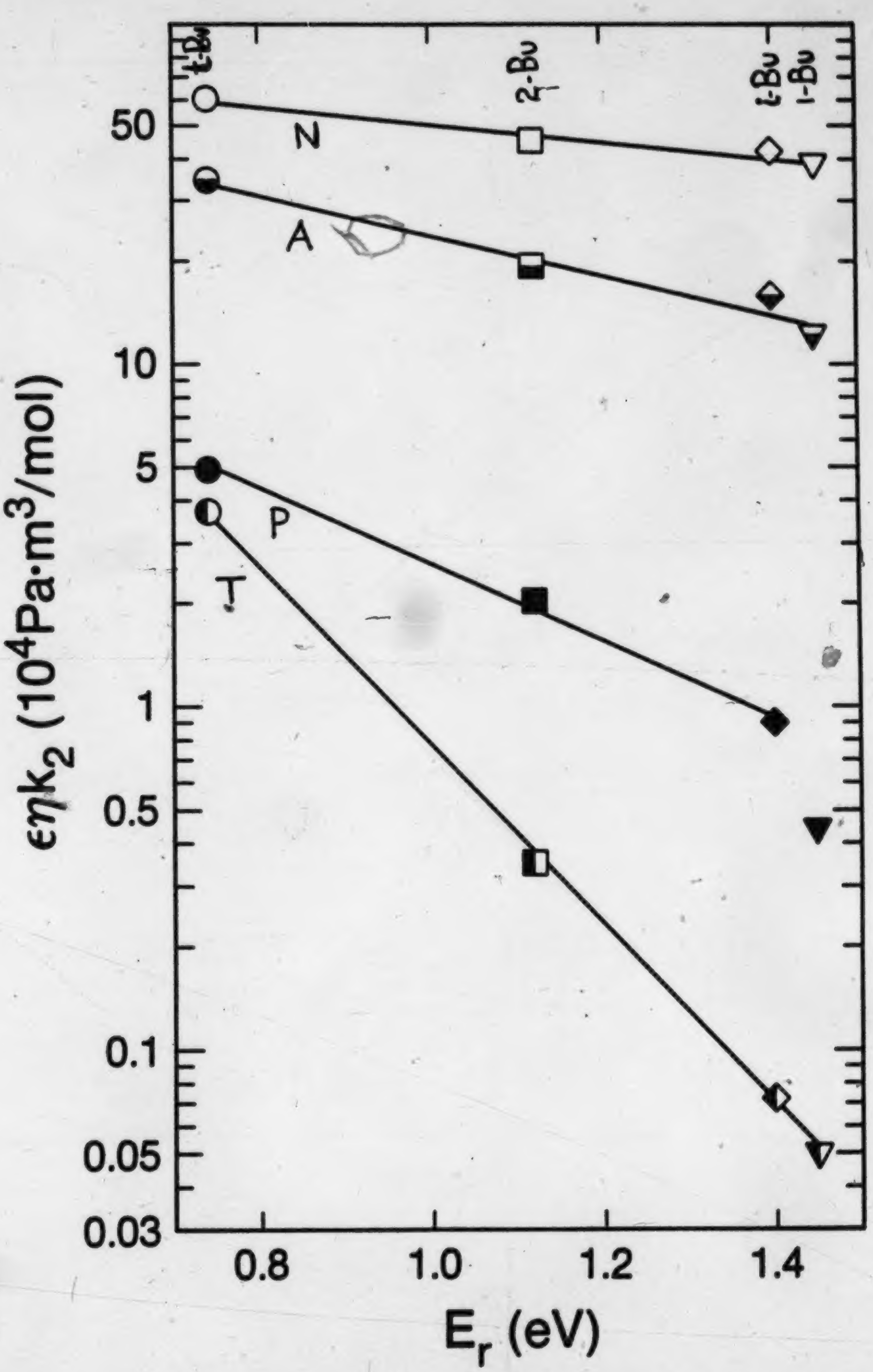

Fig 4-14: $\epsilon\eta k_2$ **against the optical absorption energy of** e_s^-.

○◒●◐t-BuOH, □⬓■◧2-BuOH, ◇⬖◆◇i-BuOH, ▽▽▼▼1-BuOH.

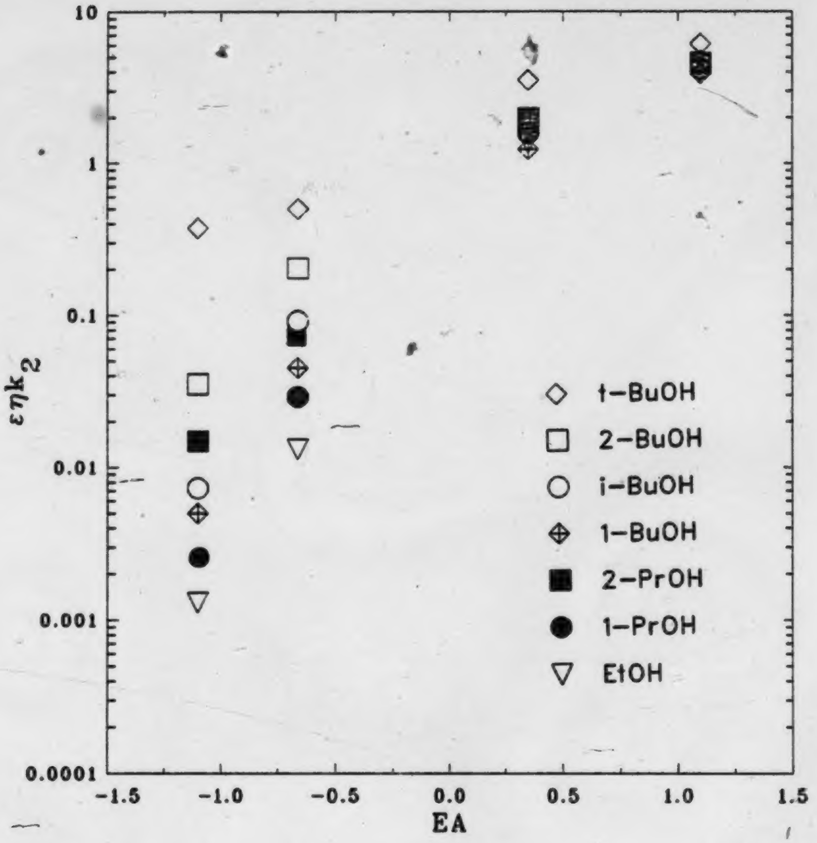

Fig 4-15: Dependence of e_s^- reactivities in alcohol/Water mixtures with electron affnity (from ref. 170, 171).

The reactants in an electron scavenging reaction first approach each other by diffusion according to the process (51),

$$e_S^- + S \rightleftharpoons [e_S^-, S] \tag{51}$$

and then react together according to reaction (52),

$$[e_S^-, S] \longrightarrow products \tag{52}$$

The observed rate constant k_2 for electron capture is,

$$k_2 = \frac{k_{51} k_{52}}{k_{-51} + k_{13}} \tag{53}$$

The rate constant for nitrobenzene, k_N , is nearly diffusion controlled, so in this case $k_{52} \gg k_{-51}$ and $k_N \approx k_{51}$. The rate constant for an inefficient scavenger is strongly affected by factors which affect step (52). Examination of the ratio k_2/k_N uncovers effects due to factors other than diffusion.

4.2.1.2(a) Pure Alcohols

In pure butanols $\log(k_2/k_N)$ is inversely proportional to E_r (Fig. 4-16). Equation (53) can be rewritten as;

$$\frac{1}{k_2} = \frac{1}{k_{51}} + \frac{k_{-51}}{k_{51} k_{52}} \tag{54}$$

Since $k_{51} \approx k_N$,

$$\frac{k_N}{k_2} = 1 + \frac{k_{-51}}{k_{52}} \tag{55}$$

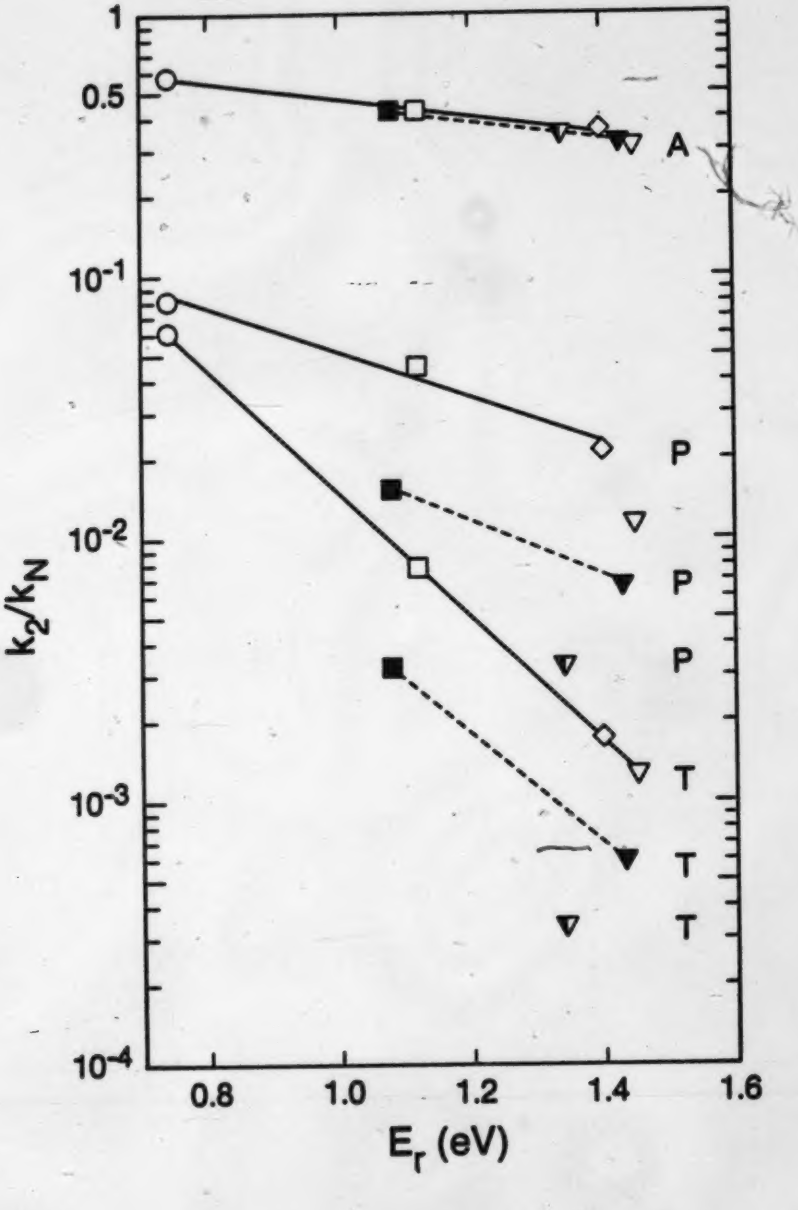

Fig 4-16: Values of (k_2/k_N) against optical absorption energy

○ *t*-BuOH □ 2-BuOH ◇ *i*-BuOH ▽ 1-BuOH

▼ EtOH ■ 1-PrOH ▼ 2-PrOH

For the inefficient scavengers $k_{-51} \gg k_{52}$, thus

$$\frac{k_N}{k_2} \approx \frac{k_{-51}}{k_{52}} \tag{56}$$

According to the transition state theory

$$k \approx \frac{k_B T}{h} exp(-\frac{\Delta G^{\neq}_{52}}{RT}) \tag{57}$$

and,

$$ln(\frac{k_N}{k_2}) \approx (\frac{\Delta G^{\neq}_{52} - \Delta G^{\neq}_{51}}{RT}) \tag{58}$$

where $\Delta G^{\neq}$ is the free energy of activation of the reaction. When $k_{-51} \gg k_{52}$, $\Delta G^{\neq}_{-51} \ll \Delta G^{\neq}_{52}$ and,

$$ln(\frac{k_N}{k_2}) \approx \Delta G^{\neq}_{52}/RT \tag{59}$$

Hence the free energy of activation of reaction (52), $\Delta G^{\neq}_{52}$ increases with the trap depth of the solvated electron .

The sensitivity of $\Delta G^{\neq}_{52}$ to trap depth, $\Delta G^{\neq}_{52}\ /E_r$, is a function of the dipole moment μ of the present scavengers (Fig. 4-17).

$$\frac{\Delta G^{\neq}_{52}}{E_r} \propto \frac{1}{f(\mu)} \tag{60}$$

For these scavengers the electron affinity appears to correlate with the dipole moment (Fig. 4-18).

When the scavenger is less efficient, as phenol or toluene, log (k_2/k_N) values in butanols are consistently higher than those in propanols ($\Delta G^{\neq}_{52}$ values are consistently lower; Fig. 4-16) , and the ratio in propanols is greater than that in ethanol at the same trap depth. Thus the differences in $\Delta G^{\neq}_{52}$ values at a constant trap depth depend on the number of carbon atoms in the alcohol; there is no isomer effect and the larger alkyl group facilitates the reaction (Fig 4-19).

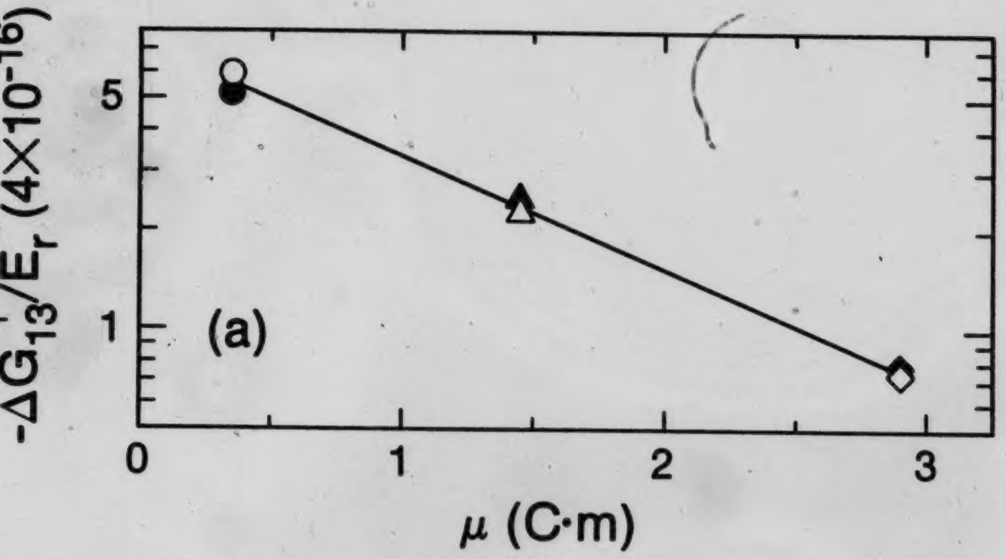

Fig. 4-17: Change of the dependence of $\Delta G_{52}^{\neq}$ for the reaction of e_s^- with inefficient scavengers, on the solvated electron optical absorption energy E_r , $\frac{\Delta G_{52}^{\neq}}{E_r}$, with the dipole moment of the scavenger μ. Scavengers: ◇,acetone; △,phenol; ○,toluene. Solutes:○◇△,butanol;●◆▲,propanol.

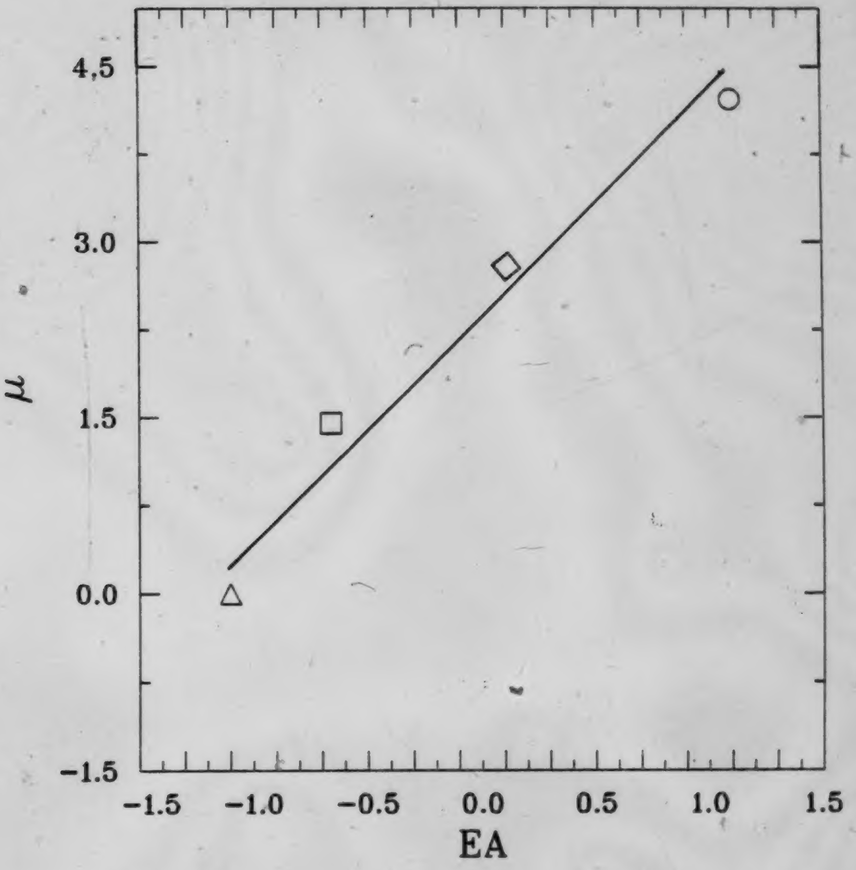

Fig. 4-18: Relationship between the electron affinity, EA, and the dipole moment, μ, of the present scavengers. Values of electron affinities are from ref.(170,) and the dipole moments from ref.(134). Solute: ○,nitrobenzene; ◇,acetone; □,phenol; 171)

△, benzene (electron affinity of toluene is unavailable),(the electron affinity of acetophenone was used instead of acetone).

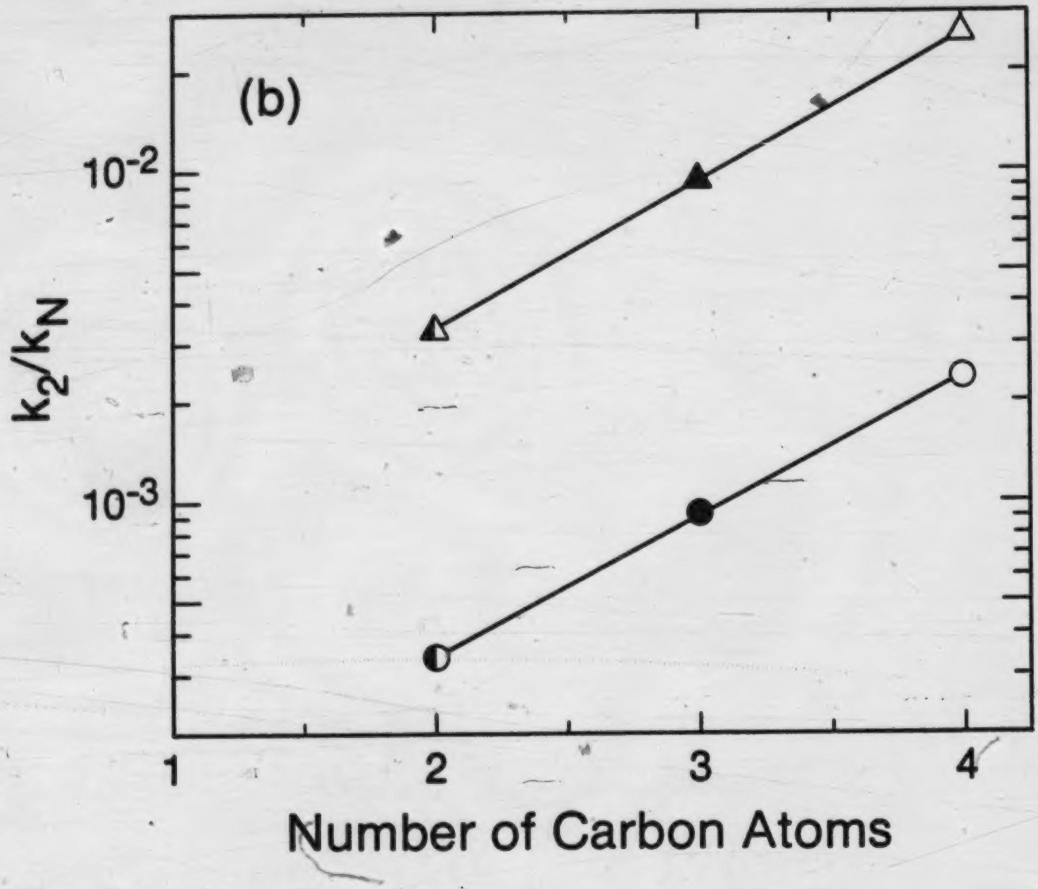

Fig. 4-19: Change of log(k_2/k_N) at the same E_r value (1.34 eV), with the number of carbon atoms. Solute:△,phenol; ○,toluene. Solvent:○△butanol; ●▲,propanol; ◐◭,ethanol.

The reaction of e_s^- with an inefficient scavenger proceeds as in reactions (47) and (48). Solvation effects on the reactants and products, e_s^- , S^-, and RO^-, control the rates of the reaction. This solvation process is apparently strongly affected by the size of the alkyl group of the alcohol.

The size of the alkyl group is reflected in the molar volume and the molecular polarizability α of the alcohol (Table 4-1).

Therefore the value of $\Delta G^{\neq}_{52}$ depends on the molar volume of the solvent in addition to the solvation energy of e_s^- ;

$$\Delta G^{\neq}_{52} \propto \frac{E_r}{f(\mu)} + f(\alpha) \qquad (61)$$

where $f(\alpha)$ is a function of solvent polarizability.

It is possible to compare this empirical equation with that of a theoretical treatment (175)

$$\Delta G^{\theta} = -EA + \Delta G_P(S^-) - \Delta G_s(e) \qquad (62)$$

where $\Delta G_P(s^-)$ is the free energy of polarization of scavenger in the solvent and $\Delta G_s(e)$ is the free energy of solvation of the electron. According to this equation,

$$\Delta G^{\neq}_{52} = EA_N - EA_S + \Delta G_P(S) - \Delta G_P(N) \qquad (63)$$

where $\Delta G_P(N)$ and $\Delta G_P(S)$ are the free energies of polarization of the nitrobenzene and the scavenger molecules.

The values of $\Delta G_P(s^-)$ are usually estimated using the Born equation (174),

$$\Delta G_P(S^-) = \frac{-e^2}{8\pi\epsilon_0 r}(1 - \frac{1}{\epsilon_s}) \qquad (64)$$

Table 4-1: Mean molar volume V_M and polarizability α of solvents at 298K.

Solvent	M 10^3 $kg.mol^{-1}$	V_M $m^3.mol^{-1}$	α^a 10^{-40} $C.m^2.V^{-1}$
Methanol	32.0	40.7^b	$3.7^{d,e}$
Ethanol	46.1	58.7^b	$5.7^{d,e}$
1-prpanol	60.1	74.8^b	7.8^d
2-propanol	60.1	76.4^b	7.8^d
1-butanol	74.1	91.5^c	$10.2^{d,e}$
i-butanol	74.1	92.4^c	10.2^f
2-butanol	74.1	91.7^c	10.2^f
t-butanol	74.1	93.9^c	10.2^f
Alcohol/water mixtures			
$x_{H_2O} = 0.10$			
i-butanol	68.5	84.8^c	
2-butanol	68.5	85.3^c	
t-butanol	68.5	87.0^c	
$x_{H_2O} = 0.35$			
i-butanol	54.5	66.0	
2-butanol	54.5	66.3	
t-butanol	54.5	67.2	

a. Conversion factor $10^{24} cm^3 = 1.1 x 10^{-40} C.m^2.V^{-1}$

b. Ref. 172

c. From densities in the present work

d. Ref. 173

e. Ref. 174

f. Assumed to be the same.

where r is the effective radius of the ion S^-, e is the charge of the electron, ϵ_0 the permittivity of the vacuum, and ϵ_s is the relative permittivity of the solvent. By application of eq.(63),

$$log(\frac{k_2}{k_N}) = \Delta G^{\neq}_{S} - \Delta G^{\neq}_{N} \tag{65}$$

where $\Delta G^{\neq}_{S}$ and $\Delta G^{\neq}_{N}$ are the free energies of activation for the reaction of e_s^- with the scavenger. Thus,

$$log(\frac{k_2}{k_N}) = EA_N - EA_S + \frac{e^2}{8\pi\epsilon_0 r_N}(1-\frac{1}{\epsilon}) - \frac{e^2}{8\pi\epsilon_0 r_S}(1-\frac{1}{\epsilon}) \tag{66}$$

$$= EA_N - EA_S + \frac{e^2}{8\pi\epsilon_0}(1-\frac{1}{\epsilon})(\frac{1}{r_N} - \frac{1}{r_S}) \tag{67}$$

In a plot of $\log(k_2/k_N)$ against $(1-\frac{1}{\epsilon})$, the slope is

$$slope = (\frac{1}{r_N} - \frac{1}{r_S}) \tag{68}$$

The values of $\log(k_2/k_N)$ for phenol and toluene in alcohols are plotted against $(1\text{-}\frac{1}{\epsilon})$ in Fig. (4-20).

The variation of $\log(k_2/k_N)$ is similar to that of Fig. (4-16). For inefficient scavengers there is much greater scatter indicating that equation (62) is not applicable to all systems. The agreement for efficient scavengers is probably due to similarities in the variation of ϵ and E_r in alcohls. The observed variations are due to the change of E_r . This is clarified by comparing Figs.(4-16) and (4-20).

According to equation (62), for solvents of similar dielectric constants the value of ΔG^{θ} for the reaction of e_s^- with the same scavenger depends only on

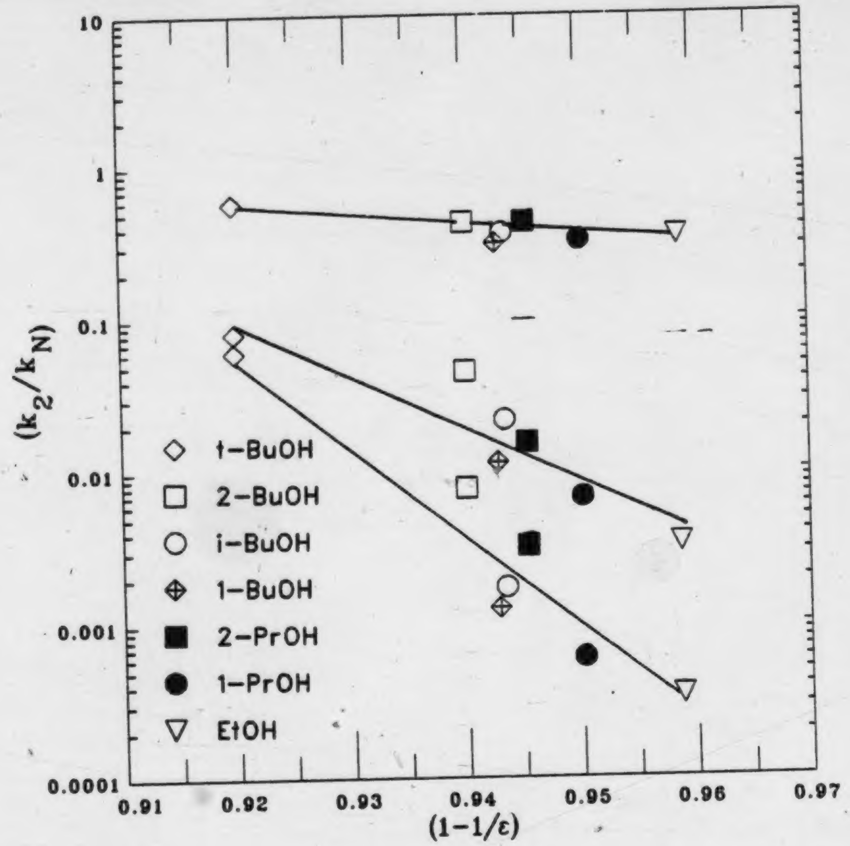

Fig. 4-20: Change of log(k_2/k_N) with $(1 + \frac{1}{\epsilon})$ in pure alcohols.

the solvation energy of the electron. But as seen from equations (65) to (67) the log (k_2/k_N) values obtained from eq.(62) do not depend on the solvation energies of the electron. In fact equation (62) does not distinguish between the efficient and inefficient scavengers, and treats those indiscriminately, except in the electron affinity term which is independent of the solvation energy and polarization energy terms. Therefore even if this equation may explain some of the differences between the reactivities of e_s^- in alcohols it is not sufficient to give a complete picture.

4.2.1.2(b) Alcohol/Water Mixtures

Values of k_2/k_N in alcohol/water mixtures decrease with increasing trap depth of the e_s^- (Fig. 4-21).

At a given water content in the different isomeric butanols, the trap depth dependence of $\log(k_2/k_N)$ is similar to that in pure butanols. This indicates that the differences in solvation by the pure isomeric alcohols persist in the water mixtures.

Although the trap-depth dependence is the same, $\log(k_2/k_N)$ values at $x_{H_2O} \approx 0.35$ are consistently lower than those in $x_{H_2O} \approx 0.10$, which are in turn lower than those in pure alcohols. The molar volume of alcohol/water mixtures decrease with increasing mole fraction of water (Table(4-1)). Here the molar mass of the solvent is,

$$M = x_1 M_1 + x_2 M_2 \tag{69}$$

where x_1 is the mol fraction and M_1 is the molar mass of the species and so on. When water is added to an alcohol the dielectric constant first slightly decreases and then increases (Fig.4-22).

The $\log(k_2/k_N)$ values correlates with the molar volumes but not with the factor $(1-\frac{1}{\epsilon})$. This implies that it is the polarization of the solvent by the scavenger anion that is important rather than polarization of the scavenger molecule

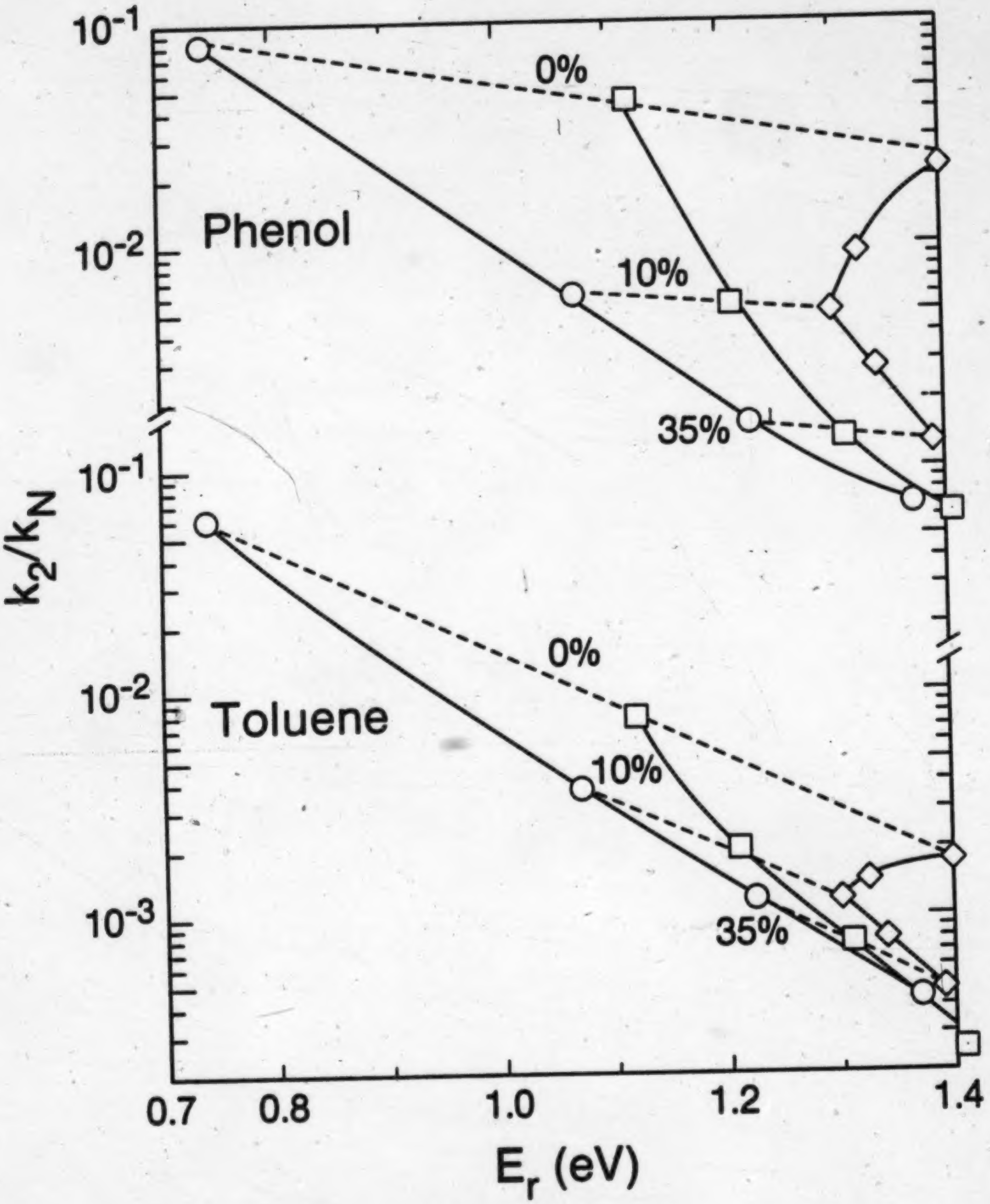

Fig. 4-21: Change of log(k_2/k_N) with E_r in butanol/water mixtures

Solvent: ◇, *i*-BuOH ; □ ,2-BuOH , ○ ,*t*-BuOH .

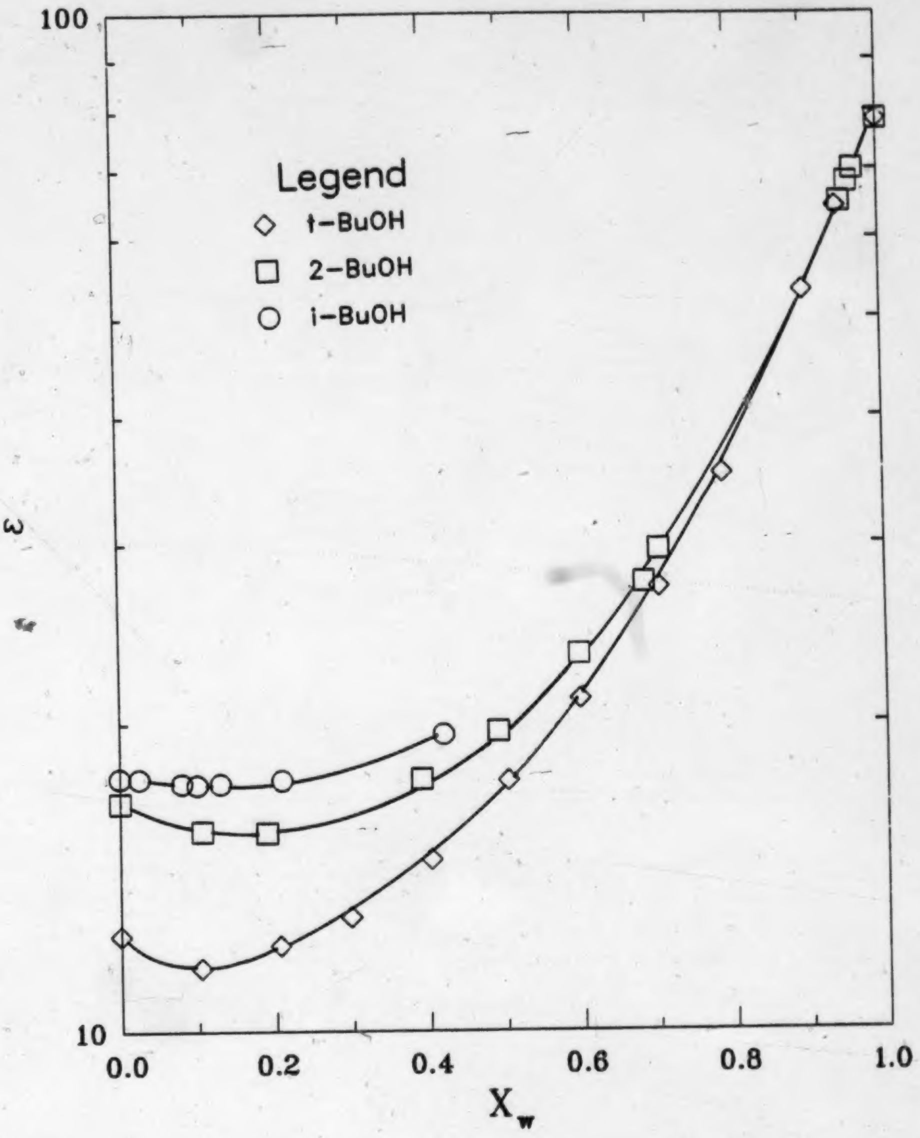

Fig. 4-22: Dependence of the dielectric constant in butanol/water mixtures on composition. (Values of ϵ are from ref. 168, 169).

by the solvent. When the polarizability of the solvent is greater the anions in eq. (47) and eq. (48) are solvated in a deeper potential well and are more stable.

Thus the factor $\Delta G_P(s^-)$ in equation (62) may be replaced by that of f(α). When water is added to alcohol the mean molar volume decreases, the effective mean polarizability of the solvent molecules around the scavenger molecule and the other participating anions decrease, the product ions become less stable and the rate constant decreases.

Thus equation (61) is also applicable to alcohol/water mixtures.

4.2.2 Energies and Entropies of Activation

The energies of activation E_2 of the electron scavenging reaction correlate with E_η , except for the reaction with toluene (Fig. 4-23).

Values of E_2 for toluene reaction are much higher than for the other scavengers. The E_2 values are also exceptionally high for the reaction with benzene.

Toluene and benzene have low electron affinities (170, 171), low dipole moments and do not hydrogen bond with the solvent. In alcohol they are solvated by the alkyl group, while the electron is solvated by the hydroxyl groups. This might create a barrier to close approach of the reactants and cause the higher activation energy of reaction. In water, all scavengers are solvated similarly since they all have hydrophobic groups and variation of E_2 among different scavengers is small.

In solvent zones (b) (c) and (d), with $x_{H_2O} > 0.1$, a lower rate constant is manifested as a more positive activation energy (Fig. 4-24).

For capture of e_s^- by a scavenger of low electron affinity a favourable arrangement of solvent dipoles about the scavenger molecule is required. A more negative entropy of activation indicates a lower probability of a sufficiently favourable arrangement of the solvent, which causes a lower capture rate constant.

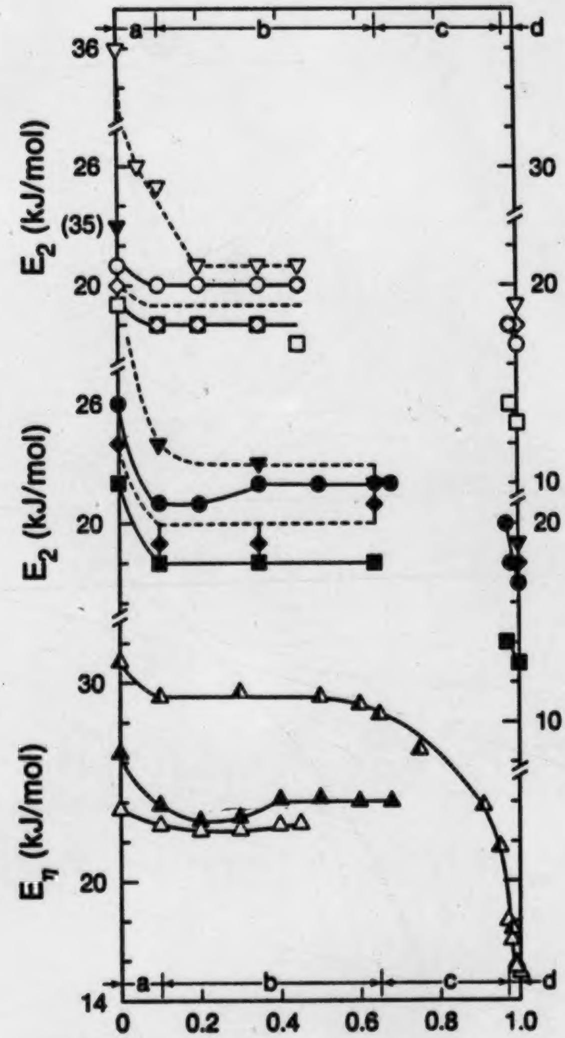

Fig. 4-23: Composition dependence of energies of activation E_2 . Solute: ○● nitro-benzene; □■ acetone; ◇◆ phenol; ▽▼ toluene Solvent: ○□◇▽ *i*-BuOH ; ▲●■◆▼ 2-BuOH ; ◭, *t*-BuOH

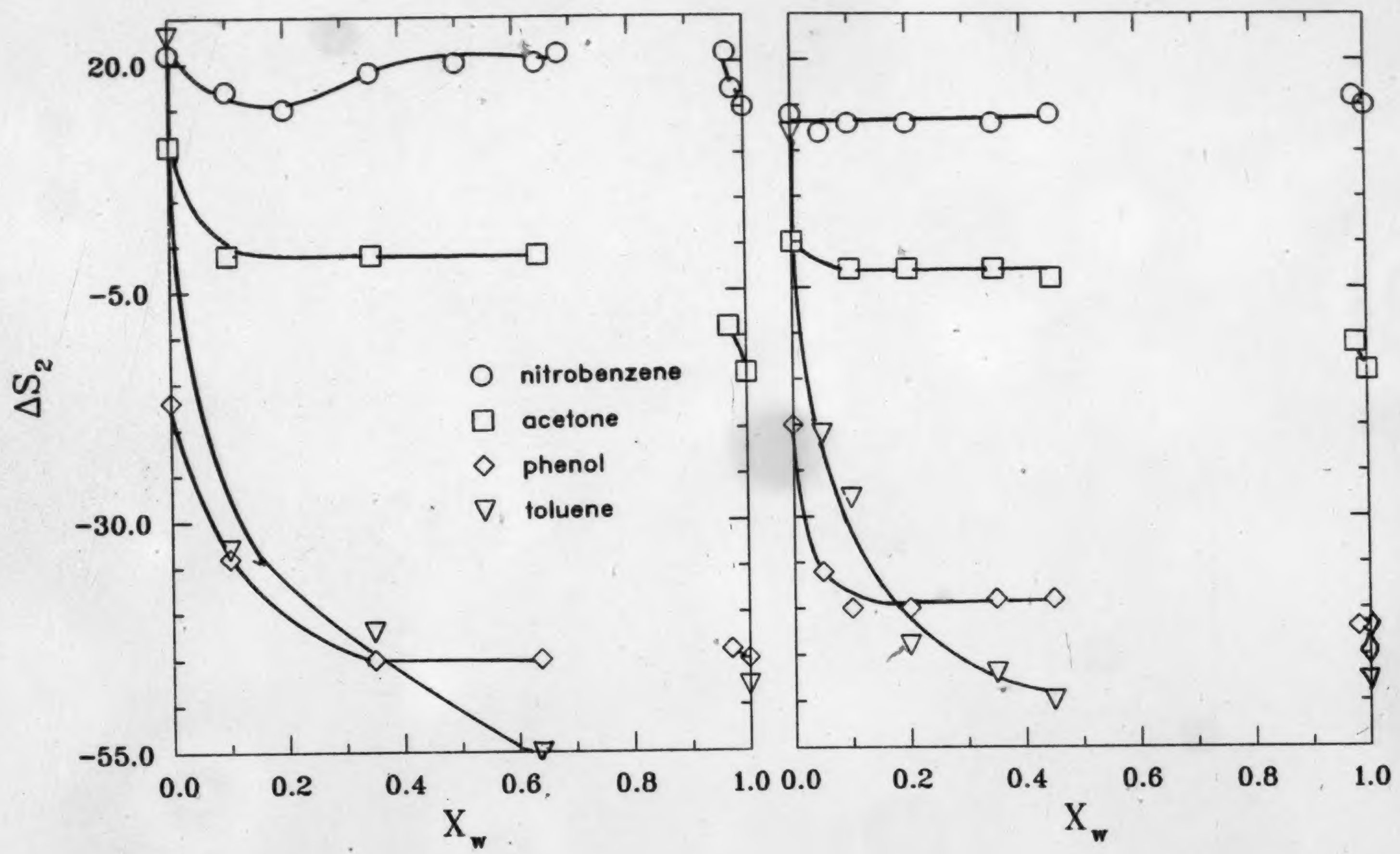

Fig. 4-24: Composition dependence of entropies of activation $\Delta S_2^{\neq}$ Solute:

4.3 Comparison of e_s^- Reactivities with Polar and Charged Scavengers in t-BuOH/Water Mixtures

The solvent effects are further investigated by comparing the reactivity of the e_s^- with charged scavengers. The major differences between these two types of scavengers are the differences of reaction radii and diffusion radii. The ions also have structure-breaking and structure-making effects which change the local viscosity around the ion (176).

The rate constants of e_s^- with the present scavengers are nearly diffusion controlled with $k_2 \geq 10^7 m^3/mol.s$. Of the scavengers studied the reactivities for negative scavengers are more solvent composition dependent than those for the positive scavengers (Fig. 4-24).

4.3.1 Positive Scavengers

The composition dependence of rate constants for the reaction with Ag^+ is similar to that of nitrobenzene (Fig. 4-25).

The application of the Stokes-Smoluchowski relation results in four composition zones (Fig. 4-26).

(a) $0 \leq x_{H_2O} < 0.10$; k_2 decreases with decreasing viscosity,

(b) $0.10 < x_{H_2O} < x_{\eta_{max}}$; k_2 slightly increases with increasing viscosity,

(c) $x_{\eta_{max}} < x_{H_2O} < 0.90$; $k_2 \propto \eta^{-1}$

(d) $0.90 < x_{H_2O} < 1.00$; $k_2 \propto \eta^{-0.54}$

In zones (a), (b) and (c) the rate constants for the reaction with Ag^+ are consistently higher than for nitrobenzene at the same composition. In zone (d) the rate constants are similar; the factor $(\frac{1}{r_e} + \frac{1}{r_S})(R_e + R_S)$ is the same for both systems

The greater rate constants for reaction with Ag^+ almost over the whole composition range are probably due to the larger interaction between the Ag^+ ion and the e_s^- that results in an increased effective reaction radius.

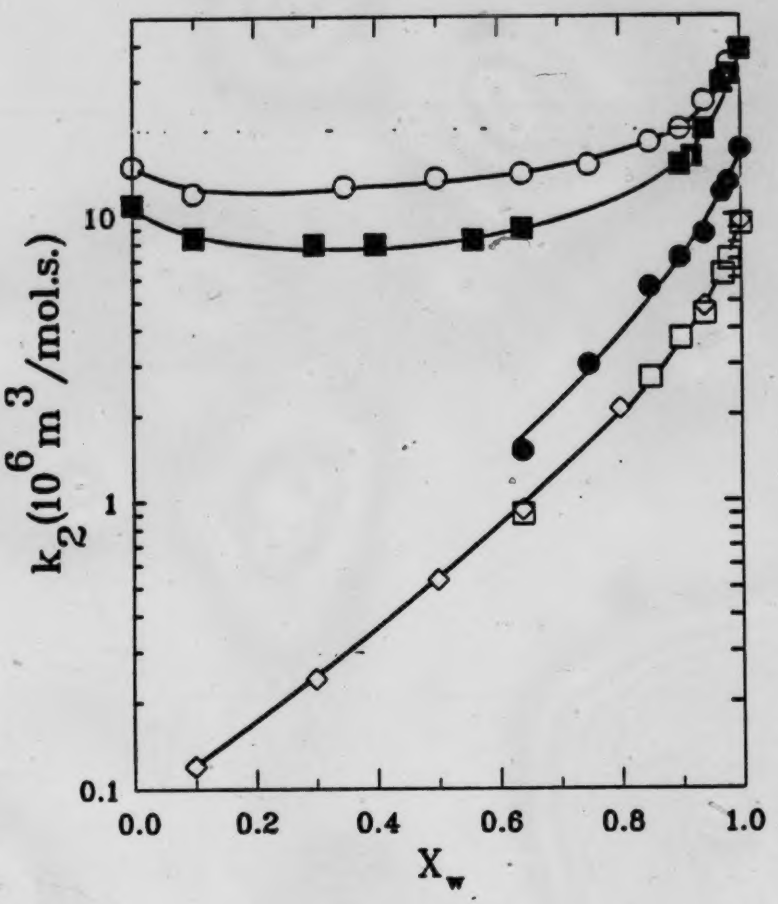

Fig. 4-25: Composition dependence of rate constants k_2 for e_s^- reaction in *t*-butanol/water mixtures. Solute: ○ , nitrobenzene; ■ , Ag^+ ; □◇, , NO_3^- ; ● , CrO_4^{2-} .

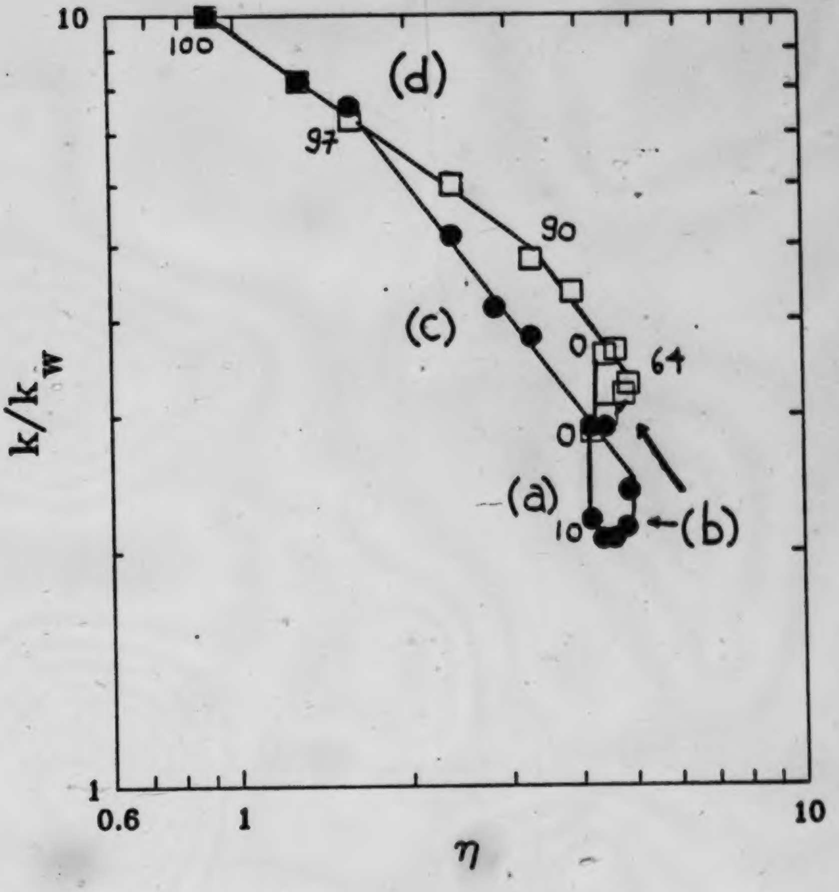

Fig. 4-26: Change of rate constant k_2 with viscosity η in *t*-butanol/water mixtures. Solute: ●, nitrobenzene; □, Ag^+.

The effects due to the potential interaction between the reactants are taken into consideration in the Debye equation (55). The correction factor due to the reactant interaction in the present case depends on the type of the potential difference. The interaction energies of ion-dipole and ion-ion encounter pairs are given in eq. (41) and (42). If the encounter pair is ion - nonpolar the potential interaction between these are given by (174),

$$U_{i,n} = \frac{\alpha e^2}{8\pi\epsilon_0\epsilon r^4} \qquad (70)$$

For an interaction distance of 0.5 nm the value of $U(r)_i$ for the reaction changes with ϵ such that

$$U(r)_i = \frac{-C}{\epsilon} \qquad (71)$$

whereas the correction factor changes as

$$f = \frac{C/\epsilon}{1 - exp(-C/\epsilon)} \qquad (72)$$

The value of constant C is 112.1 for the reaction of e_s^- with Ag^+ and 224.2 for that with Cu^{2+} , whereas for nitrobenzene (dipole moment 4.22 D) it is 19.6. The rate constants normalized with the correction factors are plotted against viscosity in Fig.(4-27).

The k_2 /f values are divided by that in water to normalize the rate constants for the effect of electron capture efficiency.

Once the differences in potential interaction energies for the reaction of e_s^- with charged and polar scavengers are taken into account, the rate constants are similar in zone (d) and part of zone (c). The value (k_2 /f) at different viscosities

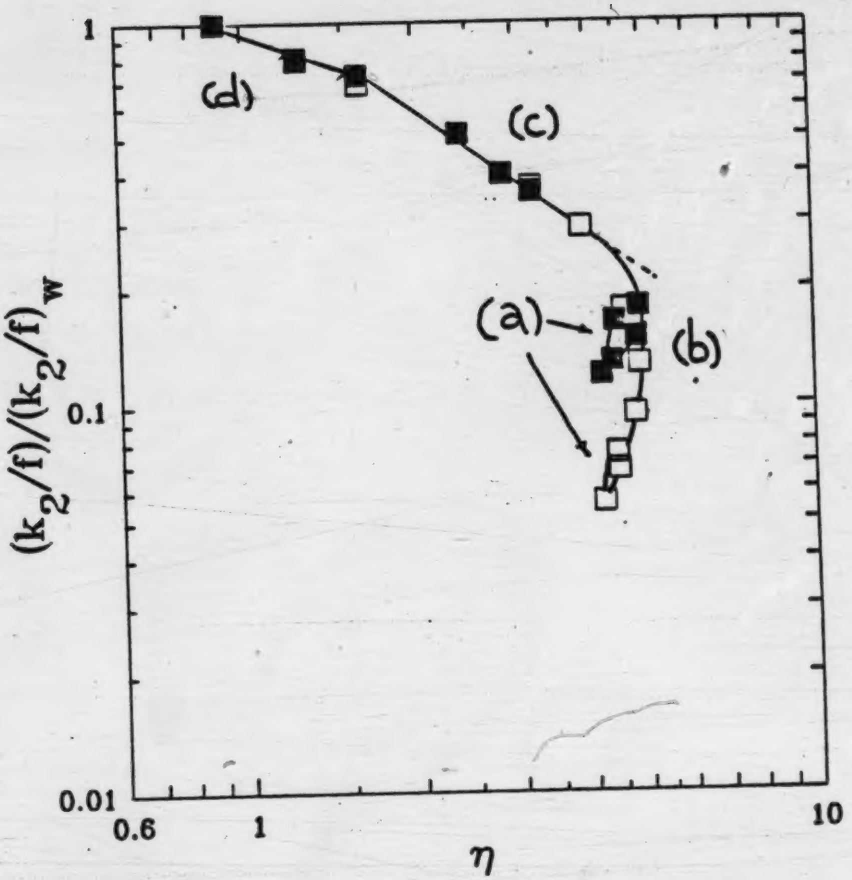

Fig. 4-27: The viscosity η dependence of normalized rate constants (k_2/f) in *t*-butanol/water mixtures. Solute: ■ , nitrobenzene; □ , Ag^+ .

displays the change of $(\frac{1}{r_e}+\frac{1}{r_S})(R_e+R_S)$. This figure imply two important solvent effects:

1. the factor $(\frac{1}{r_e}+\frac{1}{r_S})(R_e+R_S)$ is constant in the zone $0.85 < x_{H_2O} < 0.97$,
2. the factor $(\frac{1}{r_e}+\frac{1}{r_S})(R_e+R_S)$ for reaction with Ag^+ is similar to that with nitrobenzene .

Once the effect of the dielectric constant on the reaction radius is corrected, $(R_e + R_S)$ is probably equal to $(r_e + r_S)$. Therefore,

$$(\frac{1}{r_e}+\frac{1}{r_S})(R_e+R_S) \approx (\frac{r_e+r_S}{r_e r_S})^2$$

If the two solvent effects are considered,

1. constant $(\frac{1}{r_e}+\frac{1}{r_S})(R_e+R_S)$,

$$(\frac{1}{r_e}+\frac{1}{r_S})(R_e+R_S) \approx constant$$

$$\frac{(r_e+r_S)^2}{r_e r_S} \approx constant \tag{73}$$

Since the optical absorption energies imply that r_e in this zone is constant ; r_S is also constant.

2. similar values of $(\frac{1}{r_e}+\frac{1}{r_S})(R_e+R_S)$,

$$((\frac{1}{r_e}+\frac{1}{r_S})(R_e+R_S))_{Ag^+} \approx ((\frac{1}{r_e}+\frac{1}{r_S})(R_e+R_S))_{Nitrob}$$

where the subscripts Ag^+ and $Nitrob$ refers to the silver ion and nitrobenzene respectively.

$$(\frac{(r_e+r_S)^2}{r_e r_S})_{Ag^+} \approx (\frac{(r_e+r_S)^2}{r_e r_S})_{Nitrob} \tag{74}$$

Since r_e is constant ; $r_{Ag^+} \approx r_{nitrob}$

This seems to be quite impossible since the physical radius of nitrobenzene $\approx$ 0.28 nm while the Stokes radius of Ag^+ is 0.15 nm. The only possible way this could occur is if both scavengers are solvated in clathrate micro-phases.

When alcohol is added to water, clathrate structure formation is supposed to occur (109-111). With further addition of alcohol the clathrates separate into micro-phases. These micro-phases are water-rich since the maximum structure stabilization occurs at $x_{H_2O} \approx 0.97$ in t-BuOH (108,109), which correspond to a water:alcohol ratio of 33:1. Thus in this zone Ag^+ has more affinity to clathrates. Nitrobenzene as a molecule with a hydrophobic group forms clathrates. Therefore the effective diffusion radius for the scavenger is that of the micro-phase, which is the same for both nitrobenzene and Ag^+ . The constant value for $(\frac{1}{r_e} + \frac{1}{r_S})(R_e + R_S)$ indicates that micro-phases may exist up to mol fractions of 0.85 water.

In the region $0 \leq x_{H_2O} < 0.85$, the normalized k_2 /f values for nitrobenzene are consistently higher than for Ag^+ and the extent of difference increases with the alcohol content (Fig. 4-28).

Silver is a small ion (ionic radii $\approx$ 0.126 nm), leading to electrostriction in a polar medium. It acts as a structure maker and increases the local viscosity around itself (177). This leads to a lower diffusion coefficient and eventually to a lower rate constant. The structure making effect increases with the decreasing structure of the solvent (178).

As the solvent becomes richer in alcohol, the micro-phases collapse and the scavenger and the electron start to get solvated in the general medium. The structure in alcohol/water mixtures decrease with increasing alcohol content; the structure making effect of the Ag^+ ion increases, and the rate constant decreases.

4.3.2 Negative Scavengers

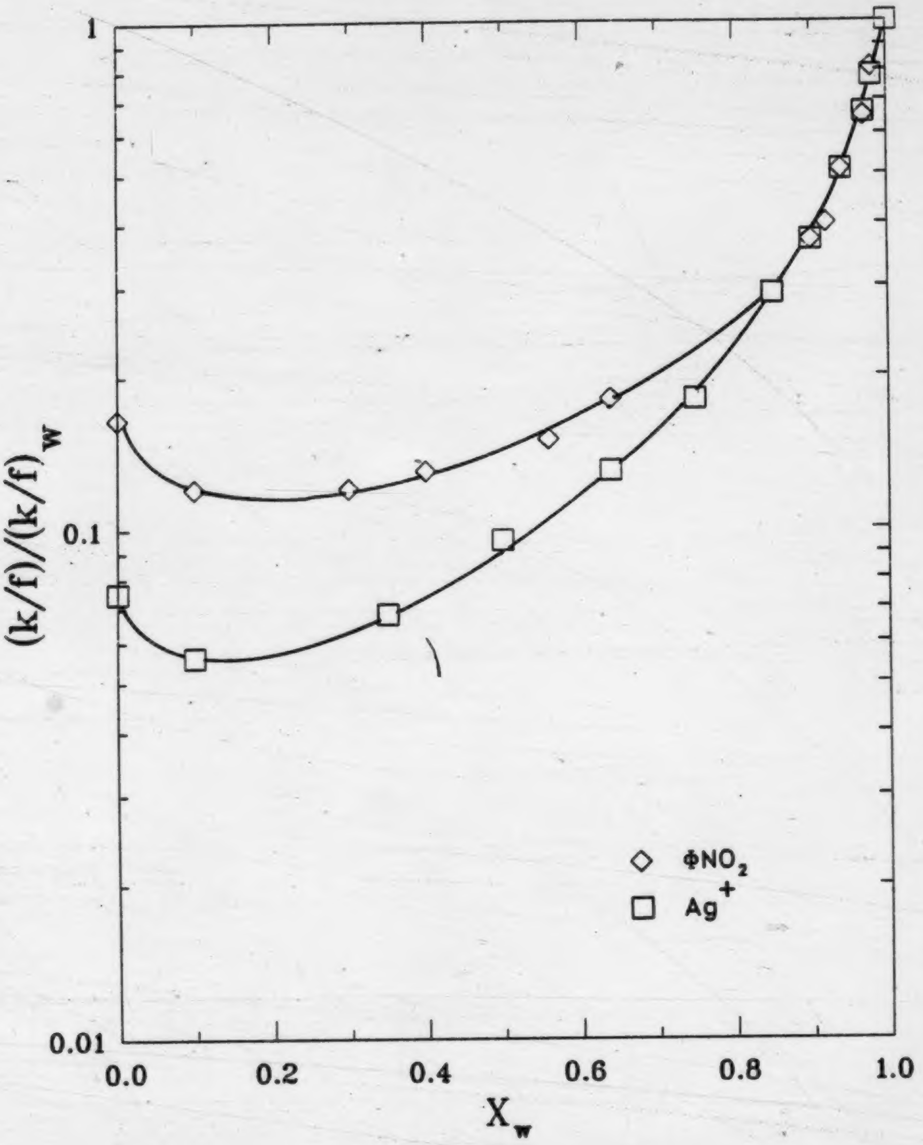

Fig:4-28: The composition η, dependence of normalized rate constants k_2 in *t*-butanol/water mixtures. Solute: □, Ag^+ ; ◇, nitrobenzene .

The rate constants for the negatively charged scavengers display greater composition dependence in the alcohol rich solvents (Fig. 4-29).

To determine if this is due to the change in the dielectric constant of the solvent, the Debye relation is applied. For an interaction distance of 0.5 nm the correction factor f changes as

$$f = \frac{112.1/\epsilon}{exp(112.1/\epsilon) - 1} \qquad (75)$$

The value of f gradually decreases from 0.45 in water, to 0.0007 in alcohol. The corresponding values for Rf are 0.23 nm in water and 0.0006 nm in pure alcohol. The values of Rf in alcohol/water mixtures are meaningless since that in water probably corresponds to the physical radius of the NO_3^- molecule.

The values of f for CrO_4^{2-} molecule are even more exaggerated. This indicates that the change in the dielectric constant does not have an effect on these two scavengers since the reactants are so close together when the reaction occurs. This is confirmed by the similarities between the reactivities of the negative scavengers and that of the normalized rate constants of positive scavengers (Fig. 4-30) in the water-rich zones. The rate constants for all three scavengers Ag^+, NO_3^-, and CrO_4^{2-}, are similar in the water-rich region $0.85 < x_{H_2O} < 1.00$ indicating that these ions are solvated in water-rich clathrates.

In the alcohol-rich regions the reactivity of NO_3^- ion is less than that of Ag^+. The reason is not electrostriction since NO_3^-, a comparatively large ion, acts as a structure breaker (176) that results in a larger diffusion coefficient. In fact, even though the ionic radius of Ag^+ is probably about half that of NO_3^-, the Stokes radii of the ions are respectively, 0.62 and 0.72 nm. The rate constant for

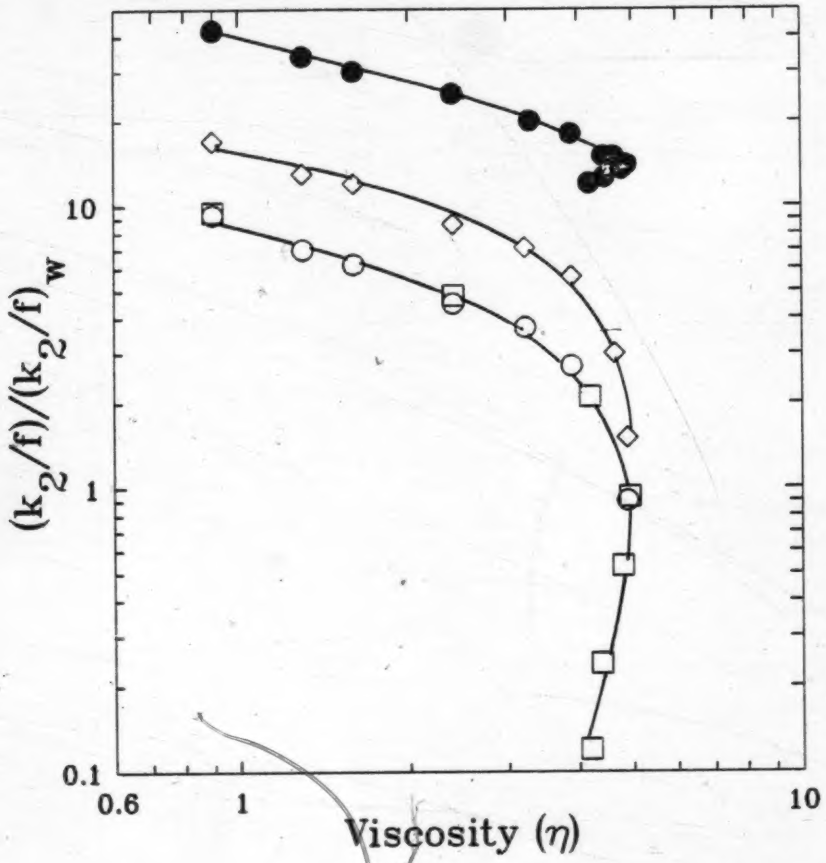

Fig. 4-29: The viscosity η, dependence of rate constants k_2 in *t*-butanol/water mixtures. Solute: ●, Ag^+ ; □○, NO_3^- ; ◇, CrO_4^{2-} .

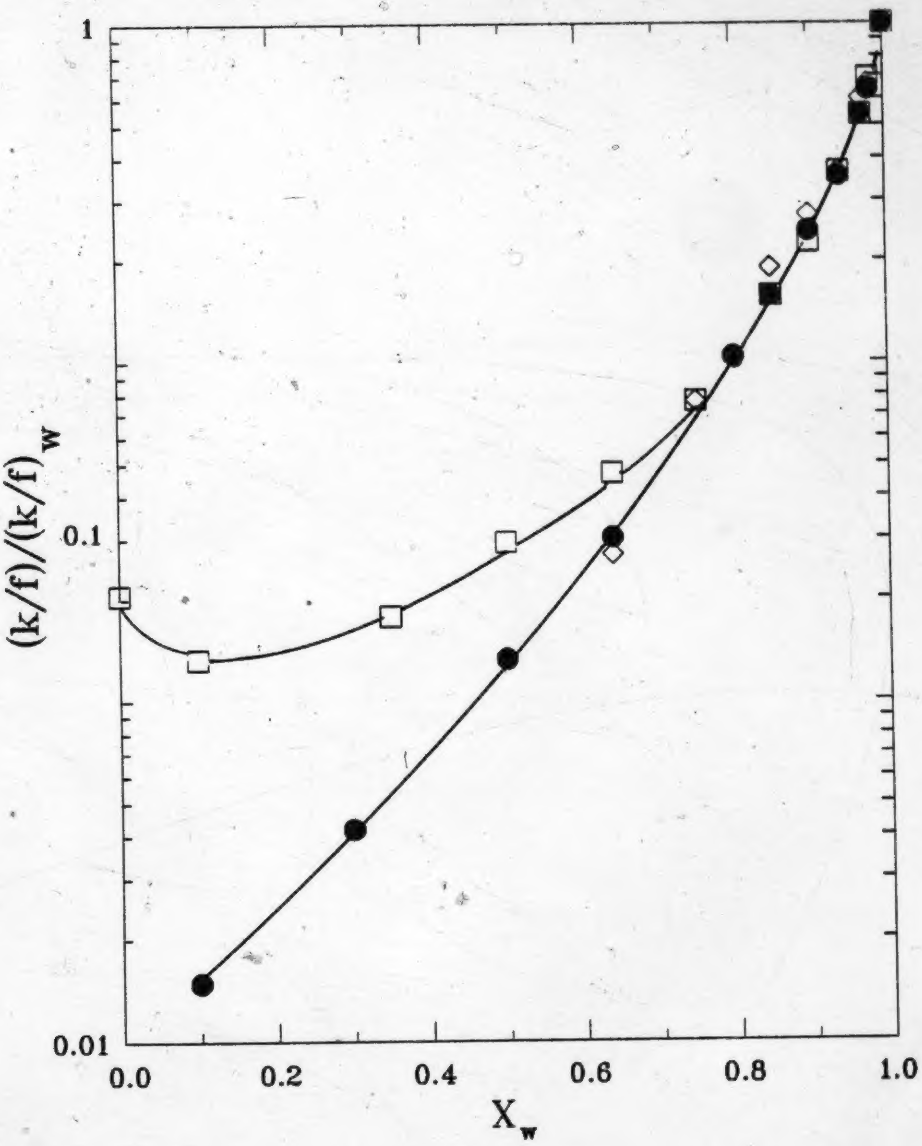

Fig. 4-30: The composition dependence of normalized rate constants in t-butanol/water mixtures. Solute:□,Ag^+ ; ●,NO_3^- ;◇,CrO_4^{2-} .

the reaction with NO_3^- at $x_{H_2O} = 0.10$ is about 4 fold lower than that with Ag^+ . The diffusion coefficient and/or the reaction radius of NO_3^- is lower. Since the Stokes radii of these two ions are comparable a lower diffusion coefficient for the reaction with NO_3^- is possible if there is hindrance to motion by ion-pair formation (association between ions) (177-179).

4.3.3 Temperature Dependence

The energies of activation in pure water are in the order $Ag^+ > Cu^{2+}$ for positive ions and $CrO_4^{2-} > NO_3^-$ for negative ions (Fig. 3-154). Thus the charge effects are manifested as activation energies. When the ions are positive there is a greater attractive interaction between the electron and the ion with larger charge density. Since Cu^{2+} has a larger charge density it attracts the e_s^- more easily than Ag^+ ; it has a lower E_2 value. For the negative ions CrO_4^{2-} has a greater repulsive interaction with the electron and thus the energy of activation is higher than for NO_3^- .

Generally the negative ions in the present study have energies of activation lower than those of positive ions. The negative ions NO_3^- and CrO_4^{2-} are large ions compared to the positive ions Ag^+ and Cu^{2+} . Thus both negative ions act as structure breakers while the positive ions act as structure makers. Therefore the positive ions are solvated in deeper potential wells and reaction with the electron is more difficult; E_2 values are greater.

In the alcohol/water mixtures, the energy of activation decreases in zone (a), is constant in zone (b) and gradually decreases in zones (c) and (d) for positive scavengers. The activation energies for Cu^{2+} are also similar. The same zone behaviour was also observed for the reaction with nitrobenzene and is correlated to the energy of activation for viscous flow.

The values of E_2 for the reaction with negative scavengers decrease in zones (c) and (d) as seen for nitrobenzene and positive scavengers but decreases gradually in zone (b).

When alcohol is added to water the composition dependence of k_2 for negative ions is similar to that for positive ions and that for nitrobenzene (Figs.4-28 and 4-30). But below $x_{H_2O} \approx 0.85$, k_2 for the negative ions decrease persumably due to ion-pair association. Existence of the scavenger ion as an ion-pair with its counter ion makes it difficult for the electron to react, and therefore increases the energy of activation. Thus the lower rate constants are not only due to lower diffusion coefficient of the pair, but also due to difficulty of approaching the scavenger ion.

4.4 Temperature and Composition Dependence of Densities and Viscosities of Butanol/Water Mixtures

Correlation of the e_s^- reactivities with the transport properties of the solvent required the temperature and composition dependence of the dynamic viscosities of the butanol/water mixtures. Since these were unavailable in literature the study of densities and kinematic viscosities was also included in the present thesis.

The composition dependence of thermophysical properties of binary mixtures is often described in terms of properties that for ideal mixtures have values Y_{id} (144,146) where,

$$Y_{id} = x_1 Y_1 + x_2 Y_2 \tag{76}$$

where $x_1 + x_2 = 1$ and Y_i is the value for pure component i. These properties are additive in mole fraction. The measured Y_{expt} is related to an excess value Y^E where,

$$Y^E = Y_{expt} - Y_{id} \tag{77}$$

4.4.1 Excess Volume

For the density the additive property is the molar volume V = M/ρ, where M is the molar mass for the mixture and (181),

$$M = \Sigma(x_i M_i) \tag{78}$$

The ideal mixture volume V_{id},

$$V_{id} = \frac{x_w M_w}{\rho_w} + \frac{x_a M_a}{\rho_a} \tag{79}$$

where subscripts w and a refer to water and alcohol respectively. Hence the ideal mixture density is,

$$\begin{aligned}\rho_{id} &= M_m/V_{id} \\ &= \frac{(x_w M_w + x_a M_a)}{(x_w M_w/\rho_w + x_a M_a/\rho_a)}\end{aligned} \tag{80}$$

The experimental densities and the ideal mixture densities calculated using eq.(81) are shown in Fig.(4-31).

Values of ρ_{expt} are larger than ρ_{id}. Therefore the liquid contracts on mixing (144, 146).

The composition dependence of the molar volume V is usually described in terms of the excess volume V^E , rather than that of ρ.

$$V^E = \frac{M_M}{\rho_{expt}} - V_{id} \tag{81}$$

The excess volumes calculated from the above equation are listed in Table (4-2) and for two temperatures are plotted in Fig.(4-32).

The excess volumes are negative indicating the contraction of the liquid. This is probably due to the breakdown of the open structure of water. The minimum in the V^E plot deepens with increasing temperature in *t*-BuOH /water solvents. In the the other two butanol/water mixtures $|V^E|$ decreases with increasing temperature (from 278 to 328K), but remains approximately the same on further heating. This implies that the increased thermal agitation of the solvent makes it less non-ideal.

4.4.2 Viscosity

The main problem in calculating an excess viscosity is the lack of agreement as to the form of the ideal mixture viscosity. Although the equations (76) and (77) can be used to define ideal viscosity (182), the only mixture that could

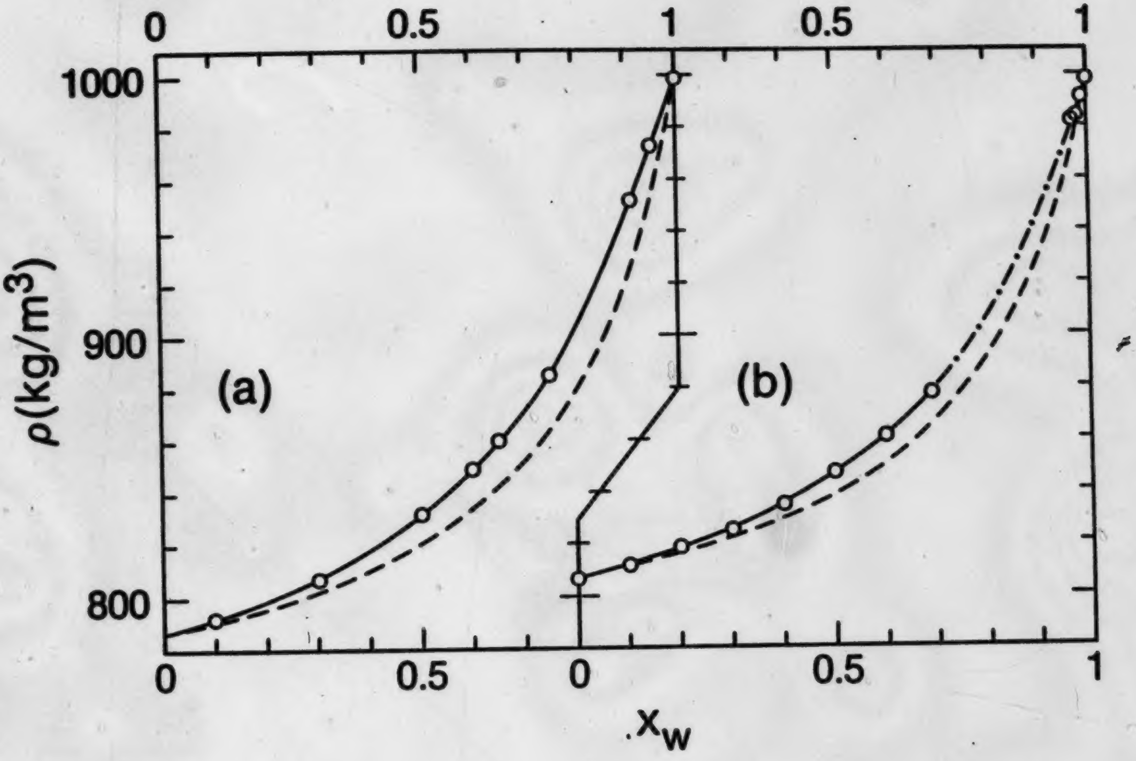

Fig. 4-31: The experimental—, and calculated----densities of *t*-butanol/water (a), and 2-butanol/water (b) mixtures.

Table 4-2: Excess volumes V^E in butanol/water mixtures.

x_{H_2O}	V^E	V^E	V^E	V^E
	Water in 2-butanol			
T	278.15	293.15	328.15	353.15
0.10	0.111	0.085	0.026	0.002
0.20	0.298	0.249	0.164	0.126
0.30	0.332	0.283	0.235	0.219
0.40	0.487	0.422	0.317	0.290
0.50	0.632	0.562	0.479	0.468
0.60	0.674	0.595	0.478	0.459
0.68	0.665	0.585	0.493	0.498
0.97	0.221	0.212	0.217	0.203
0.98	0.122	0.130	0.155	0.148
0.99	0.048	0.054	0.078	0.075
	Water in i-butanol			
T	273.150	293.150	323.150	353.150
0.10	0.309	0.244	0.146	0.061
0.20	0.381	0.298	0.199	0.123
0.30	0.515	0.392	0.254	0.128
0.40	0.613	0.491	0.346	0.243
0.45	0.737	0.568	0.368	0.202
0.99	0.061	0.055	0.072	0.066
	Water in t-butanol			
T	298.150	313.150	313.150	353.150
0.10	0.235	0.398	0.620	0.888

0.30	0.481	0.681	0.987	1.335
0.50	0.845	1.001	1.261	1.569
0.60	0.908	1.038	1.249	1.515
0.65	0.949	1.054	1.230	1.455
0.75	0.914	0.978	1.112	1.295
0.91	0.665	0.650	0.677	0.749
0.95	0.462	0.469	0.483	0.502

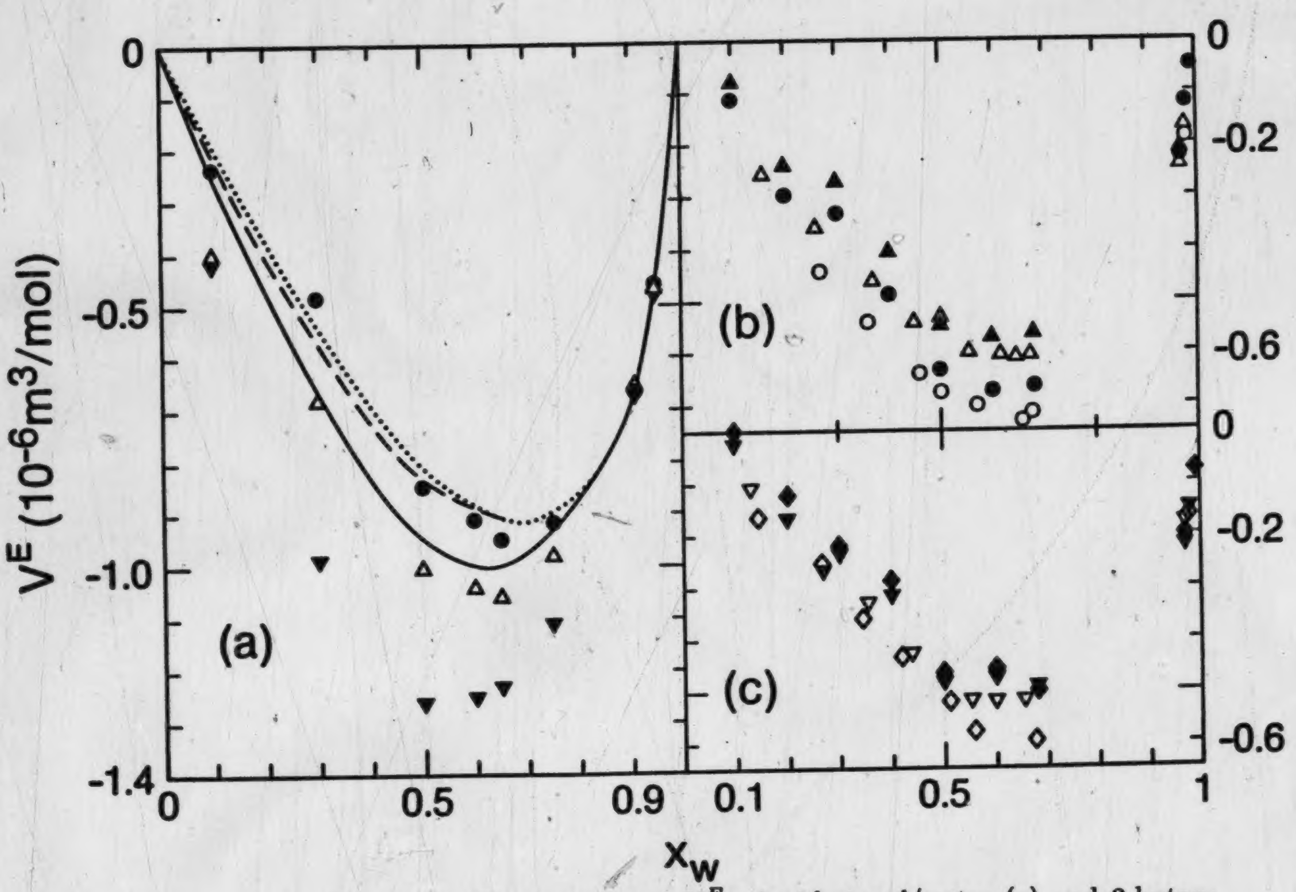

Fig. 4-32: Excess volumes V^E, in *t*-butanol/water (a) and 2-butanol/water (b and c) mixtures. Temperatures:(a)● 298K,△ 313K,▼ 353K. (b)▲ 298K, ● 278K (c)◆ 328K,▼ 353K. Open points in (b) and (c) from ref. 146

be described by it is $H_2O/HDO/D_2O$ (184) in which the components are quite similar. The most widely used relation is that of Arrhenius (185),

$$ln(\eta_{Ar}) = x_1 ln(\eta_1) + x_2 ln(\eta_2) \tag{82}$$

This is equation (76) with $Y_i = ln\eta_i$.

There is also disagreement whether the more meaningful is $[ln\eta_{expt} - ln\eta_{Ar}]$ or $[\eta_{expt} - \eta_{Ar}]$. The other models are fluidity (183, 186)

$$\Phi = x_1\Phi_1 + x_2\Phi_2 \tag{83}$$

and power-root (186, 187)

$$\eta^a = x_1\eta_1^a + x_2\eta_2^a \tag{84}$$

equations.

The experimental viscosities and the values calculated from equations (76), (82) and (83) are shown in Fig. (4-33).

In each case the calculated values are far from the experimental values. The equation (84) with a=1/3, 1/2, and 1/2.5 was also tested; calculated values lie between the values of eq. (76) and (82). Thus regardless of the form of η_{id} the present work indicates a large positive excess viscosity.

The viscosities of butanols are in the order: *t*-BuOH > *i*-BuOH > 2-BuOH > 1-BuOH . The viscosity of the alcohol increases with greater branching and rigidity of the alkyl group.

The viscosities in alcohol/water mixtures also display zone behaviour as observed in the kinetics of e_s^- reactions. In water rich zone (d) they are similar indicating that the increase in viscosity is due to hydrogen bond formation among water molecules rather than between water and alcohol. With increasing

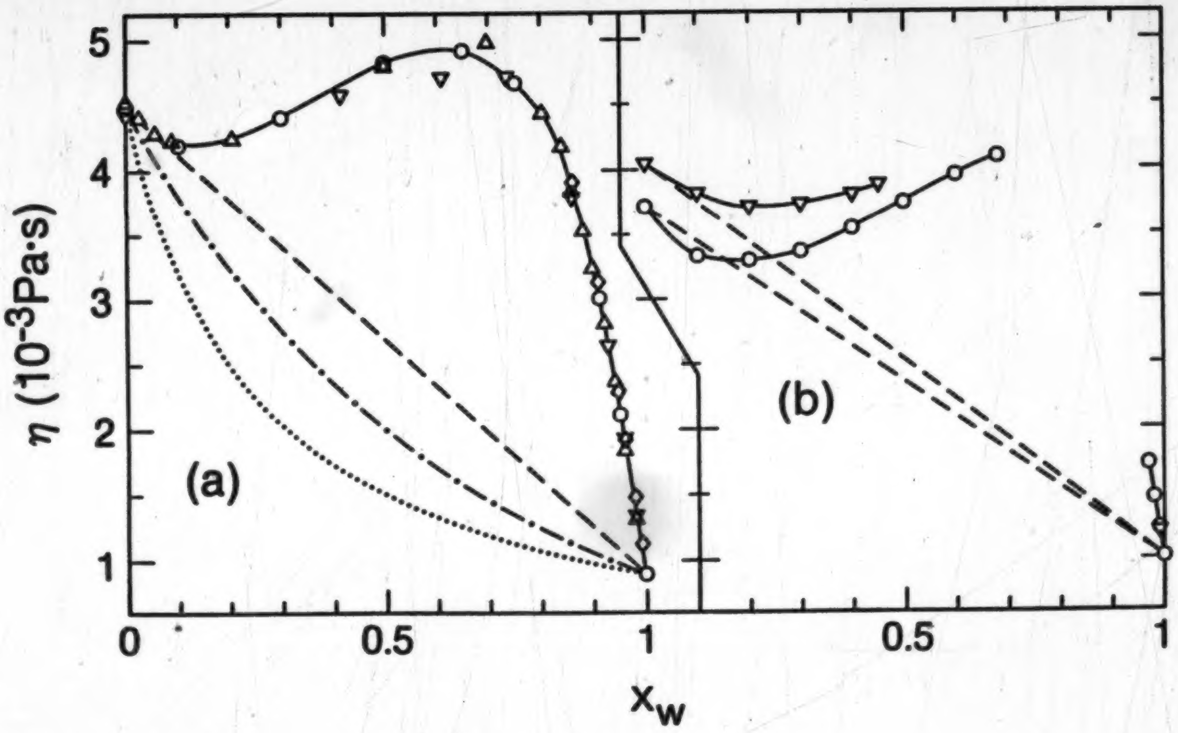

Fig. 4-33: Composition dependence of viscosity η.

(a)▽ref138,△ref148eq.(76)- -,eq.(82)-·-,eq.(83)……,

(b)○ 2-butanol/water,▽*iso*-butanol/water temperature the increased thermal agitation of the solvent makes it less non-ideal (Fig. 3-155) and thus the viscosities of the two pure solvents become similar. The decrease of viscosity with increasing temperature for the alcohol is much greater than for water; a greater energy is needed for the diffusive motion in alcohols than in water.

4.3.3 Energy of Activation for Viscous Flow

In pure alcohols, the energies of activation, E_η, are in the order ; *t*-BuOH > 2-BuOH ≥ *i*-BuOH > 1-BuOH (Fig. 4-34).

The values for 2-BuOH and *i*-BuOH are in the inverse order of viscosities. In these 2-BuOH has a more rigid alkyl group, whereas *i*-BuOH has a less sterically hindered -OH group which facilitates hydrogen bonding. Both processes are involved in the motion of alcohol molecules.

Thus higher E_η values in associated liquids are due to two processes that are responsible for the greater difficulty of molecular translational-rotational motion (123):

1. greater difficulty of motion caused by the rigid shape of the molecule,
2. greater attractive interactions between the molecules. (which pull the molecules closer together and decrease the free volume between them).

The attractive forces among the tertiary alcohols are expected to be less favourable because of the steric hindrance of the bulky and rigid alkyl group so the molar volume of *t*-BuOH is slightly greater than for the other butanols. The higher value of E_η for *t*-BuOH implies that the rigidity of the molecule is more important for the motion of the butanols than the attractive forces. The more flexible alkyl groups of the other butanols facilitate diffusion. Thus even though the α carbon atom of the *i*-BuOH molecule is less sterically hindered, which promotes hydrogen bonding, it has a lower E_η value than 2-BuOH.

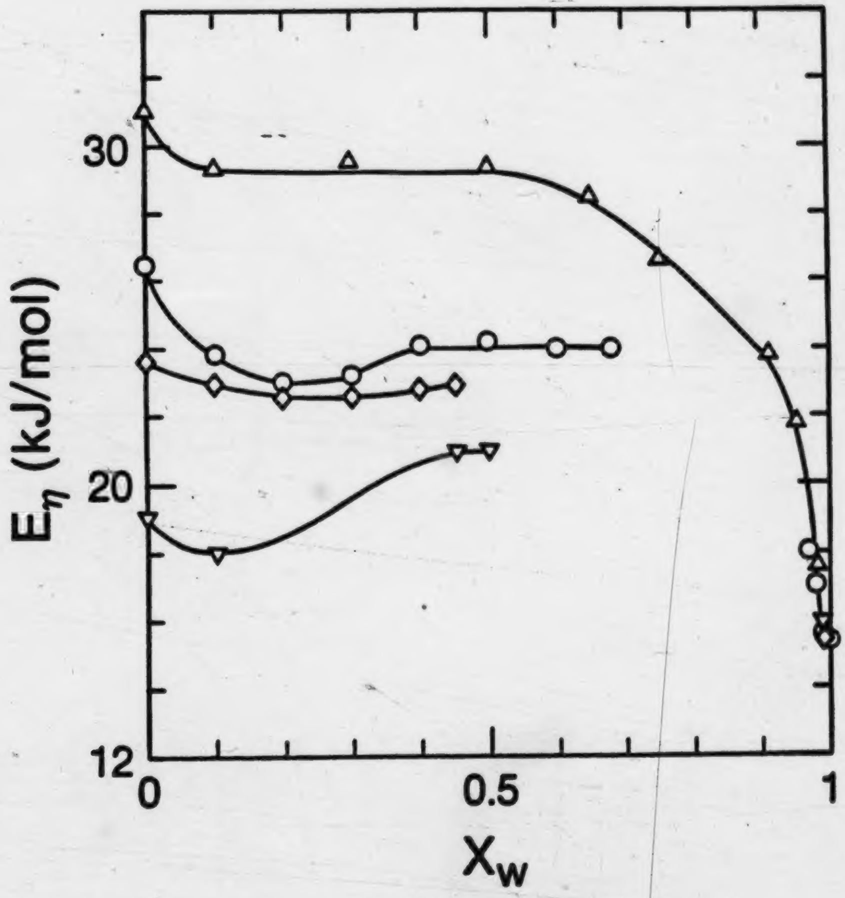

Fig. 4-34: Composition dependence of activation energy for viscous flow, E_η . Solvent:△*t*-butanol/water, ○2-butanol/water, ◇*iso*-butanol/water, ▽1-butanol/water .

When water is added the E_η value in all butanols decrease. Water, a much smaller molecule, acts as a lubricant hence the bulk viscosity lowers. The values of E_η in small alcohols (62, 63) increase with the addition of water. Water and alcohol molecules form hydrogen bonds. But in butanols the ease of motion due to water is greater than the effect due to hydrogen bonds, therefore the value of E_η decreases.

As the water content in the alcohol increases, the hydrogen bond formation increases and the result of these two competing effects are displayed. Mixtures of *i*-BuOH indicate the greatest increase in E_η in zone (b) because it has the least sterically hindered group of the butanols. The molecule with the most sterically hindered -OH group *t*-BuOH indicate E_η values in this zone that do not change with the increasing water content.

Upon addition of a small amount of butanol to water E_η increases (zone (d), Fig. 4-34). Butanol promotes structure in water, which stiffens it and hinders diffusion. Further addition of *t*-BuOH to water continues to stiffen the liquid structure. The similarities of viscosity values in the water-rich region indicate that hydrogen bonding is among water molecules rather than between water and alcohol molecules.

Conclusions

Solvent effects on electron reactivity are dependent on the shape and size of the alkyl group in the isomeric butanol solvents.

The differences in the rate constant of a specific scavenger are due to differences in solvent viscosity and electron solvation energy.

The viscosity of *t*-BuOH is highest because of the rigid, bulky alkyl group which hinders diffusion. The viscosity of 1-BuOH with the most flexible alkyl group is the lowest.

The bulkiness of the *t*-butyl group also causes a lowering of the solvation energy of the electrons, because of steric hindrance to the alignment of the -OH groups about the electron.

The viscosity and electron solvation factors have opposing effects on the magnitude of k_2 , so the net effect is a resultant of the two components.

While the rate constants for the efficient scavengers are most affected by changes in solvent transport properties, those of inefficient scavengers are most effected by the change in the solvation energy.

The free energy of reaction of the electron with an inefficient scavenger depends on the electron affinity of the scavenger, the solvation energy of the electron and the polarizability of the solvent.

REFERENCES

1. W.Weyl, Ann. Phys. **121,** 601 (1864).
2. G.W.A.Fowles, W.R.McGregor, and M.C.R.Symons, J. Chem. Soc. 3329 (1957).
3. J.E.Bennett, B.Miles, and A.Thomas, J. Chem. Soc.(A). 1393 (1967).
4. G.R.Freeman in "Non-Homogeneous Kinetics", ed: G.R.Freeman (John Wiley and Co.; New York, 1987).
5. D.C.Walker, J. Phys. Chem. **84,** 1140 (1980).
6. L.Kevan, J. Phys. Chem. **84,** 1232 (1980).
7. Y.Wang, M.K.Crawford, M.J.McAuliffe and K.B.Eisenthal, Chem. Phys. Lett. **74,** 160 (1980).
8. W.J.Chase and J.W.Hunt, J. Phys. Chem. **79,** 2835 (1975).
9. P.Bordewijk, M.Kunst and E.Rip, J. Phys. Chem **77,** 548 (1983).
10. S.Gordon, E.J.Hart, M.S.Matheson, J.Rabani and J.K.Thomas, J. Chem. Soc. 193 (1963).
11. D.Huppert, P.Avouris, and P.M.Rentzepis, J. Phys. Chem. **82,** 2282, (1978).
12. T.R.Tuttle, S.Golden, S.Lwenje and C.M.Stupak J. Phys. Chem. **88,** 3811 (1984).
13. D.C.Walker, Can. J. Chem. **55,** 1987 (1977).
14. N.Okabe, T.Kimura and K.Fueki, Can. J. Chem. **61,** 2199 (1983).
15. J.Jortner and N.R.Kestner, J. Phys. Chem. **77,** 1040 (1973).
16. Kajiwara, K.Funabashi and Naleway, Phys. Rev. **A6,** 808 (1972).
17. R.Lugo and P.Delahay, J. Chem. Phys. **57,** 2122 (1972).
18. G.L.Hug and I.Carmicheal, J.Phys. Chem. **86,** 3410 (1982).

19. K.Funabashi, I.Carmicheal and W.H.Hamill, J. Chem. Phys. **69**, 2652 (1978).

20. J.K.Baird, L.K.Lee and E.J.Meehan, J. Chem. Phys. **83**, 3710 (1985).

21. J.K.Baird and C.H.Morales, J. Phys. Chem. **89**, 774 (1985).

22. T.Ichikawa and H.Yoshida, J. Chem. Phys. **73**, 1540 (1980).

23. T.Kimura, O.Hirao, C.Okabe and K.Fueki, Can. J. Chem. **62**, 64 (1984).

24. K.F.Baverstock and P.J.Dyne, Can. J. Chem. **48**, 2182 (1970).

25. T.Shida, S.Iwata and T.Watanabe, J. Phys. Chem. **76**, 3683 (1972).

26. K.Kato, S.Takagi and K.Fueki, J. Phys. Chem. **85**, 2684 (1981).

27. R.A.Ogg, Phys. Rev. **69**, 243, (1946).

28. J.Jortner, J. Chem. Phys. **30**, 839 (1959).

29. D.A.Copeland, N.R.Kestner and J.Jortner, J. Chem. Phys. **53**, 1189 (1970).

30. D.F.Feng, K.Fueki and L.Kevan, J. Chem. Phys. **58**, 3281 (1973).

31. A.Banerjee and J.Simons, J.Chem.Phys. **68**, 415 (1978).

32. D.Chandler, J. Phys. Chem. **88**, 3400 (1984).

33. G.R.Freeman, J.Phys. Chem. **77**, 7 (1973).

34. J.G.J.Kirkwood, Chem. Phys. **7**, 911 (1939).

35. F.Y.Jou and G.R.Freeman, Can. J. Chem. **60**, 1809 (1982).

36. A.D.Leu, PH.D. Thesis, University of Alberta, 1980.

37. A.D.Leu, K.N.Jha and G.R.Freeman, Can. J. Chem. **60**, 1809 (1982).

38. R.R.Hentz and G.A.Kenney-Wallace, J. Phys. Chem. **78**, 514 (1974).

39. G.E.Hall and G.A.Kenney-Wallace, Chem. Phys. **32**, 313 (1978).

40. J.Kroh and J.Salmon, J. Phys. Chem. **85**, 2021 (1981).

41. B.Webster, J. Phys. Chem. **84**, 1070 (1980).

42. A.M.Brodsky and A.V.Tsarevsky, J. Phys. Chem. **88,** 3799 (1984).

43. N.Kato, K.Akiyama and K.Fueki, J. Phys. Chem. **85,** 3087 (1981).

44. M.Woznyj and H.D.Ludemann, Z. Naturforsch, **40a,** 693 (1985).

45. M.A.Anisimov, et al., J. Struct. Chem. **18,** 835 (1977).

46. T.H.Tran-Thi, A.M.Koulkes-Pujo, J.Sutton and O.Anitoff, Radiat. Phys. Chem. **23,** 77 (1984).

47. J.L.Dye, M.G.DeBacker and L.M.Dorfman, J. Chem. Phys. **52,** 6251 (1970).

48. F.Y.Jou and L.Dorfman, J. Chem. Phys. **58,** 4715 (1973).

49. V.V.Shornikov, G.I.Khaikin and V.A.Zhugunov. High. Ener. Chem. **15,** 226 (1981).

50. V.V.Shornikov, G.I.Khikin and V.A.Zhigunov, Radiat. Phys. Chem. **24,** (1985).

51. "The Hydrated Electron", editors: E.J.Hart and M.Anbar (Wiley-Interscience, New York, 1970).

52. B.Cercek, Int. J. Radiat. Phys. Chem. **7,** 223 (1975).

53. A.M.Afannasiev, K.Okazaki and G.R.Freeman. J. Phys. Chem. **83,** 1244 (1979).

54. M.V.Smoluchowski, Phys. Z. **17,** 557, (1916).

55. P.Debye, Trans. Electrochem. Soc. **82,** 265 (1942).

56. G.H.Weiss, J. Stat. Phys. **42,** 3 (1986).

57. R.I.Cukier, J. Stat. Phys. **42,** 69 (1986).

58. J.P.Dodelet and G.R.Freeman, Can. J. Chem. **53,** 1263 (1975).

59. P.Fowles, Trans. Faraday Soc. **67,** 428 (1971).

60. J.A.Delaire, M.O.Delcourt and J.Belloni, J. Phys. Chem **84,** 1186 (1980).

61. F.Barat, L.Gilles, B.Hickel and B.Lesigne, J. Phys. Chem. **77,** 1711 (1973).

62. B.H.Milosavijevic and O.I.Micic, J. Phys. Chem. **82,** 1359 (1978).

63. O.I.Micic and B.Cercek, J. Phys. Chem. **81,** 833 (1977).

64. A.Einstein in "Investigations on the Theory of Brownian Movement", p 75 (Dover Publications, New York, 1956).

65. Farhataziz, S.Kalachandra and M.S.Tunuli, J. Phys. Chem. **88,** 3837 (1984).

66. S.Kalachandra and Farhataziz, Chem. Phys. Lett. **73,** 465 (1980).

67. Y.Maham and G.R.Freeman, J. Phys. Chem. **89,** 4347 (1985).

68. J.Cygler and G.R.Freeman, Can. J. Chem. **62,** 1265 (1984).

69. A.Masters and P.Madden, J. Chem. Phys. **74,** 2450 (1981).

70. B.U.Feldhorf, Mol. Phys. **48,** 1283 (1983).

71. J.B.Hubbard and L.Onsager, J. Chem. Phys. **67,** 4850 (1977).

72. K.Ibuki and M.Nakahara, J. Chem. Phys. **84,** 2776 (1986).

73. K.Ibuki and M.Nakahara, J. Chem. Phys. **84,** 6779 (1986).

74. A.M.Afannasiev, K.Okazaki and G.R.Freeman, Can. J. Chem. **57,** 839 (1979).

75. K.M.Idriss-Ali and G.R.Freeman, Radiat. Phys. Chem. **23,** 89 (1984).

76. Y.Maham and G.R.Freeman, J. Phys. Chem. **91,** 0000 (1987).

77. "Physico-chemical Constants of Binary Mixtures", vol 4 (Interscience, New York, 1960).

78. F.Franks in "Physico-chemical Processes in Mixed Aqueous Solvents", editor F.Franks (Elsevier, New York,1967).

79. J.Morgan and B.E.Warren, J. Chem. Phys. **6,** 666 (1938).

80. J.D.Bernal and P.H.Fowler, J. Chem. Phys. **1,** 515 (1933).

81a. A.H.Narten, J. Chem. Phys. **56,** 5681 (1972).

81b. A.H.Narten and H.A.Levy, J. Chem. Phys. **55,** 2263 (1971).

82. J.A.Pople, Proc. Royal Soc. **A222,** 498 (1954).

83a. S.E.Rice and M.G.Sceats, J. Phys. Chem. **85,** 1107 (1981).

83b. S.E.Rice and M.G.Sceats in "Water: A Comprehensive Treatise" vol7, editor F.Franks (Plenum Press, New York, 1982).

84. F.H.Stillinger and A.Rahman, J. Chem. Phys. **60,** 1545 (1974).

85. H.E.Stanley and J.Teixeira, J. Chem. Phys. **73,** 3404 (1980).

86. H.S.Frank and Y.W.Wen, Discuss. Faraday Soc. **24,** 133 (1957).

87. G.J.Safford, P.S.Leung, A.W.Neumann and P.C.Schaffer J. Chem. Phys. **50,** 4444 (1969).

88a. G.Nemethy and H.A.Scheraga, J. Chem. Phys. **36,** 3382 (1961).

88b. A.T.Hagler, G.Nemethy and H.A.Scheraga, J. Chem. Phys. **76,** 3229 (1972).

89. M.S.Jhon, H.Eyring, J.Grosh and T. Ree, J. Chem. Phys. **44,** 1456 (1966).

90. Y.I.Naberukhin, J. Struct. Chem. **25,** 223 (1984).

91. F.H.Stillinger, Science, **209,** 451 (1980).

92. P.Huyskens, J. Mol. Struct. **100,** 403 (1983).

93. "The hydrogen Bond" editors, P.Schuster, G.Zundel and C.Sandorfy ,vol 3, p 1070 (North Holland Publishing, 1976).

94. M.C.R.Symons and V.K.Thomas, J. Chem. Soc. Faraday. Trans.1 **77,** 1883 (1981).

95. M.Magini, G.Paschina and G.Piccaluga, J. Chem. Phys. **77,** 2051 (1982).

96. A.H.Narten and A.Habenschuss, J. Chem. Phys. **80,** 3387 (1984).

97. A.H.Narten and S.I.Sandler, J. Chem. Phys. **71**, 2069 (1979).

98. H.H.Eysel and J.E.Bertie, J. Mol. Struct. **142**, 227 (1986).

99. B.M.Pettit and J.J.Rossky, J. Chem. Phys. **78**, 7296 (1983).

100. W.L.Jorgensen, J. Phys. Chem. **90**, 1276 (1986).

101. J.Liszi, L.Meszaros and I.Ruff, Acta. Chim. Accad. Scien. Hung. **104**, 279 (1980).

102. J.P.Hastead in "Aqueous Dielectrics" ,p 176 (Chapman and Hall, London, 1973).

103. A.D'Aprano, I.D.Donato, and V.Agrigento, J. Sol. Chem. **11**, 259 (1982).

104. A.D'Aprano, I.D.Donato, G.D'Arrigo, D.Bertollini, M.Cassettari and G.Salvetti, Mol. Phys. **55**, 475 (1985).

105. B.Marongin, I.Ferrino, R.Monaci, V.Solinas and S.Forraza, J. Mol. Liq. **28**, 229 (1984).

106. A.C.Brown and D.J.G.Ives, J. Chem. Soc. 1608 (1962).

107. Y.I.Naberukhin and V.A.Rogov, Russ. Chem. Rev. 207 (1971).

108. H.Tanaka, K.Nakanishi and H.Touhara, J. Chem. Phys. **81**, 4065 (1984).

109. T.M.Bender and R.Pecora, J. Phys. Chem. **90**, 1700 (1986).

110. H.Leiter, Č.Albayrak and H.G.Hertz, J. Mol. Liq. **27**, 211 (1984).

111. M.C.R.Symons and G.R.Eaton, Farad. Sympos. **17**, 31 (1982).

112. K.Shinoda, J. Phys. Chem. **81**, 1300 (1977).

113. W.L.Jorgensen, J.Gao and C.Ravimohan, J. Phys. Chem. **89**, 3470 (1985).

114. F.A.Smith and C.D.Beiling in "Positron Annhilation"; editors, P.G.Coleman, S.C.Sharma, L.M.Diana, p 838 (North-Holland Publishing, 1982).

115. V.I.Korsunski and Y.I.Naberukhin, J. Struct. Chem. **18,** 587 (1977).

116. M.Woznyj and H.D.Ludemann, Z. Naturforsch **40A,** 693 (1985).

117. A.M.Hafez and H.Sadek, Acta. Chim. Accad. Sci. Hung. **89,** 257 (1976).

118. F. Franks in "Physico-chemical Processes in Mixed Aqueous Solvents", editor F.Franks, p 67 (Elsevier, 1967)

119. A.D'Aprano, D.Donato, E.Caponetti and V.Agrigento, J. Sol. Chem. **8,** 793 (1979).

120. D.Bertollini, M.Cassettari and G.Salvetti, J. Chem. Phys. **78,** 365 (1983).

121. J.P.Perl, D.T.Wasan, P.Winsor and R.H.Cole, J. Mol. Liq. **28,** 103 (1984).

122. S.K.Garg and C.P.Smyth, J. Phys. Chem. **69,** 1294 (1965).

123. W.Dannhauser and F.Fluekinger, Phys. Chem. Liq. **2,** 37 (1970).

124. H.Sato, H.Nakamura, K.Itoh and K.Higasi, Chem. Lett. 1167 (1985).

125. D.Bertollini, M.Cassettari and G.Salvetti, J. Chem. Phys. **76,** 3285 (1982).

126. R.S.Moog, M.D.Edigar, S.G.Boxer and M.D.Fayer, J. Phys. Chem. **86,** 4694 (1982).

127. Y.Masuda, M.Suno, H.J.Yamatera, J. Phys. Chem. **89,** 3086 (1985).

128. L.A.Phillips, S.P.Webb, S.W.Yieh and J.H.Clark, J. Phys. Chem. **89,** 17 (1985).

129. S.A.Rice and G.A.Kenney-Wallace, Chem. Phys. **47,** 161 (1980).

130. E.F.J.Templeton, E.L.Quitevis and G.A.Kenney-Wallace, J. Phys. Chem. **89,** 3238 (1985).

131. S.Beddard, T.Doust and J.Hudales, Nature **294,** 145 (1981).

132. R.J.Gardner and P.C.Senanayake, Rev. Sci Instrum. **57,** 3129 (1986).

133. J.T.R.Watson, R.S.Basu and J.V.Sengers, J. Phys. Chem. Ref. Data **9,** 1255 (1980).

134. "Handbook of Chemistry and Physics", 64th edition, editor R.C.Weast (CRC Press, Boca Raton, Florida) (a) p F-11 (b) p F-33 (c) p F-39 to F-42 (d) p C-249.

135. "Operating Instructions KPG Ubbelohde Viscometers (Schott Gerate, Hofheim a. Ts., F.R.Germany, 1982).

136. D.F.Williams, C.H.Byers and C.R.Young, ORNL/TM-9410, (Oak Ridge National Laboratory, Oak Ridge, TN. 1985).

137. L.Ubbelohde, Ind. Eng. Chem. (Analyt. ed.) **37,** 85 (1937).

138. T.L.Broadwater and R.L.Kay, J. Phys. Chem. **74,** 3802 (1970).

139. N.B.Vargaftik in "Tables on Thermophysical Properties of Liquids and Gases" 2nd ed. (J. Wiley and Sons, Halsted Press, New York, 1975).

140. A.K.Doolittle and R.H.Peterson, J. Am. Chem. Soc. **73,** 2145 (1951).

141. M.A.Rauf, G.H.Stewart and Farhataziz, J. Chem. Eng. Data. **28,** 324 (1983).

142. K.Shinsaka, N.Gee and G.R.Freeman, J. Chem. Thermody. **17,** 1111 (1985).

143. C.M.Sorensen, J. Chem. Phys. **79,** 1455 (1983).

144. C. deVisser, G.Perron and J.E.Desnoyers, Can. J. Chem. **55,** 856 (1977).

145. A.Hvidt, R.Moss and G.Neilsen, Acta. Chem. Scand. **B32,** 274 (1978).

146. M.S.Chaudry and J.A.Lamb, J. Chem. Thermody. **18,** 665 (1986).

147. K.R.Harris and L.A.Woolf, J. Chem. Soc. Faraday Soc. **76,** 373 (1980).

148. "Physico-chemical Constants of Binary Mixtures", editor J.Timmermans (Interscience, New York, 1980).

149. J.P.Dodelet and G.R.Freeman, Can. J. Chem. **50**, 2667 (1972).

150. P.Fowles, Trans. Faraday Soc. **67**, 428 (1971).

151. A.V.Rudenev, A.V.Vannikovand N.A.Bakh, High Energ. Chem. **6**, 416 (1972).

152. A.V.Vannikov, E.I.Maltzev, V.I.Zolotarevsky and A.V.Rudnev, Int. J. Rad. Phys. Chem. **4**, 135 (1972).

153. "Physical Properties of Hydrocarbons", editor R.W.Gallant, vol 1 (Gulf Publishing, Houston, Texas, 1968).

154. A.D'Aprano, D.I.Donato and V.Agrigento, J. Sol. Chem. **10**, 673 (1981).

155. K.Nakanishi, K.Ikari, S.Okazaki and H.Touhara, J. Chem. Phys. **80**, 1956 (1984).

156. A.Hvidt, R.moss and G.Neilson, Acta. Chem. Scand B, **32**, 274 (1978).

157. G.Roux, D.Roberts, G.Perron and J.E.Desnoyers, J. Sol. Chem. **9**, 629 (1980).

158a. H.Tanaka, K.Nakanishi and H.Touhara, J. Chem. Phys. **81**, 4065 (1984).

158b. K.Nakanishi, K.Ikari, S.Okazaki and H.Touhara, J. Chem. Phys. **81**, 890 (1984).

160. F.Y.Jou and G.R.Freeman, Can. J. Chem. **54**, 693 (1976); J. Phys. Chem. **81**, 909 (1977); **83**, 1979 (1979).

161. K.Okazaki and G.R.Freeman, Can. J. Chem. **56**, 2313 (1978).

162. J.Jortner and R.M.Noyes, J. Phys. Chem. **70**, 770 (1066).

163. B.C.Webster and I.C.Carmicheal, J. Chem. Phys. **68**, 4086 (1978).

164. C.M.Stupak, T.R.Tuttle and S.Golden, J. Phys. Chem. **88**, 3804 (1984).

165. F.Y.Jou and G.R.Freeman, J. Phys. Chem. **88**, 3900 (1984).

166. A.D.Leu, K.N.Jha and G.R.Freeman, Can. J. Chem. **61**, 1115 (1983).

167. H.Christensen and K.Sehested, J. Phys. Chem. **80**, 186 (1986).

168. "Dielectric Properties of Binary Solutions", editor, Y.Y.Akhadov (Pergamon Press, Oxford, 1980).

169. A.C.Brown and D.J.G.Ives, J. Chem. Soc. 2, 1608 (1962).

170. J.V.Beitz and J.R.Miller, J. Chem. Phys. **71**, 4579 (1979).

171. J.M.Younkin, L.J.Smith and R.N.Compton, Theor. Chim. Acta. **41**, 157 (1976).

172. G.L.Bolton and G.R.Freeman, J. Am. Chem. Soc. **98**, 6825 (1976).

173. M.Iwahashi, Y.Ohbu, T.Kato, Y.Suzuki, K.Yamauchi, Y.Yamauchi and M.Muramatsu, Bull. Chem. Soc. Jpn. **59**, 3771 (1986).

174. J.Applequist, J.R.Carl and K.Fung, J. Am. Chem. Soc. **94**, 2952 (1972).

175. K.J.Miller and J.A.Sawchik, J. Am. Chem. Soc. **101**, 7206 (1979).

176. A.A.Kadhum and G.A.Salmon, J. Chem. Soc. Farad. Trans. **82**, 2521 (1986).

177. F.Accascina, R.De Lisi and M.Goffredi, Electrochim. Acta. **16**, 101 (1971).

178. F.Accascina, R.De Lisi and M.Goffredi, Electrochim. Acta. **15**, 1209 (1970).

179. G.D.Parfitt and A.L.Smith, Trans. Farad. Soc. **59**, 257 (1963).

180. H.Phuong-Nguyen and G.Delmas, Can. J. Chem. **64**, 681 (1986).

181. H.Vogel and A.Weiss, Ber. Bunseg. Phys. Chem. **86**, 193 (1982).

182. H.N.Solimo, R.Riggio, J.A.Espindola, S.D.V.Alonso and M.Katz, Can. J. Chem. **54**, 3125 (1976).

183. R.E.Rind, E.M.McLaughlin and A.R.Uddelohde, Trans. Farad. Soc. **56,** 328 (1960).

184. J.Kestin, N.Imaishi, S.H.Nott, J.C.Nieuwoudt and J.V.Sengers, Physica **134A,** 38 (1985).

185. S.Arrhenius, Z. Phys. Chem. **1,** 285 (1887).

186. J.Kendall and K.P.Monroe, J. Am. Chem. Soc. **39,** 1777 (1917).

187. E.P.Ivany, J. Am. Chem. Soc. **65,** 1392 (1943).